

PHYSICAL MODEL REAL-TIME AURALISATION OF MUSICAL
INSTRUMENTS: ANALYSIS AND SYNTHESIS

DISSERTATION
ZUR ERLANGUNG DES GRADES EINES DOKTORS DER PHILOSOPHIE
AM FACHBEREICH GEISTESWISSENSCHAFTEN IN DER FAKULTÄT
KULTURGESCHICHTE UND KULTURKUNDE IM FACH DER
SYSTEMATISCHEN MUSIKWISSENSCHAFT
AN DER UNIVERSITÄT HAMBURG

vorgelegt von

FLORIAN PFEIFLE

aus

HAMBURG

HAMBURG, 2016

1. Gutachter: Prof. Dr. habil. Rolf Bader
2. Gutachter: Prof. Dr.-Ing. habil. Udo Zölzer

DATUM DER DISPUTATION

07.07.2014

TAG DES VOLLZUGES DER PROMOTION

07.07.2014

*To Magali and my parents, Beate & Massimo.
Thank you for all your patience, love, and support.*

Physical modelling is a widely applied method for researching acoustical properties of musical instruments. In recent years the ever rising computational power of standard personal computers and the accessibility of dedicated accelerating hardware has fuelled manifold developments in this field of research. Most physics based methods that directly solve the underlying differential equations have the severe drawback of a high computational cost, so many simplifications of the physical models are proposed and utilised to make physical schemes faster or capable of real-time. But, with simpler descriptions of the modelled instruments, less information about the actual physical behaviour can be gained from the model. This, in turn, directly influences the sound quality of the physical model. A method that could retain high structural accuracy while being capable of calculating and synthesizing instrument models in real-time would be highly beneficial for several reasons:

- For musicological research of the influence of physical parameters on the timbre and the radiated sound of the instrument.
- For instrument makers who could test the influence of geometrical alterations on the vibrational behaviour of the respective instrument without the time delay of crafting a new instrument.
- For musicians who are interested in physics based synthesis of musical instruments.
- For composers who want to compose and perform music for a new class of instruments with changeable geometrical features in real-time. (Imagine a piano that can be manipulated in size while playing.)

This thesis presents a methodology and working implementation of real-time physical models of four musical instruments. The models are developed by using measurements taken on real instruments as a basis and implementing all acoustically relevant parts of the instruments in software and hardware. The physical models are computed using symplectic and multi-symplectic time integration methods iterating Newton's equation of motion in time. All models are implemented in C/MATLAB and on Field Programmable Gate Array Hardware. The final instrument models can be controlled from a Graphical User Interface running on a standard PC.

ACKNOWLEDGMENTS

The research described in this thesis was carried out at the Institute of Systematic Musicology at the University of Hamburg between August 2010 and December 2013.

Notwithstanding that the research project was, and still is, a matter of deep personal interest, all this would not have been possible without the help and support of several outstanding individuals. Hence, it gives me great pleasure to acknowledge all the support I have received during my years at the Institute of Systematic Musicology and outside of the University.

First of all I would like express my gratitude towards Prof. Dr. Rolf Bader who, despite his busy schedule, always found time to discuss subjects concerning my thesis. Without his efforts I would not have had the freedom to pursue my scientific ambitions with the same dedication as I have. I would like to thank Prof. Dr. Udo Zölzer who commented on several central aspects in earlier version of this thesis. Further acknowledgements go to Prof. Dr. Albrecht Schneider with whom I had several fruitful discussions regarding my work. I sincerely would like to thank the *Deutsche Forschungsgemeinschaft* (DFG) for supporting me financially during the years 2010-2012 giving me the freedom to work exclusively on my thesis.

Furthermore, I would like to thank Malte, Jan, Christian and all the others at the Institute, for supplying a collegial and friendly atmosphere. I especially would like to thank Niko for his help with several of the measurements as well as his hospitality during the last months of my work. Orië, thank you for green-tea and *Pocky*. A specially heartfelt thank you goes to Magali who supported me patiently over the last years, and to my parents Massimo & Beate for supporting me at all times.

1	Introduction	1
1.1	Background and motivation	2
1.1.1	Real-time physical modeling	5
1.2	Physical modeling or mathematical modeling?	8
1.3	Methodology of this thesis	9
2	History, organology and acoustics	11
2.1	Preliminary Remarks	11
2.2	Applied Measurement Tools	12
2.2.1	Microphone Array	12
2.2.2	High-Speed Camera	13
2.2.3	Impulse Hammer - Piezo Recordings	14
2.2.4	Dummy Head Recordings	14
2.3	American 5-String Banjo	15
2.3.1	Historic Overview	15
2.3.2	Banjo Strings	23
2.3.3	Banjo Bridge	28
2.3.4	Banjo Membrane	32
2.3.5	Banjo Body	37
2.3.6	Banjo Playing Styles	37
2.3.7	Open Questions	38
2.4	Violin	39
2.4.1	Historic Overview	39
2.4.2	Acoustical Research History	40
2.4.3	The Violin String	42
2.4.4	The Bow/String Interaction	46
2.4.5	Violin Bridge	47
2.4.6	Violin Front/Back Plate	47
2.5	<i>Ruan</i> and <i>Yueqin</i>	49
2.5.1	Historic Overview	49
2.5.2	Acoustical Properties of the <i>Ruan</i>	52
2.5.3	<i>Ruan</i> Strings	52
2.5.4	<i>Ruan</i> Bridge	55

2.5.5	Ruan Body	55
2.5.6	Acoustical Properties of the <i>Yueqin</i>	57
2.6	Pick/String Interaction	60
2.6.1	High-Speed Camera Recordings	61
2.6.2	Spectral Components	61
2.6.3	Tremolo Model Extension	62
2.7	Intermediate Results	62
3	Numerical methods	64
3.1	Numerical Methods for Physical Modeling	66
3.1.1	Single-Step Methods	67
3.1.2	Multi-Step Methods	68
3.2	Finite Difference Methods	69
3.2.1	Finite difference approximations	73
3.2.2	Finite Difference Operators	74
3.3	Finite Difference Time Domain Methods	77
3.3.1	0-dimensional Wave Equation	77
3.3.2	1-Dimensional Wave Equation	80
3.3.3	Considerations Regarding the FDTD Method	81
3.4	Discretising the Equations of Motion	81
3.4.1	0-Dimensional Equations of Motion	82
3.4.2	Derivation of the 1-Dimensional Wave Equation	85
3.5	Symplectic and Multi-Symplectic Methods	89
3.5.1	Comparison of Several Algorithms	91
3.5.2	Multi-Symplectic Schemes	96
3.5.3	Implicit Algorithms	97
3.6	Pseudo-Spectral Finite Differences	97
3.6.1	Finite Difference Grids as Convolution Kernels	98
3.7	Final High Level Algorithm	100
3.7.1	Introduction	100
3.7.2	Basic Formulation	101
3.8	Final Low Level Algorithm	102
3.8.1	Model of a Linear String	103
3.8.2	Approximating Damping Parameters	103
3.8.3	Linear Velocity Damped String	104
3.9	Error and Stability Analysis	104
3.9.1	Discretisation Error	106
3.9.2	Stability and Error Measures	107
3.9.3	Stability Analysis Used in this Thesis	110
4	Physical models	112
4.1	1-dimensional wave equation models	113
4.1.1	Linear string with damping	121
4.1.2	High Deflection String	126
4.1.3	String with Bending Stiffness	130
4.1.4	Stiff string with damping and end support losses	133
4.1.5	Discussion	134

4.2	2-dimensional wave equation models	135
4.2.1	Linear membranes	136
4.2.2	Tension modulated membranes	140
4.2.3	Plates	141
4.2.4	Stiff membranes	143
4.2.5	Frequency dependent damping	146
4.2.6	Wooden orthotropic plates	146
4.2.7	Wooden orthotropic plate with buckling	148
4.3	3-dimensional wave equation models	149
4.3.1	Closed air cavities	150
4.3.2	Air cavities with orifices	151
4.4	Coupled geometries	152
4.4.1	Elastic spring coupling	152
4.4.2	Impedance coupling	152
4.4.3	Structural coupling	153
4.5	American 5-string banjo model	155
4.5.1	Banjo string model	156
4.5.2	Banjo membrane model	157
4.5.3	Model of the bridge	158
4.5.4	Model of the air cavity	158
4.5.5	Numerical results	160
4.5.6	Discussion	161
4.6	Yueqin model	164
4.6.1	String model	164
4.6.2	Model of the front- and back-plate	165
4.6.3	Model of the enclosed air	165
4.6.4	Numerical results	166
4.7	Ruan model	168
4.7.1	String model	168
4.7.2	Model of the front- and back plate	169
4.7.3	Model of the bridge	169
4.7.4	Model of the enclosed air	169
4.7.5	Numerical results	170
4.8	Violin model	172
4.8.1	Violin string model	172
4.8.2	Violin bridge model	172
4.8.3	Violin top plate model	173
4.8.4	Air cavity	173
4.8.5	Bow string model	174
4.9	Sound integration over surfaces	177
5	FPGA - A structural overview	179
5.1	History of FPGAs	180
5.2	Features and properties of FPGAs	182
5.2.1	Structure of FPGAs	182
5.2.2	Special function blocks	184
5.2.3	Hardware Description Language	186

5.2.4	Finite State Machine	188
5.3	XUP Virtex-II Pro Development System	191
5.3.1	Virtex-2 FPGA	191
5.3.2	LM4550-AC '97 CODEC	191
5.3.3	I2S interface	193
5.4	The ML-605 Evaluation Board	194
5.4.1	Virtex-6 FPGA	194
5.5	PCIe interface	194
5.5.1	PCIe fundamentals	195
5.5.2	PCIe layer communication	195
5.5.3	Implemented design	196
5.6	Final design consideration	197
5.6.1	PCIe protocol timing	197
6	Real-time FPGA models	198
6.1	Introduction	198
6.1.1	Parallelization Considerations	199
6.1.2	Data Type Considerations	200
6.2	Routing Layer Model	203
6.2.1	Arithmetic Layer	204
6.2.2	Math Routing Layer	205
6.2.3	Control Circuit Layer	205
6.2.4	Model Routing Layer	206
6.2.5	Interface Layer	207
6.3	Hardware Operator Notation	208
6.3.1	Operator Definition	208
6.3.2	Combined Operations	208
6.3.3	Damping Approximation by Shifts	209
6.4	VHDL Translation of the Algorithm	210
6.4.1	0-dimensional Simple Harmonic Oscillator	210
6.4.2	Structurally Parallel 1-dimensional Wave Equation	216
6.4.3	Parallel/Serial 1-dimensional Wave Equation	221
6.4.4	String with Damping	221
6.4.5	Bowed String	222
6.4.6	Stiff String	223
6.4.7	2-dimensional Wave Equation	225
6.4.8	2-dimensional Plate	227
6.4.9	The Violin Bridge	229
6.4.10	3-dimensional Air Volumes	230
6.5	Instrument Models	233
6.5.1	Banjo Model	233
6.5.2	Yueqin Model	236
6.5.3	Ruan Model	237
6.5.4	Violin Model	238
6.6	Simulation Results	240
6.6.1	Banjo	240
6.6.2	Violin	241

6.6.3	Ruan	242
6.7	GUI for the Model	244
7	Results, Conclusion and Outlook	245
7.1	Central Achievements	245
7.2	Findings of Numerical Nature	246
7.2.1	Layer model	246
7.3	Findings Acoustical Nature	247
7.3.1	Banjo	247
7.3.2	Ruan	248
7.3.3	Violin	249
7.4	Future Research	250
Appendix I	252
1	High-speed recordings of banjo pick	252
2	High-speed recordings of banjo bridge	253
3	High-speed recordings of banjo string	253
Appendix II	259
1	CD contents.	259

LIST OF TABLES

2.1 Material and tension of banjo string used in this work. Values are taken from the packaging of the D'Addario 5-string Banjo strings.	23
2.2 Geometry parameters of banjo head membranes.	33
2.3 Measured vs. analytic frequency ratios of a banjo membrane.	36
2.4 Engineering constants of Paulownia wood.	55
2.5 Geometry parameters of the ruan.	56
2.6 Geometry parameters of the <i>yueqin</i>	60
3.1 Arithmetic resources of integrators.	94
4.1 Values for the linear string model.	117
4.2 Mesh grid values for arbitrary shapes.	137
4.3 Simulation parameters for the round membrane.	138
4.4 Isotropic plate theory constants.	147
4.5 Orthotropic constants for wood plate.	147
4.6 Constants for orthotropic plates.	147
4.7 Material properties for Sitka spruce.	148
4.8 Force constants for plates under buckling.	149
4.9 Simulated vs. measured ratios of a banjo membrane.	163
5.1 States for the harmonic oscillator.	188
5.2 Logic resources of a Virtex-2 XC2VP30 device.	191
5.3 Signals connected to the model.	192
5.4 Logic resources of a Virtex-6 XC6VLX-240t device.	194
6.1 Layer model signal description.	203
6.2 Digital operations for FD operators used in this work.	209
6.3 Digital operations for SHO implementation.	211
6.4 Digital operations for linear string implementation.	217
6.5 Controller data words.	223
6.6 Digital operations count for a stiff string implementation.	224
6.7 Air-plate logic block signal description.	232

1	Excitation of the string with metal pick I	252
2	Rocking motion of the bridge I	253
3	Rocking motion of the bridge II	254
4	Rocking motion of the bridge III	255
5	String movement I	256
6	String movement II	257
7	String movement II	258

LIST OF FIGURES

2.1	Transversal deflection of a plucked banjo string. Time in seconds on the abscissa and tracked pixel range on the ordinate.	25
2.2	Normalised transversal deflection of a plucked banjo string with time in seconds on the abscissa. (a)	26
2.3	Physical dimensions of the banjo bridge in [mm]. The black dot indicates the measured point.	29
2.4	Deflection of a banjo bridge normal to the membrane tracked at the left foot.	29
2.5	Spectrum of the bridge foot motion.	30
2.6	Acceleration at right bridge foot.	31
2.7	Absolute values of Banjo mode-shapes. Impulse-hammer excitation. a) : Open back, no strings. b) : Closed back, no strings. c) : Open back, strings. d) : Closed back, strings. Column a shows the position of the banjo during all measurements. For mode-shapes (4,1) and (5,1) only imaginary or real part are used for the images due to their better structural resolution.	35
2.8	Normalised transversal deflection of a plucked violin string (280 Hz) with time in seconds on the x-axis.	44
2.9	Normalised transversal deflection of a plucked violin string	45
2.10	Measured velocity of a bowed violin string.	46
2.11	Measured deflection of a bowed violin string. Discrete sample points on the abscissa.	46
2.12	Free front plate / back plate holographic interferograms	48
2.13	Chinese <i>ruan</i>	49
2.14	Chinese <i>yueqin</i>	50
2.15	Normalised transversal deflection of a plucked ruan string (104 Hz) with time in seconds on the abscissa.	53
2.16	Normalised transversal deflection of a plucked ruan string (104 Hz) with time in seconds on the abscissa.	54
2.17	Ruan radiation patterns – Impulse-hammer excitation. Column A) : Air modes. S) : Structural modes. A/S) : Coupled Air - Structure modes.	57
2.18	Transversal deflection of a plucked <i>yueqin</i> string (181 Hz), time in seconds on the abscissa.	58

2.19	Transversal deflection of a plucked <i>yueqin</i> string (181 Hz), time in seconds on the abscissa.	59
2.20	Radiation patterns of the <i>yueqin's</i> front-plate – Impulse hammer excitation.	60
2.21	Piezoelectronic recording of the pick/string interaction measured at the banjo bridge.	62
3.1	Oscillating mass-point.	78
3.2	Output of algorithm 3.53.	83
3.3	Oscillating mass-point with two springs.	86
3.4	Two oscillating mass-points with three springs.	86
3.5	Three oscillating mass-points with four springs.	87
3.6	Three oscillating mass-points, longitudinal/transversal.	88
3.7	Symplectic vs. non-symplectic integrator.	91
4.1	String segment displaced from equilibrium.	116
4.2	Time series of a linear string, deflected in triangular shape at $t = 0$	118
4.3	Simulation of linear string with triangular deflection.	118
4.4	Spectrum of the string vibration shown in Figure 4.3.	119
4.5	Time series of a linear string with Neumann boundary conditions, deflected with a Gaussian bell shape at $t = 0$	120
4.6	String with different damping factors β from undamped to highly damped.	122
4.7	Enlarged part of damped string with $\beta = 0.001$	123
4.8	Spectrum of a string with different damping factors β from undamped to highly damped.	123
4.9	String with different internal damping factors α from undamped to highly damped.	125
4.10	Spectrogram of string with non-linear Duffing-term. $\alpha = 0.001$	128
4.11	Spectrogram of string with non-linear geometric coupling.	129
4.12	Spectrogram of string with Kirchhoff-Carrier-type term.	129
4.13	Time series and spectrogram of stiff string with Euler-Bernoulli term.	132
4.14	Time series and spectrogram of stiff string with Timoshenko term.	133
4.15	Deflection over time of single point.	134
4.16	Deflection of a linear damped membrane over time.	138
4.17	Deflection of a linear membrane with opening.	139
4.18	Spectrogram of membrane with Kirchhoff-Carrier like tension change.	141
4.19	Spectrogram of membrane with geometrical coupling between longitudinal and transversal motion.	141
4.20	Time series of plate model excited by elastic hammer.	143
4.21	Deflection for several time steps of a membrane with stiffness excited by an elastic hammer.	145
4.22	Simulated spectrum of a wood plate with orthotropic and isotropic material properties.	148
4.23	Simulated spectrum of a wood plate with orthotropic and isotropic material properties.	149
4.24	Mechanical principle of Winkler bed.	159
4.25	Single string coupled to membrane.	160
4.26	Model II five strings plucked consecutively.	161

4.27	Model II knock on membrane. No strings/open back.	162
4.28	Model II knock on membrane. Resonating strings.	163
4.29	Simulation results of the yueqin. Four consecutively plucked strings. 4.29a: Time series, left and right channel. 4.29b: Spectrum.	167
4.30	Simulation results of the ruan. Four consecutively plucked strings. 4.30a: Time series, left and right channel. 4.30b: Spectrum.	171
4.31	Bow string interaction model.	175
4.32	Idealised Helmholtz motion of a bowed string.	176
4.33	Integration delays for round membrane and centred receiver.	178
5.1	Schematic overview of a Virtex-6 CLB.	183
5.2	Slicem overview	184
5.3	Schematic overview of a Xilinx column design.	185
5.4	Schematic overview of a Virtex-6 DSP48e1.	186
5.5	Schematic overview of audio CODEC LM4550.	192
5.6	AC97 protocol	193
5.7	I2S system configuration.	193
5.8	PCIe layer model.	196
6.1	Schematic overview of the Arithmetic Layer.	204
6.2	Math Routing Layer (MRL).	205
6.3	Control Circuit Layer (CCL).	206
6.4	Model Routing Layer overview.	206
6.5	Block diagram of the Interface Layer.	207
6.6	ASMD chart of the SHOs AL.	212
6.7	RTL view of FSM and Math block.	214
6.8	Timing diagram of the core functionality of the SHOs AL.	215
6.9	Timing diagram with analog output signal.	216
6.10	Parallel structure of the 1-dimensional wave equation at a random point $k \notin$ $0 \wedge L$	217
6.11	ASMD chart of the linear string AL.	218
6.12	CML of the 1-dimensional string showing the FSM and four of the ten AL blocks.	220
6.13	Serial/Parallel structure of the 1-dimensional wave equation for 80 node- points.	222
6.14	FD-shift stencil for the 1-dimensional plate operator.	225
6.15	MRL of the membrane.	226
6.16	FD-shift stencil for the 2-dimensional plate operator.	227
6.17	Logic block of the air/plate AL.	231
6.18	Partial CCL of the complete geometry implementations.	235
6.19	MoR of a complete geometry implementations.	239
6.20	Detail of banjo recording.	240
6.21	Detailed velocity of a bowed violin string.	241
6.22	Single bowed note with varying bow velocity.	241
6.23	Fast sequence of notes, changing the height of the front plate.	242
6.24	Sequence of notes played with a tremolo technique.	242

6.25 Host GUI for controlling the low level models.	244
---	-----

Abbreviations

- FPGA Field Programmable Gate Array
HDL Hardware Description Language
VHDL Very high-speed integrated circuit HDL
FEM Finite Element Method
BEM Boundary Element Method
FDTD Finite Difference Time Domain
DE Differential Equation
FPGA Field Programmable Gate Array
GPGPU General Purpose Graphics Processing Unit
ODE Ordinary Differential Equation
PDE Partial Differential Equation
SHO Simple Harmonic Oscillator

Physical Symbols

- c Velocity in the Medium
 ω Angular Frequency
 $I = \frac{\pi}{4} r^4$ Second moment of area a round geometry.
 T Linear tension in strings and membranes.
 E Young's modulus.

Layers

AL	Arithmetic Layer
MRL	Math Routing Layer
CCL	Control Circuit Layer
MRL	Model Routing Layer
IF	Interface Layer
GUI	Graphical User Interface

Mathematical Symbols

u	Temporally and Spatially Local Deflection of a System
v	Temporally and Spatially Local Velocity of a System
a	Temporally and Spatially Local Acceleration of a System
\mathbf{u}	Temporally Local Vector of Deflections of a System
\mathbf{v}	Temporally Local Vector of Velocities of a System
\mathbf{a}	Temporally Local Vector of Accelerations of a System
\mathcal{U}	Temporally and Spatially Global Deflection of the System
\mathcal{V}	Temporally and Spatially Global Velocity of the System
\mathcal{A}	Temporally and Spatially Global Acceleration of the System
Δx	Spatial Difference
u_x	First derivative of u in respect to x
∂_x	Spatial partial difference operator.
∂_t	Temporal partial difference operator.
Δt	Temporal Difference

Operators

δ_{x-}	Backward Finite Difference Operator
δ_x	Centred Finite Difference Operator
δ	Finite difference Operator
δ_{x+}	Forward Finite Difference Operator
$\bar{\delta}$	Digital Finite Difference Operator
$\hat{\delta}$	Pseudo-spectral Finite Difference Operator
τ	Temporal Shift Operator

Physical modeling sound synthesis for musicological applications is a current and active field of research at the intersection of musicology, electrical engineering, mathematics and computer science. Even though the techniques applied for physical modeling are among the oldest numerical mathematical methods, new technological advances over the past 50 years have fueled manifold applications and research in the area of numerical (sound) synthesis based on physical models. Because all physical modeling methods, utilising finite differences to solve differential equations, are computationally very expensive, their real-time capabilities were, until recently, limited to simple models or small problem sizes. Even though modern personal computers have more computational throughput than high-performance super-computer clusters of the early 1990s¹, it is still impossible to calculate full geometry models of musical instruments in real-time or even close to real-time using standard computing devices, if all subtleties of physical parameters are taken into account.

In recent years, specialised hardware devices are being utilised as co-processing units, accelerating the computations of large scale problems from weeks to mere minutes. Still, there are only few treatises regarding the implementation of real-time models of musical instruments, and, if a real-time solution is sought after, most publications concentrate on simulations of single geometries² or physical models with simplifications or linearisation in the formulation of the model³.

¹ A modern Intel Haswell i7-4770k has a theoretical throughput of 217,6 GFLOPs. This is almost four times faster compared to the 59,7 GFLOPs of the fastest supercomputer of June 1993, the CM-5/1024. See: <http://www.top500.org/lists/1993/06/>.

² For the model of a string see: J.A. Gibbons, D.M. Howard, and A.M. Tyrrell: "FPGA implementation of 1D wave equation for real-time audio synthesis", in: *IEEE Proceedings, Computers and Digital Techniques* 152.5 (2005): 619–631. For the model of a plate-like geometry see: Halil Erdem Motuk: "System-On-Chip implementation of real-time finite difference based sound synthesis", PhD thesis, Queen's University Belfast, 2006.

³ For the real-time model of a grand piano applying filter techniques to model the sound-board see: B. Bank, S.

In this thesis, real-time implementations of four music instruments are presented. These models incorporate the complete geometry with structural non-linearities and complex excitation mechanisms, and are modeled with finite difference methods, computed on a Field Programmable Gate Array (FPGA).

1.1 Background and motivation

Acoustic music instruments have been, and still are an important part of human culture throughout recorded history. There are several examples of music instruments that have a history spanning several hundred years or even thousands of years. This means they underwent constant changes and improvements throughout their developing stages, with each evolutionary step representing some sort of cultural or practical need. There are examples of music instruments that have a written history spanning several hundred years which *evolved* from archetypical instrument forms to highly valued masterpieces of craftsmanship.

Throughout their development, artisan music instrument makers have experimented with different kinds of materials and different kind of structural features, many having a visible influence on the form of the instrument as well as the sound and the timbre of the instrument. Therefore, modern versions of traditional music instruments incorporate multiple different structural features influencing their specific sound, characterising a certain manifestation of a class of instruments.

This means, there can be a multitude of different variables that shape the sound or the specific timbre of an instrument.

In many acoustic music instruments, the musically relevant part of the radiated sound is represented in the fine structure of these instruments.

A violin for instance, with its highly complex geometrical structure could not be substituted by a simple string coupled to a wooden plate without suffering loss of its characteristic sound. Additionally, these fine structural features often depend on non-linear material properties or small imperfections in the used material. This is complicated further by a coupling between different instrument parts and the interaction of different forms of acoustic vibrations, depending on the respective geometry.

In summary it is safe to state that the sound of an instrument is subject to multi-factorial influence parameters which depend on one or several of the aforementioned interactions, which in most cases cannot be understood fully by only analysing the radiated instrument sound.

Nevertheless, a very promising way to grasp the musical relevant parts of musical instruments is by modeling their whole geometries applying numerical methods, simulate the resulting

Zambon, and F. Fontana: “A Modal-Based Real-Time Piano Synthesizer”, in: *Audio, Speech, and Language Processing, IEEE Transactions on* 18.4 (May 2010): 809–821.

1 Introduction

models using a computer, and auralise and/or visualise the vibrations produced by the virtual instruments.

As this can be accomplished in a completely controllable way, the geometrical or vibrational reasons for musically interesting fine structures in the timbre can be researched systematically:

1. By changing the geometry.
2. By changing physical parameters.
3. By changing the excitation of the respective instrument.
4. By using different mathematical models.

However, a different problem arises here: Musical instruments have highly complex geometries and interaction of the respective constituent parts. This implies that there are many degrees of freedom and countless possibilities of changes in all aspects of the geometry, material properties, couplings, etc. can arise.

Hence, to arrive at a *correct* formulation for an instrument model is a typical optimisation problem of a system of nearly endless variability. Therefore, when such a model is implemented it would be beneficial to be able to apply those changes easily and fast, to arrive at estimations about the sound quality in reasonable time, preferably in real-time.

Still, the implementation of whole instrument bodies with complex interactions is very time consuming because the computational cost to solve the differential equation system rises with the complexity of the model. Solving a wind instrument with fluid dynamics, calculating 100 ms of sound may take several weeks, when implemented with FEM solvers and calculated on a standard personal computer.

When it comes to structural mechanics, computation times are faster, but still take several hours to days⁴.

Faster algorithms or methods in general would benefit the variability and applicability of whole-body models and would make them usable under more realistic research settings as well as in live music settings. At best, a real-time solution would be ideal. Then, even musicians could interact with a physical model in real-time, which would be comparable to playing a digital keyboard or a synthesizer, and change geometrical features of the modelled instrument while playing. Also, instrument makers could change design aspects of their instrument and immediately listen to the sound produced by the altered instrument.

A real-time model would enable them to research a myriad of parameter changes and not only small sets of variations, which would be feasible with non-real-time models. Instrument

⁴See: Juliette Chabassier, Antoine Chaigne, and Patrick Joly: "Modeling and simulation of a grand piano", in: *The Journal of the Acoustical Society of America* 134.1 (2013): 648–665. Here a 300 CPU Cluster calculates 24 hours, to synthesize one second of sound of a grand-piano physical model

1 Introduction

makers could test various aspects of the instruments geometry concurrently, while playing in different registers and use realistic articulations.

For researchers in musical acoustics, who want to understand instruments and their acoustically important aspects, a real-time implementation would be a great tool to parametrise simulations and compare them to measurements. Hence, a real-time solution for whole-body implementations would make the whole potential of these models available to researchers, instrument makers, and musicians.

In this thesis, a working real-time implementation for musical instruments is presented and first results, new to the field, giving a new understanding to aspects of musical sound production are presented. Furthermore, this work researches problems that can arise when comparing measured data of musical instruments to calculated data synthesised by mathematically derived models.

It is shown that the analytical models of instruments can explain effects of the vibrational behaviour of musical instruments to high accuracy for some properties but fail to do so with others.⁵

In most cases this points to an incomplete formulation of the physical model, but there are other cases where a physical effect can not be explained satisfactorily by strictly analytical methods⁶.

In this thesis, some problems that can arise when modeling musical instruments based on purely analytical approaches without comparing the results to measurements of real instruments are highlighted.

This approach is comparable to the *analysis by synthesis* methodology used in linguistic sciences.⁷

As shown in other works, a *synthesis* approach can lead to findings which extend the conventional analytical formulation and lead to more accurate mathematical descriptions of a certain problem.⁸

⁵ One example is the radiated sound of a plain membrane. The analytical solution of the 2-dimensional wave equation, describing the acoustical equations of motion of a membrane, is given by the zero-crossings of the Bessel function. But comparisons between the mathematically correct, analytical solution and real measurements reveal that there can be a discrepancy between a real, measured membrane and a mathematical membrane. Even though modern membranes of snare drums or banjos have highly isotropic material properties and very even tension distribution, the centre frequencies of the mode shapes differ considerably from the analytically expected center frequencies. See for instance the research of timpani membranes by: Thomas D. Rossing: *Science of Percussion Instruments*, World Scientific, 2008 or N. Fletcher and Th. Rossing: *Physics of Musical Instruments*, Springer, 2000.

⁶The synchronisation of organ pipes described in M. Abel, S. Bergweiler, and R. Gerhard-Mulhaupt: "Synchronization of organ pipes: experimental observations and modeling", in: *The Journal of the Acoustical Society of America* 119.4 (2006): 2467–2475 is a paragon example thereof.

⁷ Thomas G Bever and David Poeppel: "Analysis by synthesis: a (re-) emerging program of research for language and vision", in: *Biolinguistics* 4.2-3 (2010): 174–200.

⁸See for instance transversal to longitudinal vibration coupling in plates as proposed in: Rolf Bader: *Computational Mechanics of the Classical Guitar*, Springer, Oct. 2005, pp. 73-93 or non-linear effects in strings

1.1.1 Real-time physical modeling

In various areas of scientific research, the mathematical description and modeling of physical structures is a key element for understanding the behaviour and properties of *real world* objects. Especially in most fields of engineering, physical modeling in all its subsets is an important technique for simulating, implementing and verifying the behaviour of diverse devices and appliances. In structural mechanics, Finite Element Methods (FEMs) are used to simulate phenomena like transient wave propagation, impacts, deformation or steady state load distribution in large objects.⁹

The FEM is used in countless other fields of research, for instance electromagnetic simulations¹⁰ as well as instrument acoustics¹¹.

Another widely applied method, which can be seen as a successor to FEM, is the Boundary Element Method (BEM)¹² used for instance in room acoustics calculations¹³, electromagnetic models¹⁴ or models for water waves¹⁵.

Even though there are several works using FEM or BEM for modeling the mechanical properties of musical instruments,¹⁶

FEM or BEM has several drawbacks that limits their applicability for real-time¹⁷ synthesis.¹⁸

described in: David R. Rowland and Colin Pask: “The missing wave momentum mystery”, in: *American Journal of Physics* 67.5 (1998): 378–388.

⁹See the introductory chapter of: K.J. Bathe: *Finite-Element Methoden*, Springer, 2002.

¹⁰Nico Gödel: “Numerische Simulation hochfrequenter elektromagnetischer Felder durch die Discontinuous Galerkin Finite elemente Methode”, PhD thesis, Helmut-Schmidt-Universität / Universität der Bundeswehr Hamburg, 2010.

¹¹M. J. Elejabarrieta, A. Ezcurra, and C. Santamaría: “Vibrational behaviour of the guitar soundboard analysed by the Finite Element Method”, in: *Acta Acustica united with Acustica* 87.1 (2001): 128–136; N. Giordano: “Simple model of a piano soundboard”, in: *The Journal of the Acoustical Society of America* 102.2 (1997): 1159–1168.

¹²Stefan A. Sauter and Christoph Schwab: “Springer series in computational mathematics”, in: *Boundary Element Methods*, ed. by R. Bank et al., Springer Verlag, 2011.

¹³Joseph M. Corcoran and Ricardo A. Burdisso: “A diffusion boundary element method for room acoustics”, in: *12th Pan-American Congress of Applied Mechanics*, Port of Spain, Trinidad, 2012.

¹⁴M.H. Lean and A. Wexler: “Application of the boundary element method to electromagnetic scattering problems”, in: *Antennas and Propagation Society International Symposium, 1981*, vol. 19, 1981: 326–330.

¹⁵See: Frederic Dias and Thomas J Bridges: “The numerical computation of freely propagating time-dependent irrotational water waves”, in: *Fluid Dynamics Research* 38.12 (2006): 803.

¹⁶For a model of a piano sound-board see: Adrien Mamou-Mani, Joel Frelat, and Charles Besnainou: “Numerical simulation of a piano soundboard under downbearing”, in: *The Journal of the Acoustical Society of America* 123.4 (2008): 2401–2406; for the model of a base-drum see: Rolf Bader: “Finite-element calculation of a bass drum”, in: *J. Acoust. Soc. Am.* 119 (2006): 3290; or the model of a clapper see for instance: Rolf Bader et al.: “Finite-element transient calculation of a bell struck by a clapper”, in: *J. Acoust. Soc. Am.* 119 (2006): 3290.

¹⁷The term real-time in its different spelling *realtime*, *real time* and *real-time* is not really standardised. In computer science *real-time* systems are systems with predictable time steps for every sub-step of the system.

¹⁸This may be due to the fact that finite element models are known to give errors for higher wavenumbers. Another factor may be the grid construction, which can be very intricate. See Stefan Bilbao: *Numerical Sound Synthesis: Finite Difference Schemes and Simulation in Musical Acoustics*. Chichester, UK: John Wiley and Sons, 2009, pp. 16-20.

1 Introduction

Finite difference (FD) methods on the other hand do not suffer similar constraints and have been shown to be very well suited for sound synthesis of physical models.¹⁹

In current music acoustics literature, the term *physical modeling* is associated with several different ideas of sound synthesis methods, so a short clarification of the concept, utilised in this thesis, is given here.

The term *physical* denotes a direct connection to the *real* physical system of the instrument. The numerical solution method, based on the model, is adjusted to capture the physical properties to a high degree of accuracy, trying to capture all properties, at best. Next to others, there are two methods that are commonly used in the field of music and acoustics. The fundamental idea behind both approaches is to solve the differential equation by discretising the spatial and/or temporal domain and iterate this discretised system with a numerical method in space or time.

One class of physical modeling methods has its roots in filter design methodology as commonly applied in signal processing applications.²⁰ A well known and widely applied approach for instance is the digital waveguide synthesis or delay-line method.²¹ Physical models based on waveguides²² are commonly applied to solve linear differential equations, often the 1-dimensional wave equation for strings or air-columns, or the 2-dimensional equation for membranes and plates. The 1-dimensional version of this method is based on a discrete version of the d'Alembert solution of the differential equation, describing two functions travelling in both directions along a string or an air-filled tube using impedance filters at both terminations to simulate losses at the boundaries.

One fundamental advantage of this method is its computational speed. Disadvantages can arise when non-linearities must be included in a model due to coupling between geometries, non-linear excitation or complex, time-varying boundary conditions. The waveguide, or delay-line, approach is linked to filter design techniques because it is often used in combination with filters, representing the transfer-function of an instrument body or other resonator, as applied in the work of Karjalainen, Välimäki, and Janosy.²³

Another approach to synthesize instrument sounds with filter techniques can be implemented by approximating the transfer function of a vibrating object, like a linear string, with a z-transformation and reordering the resultant IIR-filter to an explicit, space-forward step,

¹⁹See Bilbao (S. Bilbao: "Robust Physical Modeling Sound Synthesis for Nonlinear Systems", in: *Signal Processing Magazine, IEEE* 24.2 [Mar. 2007]: 32–41) for an in depth consideration of the pros and cons of different strategies for physical modeling including FD methods.

²⁰K. Kroschel K.-D. Kammeyer: *Digitale Signalverarbeitung - Filterung und Spektralanalyse mit MATLAB-Übungen*, 6th ed., Wiesbaden, Germany: Vieweg+Teubner-Verlag, Apr. 2006: 587.

²¹It is utilised in many commercially available synthesizer by companies like Yamaha or Roland.

²²The concept is known as digital waveguide synthesis. JuliusO. Smith: "Digital Waveguide Architectures for Virtual Musical Instruments", in: *Handbook of Signal Processing in Acoustics*, ed. by David Havelock, Sonoko Kuwano, and Michael Vorländer, Springer New York, 2009: 399–417.

²³Matti Karjalainen, Vesa Välimäki, and Zoltan Janosy: "Towards High-Quality Sound synthesis of the Guitar and String Instruments", in: *International Computer Music Conference*, Tokyo, Japan, 1993.

1 Introduction

recursive algorithm or as an impulse response filter for different excitation forms.²⁴

Other forms of Physical Modeling found in literature are often based on lumped models, whole parts of instruments modeled as a single oscillator or other simplifications of instrument parts.²⁵

The physical modeling approach applied in this thesis utilises spatial finite difference discretisation of the respective differential equations and explicit, symplectic or multi-symplectic time integration methods. Because all important acoustical vibrations of the instruments, modeled in this thesis, can be described mathematically by the wave equation, a partial differential equation²⁶, the applied methodology is aimed at capturing its features as accurately as possible, with the smallest possible abstraction overhead resulting from mathematical or numerical methods.

Among other beneficial features of finite difference methods, they are well-suited to solve the numerical problems posed in this thesis because they are easily adaptable to varying kinds of problems, have the ability to produce stable results for various physical state variables of the modeled system and can be expressed in a straightforward and easily comprehensible, explicit form.²⁷

Even though FEM and BEM are more popular for computational simulation of mechanical problems as well as other fields, still, finite differences are used in various fields of numerical research and have by far the longest history of all three methods.²⁸

Additionally, a rising interest in the mathematical foundations of finite difference schemes has led to various optimisations and a robust mathematical framework for various numerical problems in the field of finite differences.

The driving force behind this thesis was the aspiration to model the chosen instruments with the highest perceptual accuracy possible, without resorting to simplifications in the real-time implementation due to computational restrictions²⁹ as well as creating models of musical

²⁴Robert J. Schilling and Sandra L. Harris: *Fundamental of Digital Signal Processing using MATLAB*, 2nd ed., Cengage Learning, 2012, pp. 500-503.

²⁵A perceptually reasonable simplification can be found in the physical model of a classical guitar in a Roland V-Guitar synthesizer which allows to change the height of the guitar rim, which is achieved by tuning the Helmholtz resonance using a bandpass filter, changing the center frequency of the filter.

²⁶In the case of a simple harmonic oscillator it is an ordinary differential equation.

²⁷FEM and BEM usually include the solution of a large equation system, or are solved by other implicit numerical methods. See: Bathe, *Finite-Element Methoden*, 1002ff.

²⁸An early account of finite difference methods can be found in Newton's *Principia Book 1* to solve Kepler's three body problem. See: Ernst Hairer, Christian Lubich, and Gerhard Wanner: *Geometric numerical integration : structure-preserving algorithms for ordinary differential equations*, Springer series in computational mathematics ; 31, Berlin [u.a.]: Springer, 2002, pp. 6.

²⁹This approach is utilised in several works focussing on sound synthesis. Basic parts of the model are formulated and computed with finite difference methods, whereas other parts use simplified representations for the numerical calculations to make the model capable of real-time. See for instance Teng Wei Jian: "Piano Sounds Synthesis with an emphasis on the modeling of the hammer and the piano wire.", MA thesis, University of Edinburgh, 2012.

instruments incorporating all physical and geometrical features that are important for the characteristic sound of the respective instrument. To this end, alongside the numerical aspects of the implementation, the acoustical properties of the modelled instruments are of substantial interest here because, as will be shown over the course of this work, the better the underlying physical principles of a musical instrument are understood, the more accurate a physical model can be formulated, and the more convincing the sound quality of the auralisation is.

1.2 Physical modeling or mathematical modeling?

Before presenting the methodology in more detail, a consideration regarding the problem at hand is of importance and shall be mentioned here. As stated before, the aim of this thesis is to facilitate the use of physical models for musicians, researchers, and instrument makers. This means that the physical model is designed to be as accurate as possible regarding its structural features while yielding satisfying sound synthesis results in real-time for generic as well as special cases.

In particular this means that the modeling approach used here is aimed at physically accurate representations of acoustic musical instruments and the methodology is adapted to accomplish this goal first and foremost.

Hence, the ground-truth to which the accuracy of the model is compared to, is not to a mathematical-analytical solution of the sets of equations that describe the respective instrument but physical measurements taken on real instruments.

This approach is taken because there is no guarantee that the mathematical model which is used to represent a certain feature of an instrument is the correct one, and a refinement of the numerical model towards an analytical accuracy is not goal-oriented to obtain a more physically accurate formulation.

Throughout the course of this thesis, extensive research of the acoustical properties, with a strong focus on the radiated sound of the presented instruments, as well as a comparison of numerical methods for solving the governing equations of the acoustical vibrations of these instruments, took place. And the steady comparison of the synthesis results of the physical models with the measured instruments lead to the following rules of thumb:

The most benefit towards realistic acoustical behaviour in a physical model can be reached if we do not strive for the most accurate numerical formulation compared to an analytical solution, but if we try to implement all measurable physical properties into the model as accurate as possible.

This fact gets immediately evident if we bear in mind that we are describing physical, not mathematical systems, even though mathematical tools are used approach the problems in

the first place.

Due to this numerical methods are applied that approximate the analytical equations only to a certain order of mathematical accuracy. In most cases, a higher order of analytical accuracy was not needed or even beneficial for the resulting sound, as shown in chapter 4 – an illustrative example of this is the model of a string. In this case it is quite simple to formulate a finite difference model which yields analytical results, but as shown later, methods with a lower analytical accuracy show better results when compared to the measured motion as well as sound of a real string. This does not mean that accurate mathematical modeling for musical instruments is not a crucial part of physical modeling, it means that after a certain degree of analytical accuracy is reached, the most gain in sound quality and vibrational accuracy is achieved by optimising the physical model and *not* the numerical method.

1.3 Methodology of this thesis

The methodology applied in this thesis is mainly aimed at synthesising accurate physical models of musical instruments in real-time. As a point of departure for all models, the differential equations describing the acoustic wave properties of the instrument are discretised using finite differences and coupled to form a basic model (a prototype) of the instrument. In the next step, the synthesised sounds and motions are compared to simple audio recordings of the instruments, and the models are adjusted towards a more exact representation of this sound. In the next step, more accurate measurements, using different methods are taken to compare the structural features of the modelled instruments with structural features of the real instruments. At least from this step onwards, the initial formulation of the physical model is extended to incorporate measured properties with higher accuracy. After the reformulation is implemented in the model, the synthesis results are compared again with the measurements and the recorded sound of the instrument. This *modelling-measuring-cycle* is repeated until the model of the instrument is optimised towards aural accuracy (having the right timbre) and vibrational accuracy (showing the right (modal) patterns at the measured frequencies). By fitting the numerical model of the instrument to the real instrument, much insight into the vibrational properties of the instrument is gained, and many of the mechanisms, leading to the specific timbre of an instrument, can be understood in greater detail. In all example cases, this approach helped formulating accurate numerical representations of the acoustic instruments.

This thesis commences with with a motivation and an overview on modeling and synthesis techniques, commonly applied in (instrument) acoustics, followed by an introduction and overview on the utilised methodology.

Chapter 2 starts with basic considerations regarding the instruments treated in this thesis.

1 Introduction

Alongside the historic developments of structural parts, physical measurements taken on each instrument are presented along with an introduction to important historic stages in the organological development of the respective instruments.

Chapter 3 is concerned with the mathematical and numerical methods applied in this thesis, giving an overview on the applied algorithms.

In chapter 4, the physical models, implemented in MATLAB and C are presented with a focus on the formulation of the models for the basic geometric parts of the instruments.

Chapter 5 Following that, an overview of the utilised hardware, an introduction to FPGA technology and the hardware description language (VHDL) used in this work is given in chapter 5.

Chapter 6 the implementation on the FPGA hardware and the specific structure of all final real-time models is presented.

Chapter 7 closes this treatise with an overview on the results and findings of this thesis, a conclusion and an outlook on possible future routes of research using the presented methodology and the implementation.

CHAPTER 2

HISTORY, ORGANOLOGY AND ACOUSTICS

Ut tensio, sic vis.
(As the extension, so the force)

(Hooke, 1678)

In this chapter, an introduction to the historic evolution influencing organological properties of the instruments is presented. Acoustic properties of important singular instrument parts, supported by measurements taken over the course of this thesis, are presented. A tentative consideration of factors influencing the specific timbre and temporal vibration characteristics of the respective instruments is given at the end of each section.

2.1 Preliminary Remarks

Alongside an overall knowledge of the instruments geometry as well as the basic physical parameters, as for instance material properties or boundary conditions, there are many subtle factors influencing the vibrational behaviour of musical instruments that must be taken into consideration in the formulation of a physical model.

Ideally, a physical model would include all parameters and features that are representable in a mathematical and/or computational way, if one strives for the most accurate simulation results possible. This implies that verbal attributes like *openness* or *attack* of an instrument can only be included into a physical formulation of an instrument if there are equivalent physical parameters that are measurable physically and formulated in a mathematical way. This requires an in-depth knowledge and understanding of underlying physical functional-

ties of singular instrument parts and, of equal importance, a comprehension of the interaction between those singular physical structures.

Besides material dependent constants of singular instrument constituents the underlying equations, describing the fundamental acoustic wave propagation in the respective parts are presented. All conjoining components of the instruments are taken into consideration again only if an important structural difference adds a substantial portion to the resulting acoustical vibrations.

The measurements presented here are not aimed at providing a physical description for the complete instrument class, because only one or two instruments of each family were measured. Hence, some acoustical properties may be specific to the particular instrument and not a global property of the whole instrument class. The physical models, presented in chapter 4 are based on the instruments measured in this section, and the synthesis results are compared to the measurements. Hence, all of the following measurement results are used as a *ground-truth* for the models.

In addition to the measurable, vibro-acoustic parameters, an additional contribution influencing the acoustic properties of music instruments are organologic changes in the historic development, and the effect those changes had on the timbre respectively. In accordance with the methodology proposed in the introduction it means that for a classification of a musical instruments, it is helpful to have an overview of its evolutionary steps and an insight into mechanical changes as well as the influence those changes have (had) on the timbre of the instrument sound.

In some cases, structural advancements of geometrical features were driven by practical reasons—like the *C-bouts* of the violin leading to a better playability of the outer strings, or the membrane fixation of the banjo, leading to a higher tension of the membrane and thus a higher radiated volume of the instrument—but all of these changes influenced the timbre of the instrument as well. This organologic-historic-acoustic research is one of the central aspects that can be realised with the method presented in this thesis, as shown in chapter 4.

2.2 Applied Measurement Tools

The tools and methodology used in all acoustical measurements are presented in the following section. All measurements were conducted at the Institute for Systematic Musicology at the University of Hamburg.

2.2.1 Microphone Array

For detailed imaging of radiation patterns of acoustical vibrations from surfaces of musical instruments a microphone array consisting of 128 microphones is used. The microphone

array recordings are applied as a ground truth for a comparison of radiation patterns¹ of real music instruments to the synthesised counterparts and their numerically simulated radiation patterns.

The underlying principle and the mathematical method is published in by Bader². The rationale behind this method makes use of the assumption that sound waves, radiated from an instruments surface, can be expressed as a superposition of a finite number of monopole radiators with frequency dependent radiation strength and radiation angles. Using a microphone array, sound pressure in the acoustic near-field of a sound radiating surface can be measured at discrete points. It is assumed that for each frequency every monopole has a distinct radiation characteristic, expressed as a specific radiation strength and radiation angle. Hence, a system of linear equations can be formulated and solved for every hypothetical point source on a measured surface. After propagating the measured sound pressure from the recording position back to the surface of the instrument, the method is reconstructs the distribution of the sound pressure level on the instruments surface.

For all lute instrument measurements, the array is arranged in a rectangular 11 · 11 grid with a spacing of 3.9 cm between two adjacent microphones. The microphones used in this project are self-assembled measurement microphones with an electret-capsule. All microphones are battery powered, leading to a galvanic separation of the microphones and the microphone preamplifier resulting in a better signal to noise ratio of the recorded time series. 16 *RME Mixtasy* professional studio microphone pre-amplifiers and AD/DA converters, running at a sample rate of 48,000 Hz, are used to amplify the microphone signal and for analog to digital conversion of the signal. The resulting time series are evaluated in a *Mathematica*-script, implementing the minimum energy method as described. All measurements were performed in an anechoic chamber at the Institute of Systematic Musicology, Hamburg.

2.2.2 High-Speed Camera

A high-speed camera is used to qualitatively record visibly moving parts of the instrument, as well as to track specific motions of the respective parts, like that of a string, a membrane, a finger-pick string interaction or the motion of a banjo bridge. For all measurements, a *Vision Research Phantom V711* high-speed camera is applied. Recording and qualitative evaluation of the high-speed movies is realised using the *Vision Research Phantom Camera Control* software version 1.6 and 2.7. To facilitate further analysis applying external tools, all recorded measurements are exported to an AVI-format, using the software-internal coder.

For a quantitative evaluation of the recordings, the *Innovision Systems* software *MaxTraq2D*

¹Operating deflection shapes or mode shapes of the respective instruments and geometries.

²Rolf Bader: "Reconstruction of radiating sound fields using minimum energy method", in: *The Journal of the Acoustical Society of America* 127.1 (2010): 300–308.

is used for motion tracking.

The tracked trajectories are exported to an ASCII-format file, and analysed with *MATLAB*, using the Wavelet-Toolbox for de-noising and bias-removal, and the Fourier-Transform for spectral analysis of the recorded time-series. The wavelet de-noising is realised with Daubechies-Wavelets of order 8,12, because this wavelet class is known for good de-noising characteristics.³

2.2.3 Impulse Hammer - Piezo Recordings

For researching material properties of the presented instruments, like the speed of sound in an instruments front plate for instance, an impulse hammer and piezoelectric transducer are used.

The impulse hammer, used for all measurements, is a *Kistler Impulshammer* 9722A2000, the transducer is a *Kistler* micro-piezo 352c23. The preamp is a *Kistler* 4-channel piezoelectric amplifier. All measurements are recorded using a *PicoTech Picosope 5203* digital oscilloscope and evaluated in a *Mathematica*-notebook and a *MATLAB* script using the Wavelet-Toolbox, for de-noising and bias removal, and *MATLAB*'s internal $\text{fft}^4()$ -function for spectral analysis.

2.2.4 Dummy Head Recordings

To measure the radiated sound of the instruments, dummy head recordings are taken with a *HEAD Acoustics* dummy head, consisting of two measurement microphones and an ICP preamp for the left and right channel. The instruments are recorded in an anechoic chamber with the dummy head positioned approximately one meter in front of the primary sound radiating component. The audio signals are recorded with the *HEAD Acoustics* front-end audio recording software. All recordings are evaluated using spectral analysis methods in *MATLAB*, as described before.

³Stephan Mallat: *A Wavelet Tour of Signal Processing The Sparse Way*, Elsevier, 2009, 535 ff.

⁴Fast Fourier Transform.

2.3 American 5-String Banjo

In this section, an overview on the historic, organologic evolution as well as acoustic properties of the American 5-string banjo modelled in this work is given. Besides basic physical properties of its structural parts, measurements, taken over the course of this thesis, are presented. The banjo, used for all measurements, is a *Capek* student model banjo with a *Remo* weather king head and strung with *D'Addario Light Gauge Phosphor Bronze* strings. After an overview on the historic development, an introduction to the known physical properties is given, measurements taken over the course of this work are presented thereafter.

2.3.1 Historic Overview

The following overview is divided into three sub-sections each covering a part in the history of the banjo. The first part, concerned with the pre-American and early American history is considerably more detailed than the other two because this part of the banjos history is the most vivid regarding the evolution of its idiosyncratic acoustical features.

Pre-Civil War History

The banjos history preceding the North American civil war (1861-1865), is closely linked to the Transatlantic slave trade from the 16th century to the beginning of the 19th century.⁵ This is one of the reasons a linear history before this time is hard to draw, because of incomplete historic sources due to excusatory ideologies and concealment of facts of historians of that particular time period.

*Two major forces affecting the literature of the banjo since the eighteenth century were the controversy over slavery and evangelical religion.*⁶

The whole effect of this circumstance, and the arising problems will not be discussed here because the subject area is so complex that it is far beyond the scope of this work. But due to this, there are few definite facts that support a clear scientific classification of the early evolution of the banjo and its structural parts. A well documented history began not until the second half of the 19th century, the point of time where the banjo reached the consciousness of a larger white class of population.⁷

But even since that time, far into the 20th century, there were still many myths surrounding the history and evolution of the 5-string banjo. One of the legends was that the 5-string banjo was a strictly North American instrument, which was invented in the 1820's by the white minstrel musician Joel Walker Sweeney. The other and

⁵Dena J. Epstein: "The Folk Banjo: A Documentary History", in: *Ethnomusicology* 3 (1975), ed. by Ann Arbor.

⁶Ibid., p. 347.

⁷Karen Linn: *That Half-Barbaric Twang*, 5th ed., Urbana and Chicago: University of Illinois Press, 1994, p. 1.

2 History, organology and acoustics

...most common and most confusing legend about the banjo: that it was unknown to the plantation Negro.⁸

These two myths could be proven wrong by the work of Dena Epstein.⁹ In her treatise, Epstein shows that the modern 5-string banjo was a substitution of a known instrument with deep roots in African-American slave culture. Epstein calls this instrument the *Folk Banjo* or *Calabash Banjo* in differentiation to the *modern* 5-string banjo. Through a cumulative research of historical documents from the 17th through the 19th century Epstein brings to light that the *folk banjo* was an essential part of North American *slave culture*. Epstein researches literature sources on descriptions of instruments that resemble the banjo, and focuses on three recurring features like a:

- skin covered body,
- guitar resemblance or a
- body made of gourd.

The earliest records of an instrument with comparable features on the American continent is from Martinique in 1678, where it is called a *banza*:

(...) *au son d'un tambour et d'un instrument qu'ils nomment banza*.¹⁰

Following this mentioning, Epstein presents over 30 autonomous sightings from the late 17th century to the middle of the 19th century, linking the *folk banjo* directly to an African-American culture of that particular time span.

From the same period of time, Epstein presents a series of paintings in which the banjo is shown in an African-American cultural surrounding, e.g. the colour painting *The Plantation*¹¹ from the late 18th century, where a string instrument resembling a gourd banjo is depicted at a gathering of African-Americans. Dena Epstein puts her main focus on sightings and reports on the American continent but comes to the conclusion that the roots of this folk instrument can only be found in the *Old World*, namely in Africa.

Even though the exact heritage of the banjo can not be cleared completely, as it is lost in the mist of clouded historic transmission, it is indisputable that the banjo has its roots in African-American culture.¹² But according to Dena Epstein it is fruitless to search for a direct African ancestor of the banjo:

⁸Linn, *Barbaric Twang*, p. 2.

⁹Epstein, "The Folk Banjo: A Documentary History".

¹⁰This earliest recorded account is taken from Adrien Dessalles and Pierre Regis Dessalles: *Histoire general des Antilles*, 3rd ed., Not in copyright, 1847, p. 297.

¹¹See Plate 1-2 in Philip F. Gura and James F. Bollman: *America's instrument. The banjo in the Nineteenth Century*, Chapel Hill and London: The University of North Carolina Press, 1999.

¹²See for instance other important works regarding the history of the banjo following Epstein: Maximilian Hendl: "Banjo. Altweltliche Wurzeln eines neuweltlichen Musikinstrumentes. Verschüttete Spuren zur Vor- und Frühgeschichte der Saiteninstrumente", in: *Afro-Amerikanische Schriften*, ed. by Alfons Michael

2 History, organology and acoustics

(...) any attempt in associating it with an African prototype would be at best tentative(...) ¹³

because of the diverse and fragmentary documented musical culture of Africa.

Besides the culture historic approach of Dena Epstein and other researchers like Linn ¹⁴ or Conway, ¹⁵ Maximilian Hendler ¹⁶ takes an organologic approach and researches music instruments from the *Old World* (meaning Africa and Europe) for similarities with the modern banjo. He focusses his research on three constituent parts of the banjo:

- The body and resonator with membrane cover.
- The neck.
- The strings and the adjustment of the strings.

According to Hendler, the body of the banjo has distinctive features commonly found in ancient lute instruments, due to the fact that the oldest, historically documented lute instruments had membrane covered resonators. A wall painting from ancient Egypt shows a lute instrument from the 14th century B.C. ¹⁷ Similar lutes can be found in Mesopotamian paintings from approximately 3000 B.C. ¹⁸ The geographic distribution of such instruments range from Asia, the Arabic peninsula far into Africa. But because of the intensive contact between the African continent and America, the most probable heritage for the skin covered resonator of the banjo is Africa.

The biggest gap in the history of the banjo, according to Hendler, is the transition from the round-neck, a feature that characterizes all African lutes, ¹⁹ to the flat neck that presumably arose out of an European or Asian tradition. Furthermore, Hendler notes that

...it is not very likely that the round neck never reached America. ²⁰

A notable fact is that there are no historic records of a round neck lute on the American continent. But as Hendler states,

...a systematic research of round-neck lutes in North or Central America has never been done yet, so one can only guess about the existence of such a instrument. ²¹

Dauer, vol. 1, Goettingen: Edition RE, 1995; Gura and Bollman, *America's instrument. The banjo in the Nineteenth Century*, pp. 11-75; Linn, *Barbaric Twang*; Bob Carlin: *The Birth of the Banjo. Joel Walker Sweeney an Early Minstrelsy*, Wiesbaden: McFarland & Company, Inc., Publishers, 2007, pp. 3-5.

¹³ Epstein, "The Folk Banjo: A Documentary History".

¹⁴ Linn, *Barbaric Twang*.

¹⁵ Cecelia Conway: *African Banjo Echoes in Appalachia*, Knoxville: The University of Tennessee Press, 1995.

¹⁶ Hendler, "Banjo".

¹⁷ Ulrich Wegner: *Afrikanische Saiteninstrumente*, Berlin: Staatlich Museen Preußischer Kulturbesitz, 1984, p. 94.

¹⁸ Hendler, "Banjo".

¹⁹ Wegner, *Afr. Saiteninstrumente*, 114 ff.

²⁰ Hendler, "Banjo".

²¹ Ibid.

2 History, organology and acoustics

The transition from the round-neck to a flat neck lute is an enormous progression in instrument design. A flat neck has a different fixture at the body of the instrument, and therefrom resulting, a modified contact area of the neck and the membrane. In the classical form of the *Binnenspießlaute*,²² the neck is in direct contact with the membrane. A flat neck attached at the resonator, is on the same level as the membrane, but it has no direct contact with it.

Although this is a mechanical progression, an augmentation in technical effort, it highly simplifies the playing technique, because the right and left hand coordination is not that complex and subtle as with round necked instruments.²³

This can be explained by practical reasons. Hendler suggests that enslaved Afro-Americans had not enough time to learn and master an artistic instrument like the West African *konting* or the Sudanese *ngoni*, which take year long practice to master. The African American slaves were in need to

(...)play folksongs and dances(...)without the training of a professional musician and for that a flat neck is better suited.²⁴

Hendler's research of African string instruments shows that a flat neck is a totally atypical feature for African lutes, so he concludes that the flat neck must be a mutation of prototype lutes arising out of an European tradition.²⁵

Finally, Hendler focuses on the strings and the fixation of the strings. He traces the history of string from their earliest known manifestation, the music bow, probably the oldest form of a musical instrument²⁶ to highly evolved lutes of Arabic and North African origin, with all their characteristic structural finesse.

Hendler states that most of these changes arose from practical requirements. The need for polyphony, for instance, extended the one stringed musical bow to multiple strings²⁷. A desired increase of loudness of the instrument led to resonators in form of natural products, like wood or calabash, as typically used for African lyres or lutes. But Hendler's main focus lies on the fixation of the strings, and he develops a strong case that Sudanese lutes directly inherited this feature from the oldest forms of lutes from Mesopotamia and Egypt because they lack the evolutionary organologic step from the *Spannbund* to a *Pflockwirbel*. This is an

²²Curt Sachs: *Real-Lexikon der Musikinstrumente, zugleich ein Polyglossar für das gesamte instrumentengebiet*, (Reprint d. Ausg. Berlin 1913), Stuttgart: Olms, 1972.

²³Hendler, "Banjo".

²⁴Ibid., p. 18.

²⁵A comparable instance that emerged from European and African interchange is the South African *ramkie*, a string instrument with a membrane covered calabash, first mentioned in the early 18th century. The name supposedly descends from the Portuguese *rabequinha*. The instrument itself is presumably an imitation of an Iberian lute that originated from the contact of European slave traders and South African slaves in Malabar, who brought it back to South Africa. See: Percival Robson Kirby: *The Musical Instruments of the Native Races of South Africa*, second, Johannesburg: Witwatersrand University Press, 1965.

²⁶Paintings in the *Le Trois Freres*-cave, which are dated to 15000 B.C. show a music bow. See: Hendler, "Banjo", p. 37.

²⁷Hendler calls this a Pluriarc. See: *ibid.*, p. 44.

2 History, organology and acoustics

indication that this instrument (a round neck lute with a *Spannbund*) is

(...) *in complete accordance with their [the Sudanese] sound-aesthetics*

According to Hendler, an inevitable fact of the *Spannbund*, which arises out of instrument manufacturing requirements, is the tuning of the strings. Because of the particular fixation of the string, the tuning has to be in V-form (High-Low-High pitch). The resulting descant-drone string of *Spannbund*-instruments is a very prominent feature of the *modern* 5-string banjo. This is a strong indication of a Sudanese root of the banjo because

(...) *from the [European] flat lute- or guitar-neck there is no route to the discant-bordun string.*²⁸

Mainly Sudanese instruments are taken into account because, according to Hendler, it is this area from where the main contingent of black slaves were deported during the period of the Transatlantic slave trade [sic!]. But, the assumption of a connection from North America to Sudan is an inexplicable misconception of Hendler, because at no point of history there was slave trade between the area of Sudan and the Americas. Neither slave traders nor slaves transported to the Americas came from a Sudanese area.²⁹ Even though the Sudan has a long history in slavery and slave trade, there are no records of slaves from the Sudan that were deported to the Americas. It is unclear why Hendler is convinced of the important role of the Sudan in the slave trade and in the evolution of the banjo. The only thing that can be stated is that it is very likely that the Sudanese lute tradition, which in turn arose out of Islamic traditions³⁰ influenced a large area from East Africa to West Africa deep into Sub Saharan Africa.³¹ But nonetheless, the organologic findings of Hendler are also applicable to lutes from other African areas, strongly suggesting an African heritage of the banjo.

Over the last thirty years, manifold field research on finding an African prototype of the American banjo was conducted. Among various other instruments, the West African *gimbri*³² or the Senegalese/Gambian *akonting*³³ was proposed as an African banjo prototype. Organologic features connecting both lutes with the banjo are the drone string and the skin covered resonator.

²⁸Hendler, "Banjo".

²⁹Ira Berlin: *Generations of Captivity. A history of African-American Slaves*, Cambridge, Massachusetts and London, England: The Belknap Press of Harvard University Press, 2003; Jochen Meissner, Ulrich Muecke, and Klaus Weber: *Schwarzes Amerika. Eine Geschichte der Sklaverei*, Muenchen: Verlag C. H. Beck, 2008.

³⁰Lois Ann Anderson: "The Interrelation of African and Arab Musics: Some Preliminary Considerations", in: *Music and History in Africa*, ed. by Klaus P. Wachsmann, Evanston: Northwestern University Press, 1971.

³¹Gerhard Kubik: *Africa and the Blues*, Jackson: University Press of Mississippi, 1999, pp. 63-70.

³²A Mauretanian lute played by Griot musicians. Wegner, *Afr. Saiteninstrumente*, p. 136.

³³Prominently featured in the film *Throw Down Your Heart* starring banjoist Bela Fleck. See: Sascha Paladino: *Throw Down Your Heart*, Motion picture, 2009.

The Minstrel Banjo

A written and well documented history of the *modern* banjo in North America began with the emergence of minstrel theater shows, especially the rise of *blackface* minstrelsy in the early 19th century.³⁴ The *blackface* minstrel theatre arose from a long theatre tradition of portraying Africans and African-Americans. Its roots can be dated back to the Shakespearian theatre in Great Britain³⁵.

This early accounts of white actors portraying Africans had little in common with the later minstrel theatre which based its acts on crude caricatures of African slave life.³⁶ The southern black slave and the northern black dandy were two recurring subjects of the minstrel shows and the only two subjects in the early days of minstrelsy. The first known American *blackface* minstrel performer was Andrew Jackson who performed

(...) *the first black-dialect song known to have been published in the United States(...)*³⁷

around the year 1815.³⁸ A number of other performers, including Thomas D. Rice, John Smith, or Thomas Coleman, who were well known performers in the years from 1820-1840 adapted the black face act. But the most popular minstrel actor, and supposedly one of the first white person who played the banjo³⁹ was Joel W. Sweeney⁴⁰. The misconception that he also was the inventor of the banjo has been refuted by D. Epstein. Nonetheless, the influence of J.W. Sweeney on the *blackface* minstrel was enormous and cannot be understated.⁴¹ Most historians regard him as a prototype for the whole genre of minstrel banjo, because he made the act of the black banjo player popular throughout the English speaking world.⁴² The repertoire of J.W. Sweeney and other minstrel performers contained songs that rooted in the Southern states of North America but also included adaption of Irish folk and dance tunes like reels or jigs.⁴³

A key element of these shows was the music, and a central instrument was the banjo. Or in the words of Webb:⁴⁴

(...) *none of these travelling shows could be without a banjo player(...)*⁴⁵

³⁴Carlin, *Birth of the Banjo*.

³⁵Shakespeare's *Othello* or Thomas Southern's *Oronoko* are mentioned. See *ibid.*, p. 6.

³⁶*Ibid.*, pp. 7-9.

³⁷*Ibid.*, p. 7.

³⁸*Ibid.*, p. 7.

³⁹*Ibid.*, p. 6.

⁴⁰The long held belief that the German immigrant Gottlieb Graupner performed a banjo accompanied black-face act on new years eve of 1799 in Boston has been rebutted by H. Earl Johnson in his work *Musical Interludes in Boston, 1795-1830*. Columbia University Press. New York. 1943.

⁴¹Carlin, *Birth of the Banjo*.

⁴²*Ibid.*

⁴³*ibid.*; Linn, *Barbaric Twang*; Conway, *Banjo Echoes*

⁴⁴Robert L. Webb: "Ring the banjo!", in: *Canadian folk music bulletin* 2.4 (1979).

⁴⁵*Ibid.*

2 History, organology and acoustics

This led to the circumstance that banjo became the figurehead instrument for minstrelsy, and the banjos popularity in North America and the whole English speaking world rose with the rising popularity of minstrel shows.⁴⁶ In the early years of minstrel banjo there was little doubt among the audience that the banjo was an instrument of African origin.

*The idea of the banjo was so overwhelmingly Southern black (...)*⁴⁷

J. W. Sweeney always emphasized that he had learned the banjo playing from black slaves,⁴⁸ or in the words of Cecilia Conway:

*Southern folk sources were most important to the first generations of minstrel, who borrowed and introduced Negro dance, song, and especially banjo playing to the American stage.*⁴⁹

In this period, from 1830 to 1880, the banjo underwent several structural changes.⁵⁰ It evolved from a mostly home-made instrument with a fretless wooden neck, a wooden hoop covered by a animal skin attached by nails and played with gut strings,⁵¹ to a more standardized instrument with a (metal) tension hoop for the membrane and more sophisticated attachment of the, now fretted, neck.⁵² On one hand, these changes were forced by the performers, who needed instruments with a stable pitch,⁵³ on the other hand by instrument builders who wanted to distinguish their work from amateur instruments by more advanced designs.⁵⁴ This progression in banjo manufacturing laid the foundation for the commercial banjo and the banjo fad at the end of the 19th century.

Commercial Banjo

The history of the *commercial*⁵⁵ banjo is very well documented and begins with the appearance of the banjo in minstrel shows. After the civil war, the banjo found its way from the minstrel stages, which were mostly associated with a white working-class audience, to a more elevated clientèle of *Victorian America*⁵⁶. The progression from the minstrel banjo to the commercial banjo was strongly influenced by the (imposed)⁵⁷ changing image of the banjo:

*The upper class had accepted the banjo into their parlours and parties...*⁵⁸

⁴⁶Carlin, *Birth of the Banjo*.

⁴⁷Linn, *Barbaric Twang*, p. 8.

⁴⁸Carlin, *Birth of the Banjo*, p. 20.

⁴⁹Conway, *Banjo Echoes*.

⁵⁰Gura and Bollman, *America's instrument. The banjo in the Nineteenth Century*.

⁵¹Ibid., pp. 48-49.

⁵²Ibid., pp. 49-55.

⁵³Ibid., p. 50.

⁵⁴Ibid., pp. 48-59.

⁵⁵The term commercial is applied here because the also commonly used term *Classical Banjo* could be misleading regarding the music repertoire of the instrument. Linn, *Barbaric Twang*; Carlin, *Birth of the Banjo*.

⁵⁶See *ibid.*, pp. 149-151; Linn, *Barbaric Twang*, pp. 5-40.

⁵⁷Ibid., pp. 5-36.

⁵⁸Ibid., p. 36.

2 History, organology and acoustics

This change was strongly promoted by a group of banjo players and manufacturers⁵⁹ who tried to elevate the banjo to an American made instrument put in an European music context. Because of this, banjo makers introduced structural enhancements to the instrument, like the addition of the tone ring,⁶⁰ higher frets and improved tension hoops. Their foremost goal was to change the banjos image from the plain, crude instrument of southern slaves to a modern, more artistic instrument.⁶¹ Another consequence of this *elevation* was a change in the sound of the banjo. The minstrel banjos dark timbre and short sustain of the notes were replaced by a brighter sound with a longer sustain⁶². At the end of the 19th century and the beginning 20th century, the commercial banjo had its peak in popularity. A banjo orchestra or banjo teachers could be found in almost every bigger town of North America. These banjo orchestras were often the cornerstone for ragtime orchestras⁶³ and the jazz orchestras emerging some 20 years later.

⁵⁹Linn, *Barbaric Twang*, p. 6.

⁶⁰Gura and Bollman, *America's instrument. The banjo in the Nineteenth Century*, pp. 212-213.

⁶¹Linn, *Barbaric Twang*, pp. 15-16.

⁶²ibid., p. 15; Gura and Bollman, *America's instrument. The banjo in the Nineteenth Century*, pp. 212-213.

⁶³Linn, *Barbaric Twang*, pp. 81-82.

2.3.2 Banjo Strings

In this section, the physical properties of banjo strings are presented. A focus is put on *modern* metal strings, as used for the instruments researched in this thesis.

String Material

The material of the banjo string was subject to changes forced by advancement in technology and acoustical needs over the centuries. The first gourd or folk banjos were played with strings made of animal gut⁶⁴. With the rise of the minstrel banjo, a silk string or wire wound string became the standard⁶⁵. At the turn of the 20th century the standard string material changed to metal, mainly due to the need for an increased loudness⁶⁶.

Today, materials used for banjo strings include nickel, phosphor bronze or steel. The different metals and alloys influence the sound characteristic and rigidity of strings⁶⁷. The lowest string of a standard 5-string banjo is a wound string with a steel kernel and an intermediate layer of a material depending on the manufacturer and the sound preferences. The material properties of the strings, used for the measured banjo are given in table 2.1.

String tune	Material	Diameter [mm]	Tension [kg]
d	Plain steel	0.23	5.10
B	Plain steel	0.28	5.39
G	Plain steel	0.33	4.74
D	Bronze wound steel	0.51	4.39
g	Plain steel	0.23	4.98

Table 2.1: Material and tension of banjo string used in this work. Values are taken from the packaging of the D'Addario 5-string Banjo strings.

String Adjustment

The strings of the banjo are fastened at the end of the neck (at the head), and at the lower end of the resonator.⁶⁸ The strings run over a wooden bridge, which is not fastened on the membrane, and is held in place by the net force, acting in the normal direction of the membrane. This force depends on the angle between the string under tension in normal position

⁶⁴ *...four strings of silk or dried bird gut were raised on a bridge.* Conway, *Banjo Echoes*, p. 162.

⁶⁵ *ibid.*, p. 170: *...the use of violin gut strings and one silk string wound with silver wire for the banjo.*

⁶⁶ Linn, *Barbaric Twang*, p. 83: *...switched to metal strings, which are louder... than the gut or silk strings that were used before.*

⁶⁷ David M. Brewster: *Introduction to Guitar Tone and Effects: A Manual for Getting the Sounds*, Milwaukee: Hal Leonard, 2003, p. 10.

⁶⁸ The attachment of the strings differs from banjo model to banjo model. On a modern banjo the strings are fastened at the tail piece. This concept of fixation can be found in most banjos from the mid 19th century to the present day. Other techniques prior that time can only be speculated about. Gura and Bollman, *America's instrument. The banjo in the Nineteenth Century*, p. 82.

and the bridge-elevated string under tension.

At the head, the strings run through the nut to the tuning pegs, where the strings are coiled around the tuning pegs. A comparison of two measurements, one at the head of the instrument and one at the bridge, shows that transport of the energy between the string and the coupling point of the head is smaller than at the bridge, suggesting a high impedance at the upper fixation point of the string.⁶⁹

The energy transport from the string to the membrane is comparably larger, because of the low impedance of the membrane, compared to a wooden top-plate and the flexible (not fixed) bridge.

In physical models of string instruments, Dirichlet boundary conditions are often proposed for the strings, but in real instruments the boundary conditions of strings can be considerably more complex⁷⁰. In this regard, the banjo is a special case because the non-rigid bridge has a low impedance and performs rocking motions⁷¹ on the flexible membrane. This is due to the excitation of the transversal motion of the string as well as the motion of the vibrating membrane.⁷²

In addition to this, the position of the string at the bridge influences the strength of coupling from the string to the membrane as shown in the measurements in section 2.3.3.

String Motion Measurements

The motion of a linear string can be described by the d'Alembert solution of the one dimensional wave equation as two functions travelling in opposite directions on the string.

In an ideal, linear string without damping or dispersion, using a triangular deflection as initial condition, we expect two symmetric functions travelling up and down the string as depicted in Figure 4.2. A high-speed recording depicting a banjo string can be found in appendix 3. As one can see, at time-step $t = 0$ the string is deflected in a triangular shape. When the string is released, one *function* moves towards the nut, the other *function* moves in the direction of the bridge. Because a real string is subject to several kinds of losses, the shape of the initial *function* on the string rapidly changes.

A second high-speed camera measurement, recording the deflection of the *g*-string of the banjo above the 13th fret. The motion of the point is tracked using the set-up described before. In Figure 2.1 the time series of the deflection of the string over the first 4 seconds are shown. Shorter time intervals of the deflection can be found in Figure 2.2a to 2.2c.

⁶⁹See the measurements in section 2.3.2.

⁷⁰A description for a moving end support can be found in: Fletcher and Rossing, *Physics of Instruments*, p. 52.

⁷¹A recorded image series is presented in appendix 2.

⁷²The boundary conditions at the bridge can change from one banjo to the other due to different tension of the membrane which leads to a different rigidity at feet of the bridge.

2 History, organology and acoustics

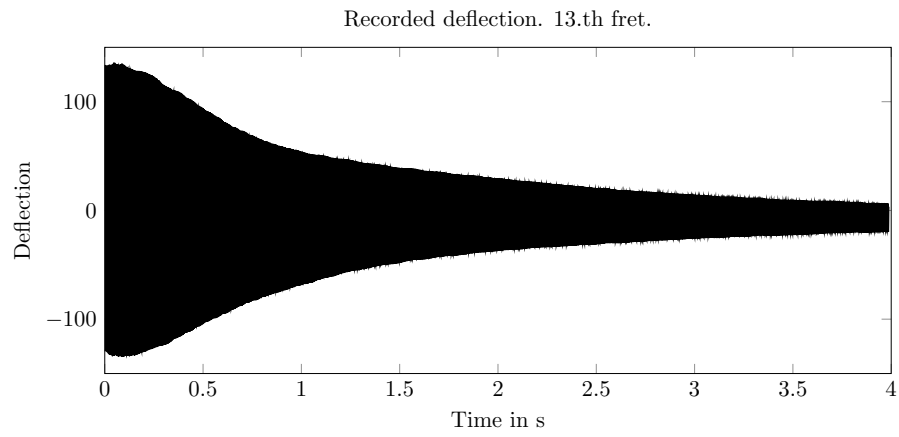
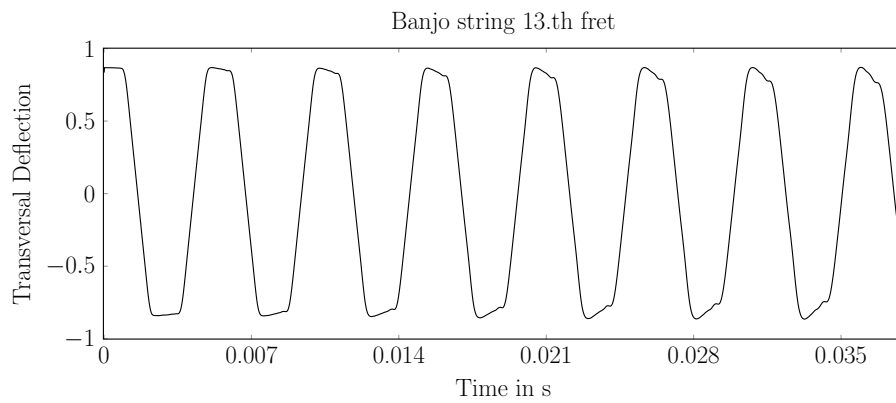
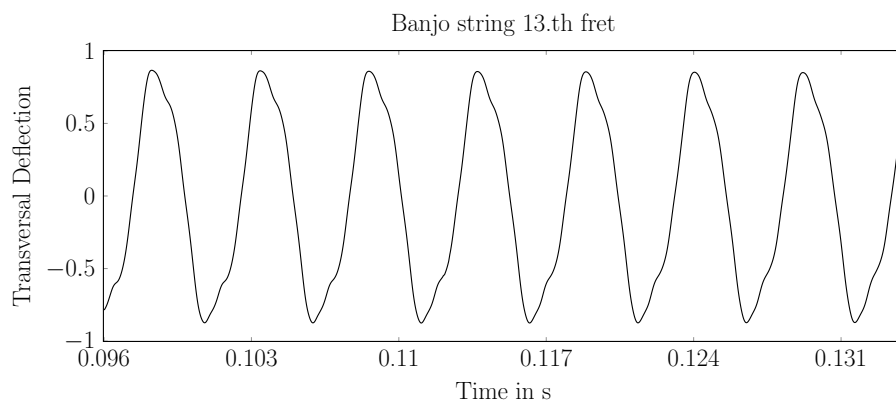


Figure 2.1: Transversal deflection of a plucked banjo string. Time in seconds on the abscissa and tracked pixel range on the ordinate.

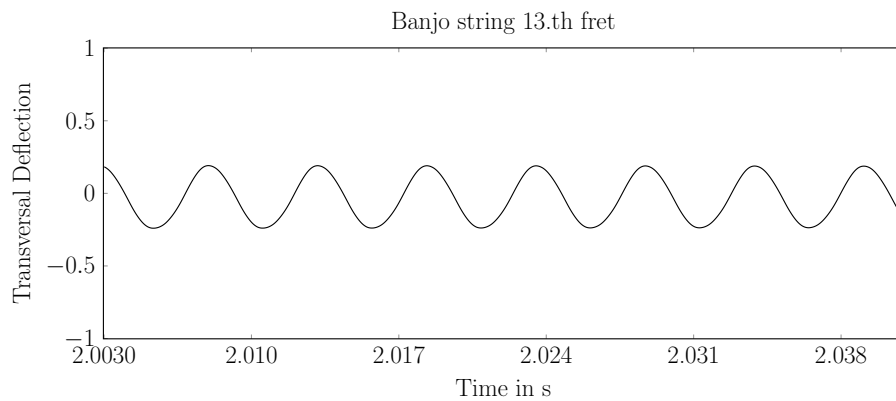
2 History, organology and acoustics



(a) Partial time series I.



(b) Partial time series II.



(c) Partial time series III.

Figure 2.2: Normalised transversal deflection of a plucked banjo string with time in seconds on the abscissa. (a)

As is visible in Figure 2.2a, the *function*, travelling up and down the string, loses its shape after the first reflection at the respective boundaries. Dispersion and dissipation effects of the string, due to material dependant non-linearities and bending stiffness, add to a increases

2 History, organology and acoustics

the decay of higher partials of the string and thus adds to immediate rounding of the initially sharp corners.⁷³ The triangular deflection of the string, with two *pulses* travelling in opposite directions, changes its shape to a quasi sinusoidal motion as visible in Figure 2.2c.

⁷³ Anders Askenfelt and Erik V. Jansson: "From touch to string vibrations. III: String motion and spectra", in: *The Journal of the Acoustical Society of America* 93.4 (1993): 2181–2196.

2.3.3 Banjo Bridge

The connecting part between banjo strings and membrane is bridge made of wood. Unlike string attachment in guitars, banjo strings are not fixed at the banjo, instead they run through carved shafts on the top-side of the bridge. The bridge is put loosely on the membrane held in place by the net force of the strings, acting in the normal direction of the membrane. This form of energy transfer from the string to the resonator can be found in many plucked lute instruments from Africa⁷⁴ as well as Asia⁷⁵.

Compared to string fixation in guitars, where the string is taut behind the immobile bridge, a non-fixed bridge incorporates several specific traits. The bridge can be moved on the surface of the membrane, thereby changing the coupling points between it and the membrane which influences the spectrum and thus the timbre of the instrument. In addition to that, it's flexibility leads to different *eigenmodes* compared to a glued on bridge because it has a less rigid foundation. This in turn, influences the transmission characteristics of the bridge and the motion at the string boundaries.

Besides the position, the mass of the bridge is important because it influences the transfer characteristic as well.⁷⁶

The influence of the banjo bridge on the timbre of the banjo sound is subject to manifold discussion among researchers, banjo builders and musicians.⁷⁷ Two aspects recognized as profoundly important by most are the geometry and the mass of the bridge. Both parameters influence the quality of the transmitted sound to the membrane⁷⁸ and audible effects on the produced sound. Bluegrass banjo players prefer thinner, lighter bridges, as they have a more *direct*, *twangy* sound characteristic.⁷⁹ A difference of banjo bridges compared to other instrument bridges is the existence of a third foot in the middle of the bridge, a structural feature that is not present in violin bridges or the bridge of the Chinese *ruan*. The middle foot of the banjo has a rounded contact area and is slightly longer than the outer feet. This enhances the rocking motion of the bridge, pivoting around the centre point of the bridge. The special geometry of the bridge feet have an additional effect on its transmission characteristics as shown in the measurement section below.

The bridge that is used in this thesis is a *Grover* 5-string maple bridge with an ebony top. The

⁷⁴Wegner, *Afr. Saiteninstrumente*, pp. 114-158.

⁷⁵See section 2.5.1.

⁷⁶Instruments like the *akonting* have a comparably larger bridge with a different geometry. This is one of the reasons for the different timbre of the instrument. As already mentioned, the folk-banjo presumably had a larger bridge and thus a *darker* timbre when compared to a modern banjo. See for instance the video at: <http://minstrelbanjo.ning.com/video/calabash-dance-cotton-pod-walkaround-test-4-stringer2>.

⁷⁷An extensive resource regarding the mechanics of the bridge is for instance <http://www.banjobridge.com/>.

⁷⁸The shape and quality of bridges can vary depending on its attributed characteristics. Some examples are: *more open*, *greater attack* or *melodious* to name just a few.

⁷⁹See <http://www.banjoteacher.com/Gear/banjobridges/index.html> for several examples.

physical dimensions are given in Figure 2.3.

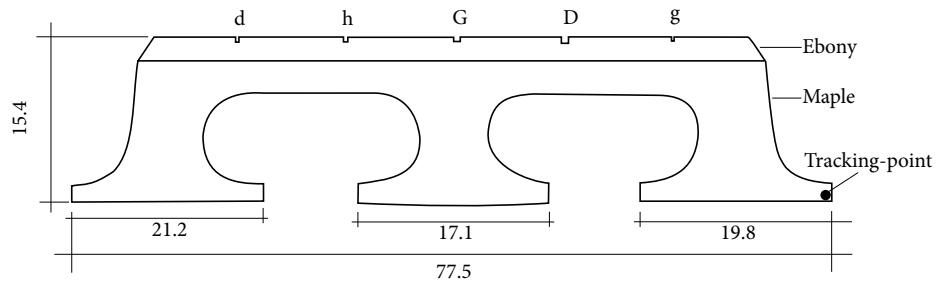


Figure 2.3: Physical dimensions of the banjo bridge in [mm]. The black dot indicates the measured point.

Measurements

The following high-speed camera recording of the banjo bridge was recorded under realistic playing conditions of a banjo. The motion of a point at the left corner of a banjo bridge when the lowest string is plucked was recorded. Figure 2 shows the rocking motion of the bridge due to excitation by a string. The time series of a this point is shown in Figure 2.4.

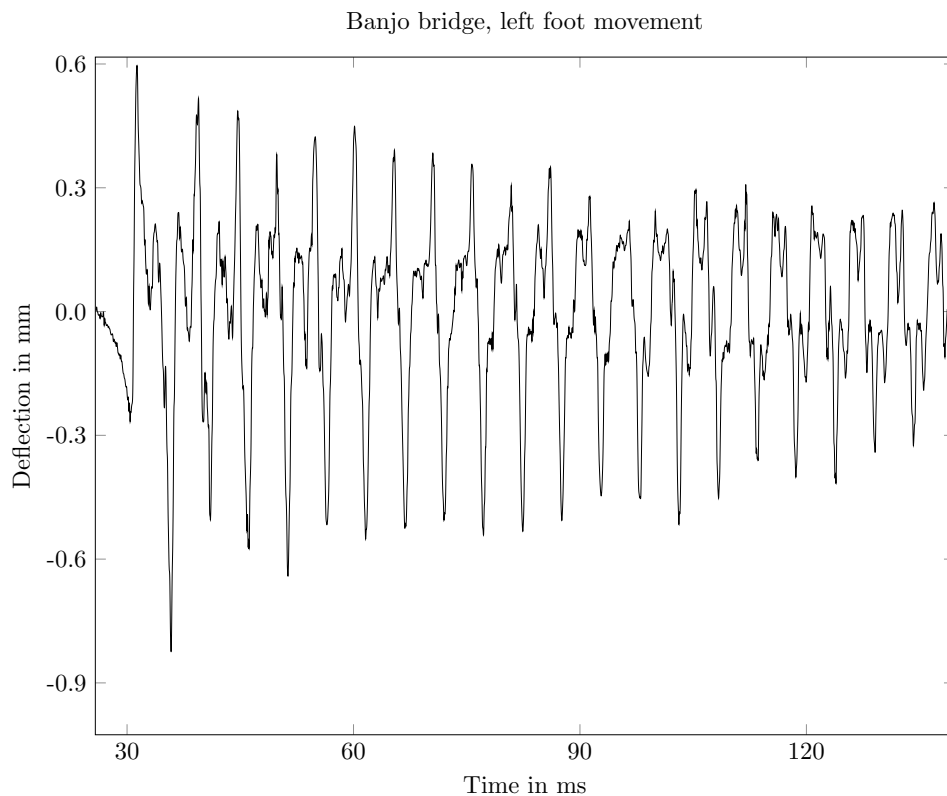


Figure 2.4: Deflection of a banjo bridge normal to the membrane tracked at the left foot.

The spectrum of the recorded time series, given in Figure 2.5, shows that the fundamental frequency of the string as well as several *harmonics* are visible. In addition to this, two modes of the membrane are visible, as indicated by the black triangles.⁸⁰

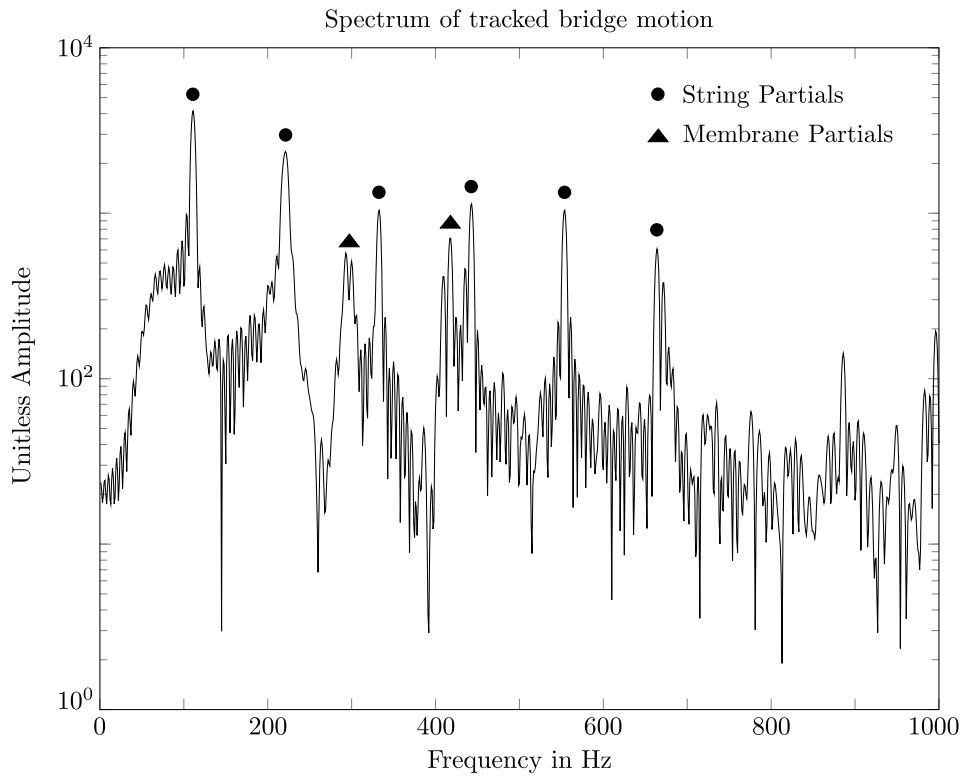


Figure 2.5: Spectrum of the bridge foot motion.

This is a strong indication that the bridge vibrates in frequencies of the string and the membrane, coupling the former to the latter and vice versa.

Figure 2.6 depicts the response to an impulse-hammer knock on the left and right top sides of the bridge, recorded with a piezoelectric transducer attached under the right foot on the back-side of the membrane, and the banjo completely assembled. As one can see, the first impulse of the left sided knock yields a much stronger response than the knock on the right side of the bridge.⁸¹ This effect is non intuitive at first, but when regarding the geometry of the middle foot as well as its contact area with the membrane, it is obvious that the foot does not pivot around its centre but around the edge on the opposite side of the excitation.

⁸⁰ Compare the frequencies (290, 434) of the membrane in Figure 2.7.c.

⁸¹ The values on the y-axis can be compared because the impulse hammer has a similar amplitude.

2 History, organology and acoustics

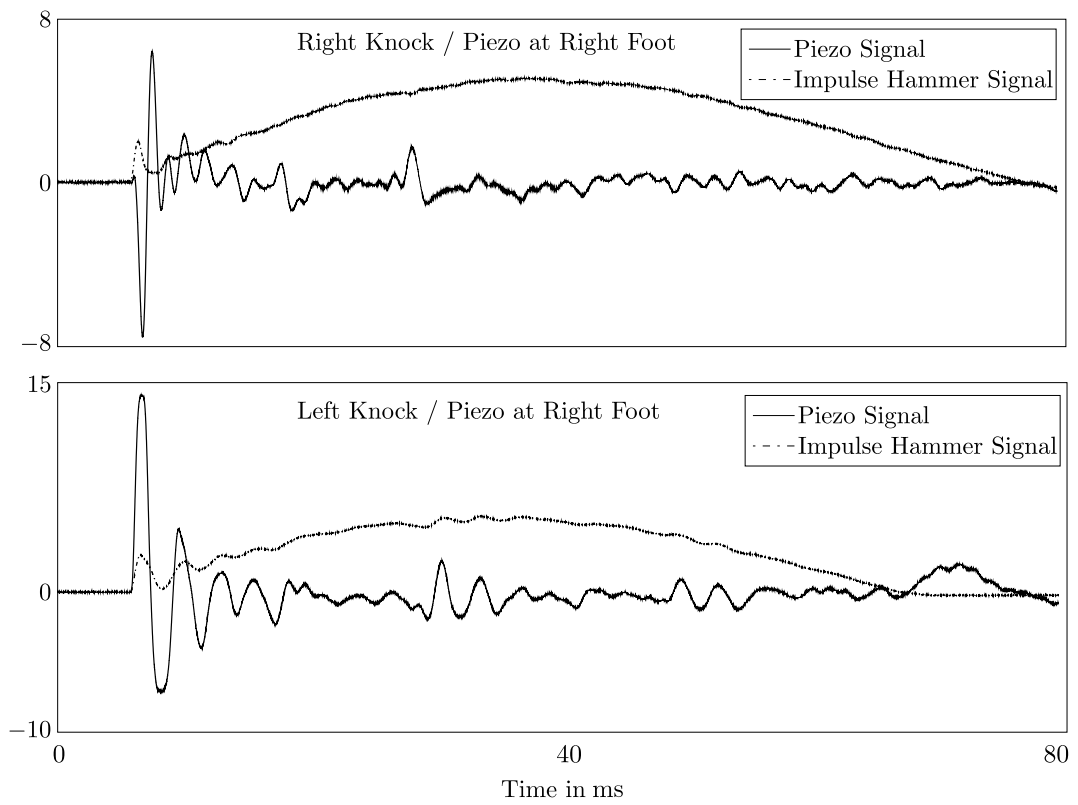


Figure 2.6: Acceleration at right bridge foot.

2.3.4 Banjo Membrane

The membrane of the banjos is of central importance for its characteristic sound. It is responsible for the amplification of the acoustical vibrations produced by the string.⁸² Due to the low impedance of a banjos membrane, compared to a wooden front plate, the sound energy, transferred from the string, is radiated with a higher amplitude in the initial transient phase of the sound, but has a shorter sustain⁸³ when compared to string instruments with a wooden front plate.

Material Properties

Analogous to the string, the properties of the membrane have undergone several changes in the evolution of the banjo. In early accounts of banjos it is mentioned that the instrument is covered by an animal skin like cat skin,⁸⁴ the skin of a ground hog⁸⁵ or sheep skin.⁸⁶ Cow skin and sheep skin were the standard material for the minstrel banjo.⁸⁷ It is widely accepted knowledge among banjo players and makers that the brightness of the sound as well as the loudness of a banjo correlates directly with the tension of the membrane. Hence, a driving force behind structural advancement of the banjo was the refinement of the membranes adjustment.⁸⁸

In the old days, banjo players generally believed that the tighter you could get the head of the banjo, the better it would sound. This was actually fairly true in the old days of goat- or calf-skin head⁸⁹⁹⁰

The sound quality improvement is characterised with a brightening of the sound resulting from higher tension as well as the reduction of non-linear large deflection effect.⁹¹ Today, the most common material for a banjo head is Mylar⁹². This material has a tensile strength

⁸²Laurie A. Stephey and Thomas R. Moore: "Experimental investigation of an American five-string banjo", in: *The Journal of the Acoustical Society of America* 124.5 (2008): 3276–3283.

⁸³Newer banjos have membranes made of Mylar. Compared to older instruments with animal skins as membranes, they can withstand a much higher tension. Hence, newer banjos are louder and have a longer sustain compared to older banjos.

⁸⁴Epstein, "The Folk Banjo: A Documentary History".

⁸⁵Conway, *Banjo Echoes*, p. 178.

⁸⁶Ibid., p. 165.

⁸⁷Gura and Bollman, *America's instrument. The banjo in the Nineteenth Century*, pp. 51, 61.

⁸⁸Ibid., p. 61.

⁸⁹Bill Palmer: *A Scientific Method for Determining the Correct Head Tension For Your Banjo*, [Online; last accessed 20-January-2014], 2006, URL: <http://www.banjowizard.com/hedtens.htm>.

⁹⁰This also holds for guitar and violin gut strings, according to instrument builders and musicians in historical performance practice, the best sound is achieved when string is under maximal tension, near its maximal tensile strength (Instrument builder M. Wichmann, personal communication).

⁹¹The more flexible a string is, the more audible a pitch-glide is. The same holds for membranes.

⁹²A brand name by Du Pont for a thermoplastic film made of ethylene glycol and dimethyl terephthalate. (*Introduction to Mylar Polyester Films*, DuPont Teijin Films, 2003)

2 History, organology and acoustics

of $20 - 24 \frac{kg}{mm^2}$ ⁹³. This is half of the tensile strength of mild steel.⁹⁴

The banjo, used for the measurements consists of a *Remo Weatherking* drum head. It is made of a single ply of Mylar with a thin layer of coating.⁹⁵

Material	Coated Mylar
Radius	15 cm
Mylar film thickness	0.36 mm

Table 2.2: Geometry parameters of banjo head membranes.

Adjustment

The membrane is attached at the rim and fastened by a tension hoop which can be tightened by tuning brackets. Many mechanical design aspects of the modern banjo found its final form at the turn of the 20th century.⁹⁶ The membrane tensioning system hasn't undergone major changes since then. Due to the fact that a tight membrane was always associated with high sound levels, mechanical enhancements make it possible to over tighten a banjo membrane⁹⁷ negatively influencing its sound characteristics.

Boundary Conditions

In correspondence to the string, the derivation of the differential equation for the membrane poses boundary conditions that are never completely satisfied in reality, and, as is shown later, is a crucial factor for realistic sounding membrane models. But for an initial analysis, fixed boundary conditions (Dirichlet) are assumed.

Measurements

The following series of measurements show the radiation of the banjo membrane resulting from a knock on a point near the left⁹⁸ bridge foot. The banjo was measured with:

- A detached back (open back banjo), no strings. ($M(a)$)
- A detached back, with strings. ($M(b)$)
- A mounted back, without strings. ($M(c)$)
- A mounted back, with strings. ($M(d)$)

⁹³See (*Mylar polyester film: Physical-Thermal Properties*, DuPont Teijin Films, 2003)

⁹⁴Hans-Jürgen Bargel: *Werkstoffkunde*, ed. by Günter Schulze, Springer, 2012, p. 132.

⁹⁵See: http://www.remoc.com/portal/products/3/11/92/130/banjo_coated_top.html.

⁹⁶Linn, *Barbaric Twang*, pp. 81-115.

⁹⁷Ibid., pp. 81-115.

⁹⁸When viewed from the front with the neck facing upward.

2 History, organology and acoustics

If the banjo is open, it has no fundamental air frequency radiating frontward because the air cavity beneath the banjos membrane is open and radiates towards its back. As depicted in Figure 2.7 the spectral maxima of the sound radiation can be characterised by membrane typical mode shapes.

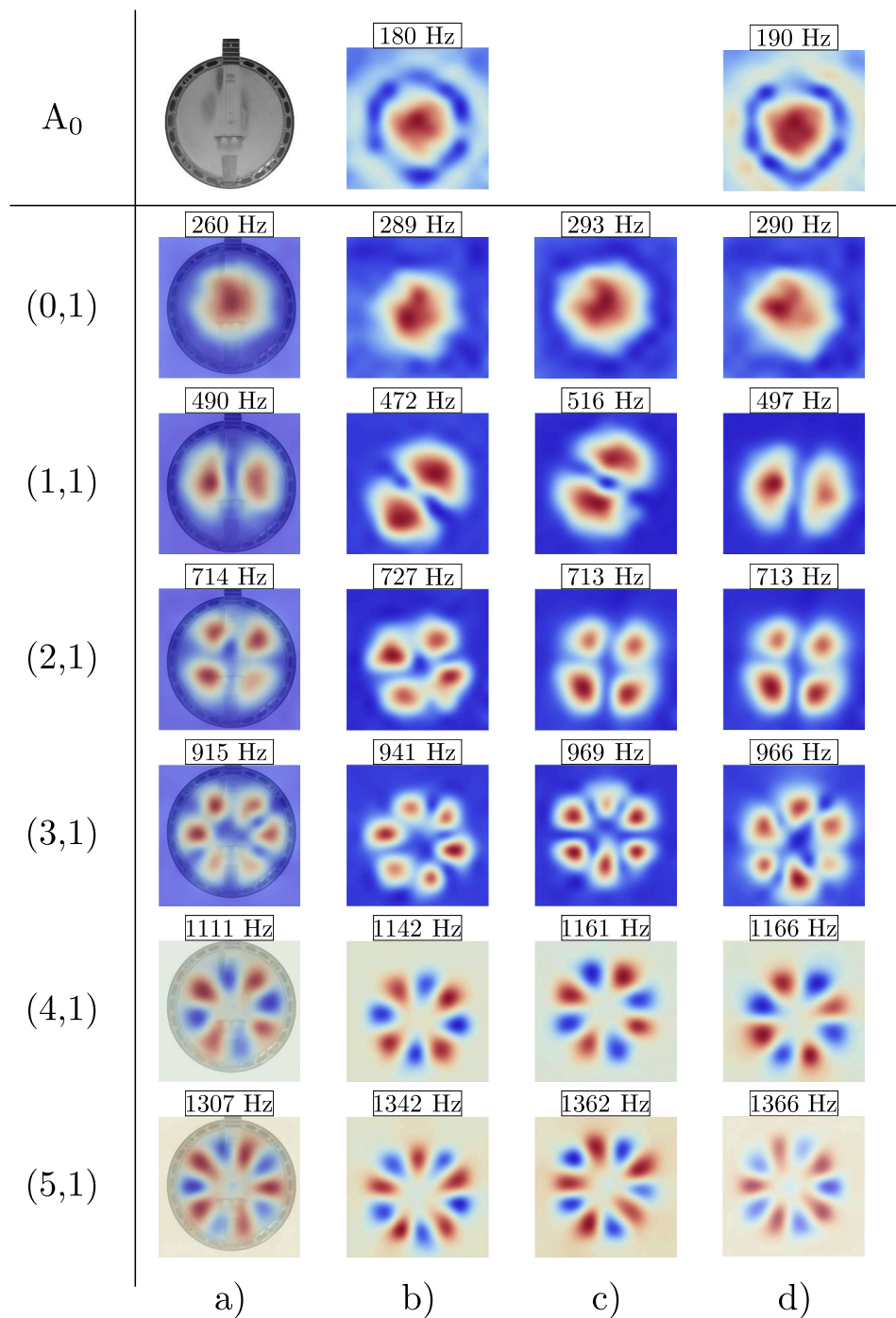


Figure 2.7: Absolute values of Banjo mode-shapes. Impulse-hammer excitation. **a)**: Open back, no strings. **b)**: Closed back, no strings. **c)**: Open back, strings. **d)**: Closed back, strings. Column **a** shows the position of the banjo during all measurements. For mode-shapes (4,1) and (5,1) only imaginary or real part are used for the images due to their better structural resolution.

2 History, organology and acoustics

The mode shapes and the ideal frequency ratios of an analytic membrane and the frequency ratios of the measurements are given in Table 2.3.

Mode	Ratio _A	Ratio _{M(a)}	Ratio _{M(b)}	Ratio _{M(c)}	Ratio _{M(d)}
(0,1)	1	1	1	1	1
(1,1)	1.59	1.88	1.63	1.76	1.71
(2,1)	2.14	2.73	2.52	2.43	2.46
(0,2)	2.30	—	—	—	—
(3,1)	2.65	3.52	3.26	3.31	3.33
(1,2)	2.92	—	—	—	—
(4,1)	3.16	4.27	3.95	3.96	4.02
(2,2)	3.50	—	—	—	—
(0,3)	3.60	—	—	—	—
(5,1)	3.65	5.03	4.64	4.65	4.71

Table 2.3: Measured vs. analytic frequency ratios of a round banjo membrane. The mode numbers indicate (axial, radial) nodal lines. Blanks indicate an absence of the mode shape. $M(*)$ are the respective measurements shown in Figure 2.7.

As shown in Table 2.3, in comparison to the analytical solution where the frequency ratios between the higher modes and fundamental membrane mode are given by the zero crossings of the real part of the Bessel function, often denoted as $J(x)$, the measured membrane under different conditions does not exhibit a comparable order. What can be stated is the fact that the influence of the bridge is much stronger on the position of the frequencies than the influence of the open or closed back. Comparing measurement $M(c)$ with $M(d)$ and $M(a)$ with $M(b)$ shows that the higher tension of the membrane due to the additional bridge force, makes it more impervious towards a changed boundary condition due to the air volume.

2.3.5 Banjo Body

African-American instruments, which influenced structural constituents of the banjo often have a body made from a hollow gourd,⁹⁹ or, more frequently, a wooden box of various kind (cigar boxes, cheese boxes...).¹⁰⁰ Because in its earliest stages the banjo was a handcrafted instrument build by musicians themselves, it can only be speculated about the knowledge about the acoustical influence of the body the builders of these instruments had.¹⁰¹ It is reasonable to suppose that the body was initially designed to fulfil load bearing functionality and wasn't designed to influence the fine structure of the banjos timbre.

As mentioned above, an important motivation of early banjo designs was the aim to produce a reasonably high membrane tension and thus a stable fixation at the body¹⁰² was needed. As is shown in the work of Linn,¹⁰³ the banjos rise to popularity was followed by many structural changes and the *elevation* of the banjo, as shown in Gura and Bollman¹⁰⁴ led to advancements in fundamental parts of the banjo, the body for instance.¹⁰⁵

(...) a group of players and makers of the banjo proposed a new set of ideas about what the banjo should be. The banjo needed "elevation", they believed, to a higher class of musical practice and a better class of people.

This was one of the main factors fuelling a redesign of several aspects of the banjos body. The wooden rim of the banjo was fitted with a metal top and metal tension screws to add more stability to the rim and the complete banjo body. Most of the features found in modern banjos were first developed around that time, as for instance the tone ring or the tension hoops with the tension screws¹⁰⁶. A modern 5-string banjo consists of a tension hoop and a metal ring to support the tension hoop. There still is discussion about the influence of the fastening of the membrane at the rim of the banjos body.

Similar to snare drums, the tension hoop can be tightened by tension screws placed equidistant around the rim.

2.3.6 Banjo Playing Styles

In traditional country music there are two schools of banjo playing styles. On the one hand there is the *old-time* playing style with its playing technique frailing or claw-hammer style, a

⁹⁹Conway, *Banjo Echoes*.

¹⁰⁰Ibid.

¹⁰¹Cecelia Conway: "Black banjo songsters in Appalachia", in: *Black music research journal* 23.1-2 (2003).

¹⁰²The round design in the banjos body could largely be due to a better distribution on the rim compared to a quadratic wood rim.

¹⁰³Linn, *Barbaric Twang*.

¹⁰⁴Gura and Bollman, *America's instrument. The banjo in the Nineteenth Century*.

¹⁰⁵Especially the attachment of the membrane changed fundamentally.

¹⁰⁶Some examples of the various different stages of the membrane attachment can be found in: Gura and Bollman, *America's instrument. The banjo in the Nineteenth Century*.

more modern banjo style, arising in the 1920 to the 1930, is the bluegrass of finger picking style. Clawhammer banjo is played with the bare hand (the backside of the nail acts as an plectrum) whereas bluegrass banjo is played with finger picks for the thumb, the index and the middle finger. Both styles can be discerned by a different playing technique and by the instrument. *Modern* bluegrass style is usually played with a closed back banjo. Old-time banjos are traditionally played with an open back.¹⁰⁷ The detachable resonator of the banjo is made out of wood and is fastened at the bottom of the instrument under the membrane. This produces an air filled cavity behind the membrane of the banjo influencing the radiated sound and the vibrational behaviour. Because the air in the cavity can radiate through small openings around the tension hoop, the radiated sound of the banjo shows a low air/cavity mode as shown in section 2.3.4.

2.3.7 Open Questions

Even though many acoustic properties of the *banjo* can be explained satisfactorily, there are several open questions regarding its acoustic vibrations, which could not be cleared completely in the scope of this thesis. One physical mechanism that can be found in most membrane covered instruments is the interaction of the enclosed air volume with the membrane.¹⁰⁸ There is always a low air-cavity resonance which can be classified as a *Helmholtz* frequency. But, the *classical* Helmholtz is only defined for cavities with rigid walls, with infinite impedance compared to the air volume and the opening of the cavity. In membrane covered lutes, the effect of the air cavity with an orifice is also present but an exact description of the physical mechanism should include the influence of the non-stiff boundary, the membrane, with finite impedance and under transient conditions.¹⁰⁹ As we will see in section 2.5.5, higher air-modes are also present in the radiated instrument sound.

The exact influence of the bridges fine structure (weight and geometry) on the radiated banjo sound could not be cleared completely in the scope of this work. An extended research regarding the influence of the bridges *eigen*-vibrations could elucidate the possibility of similar effects as found in violin bridges, especially the presence of a characteristic *bridge hill*.¹¹⁰

¹⁰⁷Dan Levenson: *Clawhammer Banjo From Scratch A Guide for the Claw-less!*, MELBAY, 2003, p. 14.

¹⁰⁸ Extensive research on this matter can be found about the kettle-drum. Several publications show the influence of the air volume on the membrane of the timpani. See: Rossing, *Science of Percussion Instruments*, pp. 5-15.

¹⁰⁹ Nonetheless, the basic Helmholtz formula for cavity modes can be applied for a first approximation of the lowest air-mode as shown in: Florian Pfeifle: "Systematic Musicology: Empirical and theoretical Studies", in: ed. by Albrecht Schneider and Arne von Ruschkowsky, Frankfurt am Main, Germany: Peter Lang Verlag, 2011, chap. Air Modes in Stringed Lute-like Instruments from Africa and China. 137–152.

¹¹⁰Erik Jansson: "On the Prominence of the Violin Bridge Hill in Notes of Played Music", in: *Journal of the Violin Society of America* 22.1 (2009): 169–176 for the influence of the bridge hill on the perceived quality of the instrument.

2.4 Violin

The classical violin is among the most researched instruments in musical acoustics as well as instrument historic organology. The vast amount of publications starting in the 15th century to today includes over ...books, papers, thesis' and other forms of literal sources.¹¹¹

Thus, the literary review given in this section focusses In this section, physical properties and an overview of the violins history as well as measurements taken over the course of this thesis are presented.

2.4.1 Historic Overview

It is assumed that the history of bowed instruments began in the 9th century A.D. in Central Asia where nomadic tribes supposedly began to use a horse hair stringed bow to excite the strings of lute instruments. These early accounts are not well documented, but the fast distribution of the bow among several cultures in the Middle East and in East Europe make a Central Asian heritage very likely.¹¹² Many figurative and pictorial sources show that bowed instruments were adopted and used in Western Europe by the 11th century.

*For the next three centuries many different types of bowed instrument, with a bewildering variety of names, were in common use throughout Europe.*¹¹³

The violin as it is played today could be recognized as an individual instrument as early as 1500¹¹⁴ and can be discerned from other classes of bowed instruments, like the *viols*. The characteristic *waist* of the instrument that

(...) gave the bow access to the outer strings (...) ¹¹⁵

was one of the multiple organologic evolutions of the instrument that led to the design of master violins by Italian instrument makers like Antonio Stradivarius (1644-1737) or Giuseppe Guarneri del Gesu (1698-1744) which are still highly valued and played today. Besides several minor structural alterations like a higher bridge, a longer neck or higher string tension that lead to a higher volume, which is required in modern concert hall acoustics, today's violins are designed after their 17th century counterparts in most regards.

¹¹¹See:

¹¹²Brigitte Geiser: "Studien zur Frühgeschichte der Violine", in: *Publikationen der Schweizerischen Musikforschenden Gesellschaft : Serie 2*, Bern: Gemeinsamer Bibliotheksverbund (GBV) / Verbundzentrale des GBV (VZG), 1974, p. 28.

¹¹³Murray Campbell and Patsy Campbell: "The Science of String Instruments", in: ed. by Thomas D. Rossing, Springer, 2010, chap. 17: 301–315.

¹¹⁴See for instance the painting of *The Madonna of the Orange Trees* by Gaudenzio Ferrari from 1529 - 1530 in: D.D. Boyden: *The History of Violin Playing from Its Origins to 1761, and Its Relationship to the Violin and Violin Music*, Oxford University Press, 1967: Plate I.

¹¹⁵Joseph Curtin and Thomas D. Rossing: "The Science of String Instruments", in: ed. by Thomas D. Rossing, Springer, 2010, chap. 13: 209–244.

2.4.2 Acoustical Research History

Compared to other string instruments, the violin is a rather small in size, nonetheless it is capable of producing sound loud enough to be audible even in large concert halls. It is probably because of its difficult structure that it exhibits very complex physical-acoustical behaviour and a complex interaction between its constituent parts. In Schelleng's words:

*The violin family presents many unsolvable problems; its shape and the peculiarities of its materials were certainly not selected with regard to convenience in analysis.*¹¹⁶

Regardless of this fact, there is a long list of publications considered with acoustic and physical properties of violins.

Felix Savart was the first researcher who discussed basic features of some of the structural and acoustic interactions. He suggested that the soundpost stiffens the treble side of the violin, transforming the rocking motion of the bridge, which excites a dipole mode of the top-plate, into a monopole mode by this unilateral stiffening of the geometry.¹¹⁷ Since a monopole radiates more effectively compared to a dipole, the violin gets louder when the soundpost is attached, especially in the low frequency range of the top plate dipole resonances. The effect of changing sound quality if the soundpost is detached is known among most professional violin players and instrument makers. In another work, Savart suggests that good violins have a special relation of top plate and back plate tap-tone resonances. In his measurements he compared disassembled front- and backplates of these instruments and found that Gesu Guaneri or Antonio Stradivari violins the fundamental resonance of both parts was between a whole tone apart whereas violins of lower quality showed intervals of a third up to a fourth. By applying his findings to violin making, he tried to develop a mathematical violin having a trapezoidal shape which showed symmetric body resonances at the fundamentals of the strings (Re, Mi, La, Sol).

One century later, C. Hutchins followed the work of Savart and suggested that if the top plate eigen-frequencies were slightly higher than the ones of the back plate, the violin sounds brighter, otherwise it sounds duller.¹¹⁸

A sophisticated discussion about the structural-acoustical interactions of the violin can be found in Bissinger¹¹⁹. There, the mechanisms of vibrational interactions leading to the violin typical radiations of the *f*-holes and lower body modes are discussed in a technical manner

¹¹⁶J. C. Schelleng: "The violin as a circuit", in: *J. Acoust. Soc. Am.* 35 (1963): 326–338.

¹¹⁷Dieter Ullmann: *Chladno und die Entwicklung der Akustik von 1750-1860*, Birkhäuser Verlag, 1996, pp. 165-166.

¹¹⁸C.M. Hutchings: "Klang und Akustik der Geige", in: *Spektrum der Wissenschaft* 2 (1981), original: *Scientific American*, October 1981: 112–122.

¹¹⁹George Bissinger: "The Science of String Instruments", in: ed. by Thomas D. Rossing, Springer, 2010, chap. 18: 317–345.

for the whole class of the Hutchins-Schelleng Violin Octet¹²⁰.

Contemporary violin research tries to find relations between the violin quality, as resulting from listening tests, and its physical properties.¹²¹ Interestingly, parameters of articulation not depending on material or geometrical properties of the instrument are found to influence the perceived quality of the instrument much more than the physical parameters. This means, the proficiency of the player has a great influence on the sound of the instrument. Still, players can tell great differences between violins and report that with some violins they are not able to perform with the same artistic intention and expression as with others. This leads to the assumption that physical parameters of the instrument are important for the interaction between the players and the instrument, and only indirectly important for the listeners.

*Since a great violinist can make a bad violin sound good, while a bad violinist cannot make a great violin sound good (...)the violinist's ability to manipulate the relative harmonic strength in the driving force, which does not in any way affect the violin itself, clearly can compensate for perceived acoustic deficiencies.*¹²²

The vocal quality of violins is discussed in Mores.¹²³ Often players reproduce the sound of a tone with their voice by choosing a vowel (a, e, i, o, u or intermediate). Mores analysis violin tones in terms of formant regions and identifies vocality by calculating height and backness, similar to speech. He finds that Stradivarius and Guaneri violins have a profound difference in their vocal quality compared to other violins. Still, the vowels perceived in listening tests are not as clear as in speech, indicating that the *vocality* of violin tones need to be measured with other methods and the underlying effect is not yet fully understood.

The importance of the interaction of the musician with the instrument stressed in the works by Bissinger is in accordance with multiple research over the last decade focussing on describing the non-linear interaction between the bow and the string, and a physical description of the mechanism based on measurements. Florens¹²⁴ presents a hardware design for interacting with a virtual model of a violin bow showing realistic simulation results. A virtual interaction model with digitized gesture data of bowing is presented in the work of Matthias

¹²⁰For a list of the Hutchins-Schelleng octet, see table 10.2 in: Fletcher and Rossing, *Physics of Instruments*, p. 325.

¹²¹Claudia Fritz, Amélie Muslewski, and Danièle Dubois: "A situated and cognitive approach of violin quality", in: *Proceedings of the 20th international Symposium on Music Acoustics* (2010).

¹²²George Bissinger: "Structural acoustics model of the violin radiativity profile", in: *J. Acoust. Soc Amer.* 124.6 (Dec. 2008).

¹²³Robert Mores: "Vowel Quality in Violin Sounds", in: ed. by R. Bader, C. Neuhaus, and U. Morgenstern, Peter Lang, 2010, chap. 6.

¹²⁴Jean-Loup Florens: "Expressive Bowing on a Virtual String Instrument", in: *Gesture-Based Communication in Human-Computer Interaction*, ed. by Antonio Camurri and Gualtiero Volpe, vol. 2915, Lecture Notes in Computer Science, Springer Berlin Heidelberg, 2004: 487–496.

Demoucron¹²⁵. Based on this work Esteban Maestre¹²⁶ shows an implementation of a similar methodology with a high level front-end. Beside the bow motion, another important factor influencing the distinct sound of the violin is the characteristic motion of the bridge, and the therefrom arising transfer function. The bridge of the violin exhibits several distinct *eigen*-oscillations (modes of vibration)¹²⁷. In addition to that, the geometry of the violins front-and back plate, as well as the enclosed air-volume radiating through the *f*-holes, play an important part in the violin specific timbre as shown in Bissinger, Williams, and Valdivia.¹²⁸

2.4.3 The Violin String

The organologic features of the violin have undergone several changes and the utilised materials and production techniques changed throughout history.¹²⁹ Early violin strings were made from animal gut, horsehair or silk. In Central Asian or Chinese bowed string instruments, these materials are still utilised today.¹³⁰ There are three different kinds of violin strings used for modern violins. Violins played for early music are often equipped with gut strings, but most strings are partially made of gut and are wrapped with silver or copper. Another kind of strings are steel core strings wound with varying material, depending on the manufacturer. The most common form of strings used today, are synthetic core strings wrapped with different metals or alloys. Compared to strings of other instruments violin strings have a carefully tuned internal damping quality, to achieve a specific sound characteristic of the string. According to string manufacturers and violinists, the specific internal damping can lead to a more controllable sound and a more easily achievable Helmholtz motion when bowing the string.¹³¹ Other important property that can be tuned by a specific string design are the brightness or the decay of a string.

In the case of upright-bass strings, this leads to the common practice of using different strings depending on the musical setting. If the instrumentalists wants to achieve a stable bowing sound and needs the best possible response from the string regarding the bow interaction, strings with higher internal damping are used. If the instrument is played in a musical setting where pizzicato notes are played, the internal damping of the string must be smaller so the

¹²⁵Matthias Demoucron: “On the control of virtual violins”, PhD thesis, School of Computer Science and Communication, 2008.

¹²⁶Esteban Maestre: “Analysis/synthesis of bowing control applied to violin sound rendering via physical models”, in: *Proceedings of Meetings on Acoustics* 19.1 (2013).

¹²⁷Lothar Cremer: *Physik der Geige*, Stuttgart, Germany: Hirzel, 1981, pp. 185-187.

¹²⁸George Bissinger, Earl G. Williams, and Nicolas Valdivia: “Violin f-hole contribution to far-field radiation via patch near-field acoustical holography”, in: *The Journal of the Acoustical Society of America* 121.6 (2007): 3899–3906.

¹²⁹Campbell and Campbell, “The Science of String Instruments”.

¹³⁰The Chinese *erhu* is one of the instruments that is still played with a horsehair bow and silk strings.

¹³¹For a comparison of violin strings from different manufacturers see: <http://www.violinist.com/wiki/violin-strings/>.

vibrational energy of the string is preserved longer and a plucked note has a longer sustain¹³².

Transverse Motion of the Violin String

The transversal motion of a string was described in section 2.3.2. As mentioned before, an important difference between violin strings and other lute instrument strings is the internal damping. The internal damping influences the transverse motion of the string in two regards:

1. The higher the internal damping, the more high partial of the string are damped, resulting in a duller, softer sound.
2. The higher the internal damping, the shorter the string vibrates due to more internal loss.

There is one important additional factor that contributes to the specific sound of the violin string: The boundary conditions. When the string is open, one boundary is the nut, which is very rigid compared to the other boundary: the bridge, which is not not as rigid but vibrates in several eigen-modes, as discussed below. When a note on a non-open string is played on the violin, the string is depressed by a finger, changing the freely vibrating length of the string and adding another boundary condition at the contact point between string, neck and finger. Because there are no frets on the neck of the violin, the boundary posed by the finger is not completely rigid, as for instance in guitars necks, and adds additional loss at the boundary due to an additional velocity damping at that point. This leads to different sustain characteristics of violin notes played on open strings compared to the same note produced by a pressed string.

Torsional Movement of the String

Among the other two modes of vibration, the longitudinal and the transversal, a violin string can exhibit a considerable amount of torsional vibrations. The physical properties of the torsional movement of the violin string was researched and described mathematically in Cremer,¹³³ he states the the torsional wave velocity is between two (for gut strings) and five (for steel strings) times faster than the transversal wave velocity.¹³⁴ Bavu, Smith, and Wolfe¹³⁵ shows that the torsional motion of a bowed strings is excited by the movement of the bow over the string in a direction orthogonal to the string. Even though they concluded that this effect is measurable, the motion is not transferred to the sound radiating front plate of the violin because the coupling of the strings torque movement to the violin bridge is too small.

¹³² As for instance an upright-bass in a Jazz or Rock'n Roll ensemble.

¹³³ Cremer, *Physik der Geige*.

¹³⁴ *ibid.*, p. 103.

¹³⁵ E. Bavu, J. Smith, and J. Wolfe: "Torsional Waves in a Bowed String", in: *Acta Acustica united with Acustica* 91.2 (2005): 241–246.

Nonetheless, further research showed that the torsional movement has an important impact on the interaction of the violin bow and the violin string. Bavu, Smith, and Wolfe¹³⁶ concluded that a skilled violinist instinctively adapts the pressure and the velocity of the violin bow in way that the transversal wave and the torsional wave of the string have rational proportion, whereas an amateur player does not have the necessary control over the bow, which leads to an unstable sound with inharmonic parts in the spectrum, audible as noise. Even though the torsional motion of the string is important for the interaction of the violinist with the instrument, it is only of marginal importance for the radiated sound of the violin.

Measurements

A tracked high-speed camera recording of the transversal deflection of a plucked violin string is shown in Figure 2.8.

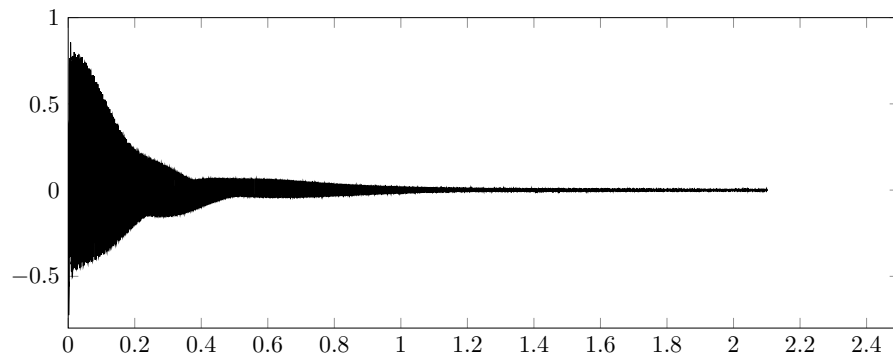
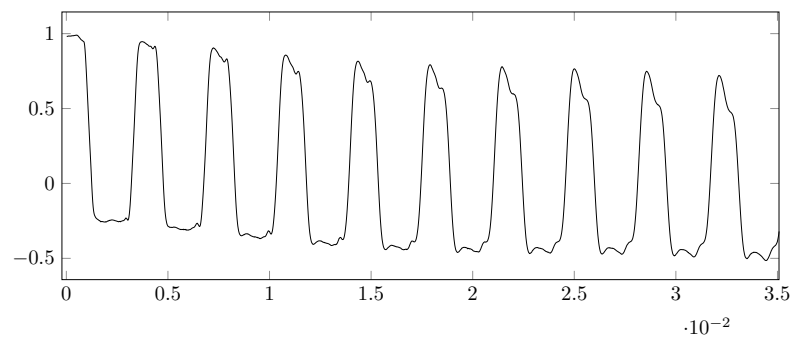
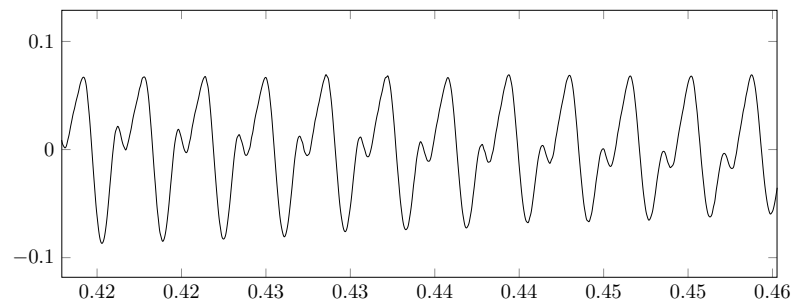


Figure 2.8: Normalised transversal deflection of a plucked violin string (280 Hz) with time in seconds on the x-axis.

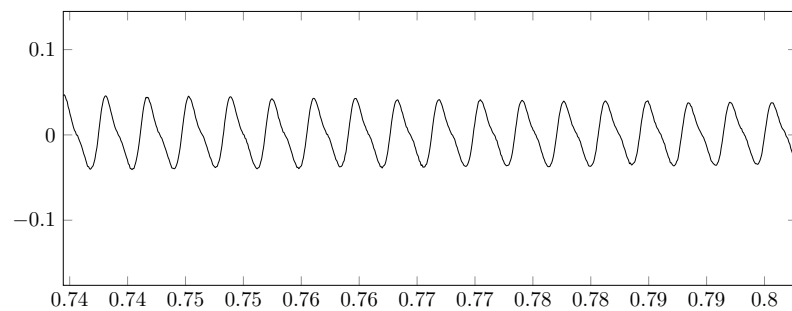
¹³⁶Bavu, Smith, and Wolfe, “Torsional Waves in a Bowed String”.



(a) Partial time series I.



(b) Partial time series II.



(c) Partial time series III.

Figure 2.9: Normalised transversal deflection of a plucked violin string (280 Hz) with time in seconds on the x-axis.

As visible in Figure 2.9a to 2.9c the initial shape of the plucked string loses its shape after the first reflection at the respective boundary.

Figure 2.10 shows the measured velocity of a bowed violin string (293 Hz/*d*-String).

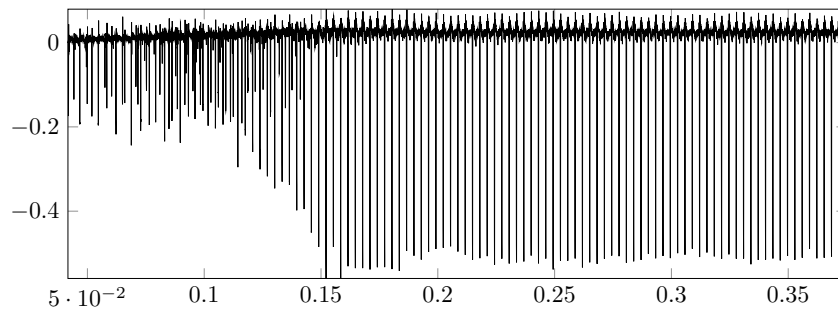


Figure 2.10: Measured velocity of a bowed violin string.

Figure 2.11 shows the deflection of a bowed violin string at the beginning of a stable Helmholtz motion.

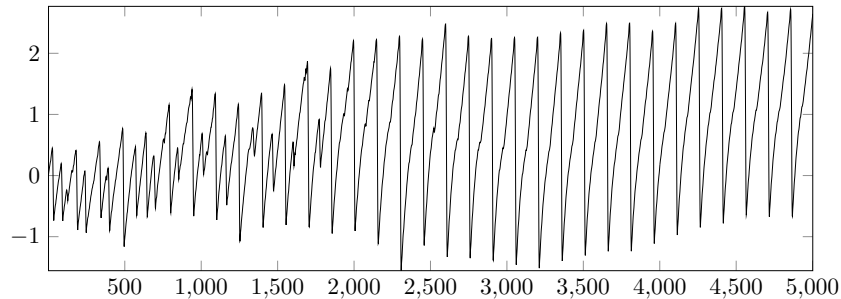


Figure 2.11: Measured deflection of a bowed violin string. Discrete sample points on the abscissa.

2.4.4 The Bow/String Interaction

The most salient feature of the violin, regarding its specific sound, is the bow/string interaction. Fundamental research regarding the bow/string interaction and the resulting wave form of the violin string was conducted by Hermann von Helmholtz¹³⁷ To research the motion of the violin string Helmholtz utilised a *Vibrationsmikroskop*, which enabled him to visualise Lissajou figures of a bowed violin string and sketch the resulting motion by hand.¹³⁸ In 1918, Raman¹³⁹ researched string vibrations and body vibrations of the cello and provided a detailed analysis of the dynamical properties of bowed strings. In 1920¹⁴⁰ published experimental data, done with a mechanical bowing machine that showed the influence of

¹³⁷Hermann von Helmholtz: *Die Lehre von den Tonempfindungen als psychologische Grundlage für die Theorie der Musik*, Vieweg, 1870, 595 ff.

¹³⁸The characteristic motion of a bowed a violin string is called Helmholtz-motion in honour of Hermann von Helmholtz.

¹³⁹C. V. Raman: “On the mechanical theory of vibrations of bowed strings”, in: *Indian Assoc. Cult. Sci. Bull.* 15 (1918): 243–276.

¹⁴⁰C. V. Raman: “Experiments with mechanically played violins”, in: *Proc. Indian Association for the Cultivation of Science* 6 (1920): 19–36.

different bowing velocities and changing distances of the bow to the bridge. F.G. Friedlander¹⁴¹ showed the importance of the dissipation of energy for the production of a stable Helmholtz motion by deducing a mathematical formulation for a string bowed at its centre. In his work, Friedlander assumes a perfectly sharp Helmholtz corner, an assumption that is not met in real strings because of the bending stiffness of the string and losses at the boundaries. Lothar Cremer¹⁴² shows the effects of a rounded Helmholtz corner on the stick-clip circle of a bow/string interaction. More recent research on the interaction between the bow and the violin string tries to include additional effects, like the motion of the bow-hairs¹⁴³, the torsional motion of the string¹⁴⁴ or the frictional behaviour of rosin¹⁴⁵.

2.4.5 Violin Bridge

In accordance to the function of the banjo bridge, the violin bridge transmits the vibrations of the four bowed strings to the soundboard of the instrument. As is shown in Cremer,¹⁴⁶ the bridge of the violin shows distinct vibrational modes which are important for the specific sound production of the violin and other bowed string instruments. As the figures in Cremer¹⁴⁷ indicate, in addition to its rocking motion, transferring the transversal pulses of the violin string, the violin bridge shows distinct *eigen*-oscillations. This adds to the specific transfer characteristics of the violin bridge which results in an important violin specific acoustic feature known as the *bridge hill* that can be identified as a peak in the radiated spectrum around a frequency of 2.5 kHz. Woodhouse¹⁴⁸

2.4.6 Violin Front/Back Plate

Acoustical properties of the violins front- and back plate were subject to research in a multitude works over the past 200 years. One of the earliest acoustic research on violins was performed by Felix Savart who compared disassembled front- and backplates working with the violin maker. There are several works that measure front plate modes with time-averaged holographic interferometry, like the work of Hutchins, K.A., and P.A.,¹⁴⁹ who visualises *tap*

¹⁴¹F.G. Friedlander: "On the oscillations of a bowed string", in: *Proceedings of the Cambridge Philosophical Society* 49 (1953): 516–530.

¹⁴²Cremer, *Physik der Geige*, pp. 79–83.

¹⁴³R. Pitteroff and J. Woodhouse: "Mechanics of the contact area between a violin bow and a string. Part I: Reflection and transmission behaviour", in: *Acta Acustica united with Acustica* (1998): 543–562.

¹⁴⁴Bavu, Smith, and Wolfe, "Torsional Waves in a Bowed String".

¹⁴⁵J. Woodhouse and P.M. Galluzzo: "The bowed String As We Know It Today", in: *Acta Acustica united with Acustica* 90 (2004): 579–589.

¹⁴⁶Cremer, *Physik der Geige*, pp. 171–203.

¹⁴⁷*Ibid.*, p. 185.

¹⁴⁸J. Woodhouse: "On the "Bridge Hill" of the Violin", in: *Acta Acustica united with Acustica* 91 (2005).

¹⁴⁹C.N. Hutchins, Stetson K.A., and Taylor P.A.: "Clarification of the plate tap tones by holographic interferometry", in: *Catgut Acoust. Soc. Newsletter* 16.15 (1971).

2 History, organology and acoustics

tones¹⁵⁰ of violins front and backs, or in the work of Saldner, Molin, and Jansson.¹⁵¹ As shown in these publications, the violin exhibits complex radiation patterns from the front and the back plate mainly due to its intricate structure. Figure 2.12 shows mode shapes published in Hutchins, K.A., and P.A.¹⁵²

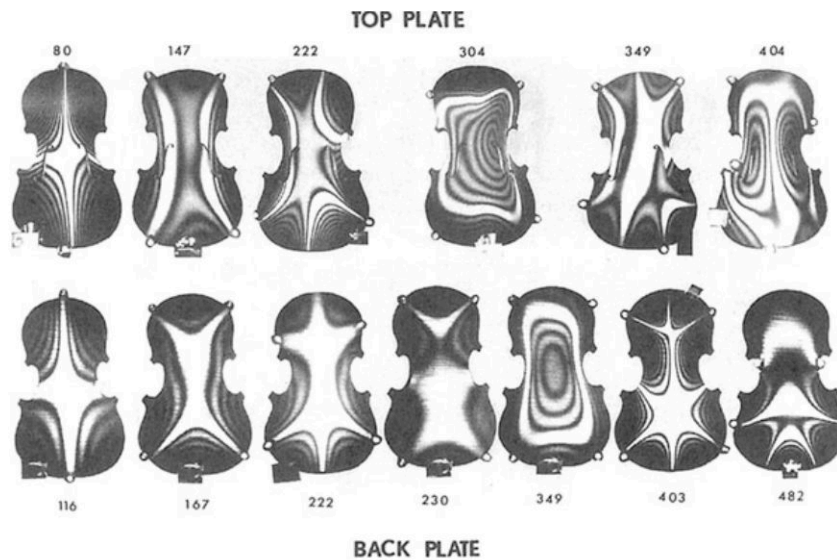


Figure 2.12: Free front plate / back plate holographic interferograms.¹⁵³

Material and Geometry Parameters

Because of its intricate geometry, it is cumbersome to find an exact description of the front plate and back plate of the violin. A description of the violin's body as a decomposition into a system of only few degrees of freedom proposed in Cremer¹⁵⁴ is capable to capture acoustic features of a violin in the low frequency range. As an extension to this model, the front plate and back plate can be realised by implementing them as thin plates.¹⁵⁵

¹⁵⁰Tap tones are commonly used by violin builders by holding the violin back or front softly, and tapping them with two fingers. By that, plate modes can be made audible. Curtin and Rossing, "The Science of String Instruments"

¹⁵¹H.O. Saldner, N.E. Molin, and E.V. Jansson: "Vibration modes of the violin forced via the bridge and action of the soundpost.", in: *J. Acoust. Soc. Am.* 100 (1996): 1168.

¹⁵²Hutchins, K.A., and P.A., "Clarification of the plate tap tones by holographic interferometry."

¹⁵⁴Cremer, *Physik der Geige*, 205ff.

¹⁵⁵This approach is also proposed in: *ibid.*, 237ff.

2.5 Ruan and Yueqin

The *yueqin* and *ruan* are two *traditional* Chinese lutes that share parts of their historic evolution and organologic features. After the organologic classification scheme of Sachs,¹⁵⁶ they can be classified as plucked round body lutes.¹⁵⁷ According to Shen,¹⁵⁸ the history of both instruments is closely connected and they play a central role in the history of Chinese lute instruments as a whole. The instruments measured in this thesis are shown in Figure 2.13 and 2.14. As one can see, comparable attributes of both lutes are the round body, the tuning mechanism as well as the wood for the front- and backplates which are made of Paulownia wood.

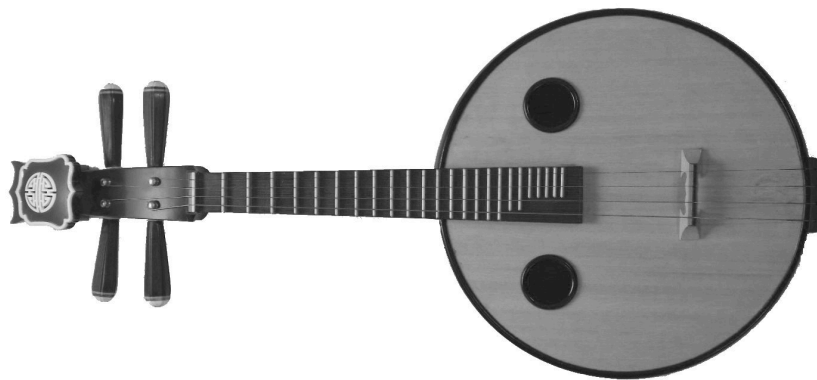


Figure 2.13: Chinese *ruan*.

A distinguishing feature is the string to soundboard coupling and there from arising a different string fixation. In the case of the *ruan*, the strings run over a two-footed bridge and are fastened at a tail piece. The strings of the *yueqin* however are fastened at a glued on bridge by a sling-knot fixation. Another discerning property is are the air holes of the *ruan* and the glued-on frets on the *yueqin*'s soundboard. Other structural differences are explained in more detail below.

2.5.1 Historic Overview

The history of Chinese plucked lute instruments comprises a time span of at least 2000 years.¹⁵⁹ But, comparable to other areas of Chinese history, it is difficult to draw a straight line in the historic-organologic development of Chinese lutes instruments because

¹⁵⁶Sachs, *Real-Lexikon der Musikinstrumente, zugleich ein Polyglossar für das gesamte instrumentengebiet*.

¹⁵⁷John Myers: *The Way of the Pipa*, Kent, Ohio: Kent State University Press, 1992.

¹⁵⁸Sin-Yan Shen: *Chinese Music and Orchestration: A Primer on Principles and Practice*, Chicago: Chinese Music Society of North America, 1991.

¹⁵⁹Myers, *Pipa*, pp. 6-31.

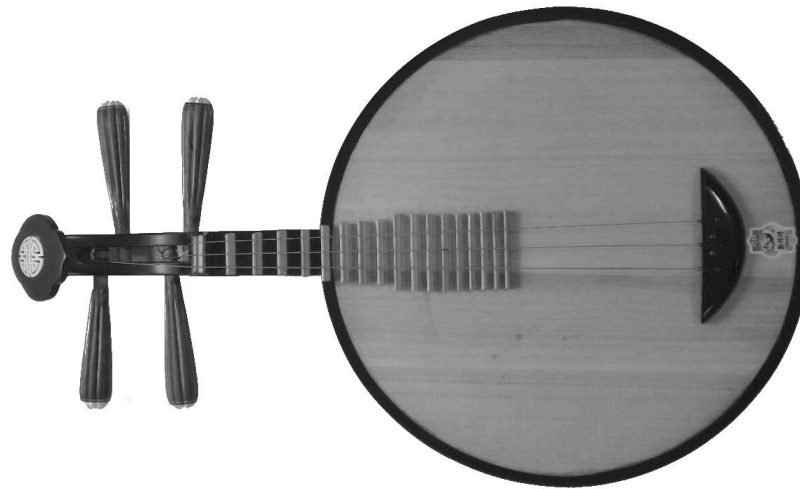


Figure 2.14: Chinese *yueqin*.

*[A]n all-embrasive periodization of China's long history is difficult and definitely controversial, as evidence by the number of different styles in scholarly practice.*¹⁶⁰

Hence, there are stages in the history of the *ruan* and the *yueqin* that escape a scientific, historic classification. A prime example would be the development of the string attachment and the already mentioned differences between both fixations. Even though the *ruan* counts as the predecessor of the *yueqin*, the organologic differences of both instruments make this claim doubtful.

Traditionally, Chinese instruments were classified by the utilised acoustical material or the sort of music that could be performed on a certain instrument. Depending on the era and the respective scholar, music instruments were classified into different classes influenced by spiritual, religious as well as social factors.¹⁶¹

This is one of the reasons, that organologic changes are not as well documented as in classical European instruments like for instance the well documented organologic history of the guitar or the piano.

Among historians, it is a widely accepted fact that the *ruan* is the oldest Chinese lute:

*The ruan is said to be the ancestor of other Chinese plucked lutes.*¹⁶²

It is associated with a lute mentioned first in the Qin¹⁶³ period where it was known as the *qin pipa*.

¹⁶⁰See the complete paragraph in: Liang Mingyue: *Music of the Billion*, ed. by Ivan Vador, New York: Heinrichshofen Edition, 1985, pp. 12-13

¹⁶¹M.J. Kartomi: *On Concepts and Classifications of Musical Instruments*, Chicago Studies in Ethnomusicology, University of Chicago Press, 1990, pp. 37-54. For an overview of a classification system consisting of 9 classes see Shen, *Chinese Music and Orchestration: A Primer on Principles and Practice*, p. 146.

¹⁶²Mingyue, *Music of the Billion*, p. 272.

¹⁶³The first Chinese dynasty from 221 B.C. to 206 B.C.. See (ibid., p. 16).

2 History, organology and acoustics

... This qin pipa (...) was created by applying strings to the taogu, a (membrane covered) percussion instrument (...)¹⁶⁴

The instrument described here, was also known by the name *xiantao* which, literally means:

(...) to stretch strings across the surface of the drum, and play it.¹⁶⁵

Due to its membrane covered resonance body this instrument maybe also an ancestor of the *sanxian*, a python skin covered long-neck lute used in modern Chinese orchestral music as well as a solo instrument.¹⁶⁶ The transition from a membrane covered lute to a wooden round body lute is not described in the accessible sources of Chinese lute instruments history. Nonetheless, it is an accepted assumption that the modern *ruan* is similar to the instrument the musician Ruan Xian, who lived approximately 300 C.E. and who was one of the *Seven sages of the bamboo grove*¹⁶⁷, played. In honour of Ruan Xian the instrument was named *ruanxian* or in short form *ruan*.¹⁶⁸

From the known pictorials and written accounts, it is not conclusively observable, if the ruan of that time was similar to the modern ruan or if it was a prototype of a stringed lute instrument from which several other lutes arose of.

The same Ruan Xian was accredited with the invention of the *yueqin*,

The *yueqin* which has a short neck, was said to be made by Ruan Xian (...). Sin-Yan Shen: *Chinese Music and Orchestration: A Primer on Principles and Practice*, Chicago: Chinese Music Society of North America, 1991, p. 108

In modern Chinese orchestral music, the ruan is often played as a bass instrument and the *yueqin* as a higher melody instrument. Liang Mingyue: *Music of the Billion*, ed. by Ivan Vantor, New York: Heinrichhofen Edition, 1985, pp. 272-273

Remarks

The differences of both instruments in their timbre and their radiated sound quality, due to their structural differences, like the presence of large sound holes or the fastening of the strings, is not part of the known and accessible historical consideration. These two superficial differences sets both instruments apart from each other and leads to the presumption, which can not be verified or falsified at this point, that both instruments have a different organologic origin. The evolution from an unmounted bridge to a glued on bridge as the primal string attachment, and from a front plate with sound holes to a front plate without sound holes is

¹⁶⁴Myers, *Pipa*, p. 7.

¹⁶⁵Shen, *Chinese Music and Orchestration: A Primer on Principles and Practice*, pp. 103-104.

¹⁶⁶The role of the instrument in the various Chinese operas can be found in table 1 in Shen (ibid., pp. 26-27)

¹⁶⁷ A group of artists, musicians and literates that lived in a bamboo grove to flee the restrictive politics at that time. Myers, *Pipa*.

¹⁶⁸ Shen, *Chinese Music and Orchestration: A Primer on Principles and Practice*, p. 102 or Myers, *Pipa*, p. 7.

very unlikely to be the manifestation of an organic and linear process. The known history of both instruments is likely to be shaded by mythical influences as is the case in other historic traditions related to Chinese instrument organology. Hence, using accessible historic sources, an exact classification of relevant evolutionary steps can not be reconstructed here and could be part of further investigations.

2.5.2 Acoustical Properties of the Ruan

In this section, an overview on the acoustical properties of the Chinese lute ruan is given. Even though the ruan is played in similar musical idioms like the *yueqin*, both instruments differ in certain aspects of playing style and qualitative sound features.

2.5.3 Ruan Strings

The strings of the ruan traditionally were made of silk. Today, ruan strings are made of metal wound nylon for the lowest string or nylon for all higher strings. Compared to the strings of the banjo, ruan strings are thicker and much shorter. They exhibit a faster decay of higher partials, resulting in a darker timbre and a more percussive sound. The instrument is played with a plectrum made of animal bone¹⁶⁹ or plastic utilising a playing technique that is based in the *tantiao* plucking technique, similar to many Chinese lutes.¹⁷⁰ Other commonly utilised techniques are tremolo techniques, resembling the playing technique of the Italian mandolin.

String Fixture

The fixation of the strings at the head of the ruan is similar to the fixation of the banjo string. The strings run over the nut and are wound around wooden tuning pegs. The tuning pegs are similar to tuning pegs of other Chinese string instruments. The mechanical principle of the tuning pegs is comparable to the tuning pegs of European bowed instruments, they differ in size and shape but are conceptually friction pegs as found in violins, violoncellos, or other stringed lutes like the Georgian *panduri*. Comparable to the banjo, the ruan has a moveable wooden bridge, which is held in position by the downward force exerted by the tightened strings.

Measurements

A high-speed camera recording of the transversal deflection of a plucked ruan string is shown in Figure 2.16.

¹⁶⁹Due to the instruction booklet that came with the author's ruan, it traditionally was made from swan bone.

¹⁷⁰The word *tantiao* is synonymous to the word *Pi'Pa* and means leftward rightward (downward upward). Shen, *Chinese Music and Orchestration: A Primer on Principles and Practice*, pp. 102-103.

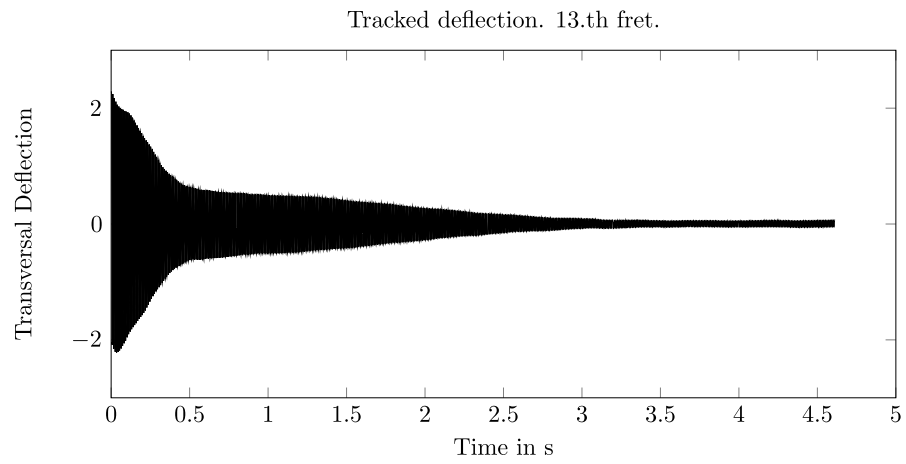


Figure 2.15: Normalised transversal deflection of a plucked ruan string (104 Hz) with time in seconds on the abscissa.

2 History, organology and acoustics

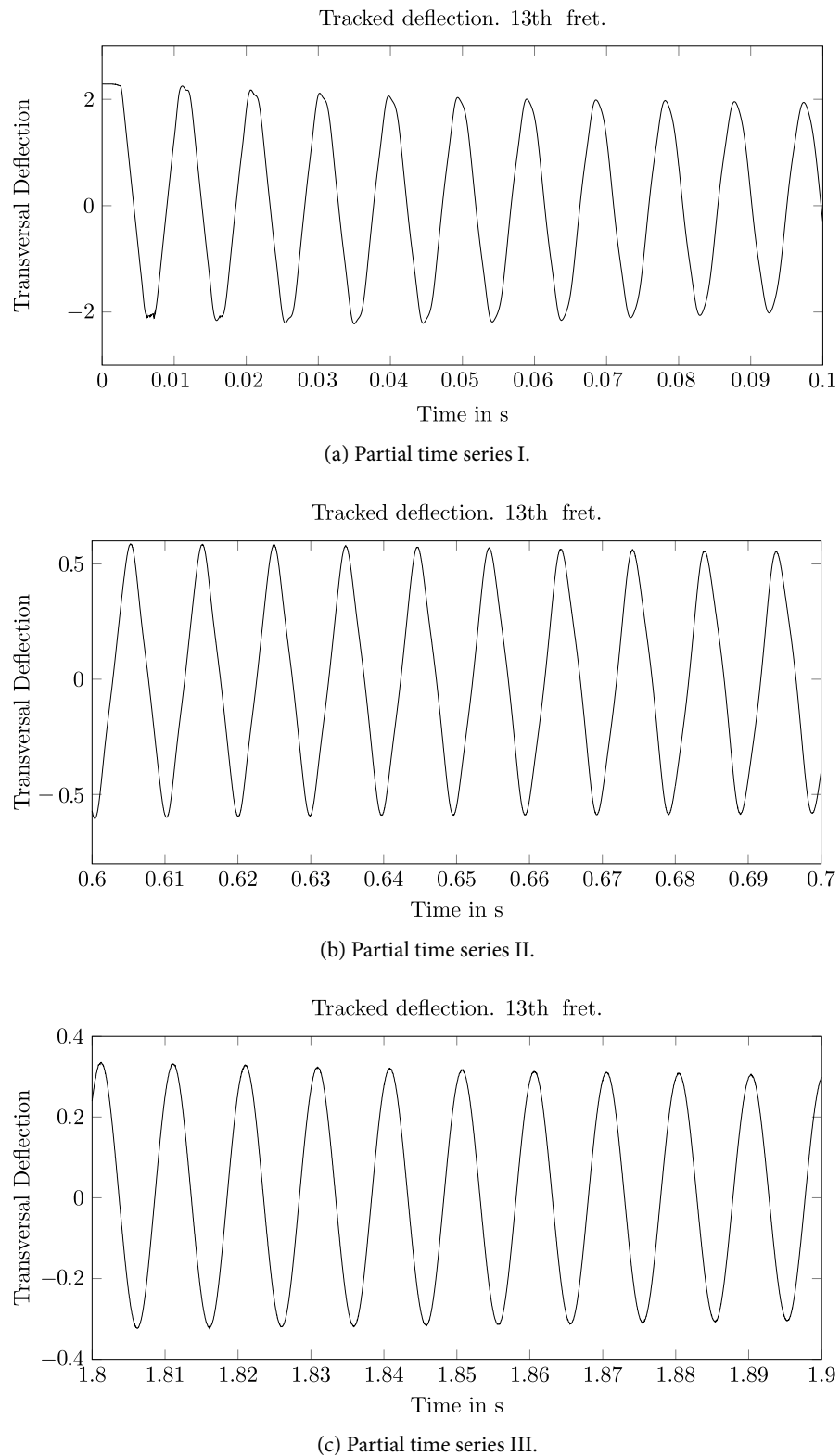


Figure 2.16: Normalised transversal deflection of a plucked ruan string (104 Hz) with time in seconds on the abscissa.

2.5.4 Ruan Bridge

Similar to the bridge of the banjo, the bridge of the ruan is carved out of wood. It is made of two separate sorts of wood. The upper part, the contact point with the strings, is made of hardwood or ebony, depending on the quality of the instrument. The lower part of the bridge is generally made of maple.

In contrast to the banjo it only has two feet. It is considerably bigger and heavier than a standard bluegrass banjo or violin bridge. Both feet have 2.1×1.3 cm large contact areas with the front plate of the instrument.

2.5.5 Ruan Body

Material properties

The front and back plate of the ruan is made of Paulownia spruce, a wood which is relatively unknown to western luthiers¹⁷¹. Its material properties taken from the *wood database*¹⁷² are listed in table 2.4.

Scientific name	Paulownia tomentosa
Average Dried Weight:	280 $\frac{kg}{m^3}$
Elastic Modulus:	4.28 GPa

Table 2.4: Engineering constants of Paulownia wood.

Paulownia is utilised in many Asian lutes as the wood for the whole body or for the sound-board. The *pi'pa*, the *qin*, the *liuqin* or the *yueqin* are all Chinese lutes with Paulownia front plates.

The front plate

The two large orifices on the front plate act as sound-holes having a comparable acoustical function as the sound-hole of the classical guitar, enhancing the radiation of lower register of the instrument. The effect of the air volume radiating through the openings can be described by the extended Rayleigh-Helmholtz formula:

$$f_H = \frac{c}{2 \cdot \pi} \sqrt{\frac{A_O}{V \cdot (l_O + 2 \cdot \delta_R)}}, \quad (2.1)$$

¹⁷¹Personal communication with a local guitar builder. But it is used as wood for custom guitars. See: Ron Kirn: *Paulownia research*, [Online; accessed 5-October-2013], 2013, URL: <http://www.tdpri.com/forum/tele-home-depot/173208-paulownia-research.html>.

¹⁷²The Wood Database: *Paulownia*, [Online; accessed 5-October-2013], 2013, URL: <http://www.wood-database.com/lumber-identification/hardwoods/paulownia/>.

2 History, organology and acoustics

with $\delta_R = \delta \cdot r_O$, A_O the area and l_O the height of the opening and r_0 the radius of the orifice.¹⁷³ The Volume V can be calculated by using the volume formula for an equivalent cylinder which is given by $\pi \cdot r^2 \cdot h$ with r and h the radius and height respectively.

Parameters	Physical values
Radius of body:	17cm
Height of body:	6.5cm
Height of opening	1cm
Area of opening:	1.26mm ²

Table 2.5: Geometry parameters of the ruan.

Inserting all values given in Table 2.5 to equation 2.1 yields a Helmholtz frequency of ≈ 147.8 Hz, which is in very good concordance with the measured frequency as visible in Figure 2.7.

Measurements

The following measurements of the ruan front plate are conducted with the microphone array as descibed in section 2.2.1. The focus of the measurements is put on the radiated spectrum of the front plate and the coupling between the enclosed air volume inside the wooden resonating body. Both orifices on the front plate of the ruan influence the radiated timbre of the instrument due to the interaction between the front plate and the enclosed air. The measurements shown in Figure 2.17 are radiation patterns of the ruan resulting from a single impulse-hammer knock on the front plate of the instrument near the left foot of the bridge.

¹⁷³ δ is the end correction of the Helmholtz formula and has a value of 0.85. See: Fletcher and Rossing, *Physics of Instruments*, p. 16.

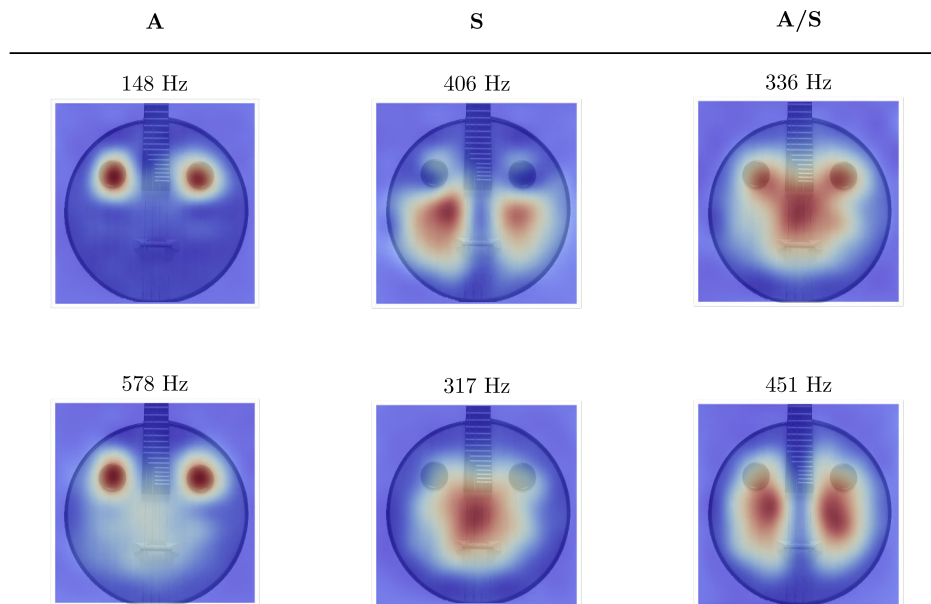


Figure 2.17: Ruan radiation patterns – Impulse-hammer excitation. Column **A**): Air modes. **S**): Structural modes. **A/S**): Coupled Air - Structure modes.

The radiation patterns of the ruan show radiation from the front plate as well as from the orifices. In Pfeifle¹⁷⁴ it was shown that the radiation of the ruan is a mixture of front plate modes, air-modes and back plate-modes radiating through the orifices.

2.5.6 Acoustical Properties of the *Yueqin*

In this section, an overview of the physical properties of the *yueqin* is presented.

Strings Material

The strings of the *yueqin* used for the measurements in this thesis, have the same material properties as the strings of the ruan. The lower string, tuned to a G1 is a steel-wound string with a nylon kernel, the two higher strings, tuned to D2 and G2, are nylon strings.

String Fixature

Compared to the other string instruments modeled in this thesis, the *yueqin* is the only instrument that does not have a separated bridge and fixture of the strings. The mechanism of the energy transfer from the string to the top-plate differs from the other instruments as it is transmitted at the tail-piece of the instrument, the point where the strings are fastened. The

¹⁷⁴Pfeifle, “Systematic Musicology: Empirical and theoretical Studies”.

elliptic quarter shell formed tail piece is glued directly onto the top-plate of the instrument as shown in Figure 2.14.

Measurements

A high-speed camera recording of the transversal deflection of a plucked *yueqin* string is shown in Figure 2.18 and Figure 2.19.

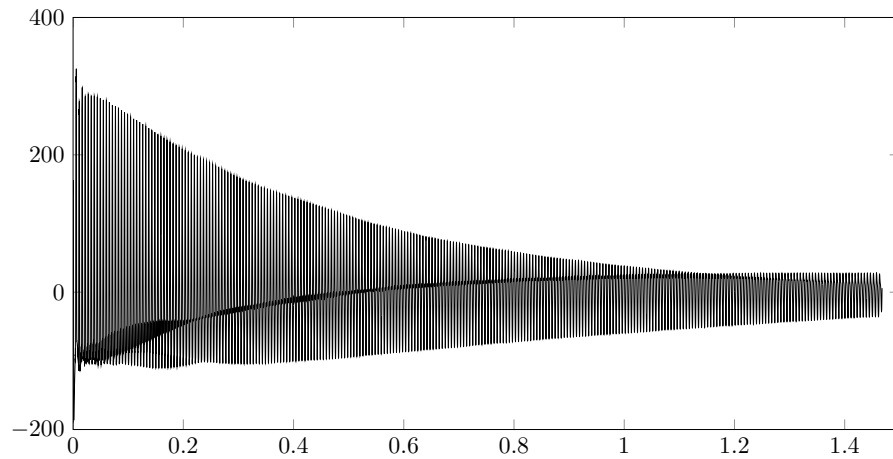


Figure 2.18: Transversal deflection of a plucked *yueqin* string (181 Hz), time in seconds on the abscissa.

2 History, organology and acoustics

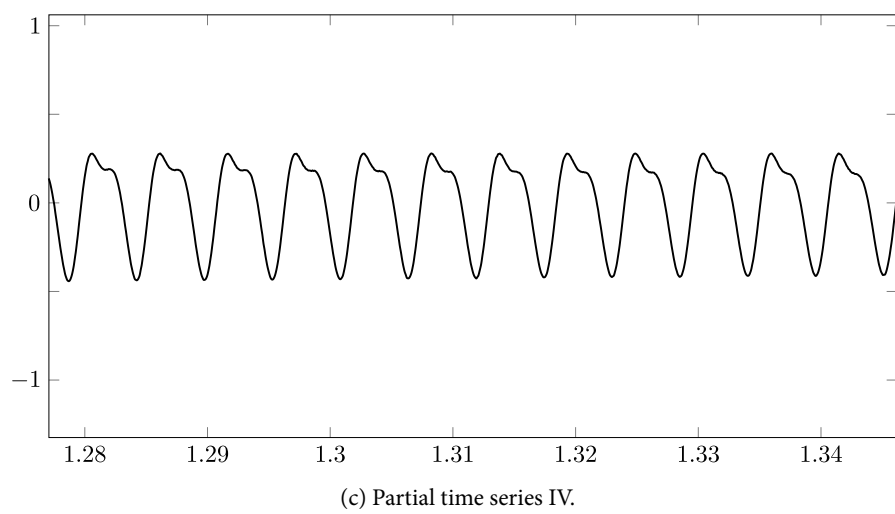
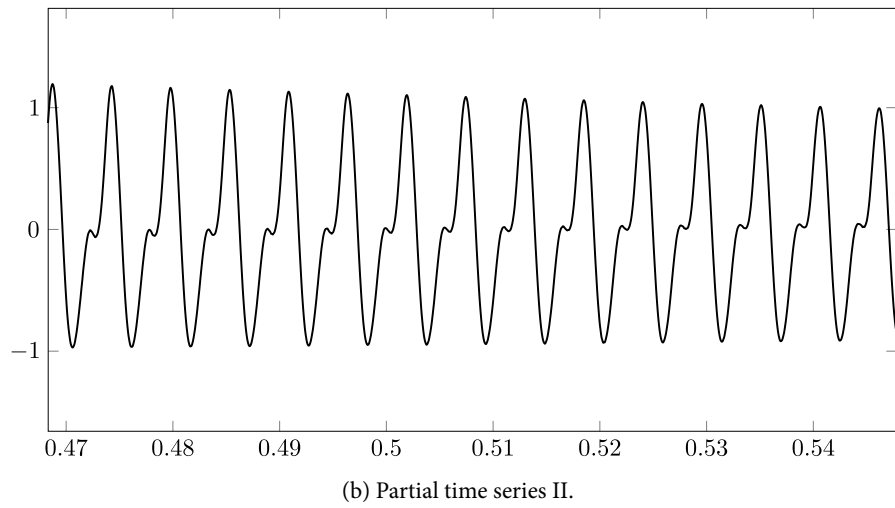
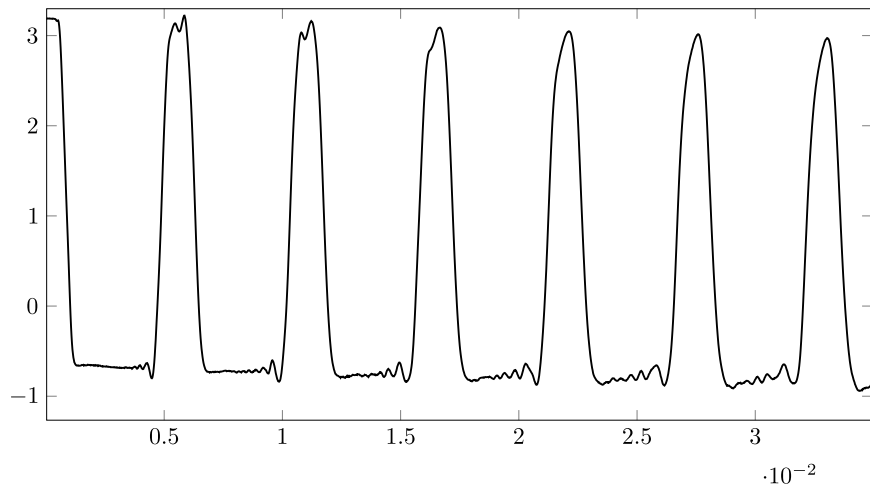


Figure 2.19: Transversal deflection of a plucked *yueqin* string (181 Hz), time in seconds on the abscissa.

Yueqin Body

The body of the *yueqin* is round and consists of a front and backplate with an enclosed air volume. Contrary to the ruan it has no orifices on the front plate but has one 21x17mm small opening located directly under the tail-piece. The front and back plate of the *yueqin* are made of Paulownia wood similar to the ruan.

Parameters	Physical values
Radius of body:	23.7cm
Height of body:	4cm

Table 2.6: Geometry parameters of the *yueqin*.

Microphone Array Measurements

The following measurements are performed with a similar set-up as the microphone array measurements shown before. The results shown in Figure 2.20 are recorded from a single impulse-hammer knock on the front plate of the instrument in the left¹⁷⁵ center of the front plate.

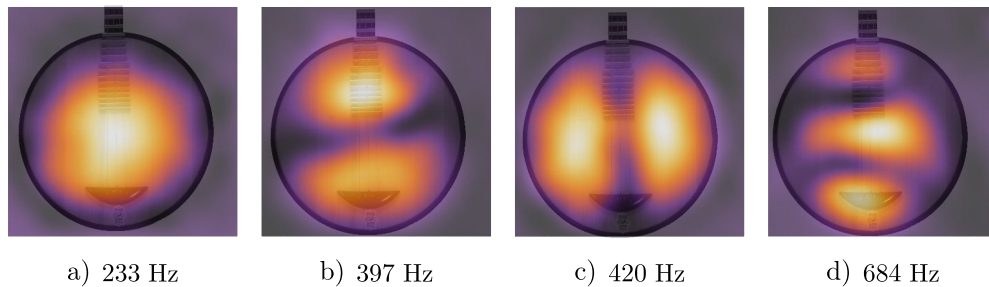


Figure 2.20: Radiation patterns of the *yueqin*'s front-plate – Impulse hammer excitation.

2.6 Pick/String Interaction

The interaction between a plectrum or a finger pick, as commonly utilised by string instrument players, and the string of an instrument adds a high frequency slipping noise to the sound of the string. Besides the excitation point, the position of the pick/string interaction), the material parameters and plucking velocities have an influence on the timbre of the slipping noise. Similar effects have been found in harps¹⁷⁶ and guitars¹⁷⁷. Measurements of a banjo-pick string interaction are presented here.

¹⁷⁵With the neck facing upward and viewed from the front.

¹⁷⁶Mentioned in Delphine Chadeaux et al.: “Experimentally based description of harp plucking”, in: *The Journal of the Acoustical Society of America* 131.1 (2012): 844–855.

¹⁷⁷ Bader, *Computational Mechanics of the Classical Guitar*, pp. 161-166.

2.6.1 High-Speed Camera Recordings

The interaction between a banjo pick and a banjo string is researched using high-speed camera recordings and qualitatively evaluating the measurements¹⁷⁸. By analysing the recorded interaction, three phases can be discerned that can be categorised as:

1. Phase 1: The string sticks to the finger pick and is deflected towards the direction of the finger movement.
2. Phase 2: When the restoring force of the string gets larger than the force exerted by the finger and the string, it starts to perform a slipping (gliding) motion on the surface of the finger-pick.
3. Phase 3: The string slips over the edge of the plectrum, is released from the sticking Phase 2 and starts to vibrate freely without the influence of the finger-pick.

There are three physical parameters that influence and control the progression of this three phase model, the velocity of the finger, the force exerted by the finger and the net force of the string, depending on the position of the interaction. This model resembles the model of the bow-string interaction but it is different in one regard: The pick, plectrum or finger has a finite length. Hence, the interaction between it and the string ceases once the plectrum, finger-pick or finger has lost contact with the string.¹⁷⁹

2.6.2 Spectral Components

Figure 2.21 shows the time-series of damped banjo string, excited with a metal finger pick and plucked at different positions, starting from the bridge to the string centre above the 12th fret. The sound is recorded with a piezoelectric transducer, mounted at the bridge in direct contact with the plucked string.

¹⁷⁸The image series is attached in appendix 2.

¹⁷⁹ In contrast to the violin bow/string interaction, this model has a higher accuracy. Due to the fact that a metal finger pick has no motion of its own, unlike the hairs of a violin bow, a linear approximation as a completely rigid object is more feasible than in the case of the violin bow.

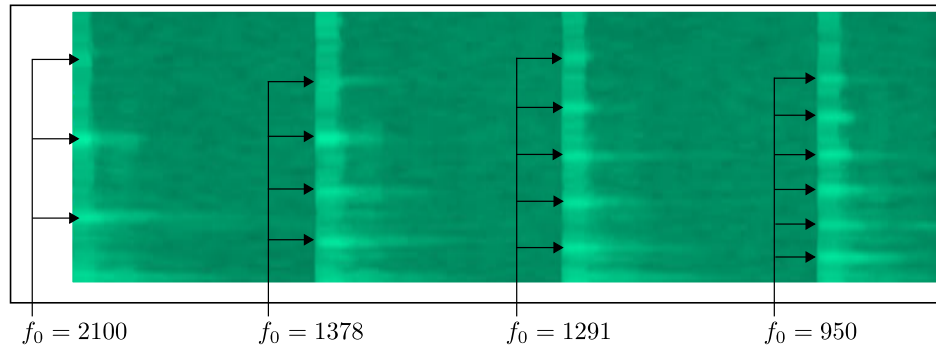


Figure 2.21: Piezoelectronic recording of the pick/string interaction measured at the banjo bridge.

As indicated by the arrows, the slipping sound produced by the metal pick can be seen in the spectrogram containing of a fundamental note and several partials. This points to the fact that the frequency content of the slipping sound is highly dependent on the position of the plectrum on the string. At the moment of contact, the plectrum adds an additional boundary condition, separating the string into two parts. The part between finger pick and bridge determines the fundamental of the perceived slipping-sound. This means that if the string is plucked directly over the 12th fret, the slipping sound has strong frequency components one octave above the fundamental frequency of the string. The farther the contact point moves towards the bridge, the higher the fundamental frequency f_0 of the slipping sound is. This effect is audible in the acoustic near-field of the banjo and has an influence on the vibration of the string.

2.6.3 Tremolo Model Extension

The ruan and the *yueqin* are traditionally played with a tremolo technique¹⁸⁰ comparable to the playing style of the Italian mandolin. The interaction of a ruan plectrum with a string is modelled as an extension to the model of the banjo string/pick interaction. One difference between both models that plays a role in the excitation of the string is the fact that the plectrum has a very short contact time with the string. After phase III of the model the excitation is repeated after a short pause, depending on the speed of the tremolo.

2.7 Intermediate Results

The measurements presented in this section show basic physical properties of the four string instruments researched in this thesis. On the one hand, the measurements act as a foundation for the physical models presented in chapter 4, on the other hand they help to stress the

¹⁸⁰Myers, *Pipa*.

2 History, organology and acoustics

importance of incorporating geometrical features of an instrument into a numerical formulation as exact as possible because every specific part influences the radiated acoustic vibration of the respective instrument and its specific timbre.

A significant example is the motion of the string. Even though the description of the transversal movement of the string is well understood mathematically, the string motion of each instruments differs in basic qualities. Like for instance the shape of the pulse after several periods or the decay characteristics of the sound. Hence, predicting the string motion without taking other information into account is impossible.

A second finding supporting the argument are the measurements of the banjo membrane. They show that the effects acting on the membrane can not be modelled by an analytical membrane and by linear adaptations. The banjo bridge and the back of the banjo have a non-linear influence on the frequency position of the visible mode shapes. Hence, both effects have to be implemented in a physical model, including the coupling of the bridge to the membrane as well as the air volume beneath the membrane. The measurements of the banjo bridge show that fine structure elements, like the special form of the bridge feet, have to be included in a numerical formulation. Due to the fact that the geometrical form influences the mechanical behaviour, the bridge influences acoustical vibrations of the banjo. Additionally, the measurements of the ruan show that geometrical constituents which supposedly are of minor importance, like the back plate of the instrument, have to be included in a formulation, because they can add spectral information to the radiated sound of the instrument. These arguments support the approach of this thesis: To model every specific feature of each instrument with greatest care. Only then, physically plausible results can be expected. This includes correct material properties and correct boundary conditions as well as couplings between the singular parts.

The two lessons that can be learned from the presented findings are 1) that it is impossible to model *the* string or *the* membrane but rather *a* string or *a* membrane, but 2) show us that the characteristic vibration responses of the respective instruments can aid us at the development of geometrically and acoustically *correct* formulations for one instrument. Because the string vibrations, membrane modes or soundboard radiations show such distinct characteristic for each instrument, it is possible to use these informations as *ground truths* and steady control items in the development of the models.

CHAPTER 3

NUMERICAL METHODS

$$x1 = x1 - x2$$

$$x2 = x1 + x2$$

(Iteration)

Physical modeling sound synthesis differs from other synthesis techniques in central aspects because laws of physics are applied to describe a system and, often using an iterative process, calculate its evolution over time by discretising one or several physical parameters characterising the system.

To this end, there exist a large variety of numerical methods that are used in physical modelling problems. In this section numerical methods that can be applied to compute physical models are presented and compared.

Before starting the considerations of numerical methods, a set of *guidelines* is developed to act as basis for decision-making for the selection of feasible methods for simulating musical instruments with finite differences in real-time on a FPGA or as close to real-time as possible on a PC.

As a point of departure, the 0-dimensional coupled mass-spring oscillator, also known as simple harmonic oscillator SHO, is chosen.¹

Thereafter, the method is exemplified on more complex models, like a stiff string with internal damping or a wooden plate with buckling and orthotropic material properties.

The numerical methods used in this thesis are derived in two ways: **a)**, from a mathematical point-of-view, in the form of a finite difference approximation of the analytic, continuous

¹The simple harmonic oscillator is the canonical introductory example for harmonic vibrations. See for instance: Fletcher and Rossing, *Physics of Instruments*, p. 4 or Hermann Haken: *Synergetik*, 2nd ed., Berlin, Heidelberg, New York, Tokio: Springer-Verlag, 1983, 115 ff. and multiple others.

3 Numerical methods

representation of the governing equation. **b**), a physically motivated derivation of the method is developed, by discretising the Newtonian and/or Hamiltonian equations of motion. This leads to a system of coupled ODEs comparable to a finite particle system.

Approach **a** can be labeled as the *classical* finite difference approach². For electromagnetic simulation this algorithm is known as the finite difference time domain approach (FDTD)³

Approach **b** is comparable to a lumped-system synthesis approach⁴ or particle method approach⁵

Even though both approximation methods make use of different assumptions in the derivation, they yield comparable numerical algorithms with differences mostly in regards to notation of variables. Thus, both approaches can be expressed in nearly identical form, as will be shown further below. After an introduction to finite difference methods, several time stepping methods, also known as time integrators, or simply integrators⁶, that are applied in this work to compute the evolution of finite difference approximations in time, are presented. Following this, basic properties of symplectic and multi-symplectic integrators (SI/MSI) are presented and a short on the mathematical background is given. After an error analysis of the numerical methods and some considerations regarding the stability of coupled problems, the basic form of the algorithm is extended to a Pseudo-Spectral finite difference formulation. The final form of the algorithm that is used for all real-time models is presented thereafter.

² Bilbao, *Numerical Sound Synthesis*. for a complete methodology for musical sound synthesis applications implementing this method.

³ See: Kane Yee: "Numerical solution of initial boundary value problems involving maxwell's equations in isotropic media", in: *IEEE Transaction on Antennas and Propagation* 14.3 (1966): 302–307 for an early work.

⁴ Bilbao, *Numerical Sound Synthesis*. pp. 9-10.

⁵ Donald Greenspan: "Discrete Mathematical Physics and Particle Modeling.", in: *IMACS European Simulation Meeting*, 1984: 39–46.

⁶ See: Hairer, Lubich, and Wanner, *Geometric numerical integration*. pp. 27ff.

3.1 Numerical Methods for Physical Modeling

Physical modeling (PM) for acoustical engineering applications can be classified by a comparison of their underlying rationale. Ideally, PM methods are a direct mapping of a certain object, which in this thesis are musical instruments, to a physical system which obeys our perceivable laws of classical mechanics, or Newtonian mechanics, and are describable by a set of equations, in most cases partial differential equations PDEs.

Because an analytical solubility of such a complex system is only given for simple cases, numerical methods are applied to solve the problem.

For modeling and synthesizing musical instruments, there are two differing methods commonly applied to solve the equations characterising a physical system numerically.

Type I methods : The first, and older methodology, works by discretising and iterating the state variables of a physical system, for mechanical problems this is mostly the deflection, stress-strain relationships or other forms of deformation. This approach is used in finite difference methods, finite element methods, boundary element methods to mention just a few.

Type II methods : These approaches can be labeled as traveling wave methods or scattering method. Instead of discretising the physical object, they aim at discretising a solution of the wave-equation, for instance the d'Alembert equation, which consists of two travelling waves in opposite directions, and iterate this solution in time. Among the most commonly used methods for physical based sound synthesis there are digital waveguide methods, digital filter methods and transmission line methods.⁷ An introduction and comparison of both methods is published in Bilbao.⁸

In this thesis, only methods of type I are employed, thus, the numerical schemes regarded in this thesis are just a small part of the multitude of numerical methods and schemes used in other works to discretise and iterate differential equations.

Even though the rationale behind most type I methods is comparable, there are several different classes of algorithms, that can be employed for similar numerical problems as presented in this thesis, having different characteristic properties. A short overview on several standard methods is presented in the following.

⁷Another not so common method is the wave digital filter method proposed by Alfred Fettweis, See: A. Fettweis: "Wave digital filters: Theory and practice", in: *Proceedings of the IEEE* 74.2 (Feb. 1986): 270–327. They are mentioned here because they can be used to efficiently compute digitised versions of analog circuits on FPGA hardware.

⁸Stefan Bilbao: "Wave and Scattering Methods for the Numerical Integration of Partial Differential Equation", phd, Stanford, California: Department of Electrical Engineering, Stanford University, May 2001.

3.1.1 Single-Step Methods

A widely applied class of methods to solve differential equations numerically are known as Runge-Kutta (RK) methods or RK schemes. RK schemes are named after the German mathematicians Carl Runge and Martin Wilhelm Kutta who developed the method at the beginning of the 20th century.⁹ The RK method is an umbrella term for a family of multiple schemes differing in their order. RK methods can be formulated explicitly as well implicitly to solve initial value problems of differential equations.

An extension to RK methods was developed by C. Butcher, who proposed the Butcher tableau as a tool to efficiently represent the coefficients of a RK scheme.¹⁰ The rationale behind RK methods draws on the idea that values on discrete grid points in an interval $[y_x, y_{x+\Delta x}]$ can be calculated by values from given grid points $u_x, u_{x+\Delta x}$ as well as s intermediate steps by evaluating

$$y_{x+\Delta x} = y_x + \Delta x \sum_{i=1}^s b_i k_i(y_x, y_{x+\Delta x}). \quad (3.1)$$

The coefficients b are the weights for the intermediate values k which are given as

$$k_i = f \left(t_x + \Delta x c_i, y_x + \Delta x \sum_{l=1}^s a_{il} k_l \right), \quad i = 1, \dots, s. \quad (3.2)$$

Schemes that can be classified as RK methods can be subdivided further into explicit and implicit methods. Explicit schemes with adaptable step size are the Fehlberg¹¹ scheme or the Heun-Euler scheme¹². Implicit methods that can be classified as RK schemes are Lobatto-Gauss¹³ schemes or Radau methods¹⁴.

A widely applied method in FEM computations is the Newmark-beta ($N\beta$) scheme, an implicit solution scheme. It is often utilised to compute the responses of structural mechanics problems.¹⁵ The idea of the $N\beta$ scheme is that the velocity (v) and the deflection (u) in the equations of motion can be computed as:

$$\begin{aligned} v(t + \Delta t) &= v(t) + \Delta t[(1 - \gamma)v_t(t) + \gamma v_t(t + \Delta t)] \\ u(t + \Delta t) &= u(t) + \Delta t v(t) + \Delta t^2 \left[\left(\frac{1 - 2\beta}{2} \right) v_t(t) + \beta v_t(t + \Delta t) \right] \end{aligned} \quad (3.3)$$

The accuracy and the stability can be aligned by parameters β and γ . A $N\beta$ -scheme with a

⁹ Hans Rudolf Schwarz and Norbert Köckler: *Numerische Mathematik*, 6., Wiesbaden: Treubner Verlag, 2006.

¹⁰ Walter Zulehner: *Numerische Mathematik*, Mathematik Kompakt, Basel: Birkhäuser Verlag, 2011, pp. 58-60.

¹¹ *ibid.*, p. 67.

¹² MS Chandio and AG Memon: "Improving the Efficiency of Heun's Method", in: *Sindh University Research Journal (Science Series)* 42.2 (2010): 85-88.

¹³ A. Aydın and B. Karasözen: "Symplectic and multisymplectic Lobatto methods for the 'good' Boussinesq equation", in: *Journal of Mathematical Physics* 49.8 (2008): NA.

¹⁴ <http://www.springerreference.com/docs/html/chapterdbid/333757.html>.

¹⁵ Bathe, *Finite-Element Methoden*, pp. 930-932.

constant acceleration can be constructed by setting $\beta = \frac{1}{4}$, a linear acceleration scheme is achieved by setting ($\beta = \frac{1}{6}$). In both cases the other constant is set to $\gamma = \frac{1}{2}$.

3.1.2 Multi-Step Methods

All previously mentioned methods are single step methods, meaning that only the calculated values of one preceding grid point ($t - 1$) and the grid point itself (t) are used for the calculation of the actual values of grid point (t). Multi-step methods, like the explicit Adams-Bashforth (AB) method or the implicit Adams-Moulton method, use the information of several previous steps in the calculation of a new grid value. Hence, the first iterated values of the algorithm are approximated by a different scheme¹⁶, until the number of grid points, depending on the order of the scheme, are calculated. The explicit AB method can be expressed in the following form

$$y(x + \Delta x) = y(x) + \Delta x \sum_{i=0}^{s-1} b_i f(t(x - i), y(x - i)), \quad (3.4)$$

with the coefficients b_i for the previous steps. The coefficients can be computed by using a Lagrange interpolation as

$$b_i = \frac{(-1)^i}{i!(s-i)!} \int_0^1 \prod_{j=0, j \neq i}^s (x + j) dx, \quad i = 0, \dots, s, \quad (3.5)$$

¹⁶Mostly the Euler scheme is applied for the initial step of the method.

3.2 Finite Difference Methods

The basic rationale behind finite difference methods is among the oldest techniques to solve analytical mathematics problems numerically. The idea can be found as early as 1687 in Newton's *Principia*¹⁷, works of Euler¹⁸ as well as other important works throughout the last 350 years.¹⁹ In this thesis, finite difference methods are used to solve Ordinary Differential Equations (ODE) and Partial Differential Equations (PDE) numerically using explicit schemes.

The numerical computation of structural mechanics problems that are expressible as PDEs or ODEs, is a central field of research in theoretical physics²⁰ and applied mathematics²¹. This means there is a large body of work regarding numerical solution methods for problems that can be solved with finite difference methods.

Canonical formulations of finite difference operators used in numerical mathematics and the appertaining calculus were formulated as early as 1860²². A notable work, that is often cited as the cornerstone of *modern* finite difference methods,²³ is the publication by Courant, Friedrichs, and Lewy.²⁴ It summarises basic properties of finite difference methods and formalises several traits of numerical schemes for DEs. In that treatise, a method for discretising continuous wave equations is presented and a convergence condition, later named CFL (Courant-Friedrich-Lewy) condition or CFL constant, is developed for spatial and time discretisation step widths. The CFL number (λ) can be defined as $\frac{c \cdot k}{h} = \lambda$, with c the wave velocity in the medium, k the discrete time-step and h the discrete spatial step-width. This number can be applied as a condition for stability and convergence properties of numerical finite difference schemes and is commonly used as an initial tool for assuring a valid selection of time and spatial step width sizes. A more thorough explanation follows below.

A step forward in the development of finite difference methods was the invention of the computer:

¹⁷See the historical remark in: Hairer, Lubich, and Wanner, *Geometric numerical integration*. P. 402 or Iantweddle: *James Stirling's Methodus Differentialis: An Annotated Translation of Stirling's Text*, Springer Verlag, 2003, p. 2.

¹⁸Leonhard Euler and John D. Balnton: *Foundations of Differential Calculus*, springer verlag, 2000.

¹⁹See the introduction of: Charles Jordan: *Calculus of Finite Differences*, new york, n.y.: Chelsea Publishing Company, 1950 or *ibid.*, 1 ff. Ernst Hairer, Christian Lubich, and Gerhard Wanner: "Geometric numerical integration illustrated by the Störmer/Verlet method", in: *Acta Numerica* 12 (2003): 399–450, p. 402.

²⁰Bathe, *Finite-Element Methoden*.

²¹Hairer, Lubich, and Wanner, *Geometric numerical integration*.

²²A first treatise regarding the calculus of finite differences is the first edition of: George Boole: *A Treatise on the Calculus of Finite Differences* -, 3rd ed., London: MacMillan and Company, 1880. Other works are mentioned in the introduction of: Jordan, *Calculus of Finite Differences*.

²³See the introduction of: Vidar Thomèe: "From finite differences to finite elements: A short history of numerical analyses of partial differential equations", in: *journal of computational and applied mathematics* 128.1-2 (2001): 1–54.

²⁴R. Courant, K. Friedrichs, and H. Lewy: "Über die partiellen Differenzgleichungen der mathematischen Physik", in: *Mathematische Annalen* 100.1 (1928): 32–74.

3 Numerical methods

For time-dependent problems considerable progress in finite difference methods was made during the period of, and immediately following, the Second World War, when large-scale practical applications became possible with the aid of computers.

25

Since that time, there has been very active research regarding properties and the applicability of finite difference methods. A dominating interest in early works was a thorough definition of stability conditions for finite difference schemes²⁶. From this time on, finite difference methods have proven to be a stable tool for solving linear and non-linear²⁷ DEs.

Today, finite difference methods are applied in various areas of science to solve numerical problems. These range from medical engineering²⁸, to molecular dynamics²⁹. Finite difference methods are applied in fluid simulations³⁰ or physically based graphics simulations³¹, they are applied for simulations in Nanotechnology and Optoelectronics³².

One important factor fuelling the increasing usage of finite difference methods in the last decade is the rising computational power and the steadily advancing computational throughput in the giga-FLOP/tera-FLOP³³ range, on easily accessible, conventional personal computers.³⁴ A trend that is still continuing, even though the focus of current research lies more on developing dedicated co-processor platforms or parallel structures than on the mere acceleration of CPUs.³⁵ This led to an increasing research interest in stable and robust finite difference algorithms over the last twenty years³⁶. In musical acoustics, FD methods are utilised as a numerical tool since the late 1950s³⁷ at least.

²⁵Thom e, "Short history of finite differences".

²⁶As for instance in the works of Lax and Wendroff P.D. Lax and Richtmyer R.D.: "Survey of the stability of linear finite difference equations", in: *Communications on Pure and Applied Mathematics* 9 (1956): 267–293 or the works of Richtmyer, who formalised the CFL condition as a stability analysis measure.

²⁷For instance the Korteweg-de-Vries equations as found in: B. Fornberg: *A practical guide to pseudospectral methods*, vol. 1, Cambridge university press, 1998, p. 130.

²⁸Z. Jackiewicz, B. Zubik-Kowal, and B. Basse: "Finite-Difference and Pseudo-Spectral Methods for the Numerical Simulations of In Vitro Human Tumor Cell Population Kinetics", in: *Mathematical Biosciences and Engineering* 6.3 (2009): 561–572.

²⁹Loup Verlet: "Computer "Experiments" on Classical Fluids. I. Thermodynamical Properties of Lennard-Jones Molecules", in: *Phys. Rev.* 159.1 (July 1967): 98–103.

³⁰N. Foster and D. Metaxas: "Realistic animation of liquids", in: *Graph. Models Image Process.* 5.58 (1996): 471–483.

³¹See the section on finite difference methods in: Andrew Nealen et al.: "Physically Based Deformable Models in Computer Graphics", in: *Computer Graphics Forum* 25.4 (Dec. 2006): 809–836.

³²Fernando L. Teixeira: "FDTD/FETD Methods: A Review on Some Recent Advances and Selected Applications", in: *J. of Microwaves and Optoelectronics* 6.1 (2007): 83–95.

³³Floating Point Operations per Second. See: R. Weitowitz and K. Urbanski: *Digitaltechnik*, 5th ed., Berlin, Heidelberg: Springer, 2007, p. 352.

³⁴A current consumer graphics card, a Nvidia GeForce GTX 770 has a theoretically processing power of 3,3 tera-FLOPS which is in the range of supercomputers of the late 90s. See: <http://www.top500.org/lists/1999/06/>.

³⁵More on this in chapter 5.

³⁶Hairer, Lubich, and Wanner, *Geometric numerical integration*.

³⁷Bilbao, *Numerical Sound Synthesis*. P. 2.

3 Numerical methods

An overview of physical modeling and related signal processing applications is presented in the works of Zölzer et al.,³⁸ Bilbao,³⁹ K.-D. Kammeyer⁴⁰ or in Välimäki et al.⁴¹

An early treatise in the field of musical acoustics and musical sound synthesis is the work of Hiller and Ruiz (1971)⁴². In their work, a finite difference method is applied to solve the wave equation for sound synthesis. Following their work, throughout the 1970s and 1980s, there were several works in the field of musical synthesis or musical acoustics that utilised finite difference methods comparable to the earlier attempts by Hiller and Ruiz. Notable works include Bacon and Bowsher,⁴³ who presented a model of a struck string solved with finite differences or Boutillon,⁴⁴ who presented a physical model of a piano hammer. A work, which can be viewed as a stepping stone in regards to model accuracy and refinement of the physical parameters is the work by Askenfeld and Chaigne (1994)⁴⁵. Since that time, the increasing number of publications shows the rising interest in finite difference methods for physical models of musical instruments. These works include physical models for such diverse instruments as the guitar⁴⁶, piano⁴⁷, banjo⁴⁸, ruan⁴⁹, trumpets⁵⁰ and others.

An analysis and comparison of the results of the mentioned works shows some recurring statements which can be summarised as follows⁵¹:

1. Finite difference models are straight-forward to implement, compared to other numerical methods like finite element methods or boundary element methods.

³⁸Udo Zölzer et al.: *DAFX: Digital Audio Effects*, ed. by Udo Zölzer, John Wiley & Sons, May 2002.

³⁹Bilbao, *Numerical Sound Synthesis*.

⁴⁰K.-D. Kammeyer, *Digitale Signalverarbeitung*.

⁴¹Vesa Välimäki et al.: "Model-Based Sound Synthesis", in: *EURASIP Journal on Applied Signal Processing*, Hindawi Publishing Corporation, 2004.

⁴²Lejaren Hiller and Pierre Ruiz: "Synthesizing Musical Sounds by Solving the Wave Equation for Vibrating Objects: Part 1", in: *J. Audio Eng. Soc.* 19.6 (1971): 462–470; Lejaren Hiller and Pierre Ruiz: "Synthesizing Musical Sounds by Solving the Wave Equation for Vibrating Objects: Part 2", in: *J. Audio Eng. Soc.* 19.7 (1971): 542–551.

⁴³R. A. Bacon and J. M. Bowsher: "A Discrete Model of a Struck String", in: *Acta Acustica united with Acustica* 41.1 (1978): 21–27.

⁴⁴Xavier Boutillon: "Model for piano hammers: Experimental determination and digital simulation", in: *The Journal of the Acoustical Society of America* 83.2 (1988): 746–754.

⁴⁵Antoine Chaigne and Anders Askenfeldt: "Numerical simulations of piano strings. I. A physical model for a struck string using finite difference methods", in: *The Journal of the Acoustical Society of America* 95.2 (1994): 1112–1118; Antoine Chaigne and Anders Askenfeldt: "Numerical simulations of piano strings. II. Comparisons with measurements and systematic exploration of some hammer-string parameters", in: *The Journal of the Acoustical Society of America* 95.3 (1994): 1631–1640.

⁴⁶Rolf Bader: "Complete Geometric Computer Simulation of a Classical Guitar", in: *Lay-Language paper of the American Acoustical Society 05* (2005), http://www.aip.org/149th/bader_Guitar.htm.

⁴⁷Boutillon, "Model for piano hammers: Experimental determination and digital simulation" or more recently Juliette Chabassier and Antoine Chaigne: "Modeling and numerical simulation of a nonlinear system of piano strings coupled to a soundboard", in: *Proceedings of 20th International Congress on Acoustics*, 2010.

⁴⁸F. Pfeifle and R. Bader: "Musical Acoustics, Neurocognition and Psychology of Music", in: Frankfurt am Main, Germany: Rolf Bader, 2009: 71–86

⁴⁹F. Pfeifle and R. Bader: "Measurement and physical modelling of sound hole radiations of lutes", in: *J. Acoust. Soc. Am.* 130.4 (2011): 2507–2507.

⁵⁰Bilbao, *Numerical Sound Synthesis*.

⁵¹The following list is mainly based on: *ibid.*, pp. 17–18; Välimäki et al., "Model-Based Sound Synthesis".

3 Numerical methods

2. Finite difference models can yield realistic sound quality and accurate motion simulations.
3. Finite difference formulations are intuitive.
4. Finite difference models have a high computational cost compared to other physics based methods like filters.
5. The Stability of finite difference algorithms is an important criterion regarding the usability of the method for the problem under consideration.

Based on these findings, several requirements for real-time physical modeling sound synthesis of musical instruments, and the demands it poses on a numerical method shall be formulated in the following:

1. The error must be reasonably small over the audible frequency range:

Because the ear is proficient in detecting subtle differences and errors in time varying signals, it is important that there are no artificial components in the spectrum added by a numerical method.

2. Solutions to long-time behaviour must be as accurate as possible:

A numerical method should be able to produce results that are accurate for arbitrarily long simulation times, at best.

3. The algorithm should be stable over a large time and frequency range:

A numerical method should produce stable results over the audible frequency range and ideally an infinitely long simulation time.

4. All physical parameters should be accessible at any point of the simulation:

A numerical method should facilitate the possibility to interact with important parameters of the model, like coupling or internal material constants.

5. The computational cost should be as small as possible and assessable up front in terms of resource utilisation and timing constraints:

Real-time implementations of numerical methods require an accurate knowledge of the internal timing and an overview on the required hardware resources.

With this set of requirements, purposeful guidelines to find a feasible method for modelling the acoustically relevant properties of musical instruments are given. To add one more requirement to the numerical method, one has to recapitulate the basic physical principles of Newtonian mechanics.

Most musical instruments can be described in terms of classical mechanics as coupled (linear or non-linear) system governed by coupled ODEs and PDEs⁵². Compared to other, more advanced mechanical systems, they can be described using Newtons equation of motion to a high degree of accuracy⁵³, because the defining physical parameters are directly accessible and are well understood regarding their influence on the acoustic vibrations of the respective instrument.

In most cases, acoustical phenomena can be described by one of the various forms of the wave equation of differing order and dimension, and the equations of motion are directly deducible from these equations, using Newton's fundamental theorems. Newton's second axiom states that forces are only dependent on the position and on the velocity⁵⁴. Thus, we can describe the underlying system by using the equations of motion to a high degree of accuracy if we know these two physical values. To summarise this thought: it is favourable to use numerical schemes which include formulations for the deflections, velocities and forces in an explicit form for every discrete sampling point in space and time.

3.2.1 Finite difference approximations

Finite difference approximations can be derived by using a Taylor series approach, which follows the assumption that any point $f(x_i)$ of a function $f(x)$, given that the function is well-defined, can be approximated by a Taylor series expansion. Using this series, finite difference expressions for differential terms can be deduced by approximating a continuous function with a Taylor series expansion, which allows us to approximate the value of a function $f(x)$ at position $x = x_0 + h$ by

$$f(x_0 + h) = f(x_0) + h \cdot f(x_0)_x + \frac{h^2}{2!} \cdot f(x_0)_{xx} + \frac{h^3}{3!} \cdot f(x_0)_{3x} + \frac{h^4}{4!} \cdot f(x_0)_{4x} + O(h^5) \quad (3.6)$$

with the Landau Symbol O , approximating the remainder term and the subscript x indicating a derivation by x . For now, we are only interested in the linear terms, so we strip equation 3.6 and reorder it to $f(x_0)_x$ to get

$$f(x_0)_x = \frac{-f(x_0) + f(x_0 + h)}{h} + O(h). \quad (3.7)$$

⁵² Philip M. Morse and K. Uno Ingard: *Theoretical Acoustics*, Princeton University Press, 1968; Fletcher and Rossing, *Physics of Instruments*; Bader, "Complete Geometric Computer Simulation of a Classical Guitar".

⁵³ Some musical instruments show effects that can only be explained by statistical methods, like the synchronisation of organ pipes. See: Abel, Bergweiler, and Gerhard-Multhaupt, "Synchronization of organ pipes: experimental observations and modeling".

⁵⁴ In the case of a conservative field-the velocity. See: F. Kuypers: *Klassische Mechanik*, 8th ed., Weinheim: Viley-VHC, 2008, p. 6.

This is called a forward approximation of the derivative $f(x_0)_x$ at the point x . Approximating $f(x_0 - h)$ in the same manner gives an expression for a backward difference of derivative $f(x_0)_x$

$$f(x_0)_x = \frac{f(x_0) - f(x_0 - h)}{h} + O(h). \quad (3.8)$$

If equations 3.7 and equation 3.8 are combined, we obtain an expression for centered finite differences around point x

$$f(x_0)_x = \frac{f(x_0 + h) - f(x_0 - h)}{2 \cdot h} + O(h^2). \quad (3.9)$$

It is important to note that the order of the error is quadratic instead of linear when using centered finite difference approximations.⁵⁵ In the remainder of this work, centered finite difference approximations are used if applicable because of the smaller error term introduced by the discretization. The approximation of a derivative of a continuous function at a given grid (sample) point, presented here, is the basic rationale behind all finite difference schemes used in this thesis.

3.2.2 Finite Difference Operators

There are several standard finite difference operators which are commonly used in many works as well as in this thesis. A classical central difference approximation of a first order differential expression was presented above. The notation of finite difference approximations can be condensed to an operator notation. This generalized operator notation is applied throughout the remainder of this thesis. It is based on the notation used in works like Jordan,⁵⁶ Strikwerda⁵⁷ and Bilbao.⁵⁸

A discrete shift operator acting on a 1-dimensional function \mathbf{y} at position x and time instant t is indicated by τ with

$$\begin{aligned} \tau_{t-}(y(t, x)) &= y(y - \Delta t, x) \text{ or} \\ \tau_{x-}(y(t, x)) &= y(t, x - \Delta x) \end{aligned} \quad (3.10)$$

and $\Delta t, \Delta x$ the discrete step width in the temporal or spatial dimension respectively. A difference approximation in the forward (+) and backward (−) direction at discrete position i can thus be written as

⁵⁵For first derivatives employing a two-point stencil, the centered finite difference approximation has a frequency limitation, reducing the usable bandwidth as shown in: Terry A. Bahill, Jeffrey S. Kallman, and Jon E. Liberman: “Frequency Limitations of the Two-Point Central Difference Differentiation Algorithm”, in: *Biological Cybernetics* 45 (1982): 1–4.

⁵⁶Jordan, *Calculus of Finite Differences*.

⁵⁷J. Strikwerda: *Finite difference schemes and partial differential equations*, 2nd ed., Philadelphia: SIAM, 2005.

⁵⁸Bilbao, *Numerical Sound Synthesis*.

$$\delta_{x+}\mathbf{y}|_i = \frac{1}{\Delta x}(y(i + \Delta x) - y(i)) = \frac{1}{\Delta x}(\tau_{x+} - 1)\mathbf{y}, \quad (3.11)$$

$$\delta_{x-}\mathbf{y}|_i = \frac{1}{\Delta x}(y(i) - y(i - \Delta x)) = \frac{1}{\Delta x}(1 - \tau_{x-})\mathbf{y}. \quad (3.12)$$

Higher order operators can be derived by combining first order operators as

$$\delta_{xx} = \delta_{x+} \cdot \delta_{x-} \quad (3.13)$$

Expanding both operators leads to

$$\begin{aligned} \delta_{xx} &= \delta_{x+} \cdot \delta_{x-} = \frac{1}{\Delta x}(\tau_{x+} - 1) \cdot \frac{1}{\Delta x}(1 - \tau_{x-}) \\ &= \frac{1}{\Delta x^2}(-1 + \tau_{x-} + \tau_{x+} - \tau_{x-}\tau_{x+}) \end{aligned} \quad (3.14)$$

with $\tau_{x-}\tau_{x+} = 1$ this can be rewritten as

$$\delta_{xx} = \frac{1}{\Delta x^2}(\tau_{x-} - 2 + \tau_{x+}), \quad (3.15)$$

which is a second order centered difference in operator notation. Higher order operators can be constructed in a similar fashion.

Finite difference operators can also be thought of as weights at the respective grid locations. Meaning, for an approximation of a differential function the actual grid node, where the derivative is calculated, is taken into account as well as several adjacent grid points to calculate the derivative, depending on the order of the approximation and the order of the differential operator. These weights can be calculated using the discrete grid and the respective order of differential equation.

Taylor Series Derivation

All finite difference operators used in this thesis can be derived from a Taylor series expansion around a point i or as a series of first order differences. Take for example the second derivative of y in respect to x , remember that we can write the second derivative of a function at point i as two first derivatives⁵⁹

$$y_{xx}|_i = (y_x)_x|_i. \quad (3.16)$$

Now it is possible to combine the first order backward difference (equation 3.8) and the first order forward difference (equation 3.7) to get the centered finite difference expression of

⁵⁹We suppose the function is analytic, meaning continuous and well defined around i .

3 Numerical methods

second order. Replacing the differential with a finite difference expression we obtain

$$(y_x)_x|_i \approx \frac{-\frac{y(i-\Delta x)+y(i)}{\Delta x}|_i + \frac{-y(i-\Delta x)+y(i)}{\Delta x}|_{i+\Delta x}}{\Delta x}. \quad (3.17)$$

If we now reorder this equation we get

$$(y_x)_x|_i \approx \frac{1}{\Delta x^2} \cdot (y(i-\Delta x) - 2 \cdot y(i) + y(i+\Delta x)) = \delta_{xx}, \quad (3.18)$$

which is the finite difference equation for the second order differential equation in *standard* notation. Higher order approximations can be derived by taking higher order terms of the Taylor expansion into account⁶⁰. Difference operators of higher dimension can be approximated accordingly by a Taylor series expansion.⁶¹

Padé/Lagrange Series Derivation

Even though the derivation with Taylor series is a robust method for calculating finite difference weights, it has one drawback. It can only be applied for regular, equidistantly spaced grids. As an extension to this basic derivation of finite difference weights, Fornberg⁶² presents an algorithm, based on a Padé approximant⁶³ and Lagrange interpolation polynomial which can be used to calculate finite difference weights of arbitrary order and accuracy, only limited by the lower bounds of the digital number representation. This algorithm is published in FORTRAN⁶⁴ and translated to C and MATLAB over the course of this thesis. All finite difference weights used in this work are calculated with these functions.

The idea of this algorithm is to approximate the finite difference weights by either a Padé polynomial approximant⁶⁵ or a Lagrange interpolation polynomial⁶⁶.

A Padé series can be used to approximate a function f that can be approximated by a power series

$$f(z) = \sum_{k=0}^{\infty} c_k z^k \quad (3.19)$$

⁶⁰A one-dimensional second order centered finite difference stencil is presented in 3.6, higher order weights can be derived in a similar way.

⁶¹Higher order finite difference operators are derived in: Bathe. (Bathe, *Finite-Element Methoden*, p. 159)

⁶²B. Fornberg: "Calculation of weights in finite difference formulas", in: *SIAM Rev.* 40.3 (1998): 685–691.

⁶³A Padé approximation is also derived from a Taylor approximation.

⁶⁴B. Fornberg: "Generation of finite difference formulas on arbitrarily spaced grids", in: *Math. Comput* 51.184 (1988): 699–706.

⁶⁵For the case of equispaced grids

⁶⁶For arbitrarily spaced grids.

3.3 Finite Difference Time Domain Methods

In this section, a short introduction to the Finite Difference Time Domain (FDTD) method is given. It is commonly used in room acoustics⁶⁷ and implemented as solution method in many other fields of numerical simulations. In instrument acoustics, it is applied in the works of Askenfelt and Jansson⁶⁸, Boutillon⁶⁹ or, most prominently, in works like Bilbao,⁷⁰ Bilbao⁷¹ and Bilbao.⁷² At first, the numerical solution for a simple harmonic oscillator is presented. Afterwards this method is applied to solve the differential equation of a damped linear string numerically.

3.3.1 0-dimensional Wave Equation

In mechanical physics, a simple example of a harmonic oscillator is a 0-dimensional (point-) mass m coupled to a massless spring with a spring constant k , indicating the linear stiffness of the spring. This system is often referred to as a mass-spring model⁷³ or a simple harmonic oscillator⁷⁴. The governing equation for the force acting on the oscillating mass can be written as

$$F_{osc} = -k \cdot x \quad (3.20)$$

with F_{osc} the restoring force of the system, k the stiffness of the massless spring and x the deflection of the mass relative to equilibrium as depicted in Figure 3.1. Equation 3.20 is also known as *Hooke's Law*⁷⁵ and is one of the fundamental laws of physics, which finds application in such diverse fields as molecular dynamics⁷⁶.

⁶⁷It is used since the late 1960s and was first proposed by Yee, "Numerical solution of initial boundary value problems involving Maxwell's equations in isotropic media" to solve Maxwell's equation for electro-magnetic waves.

⁶⁸Anders Askenfelt and Erik V. Jansson: "From touch to string vibrations. II: The motion of the key and hammer", in: *The Journal of the Acoustical Society of America* 90.5 (1991): 2383–2393.

⁶⁹Boutillon, "Model for piano hammers: Experimental determination and digital simulation".

⁷⁰Bilbao, "Robust Physical Modeling Sound Synthesis for Nonlinear Systems".

⁷¹Bilbao, *Numerical Sound Synthesis*.

⁷²Stefan Bilbao: "Conservative numerical methods for nonlinear strings", in: *The Journal of the Acoustical Society of America* 118.5 (2005): 3316–3327.

⁷³Kuypers, *Klassische Mechanik*

⁷⁴See chapter 3 (pp. 45-77) of: Bilbao, *Numerical Sound Synthesis*.

⁷⁵The dictum at the beginning of this chapter was first published by Hooke as an Latin anagram *ceiiinosssttuv* in 1660. The solution of the anagram was published in 1678.

⁷⁶Massimo Blasone and Petr Jizba: "Quantum mechanics of the damped harmonic oscillator", in: *Can. J. Phys.* 80 (2002): 645–660 or solid mechanics Vitali F. Nesterenko: *Dynamics of Heterogeneous Materials*, ed. by Lee Davidson and Yasuyuki Horie, Springer-Verlag, 2001.

3 Numerical methods

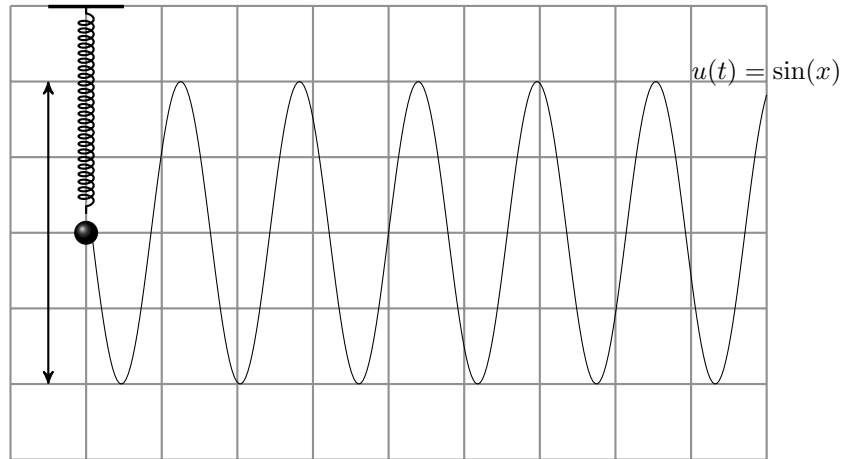


Figure 3.1: Oscillating mass-point.

To derive the equations of motion, Newton's second axiom $F = p_t$ can be applied. p is the impulse (or the momentum) of mass m , the subscript t denotes a derivation by time⁷⁷. If the mass is constant over time, one can rewrite equation 3.20 into following form:

$$F_{osc} = p_t = m \cdot a = -k \cdot x. \quad (3.21)$$

From classical physics, we know that the acceleration a is the second derivative of the deflection by time. With this, equation 3.21 can be written as:

$$F_{osc} = m \cdot a = -k \cdot x \Leftrightarrow x_{tt} = -\frac{k}{m} \cdot x. \quad (3.22)$$

From basic analysis, we know that an analytical solution to this Ordinary Differential Equation (ODE) can be a trigonometric function. If we set $x = \sin(\omega \cdot t)$, we get the expected solution

$$x_{tt} = -\omega^2 x. \quad (3.23)$$

A comparison of coefficients shows that the right hand side multiplicand is $\frac{k}{m} = \omega^2$. A straight-forward way to find a numerical solution to this problem is the approximation of the differential expression on the left hand side of equation 3.22 with a centered finite difference term⁷⁸ as developed in section 3.2:

$$x_{tt} \approx \frac{x(t - \Delta t) - 2 \cdot x(t) + x(t + \Delta t)}{\Delta t^2}. \quad (3.24)$$

⁷⁷In most classical physics textbooks the derivative by time is indicated by a *dot* superscript. In this work we follow the index notation which is commonly used in the scope of finite difference related work Jordan, *Calculus of Finite Differences*. The notation for derivatives can be written as $x_t \equiv \dot{x} \equiv \frac{\partial x}{\partial t} \equiv \frac{dx}{dt}$. The last two cases are the differential operators for partial differential equations (PDE) and ordinary differential equations (ODE).

⁷⁸Schwarz and Köckler, *Numerische Mathematik*, Bilbao, *Numerical Sound Synthesis*.

3 Numerical methods

Inserted into equation 3.22 yields

$$\frac{x(t - \Delta t) - 2 \cdot x(t) + x(t + \Delta t)}{\Delta t^2} = -c^2 \cdot x. \quad (3.25)$$

with $c = \sqrt{\frac{k}{m}}$. Now one can rewrite equation 3.25 into the recursive form

$$x(t + \Delta t) = -c_{acc} \cdot x(t) \cdot \Delta t^2 - x(t - \Delta t) + 2 \cdot x(t) = \kappa \cdot x(t) - x(t - \Delta t) \quad (3.26)$$

with $acc = -c^2 \cdot \Delta t^2 + 2$. The values for $x(t + \Delta t)$ depend only on the values of $x(t)$, κ and $x(t - \Delta t)$. This means, the deflection of the oscillating mass-point can be calculated by applying an constant deflection for the time steps $t = 0 - \Delta t$ and $t = 0$. Rewritten in a computable pseudo-code the algorithm looks like:

1. With the given constant κ and the deflection of the mass at point of time t and $t - \Delta t$, compute the next time step $t + 1$.
2. Set the value of the calculated deflection $x(t + 1)$ to the variable $x(t)$ and the value of $x(t)$ to the variable $x(t - 1)$. Then return to step 1.

Resulting Waveforms

A plot of the deflection over time is shown in Figure 3.1. As expected, the deflection has a sinusoidal characteristic.

Analysis of the Algorithm

A short analysis of algorithm 3.26 shows that an explicit expression for the deflection at each discrete instant of time is computed. The two terms on the right side $x(t) - x(t - \Delta t)$ are related to a backward finite difference approximation of the velocity⁷⁹ and the other term $-c_{acc}x(t)$ is related to the force expression of the SHO⁸⁰. This shows that the deflection, the velocity and the acceleration are represented in this equation, but are not explicitly given.

Regarding the set of rules, developed at the beginning of this chapter, this poses one fundamental problem when using this algorithm: The physical values velocity and acceleration are not accessible in an explicit way

In the scope of physical modeling of musical instrument acoustics, this is the main drawback of the FDTD method. Mechanically coupled systems can be fully described by the equations of motion and Newtonian mechanics, by a coupling of impedances or a coupling of acting forces, omitting the need for finding a monolithic formulation of the whole geometry. In the

⁷⁹Velocity $v = \dot{x}_t \approx \frac{x(t) - x(t-1)}{\Delta t}$.

⁸⁰With $F_{osc} = -k \cdot x$

presented form of the FDTD algorithm, despite its simplicity and elegance, a straight forward coupling of singular parts is not possible.

3.3.2 1-Dimensional Wave Equation

In this section a FDTD scheme for the 1-dimensional wave equation for a linear, velocity damped string is presented.

Numerical Solution of a Linear String

As seen in chapter 2, the differential equation of the linear string is a partial differential equation of the following form

$$\mathbf{u}_{tt} = c^2 \cdot \mathbf{u}_{xx} , \quad (3.27)$$

with the already introduced constant $c = \sqrt{\frac{T}{\sigma}}$. As before, both differential terms can be discretised by finite difference approximations. For this example, second order centered finite differences are used, yielding following equation

$$\frac{u(x, t + \Delta t) - 2 \cdot u(x, t) + u(x - \Delta t)}{\Delta t^2} = c^2 \cdot \frac{u(x + \Delta x, t) - 2 \cdot u(x, t) + u(x - \Delta x, t)}{\Delta x^2} . \quad (3.28)$$

Rearranging this equation into a recursive form yields:

$$u(x, t + \Delta t) = c_{acc} \cdot [u(x + \Delta x, t) - 2 \cdot u(x, t) + u(x - \Delta x, t)] + 2 \cdot u(x, t) - u(x, t - \Delta t), \quad (3.29)$$

with $c_{acc} = \frac{c^2 \cdot \Delta t^2}{\Delta x^2}$.

Resulting Time Series

The algorithm is iterated in time, utilising the same method as presented before. More precisely, calculating the value for $t + 1$, reassigning the values for t and $t - 1$ and continuing the computation. Figure 4.2 shows the movement of the string for several time steps resulting from a triangular deflection. Figure 4.3 shows a time series of the string over five seconds. In the next Figure 4.4, the spectrum of the time series is shown. In Figure 4.5, one can see a moving Gauss impulse starting at a centered position. In Figure 4.6, time series of different damped strings are shown.

Analysis of the Algorithm

An analysis of the algorithm reveals three terms that are related to physical properties. A formulation for the acceleration is recognisable in the term $c_{acc} \cdot [u(x + \Delta x, t) - 2 \cdot u(x, t) +$

$u(x - \Delta x, t)]$ ⁸¹. The other terms are related to a backward approximation of the velocity.
⁸² In concordance to the algorithm of the 0-dimensional harmonic oscillator, all physical quantities represented in the equations of motion are recognisable, but only the deflection is computed explicitly.

3.3.3 Considerations Regarding the FDTD Method

In contrast to many positive features of FDTD methods, like the intuitive formulation and the explicit formulation for the deflection, there is a drawback: Two physical quantities that are important to describe the equations of motion in Newtonian mechanics are not calculated explicitly: The acceleration and the velocity. This limitation coerces one to find formulations for a complete instrument body in monolithic form, which, in most cases, proves to be challenging or even impossible. As already stated, the coupling of the instruments parts can be described by Newtonian forces. This means, if one can calculate these quantities explicitly, one can describe complete instruments as a system of coupled differential equations. As we will see in this chapter, it is easier to find formulations for coupled geometry models, when these properties are know. This is the main reason why for most parts of the physical models, the method described in the next section is applied. As we will see later in this chapter, using another time discretisation and time iteration method for finite difference models, results in a compact formulation of finite difference physical models of musical instruments.

3.4 Discretising the Equations of Motion

In the next section, a finite difference time stepping algorithm is derived taking basic physical laws into account. It is built upon the discretisation of Newton's equation of motion and integrating them numerically. This method is directly linked to the earliest known methods applied to solve the equations of motion.⁸³

As shown in section , one way of discretising a PDE with a finite difference approximation in dimensions > 0 can be achieved, when the differential expressions of the PDE are replaced by difference expressions. At this point, a different route is taken, by starting with a discrete expression to derive the equations of motion for a discrete point (mass point) and a quasi particle on a 1-dimensional string.⁸⁴

⁸¹Comparing the linear undamped wave equation for the string $u_{tt} = c^2 u_{xx} \approx \delta_{xx} u$.

⁸²Velocity = $x_t \approx \delta_{t-}$.

⁸³Newton used the method to solve the three body problem for planetary movement, known as the Kepler problem, in his *Principae*. See: Hairer, Lubich, and Wanner, *Geometric numerical integration*.

⁸⁴The 1-dimensional wave equation can be derived in this manner as shown by Lagrange and many others in Pierce (A.D. Pierce: *Acoustics*, New: McGraw, 1981) by taking the limit of the discrete formulation for the 1-dimensional wave equation.

3.4.1 0-Dimensional Equations of Motion

In this section, a time stepping algorithm for the 0-dimensional oscillating mass point is derived from the Newtonian equations of motion. For this, we use the assumption that acoustical vibrations fundamentally obey Newton's second law of motion. Under the premise that the force is a function of deflection, velocity and time

$$F = f(x, x_t, t). \quad (3.30)$$

we can formulate the equations of motion for a mechanical system by considering the acting forces and integrate the resulting function in time by employing an appropriate (numerical) integration method. Using a Hamiltonian formalism, the globalised position coordinate q and the globalised impulses p , the equations of motion can be written in the following form

$$\begin{aligned} p_t &= -H_q(p, q) \\ q_t &= H_p(p, q). \end{aligned} \quad (3.31)$$

with H_p, H_q a differentiation by p or q respectively. Inserting the Hamiltonian H for the oscillating mass-point, $H = T(p) + V(q) = \frac{p^2}{2m} + \frac{1}{2}k \cdot q^2$, to equation 3.31 yields following equation

$$\begin{aligned} p_t &= -k \cdot q \\ q_t &= \frac{p}{m}. \end{aligned} \quad (3.32)$$

Comparing equations 3.32 with 3.34 one can see that the formulation for the acceleration a is comparable to the formulation of the time differentiated global impulse p_t , only differing in the inclusion of the mass in the Newtonian formulation.

Discretising the Newtonian Equations of Motion

The discretisation of equation 3.34 is straightforward. The velocity of can be approximated by a backward step as the limit

$$v(t + \Delta t) = \lim_{\Delta t \rightarrow 0} \frac{x(t + \Delta t) - x(t)}{\Delta t}. \quad (3.33)$$

The same can be done for the acceleration with a forward step

$$a(t) = \lim_{\Delta t \rightarrow 0} \frac{v(t + \Delta t) - v(t)}{\Delta t}. \quad (3.34)$$

3 Numerical methods

Letting the time step $\Delta t = \frac{1}{\text{SampleFrequency}}$ be a discrete value > 0 , equation 3.33 can be reordered to

$$x(t + \Delta t) = v(t) + x(t), \quad (3.35)$$

and equation 3.34 to

$$v(t + \Delta t) = v(t) + a(t). \quad (3.36)$$

With this two steps we can rewrite the continuous algorithm, using the basic equations of motion for Newtonian systems into the following form

$$\begin{aligned} a(t) &= -k \cdot x(t) \\ v(t + \Delta t) &= v(t) + a(t) \cdot \Delta t \\ x(t + \Delta t) &= x(t) + v(t + \Delta t) \cdot \Delta t. \end{aligned} \quad (3.37)$$

When algorithm 3.53 is implemented numerically, it yields an output for the deflection (blue), velocity (black) and the acceleration (red) given in Figure 3.2, as expected, all three physical values show sinusoidal behaviour. The phase between all three is 90 degrees. The acceleration is 90 degrees behind the velocity which is 90 degrees behind the deflection.

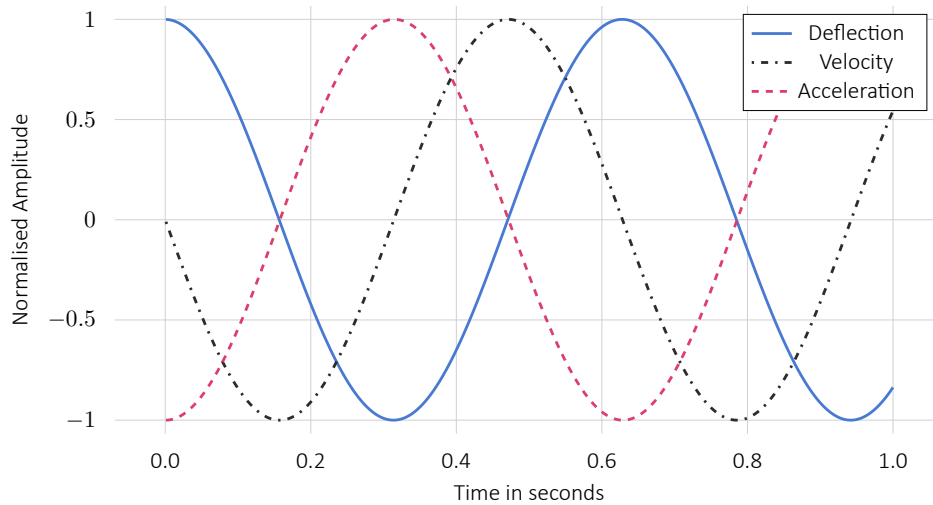


Figure 3.2: Output of algorithm 3.53.

As visible in Figure 3.2, the three-step algorithm 3.37 calculates three physical parameters: The acceleration, the velocity and the deflection of the oscillating mass-point explicitly for every sample point. In the presented form, the algorithm is also known as *Symplectic Euler* algorithm and is a mixture of the explicit Euler time step for the deflection, and an implicit Euler time step for the velocity. In difference to the explicit Euler, which has an growth in energy over time, and the implicit Euler, which loses energy over time, the symplectic Euler does not vary in its energy balance as further elucidated in section 3.5. Another multi-step

3 Numerical methods

method which computes the velocity and the deflections from Newton's equations of motion, is known as *Beeman's algorithm*⁸⁵, which can be formulated as

$$\begin{aligned}u(t + \Delta t) &= u(t) + v(t)\Delta t + \frac{1}{6}(4a(t) - a(t - \Delta t))\Delta t^2 \\v(t + \Delta t) &= v(t) + \frac{1}{6}(2a(t + \Delta t) + 5a(t) - a(t - \Delta t))\Delta t.\end{aligned}\tag{3.38}$$

Here u , v are the deflection and velocity respectively and a is the acceleration.

This algorithm is comparable to the Velocity-Verlet algorithm, presented in this section because it computes the deflection and the velocity explicitly. In contrast to the NVS scheme, it has a higher computational complexity as will be elucidated further below.

Algorithms applied to compute the equations of motion are used in various fields of physical simulations like for instance in molecular dynamics⁸⁶, fluid dynamics or particle-simulation⁸⁷.

⁸⁵D. Beeman: "Some multistep methods for use in molecular dynamics calculations", in: *Journal of Computational Physics* 20.2 (1976): 130–139.

⁸⁶S.K. Gray, D.W. Noid, and B.G. Sumpter: "Symplectic integrators for large scale molecular dynamics simulations: A comparison of several explicit methods", in: *The Journal of chemical physics* 101 (1994): 4062.

⁸⁷Verlet, "Computer "Experiments" on Classical Fluids. I. Thermodynamical Properties of Lennard-Jones Molecules".

Discretising the Hamiltonian Equations of Motion

Similar to the discretisation of the Newtonian equations of motion, the continuous Hamiltonian system can be discretised by applying a finite difference approximation. Equation 3.32 can be discretised by applying a midpoint approximation for the time derivative of the velocity and the deflection

$$\begin{aligned}\frac{p(t + \Delta t) - p(t - \Delta t)}{2 \cdot \Delta t} &= -k \cdot q(t) \\ \frac{q(t + \Delta t) - q(t - \Delta t)}{2 \cdot \Delta t} &= \frac{p(t)}{m},\end{aligned}\tag{3.39}$$

or reorganised

$$\begin{aligned}p(t + \Delta t) &= -2 \cdot \Delta t \cdot k \cdot q(t) + p(t - \Delta t) \\ q(t + \Delta t) &= \frac{p(t)}{m} 2 \cdot \Delta t + q(t - \Delta t),\end{aligned}\tag{3.40}$$

Applying a central difference discretisation around $t + \frac{\Delta t}{2}$ for the time derivative of the velocity, leads to the well established *Leap-Frog* algorithm given as

$$\begin{aligned}p\left(t + \frac{\Delta t}{2}\right) &= -k \cdot q(t) \cdot \Delta t + p\left(t - \frac{\Delta t}{2}\right) \\ q(t + \Delta t) &= \frac{p\left(t + \frac{\Delta t}{2}\right)}{m} \cdot \Delta t + q(t).\end{aligned}\tag{3.41}$$

Both time integrators capture the Hamiltonian properties of the DE, describing the harmonic oscillator as shown in Hairer, Lubich, and Wanner.⁸⁸

3.4.2 Derivation of the 1-Dimensional Wave Equation

In the following section, the oscillating mass-point is used as a starting point to develop a finite difference approximation of the equation of motion of a 1-dimensional structure (a taut string). Unless mentioned otherwise, the spring is massless and has a linear stiffness k . The mass m is a point-mass without air friction, the deflection of the mass is denoted as $u[m]$ and the acceleration as $u_{tt}[m]$. A simple extension of the oscillating mass-point can be achieved by adding a second spring to the mass, as depicted in Figure 3.4.

⁸⁸Hairer, Lubich, and Wanner, *Geometric numerical integration*. Pp. 4-9.

3 Numerical methods

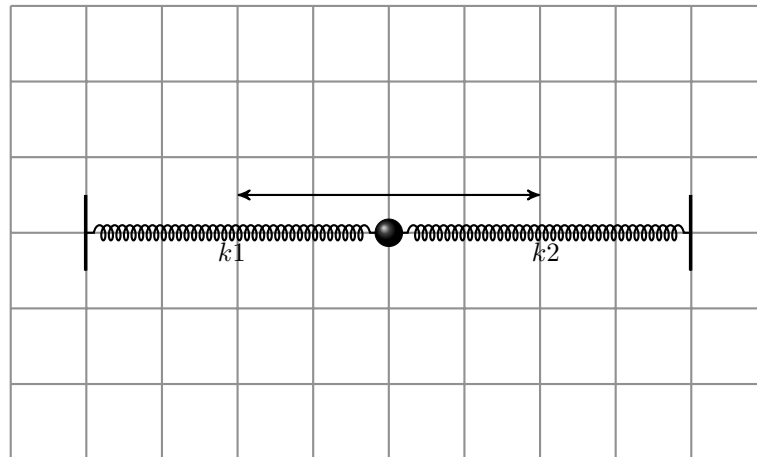


Figure 3.3: Oscillating mass-point with two springs.

With the proposition that the mass m only moves in x-direction and the stiffness of both springs is linear, then the equation of motion for the mass can be written as

$$m \cdot u_{tt}[m] = -(k_1 + k_2) \cdot u[m]. \quad (3.42)$$

This (analytical) ODE is similar to equation 3.22 and can be solved as with the methodology presented above. If we extend this model to two mass-points, as depicted in Figure 3.4, we now have three springs and the equation of motion for

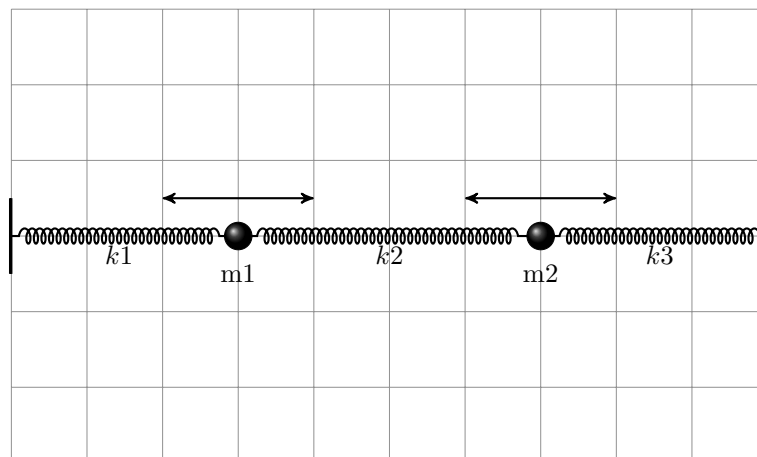


Figure 3.4: Two oscillating mass-points with three springs.

mass-point m_1 can be written as

$$m \cdot u_{tt}[m_2] = -(k_3 + k_2) \cdot u[m_2] + k_2 \cdot u[m_1]. \quad (3.43)$$

The next example consists of three masses coupled by four springs as is shown in Figure 3.5.

3 Numerical methods

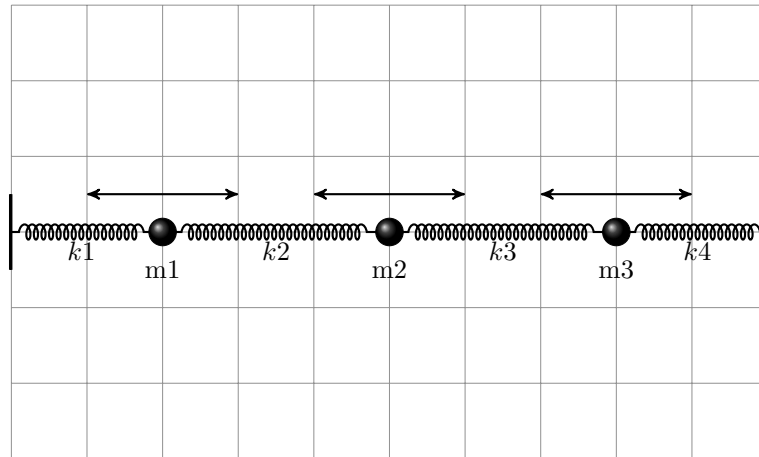


Figure 3.5: Three oscillating mass-points with four springs.

Here, the equation of motion for mass $m1$ is given as

$$m \cdot u_{tt} [m2] = -(k_3 + k_2) \cdot u [m2] + k_2 \cdot u [m1] + k_3 \cdot u [m3]. \quad (3.44)$$

If we now say that all string constants are equal and linear, $k = k_1 = k_2 = k_3 = k_4$ then we can rewrite equation 3.44 to

$$m \cdot u_{tt} [m2] = k \cdot (-2 \cdot u [m2] + u [m1] + u [m3]). \quad (3.45)$$

Equation 3.46 is an explicit formulation of the acceleration and can be recast to

$$u_{tt} [m2] = c^2 \cdot (-2 \cdot u [m2] + u [m1] + u [m3]), \quad (3.46)$$

with $c^2 = \frac{k}{m}$. Up to this point, we are only looking at longitudinal oscillations of the mass point. If we extend our model to allow movement in the y -direction, as depicted in Figure 3.6

3 Numerical methods

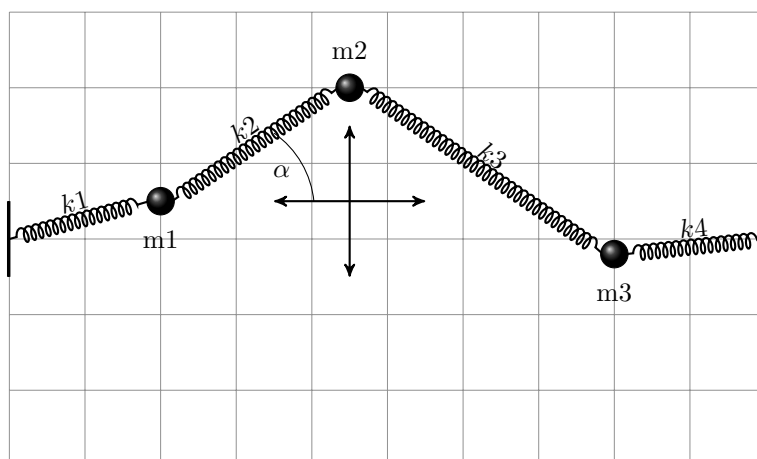


Figure 3.6: Three oscillating mass-points with four springs longitudinal/transversal motion.

In this example, we propose that the spring k_1 and k_4 are coupled to a solid object. All springs are extended to an equilibrium-state with force F_0 acting in the horizontal direction. If the vertical deflection is small, we can say that the acting force on mass-point m_2 is approximately $F_{m_2} = F_{left} + F_{right}$ with

$$\begin{aligned} F_{left} &= -F_0 \cdot \text{Sin}(\alpha_l) \\ F_{right} &= -F_0 \cdot \text{Sin}(\alpha_r). \end{aligned} \quad (3.47)$$

The values for α can be written as

$$\alpha = \text{ArcSin}\left(\frac{\Delta_y u}{\Delta_l u}\right). \quad (3.48)$$

with

$$\begin{aligned} \Delta_y(u_{left}) &= u[m_2] - u[m_1] \\ \Delta_l(u_{left}) &= \sqrt{\Delta_x^2 + \Delta_y^2}. \end{aligned} \quad (3.49)$$

If we combine equation 3.47 and equation 3.48, the Sinus and ArcusSinus functions cancel each other out⁸⁹, yielding following equation

$$\begin{aligned} F_{left} &= -F_0 \cdot \frac{u[m_2] - u[m_1]}{\sqrt{\Delta_x u^2 + \Delta_y u^2}} \\ F_{right} &= -F_0 \cdot \frac{-u[m_3] + u[m_2]}{\sqrt{\Delta_x u^2 + \Delta_y u^2}}. \end{aligned} \quad (3.50)$$

⁸⁹The ArcusSinus is only bijective over the interval $[-1; 1]$, so the angle between two adjacent points can't be larger than than $[-\frac{\pi}{2}; \frac{\pi}{2}]$. For a physically plausible problem, this constraint is met, because the angle between two points in the same dimension must be always smaller than $\frac{\pi}{2}$, if we have a Cartesian coordinate system.

3 Numerical methods

For small deflections, we can say that $\Delta_l \approx \Delta_{x_0}$. Using this inequality, we obtain the equation of motion for the deflection in the y -direction of mass point m_2

$$m \cdot u_{tt} [m_2] = F_0 \cdot (-2 \cdot u [m_2] + u [m_1] + u [m_3]) \cdot \frac{1}{\Delta x_0}. \quad (3.51)$$

Now, we can replace the globally acting force F_0 with the local force, which is the spring constant k , divided by Δx that acts between two masses in the horizontal (direction): $F_0 = \frac{k}{\Delta x}$ and replace the discrete points $u[m]$ with the continuous variable x , to obtain⁹⁰

$$u(x, t)_{tt} = \frac{k}{\Delta x_0 m} \cdot \left(\frac{u(x + \Delta x_0, t) - u(x, t)}{\Delta x_0} - \frac{u(x, t) - u(x - \Delta x_0, t)}{\Delta x_0} \right). \quad (3.52)$$

With equation 3.52, we now have a finite difference expression for the acceleration at one point of the string. If we want to iterate the deflection of the point on the string, we can combine time stepping equation 3.53 with 3.52

$$\begin{aligned} a [m_2] (t) &= c^2 \cdot \frac{1}{\Delta x^2} \cdot (-2 \cdot u [m_2] (t) + u [m_1] (t) + u [m_3] (t)) \\ v [m_2] (t + \Delta t) &= v [m_2] (t) + a [m_2] (t) \cdot \Delta t \\ u [m_2] (t + \Delta t) &= u [m_2] (t) + v [m_2] (t + \Delta t) \cdot \Delta t \end{aligned} \quad (3.53)$$

with $c^2 = \frac{k}{m}$. The time integrator uses a finite difference approximation of the equations of motion in space and time and calculates all three physical parameters explicitly. The motion of the complete string can be calculated by integrating the motion of every virtual quasi-particle over the complete string, as shown in section 3.7 and to a greater extend in chapter 4.

3.5 Symplectic and Multi-Symplectic Methods

In recent years, a paradigm for the classification of numerical time integrators has become an actively researched area in numerical mathematics and physics especially in molecular dynamics simulations.

Symplectic integrators (SI) and multi-symplectic integration (MSI) methods are researched extensively because they possess several advantageous features, when compared to non-symplectic methods. The methodology is derived from a Hamiltonian formalism, showing that SI and MSI preserve the Hamiltonian flow of a system more accurately, in other words, they preserve the geometrical features of the Hamiltonian more precisely than non-symplectic methods. In several publications⁹¹ it was shown that

⁹⁰When $\Delta x_0 \rightarrow 0$, equation 3.52 becomes the continuous (analytic) wave equation.

⁹¹D.W. Markiewicz: "Survey on symplectic integrators", in: *Preprint Univ. California at Berkeley, Spring*

3 Numerical methods

(...) [S]ymplectic integrators have a remarkable capacity for capturing the long-time dynamics of Hamiltonian systems correctly and easily.⁹²

Initially, symplectic properties were only formulated for non-dispersive, linear ODEs⁹³, but later extended to linear PDEs and dispersive ODEs and PDEs.⁹⁴ To define symplectic properties of a method, a generalised position q and the generalised velocity $p = \dot{q}$ is introduced. Using both variables to construct a continuous-time Hamiltonian system

$$\begin{aligned} \dot{q} &= +\nabla_p H(q, p) \\ \dot{p} &= -\nabla_q H(q, p) \end{aligned} \quad \text{label}eq : \text{Hamilt} \quad (3.54)$$

If we propose a numerical scheme (numerical method) Φ that maps a Hamiltonian flow in a way that

$$\left(q^{t+1}, p^{t+1} \right) = \Phi \left(q, p \right), \quad (3.55)$$

it is called symplectic if Φ satisfies

$$\Phi' \left(q, p \right) \begin{bmatrix} 0 & 1 \\ -1 & 0 \end{bmatrix} \Phi' \left(q, p \right) = \begin{bmatrix} 0 & 1 \\ -1 & 0 \end{bmatrix} \quad (3.56)$$

with $\Phi' =$ the Jacobian of Φ .⁹⁵ A qualitative representation of a symplectic and non-symplectic method for a first order ODE is shown in Figure 3.7.

(1999); Brian E. Moore: “Conformal multi-symplectic integration methods for forced-damped semi-linear wave equations”, in: *Mathematics and Computers in Simulation* 80.1 (2009): 20–28; Hairer, Lubich, and Wanner, *Geometric numerical integration*. Ernst Hairer, Christian Lubich, and Gerhard Wanner: “Geometric numerical integration illustrated by the Stoermer-Verlet method”, in: *Acta Numerica* 12 (2003): 399–450.

⁹²Robert Mclachlan: “Symplectic Integration of Hamiltonian Wave Equations”, in: *Numer. Math* 66 (1994): 465–492.

⁹³Hairer, Lubich, and Wanner, *Geometric numerical integration*. P. 54.

⁹⁴Mclachlan, “Symplectic Integration of Hamiltonian Wave Equations”; Moore, “Conformal multi-symplectic integration methods for forced-damped semi-linear wave equations”.

⁹⁵For a mathematical derivation and proof see: (Hairer, Lubich, and Wanner, *Geometric numerical integration*. Pp. 182-187).

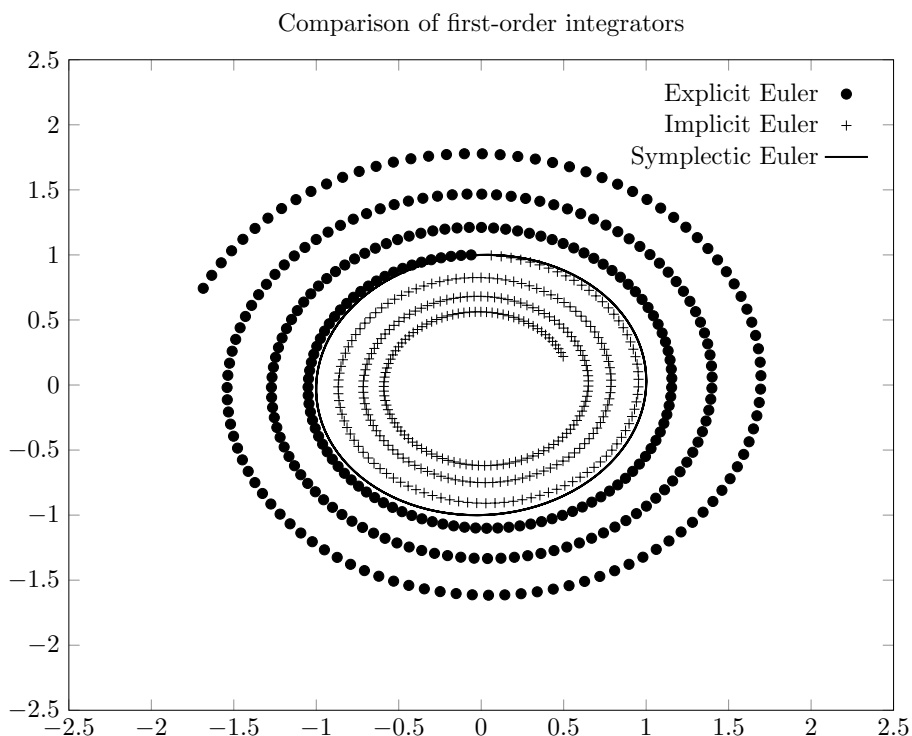


Figure 3.7: Symplectic vs. non-symplectic integrator.

As shown in Figure 3.7, symplectic methods are closer to the real Hamiltonian flow than non-symplectic methods, with a similar discretisation step width. Before an overview on the most frequently utilised SIs and MSIs is given, it is shown that the basic formulation of all of these methods can be derived in a physical way.

3.5.1 Comparison of Several Algorithms

The main feature of a symplectic algorithm is that it conserves the Hamiltonian flow of a system. Therefore, stability problems, arising from energy fluctuations of the numerical method, have a smaller impact here. This is only true, when the appropriate stability properties for the numerical integrator are chosen. This feature is crucial for long time simulation of musical instruments⁹⁶. To gain more insight into this feature, the non-symplectic version of the *Explicit Euler* algorithm is presented here. For the simple harmonic oscillator, the

⁹⁶In the scope of numerical simulation, a few seconds of sound can already have calculation step counts in hundreds of thousands or even millions. This means, even five seconds of a simulated string is a long-time simulation.

3 Numerical methods

non-symplectic *Euler* algorithm can be written as follows

$$\begin{aligned}
 a(t) &= -k \cdot x(t) \\
 v(t + \Delta t) &= v(t) + a(t) \cdot \Delta t \\
 x(t + \Delta t) &= x(t) + v(t) \cdot \Delta t.
 \end{aligned} \tag{3.57}$$

The difference compared to equation 3.53 is that the deflection $x(t + \Delta t)$ is calculated as the sum of $x(t)$ and $v(t)$. This minimal change in the algorithm results in an method which has different stability conditions, as shown in the figures on pages 105-106 of this work.⁹⁷

Another symplectic integrator that is widely applied in numerical simulations of different kinds, is the Stoermer-Verlet scheme. It can be composed of two symplectic Euler schemes⁹⁸ and can be written as

$$\begin{aligned}
 a(t + \frac{\Delta t}{2}) &= -k \cdot x(t) \\
 v(t + \frac{\Delta t}{2}) &= v(t) + a(t + \frac{\Delta t}{2}) \cdot \frac{\Delta t}{2} \\
 x(t + \frac{\Delta t}{2}) &= x(t) + v(t + \frac{\Delta t}{2}) \cdot \frac{\Delta t}{2} \\
 a(t + \Delta t) &= -k \cdot x(t + \frac{\Delta t}{2}) \\
 v(t + \Delta t) &= v(t + \frac{\Delta t}{2}) + a(t + \Delta t) \cdot \frac{\Delta t}{2} \\
 u(t + \Delta t) &= u(t) + v[t + \Delta t] \cdot \frac{\Delta t}{2}.
 \end{aligned} \tag{3.58}$$

Comparing algorithm 3.58 and 3.57, one sees that the Störmer- Verlet scheme has an additional calculation for the acceleration of the simple harmonic oscillator. It is noticeable that this algorithm is comparable to the leap-frog algorithm, which is also symplectic. Higher order symplectic integrators can be developed by different means⁹⁹ and are a direct extension of lower order methods. A fourth-order symplectic integrator, as presented by Omelyan, Mryglod, and Folk,¹⁰⁰ called 'position extended Forest-Ruth like algorithm (PEFRL)' can be written in the following form

⁹⁷The explicit euler is of first order and non-symplectic, as shown in: Hairer, Lubich, and Wanner, *Geometric numerical integration*. P. 3.

⁹⁸ibid., p. 189.

⁹⁹ See for instance: Quandong Feng et al.: "Implementing arbitrarily high-order symplectic methods via krylov deferred correction technique", in: *International Journal of Modeling, Simulation, and Scientific Computing* 01.02 (2010): 277–301; Wei Sha et al.: "Survey on Symplectic Finite-Difference Time-Domain Schemes for Maxwell's Equations", in: *IEEE Transactions on Antennas and Propagation* 56.2 (Feb. 2008): 493–500 or Jing Shen et al.: "High-order symplectic FDTD scheme for solving a time-dependent Schrödinger equation", in: *Computer Physics Communications* (2012).

¹⁰⁰Igor Omelyan, Ihor Mryglod, and Reinhard Folk: "Optimized Forest-Ruth- and Suzuki-like algorithms for integration of motion in many-body systems", in: *Computer Physics Communications* 146.188 (2001).

3 Numerical methods

$$\begin{aligned}
x1 &= x(t) + v(t)\xi\Delta t \\
a1 &= -k \cdot x1 \\
v1 &= v(t) + a1(1 - 2\lambda)\frac{h}{2} \\
x2 &= x1 + v1(t)\Xi\Delta t \\
a2 &= -k \cdot x1 \\
v2 &= v1 + a2\lambda h \\
x3 &= x2 + v2(1 - 2(\Xi + \xi))\Delta t \\
a3 &= -k \cdot x3 \\
v3 &= v2 + a4\lambda h \\
x4 &= x3 + v3\xi\Delta t \\
a(t + \Delta t) &= -k \cdot x4 \\
v(t + \Delta t) &= v3 + a(t + \Delta t)(1 - 2\lambda)\frac{\Delta t}{2} \\
x(t + \Delta t) &= x4 + v(t + \Delta t) \cdot \xi\Delta t,
\end{aligned} \tag{3.59}$$

with the constants¹⁰¹

$$\begin{aligned}
\xi &= 0.1786178958448091E + 00, \\
\lambda &= -0.2123418310626054E + 00, \\
\Xi &= -0.6626458266981849E - 01.
\end{aligned} \tag{3.60}$$

The time stepping algorithm 3.60 requires four acceleration calculations per time step.

Comparison of Different Time-Stepping Methods

All presented time stepping algorithms are compared regarding their stability, accuracy and computational cost. For this, the presented methods are implemented in MATLAB solving the ODE of an oscillating mass-point. Figure 6.10 shows phase plots of five algorithms for different ratios of $\omega^2 \cdot \Delta t$. The sample rate is fixed to $SR = 2^{16}$, so we have a $\Delta t = \frac{1}{2^{16}}$. The green line is a phase plot of an analytical solution of a harmonic oscillator.

Discussion

As one can see in Figure 3.8a and Figure 3.8b, the accuracy and speed of convergence for the presented integrators directly depends on the number of force evaluations per time-step. If the algorithms are analyzed in terms of resource utilisation, i.e. computational cost per

¹⁰¹These values are taken from Omelyan, Mryglod, and Folk, "Optimized Forest-Ruth- and Suzuki-like algorithms for integration of motion in many-body systems".

3 Numerical methods

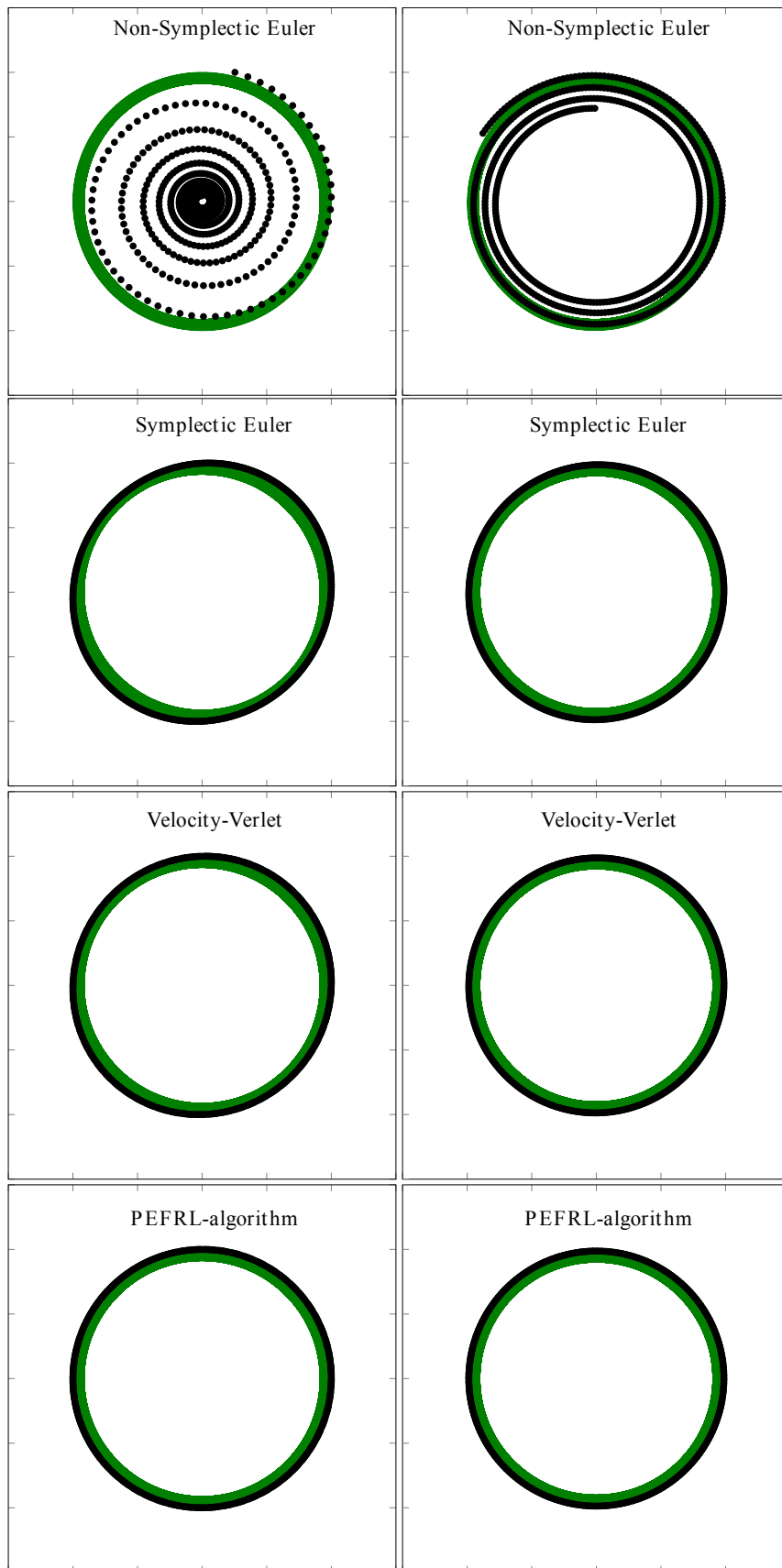
algorithmic step, one finds that an increasing number of force evaluations means an increase in arithmetic function utilisation, as shown in table 3.1.¹⁰²

Integrator	Add. Subt.	Mul.
Sym. Euler	2	3
Vel. Verlet	4	6
PERFL	9	12

Table 3.1: Arithmetic resources of integrators.

¹⁰²All divisions and multiplications of constant values are not included in the table. They do not impact the computation time inside the main loop of the algorithm because they can be calculated outside the larger time loop.

3 Numerical methods



(a)

(b)

Interim Conclusion

As shown in the preceding sections, one can minimize the error of the presented integrators by increasing the number of force evaluations, which in turn means an approximately linear increase in computational cost. This leads to a lower discretisation error in the time axis, meaning, we could implement larger time steps for the same order of accuracy compared to a method of lower order. But in an audio application we are bound by a (positive) restriction, the sample rate. In modern synthesis applications, a sample rate of at least 44,100 Hz is needed.¹⁰³ This means that we have a discretisation step wide of at least $\Delta t_{min} = \frac{1}{44100} = .22676E-06$. With an error of order (Δt^2) , we would get an error of $\epsilon \approx \Delta t^2 = 5.1410E-10$. Taking this into consideration, we can conclude that the error introduced by the time discretisation is negligibly small and a higher order time integrator is not needed for the presented methods.

3.5.2 Multi-Symplectic Schemes

As an extension to symplectic algorithms for ODEs, the same concept can be applied to PDEs. The requirement developed in section 3.5 is now called *multi-symplecticness* and is defined by similar conditions as symplecticity.¹⁰⁴

A simple multi-symplectic scheme for PDEs is the Euler-Box scheme. For a linear first order wave equation, it can be written in the following form:¹⁰⁵

$$\begin{aligned}
 \mathbf{a}(t) &= -c^2 \delta_{xx} \cdot \mathbf{x}(t) \\
 \mathbf{v}(t + \Delta t) &= \mathbf{v}(t) + \mathbf{a}(t) \cdot \Delta t \\
 \mathbf{x}(t + \Delta t) &= \mathbf{x}(t) + \mathbf{v}(t + \Delta t) \cdot \Delta t,
 \end{aligned} \tag{3.61}$$

which is of similar form as the symplectic integrator for the harmonic oscillator. The only difference is that the values for the deflection, velocity and acceleration are now vectors, as indicated by the *bold* notation. If the expression for the acceleration (3.52) developed in section 3.4.2, is inserted into line 1 of equation 3.61, the algorithm has the same form as equation 3.53 that was developed by discretising the equations of motion in section 3.4. As presented in Gotay and Isenberg,¹⁰⁶ the equations of motion for the simple oscillator are symplectic,

¹⁰³For the real-time models the sample rate lies between 2^{16} and 2^{18} .

¹⁰⁴The mathematical derivation of multi-symplecticity can be found in the works of: Brian Moore and Sebastian Reich: "Backward error analysis for multi-symplectic integration methods", in: *Numerische Mathematik* 95.4 (2003): 625–652; Brian E. Moore and Sebastian Reich: "Multi-symplectic integration methods for Hamiltonian PDEs", in: *Future Generation Computer Systems* 19.3 (2003): 395–402 or Uri M. Ascher and Robert I. McLachlan: "Multisymplectic box schemes and the Korteweg-de-Vries equation", in: *Applied Numerical Mathematics* 48.34 (2004), Workshop on Innovative Time Integrators for PDEs: 255–269.

¹⁰⁵Moore and Reich, "Backward error analysis for multi-symplectic integration methods".

¹⁰⁶Mark J. Gotay and James A. Isenberg: "The symplectization of Science", in: *Gazette des Mathématiciens* 54 (1992): 59–79.

hence it is beneficial to solve the equations of motion with symplectic methods.¹⁰⁷

3.5.3 Implicit Algorithms

Up to this point, only explicit algorithms were presented. Implicit algorithms are applied in numerical computations to a greater extent than their explicit counterparts. Most implicit algorithms have the advantage that they have superior stability conditions compared to explicit ones.¹⁰⁸ One drawback of implicit methods in the scope of real-time, or close to real-time, physical modeling is their numerical structure. Because implicit methods must be solved by a linear equation system, some of the strength of the aforementioned algorithms, like accessibility of physical parameters or intuitive representation of the underlying equations, are lost. Another drawback of implicit methods is the vulnerability to numerical instabilities, due to sparsely populated or ill-posed matrices. In some cases, these numerical instabilities may become larger than the influence by the discretisation error of the initial problem.¹⁰⁹ All presented methods can also be formulated in an implicit form, but in this work we only apply explicit versions of the presented algorithms.

3.6 Pseudo-Spectral Finite Differences

As mentioned before, one of the drawbacks of finite difference methods is their computational cost, especially in higher dimensions. One solution to approach this problem is to minimize the discretization step width in the temporal or the spatial domain. This directly influences the accuracy and stability of a finite difference scheme and antagonizes the maximal frequency resolution of the discretised problem¹¹⁰. In this section, a method that simplifies several aspects of finite difference methods and enhances the geometrical accuracy, only limited by the spatial grid size, is presented. Finite difference methods known as pseudo spectral (PS) methods are an extension to finite difference methods can be applied in various fields of numerical mathematics¹¹¹.

Even though PS methods are used in other fields of research, there are only a few published works considering the subject for modeling of musical instruments.¹¹²

¹⁰⁷ The symplecticness of the equations of motion is known in physics and is explored in mathematics extensively for at least 50 years. See Gotay and Isenberg, “The symplectization of Science”.

¹⁰⁸ In many cases, implicit time stepping algorithms are unconditionally stable.

¹⁰⁹ Eventhough there are highly optimised versions of solvers like BLAS, LAPACK, Armadillo and many others, the transition of an implicit time stepping method from a high level language, like C++ or MATLAB, to a hardware language (VHDL) is much more complex than the implementation of direct, explicit methods.

¹¹⁰ This effect can often be neglected in steady state calculations because only the first few *eigenmodes* of a system are of interest. In musical applications, on the other hand, it is important to have a frequency resolution that matches at least twice the human hearing range (Nyquist theorem).

¹¹¹ Fornberg, *A practical guide to pseudospectral methods*.

¹¹² To the best of my knowledge, there is only one paper regarding instrument acoustics applying a PS-approach see: G. Sathej and R. Adhikari: “The eigenspectra of Indian musical drums”, in: *arXiv preprint*

In the following section properties and applications of PS methods are shown. It is shown how they can be applied to optimise and enhance several aspects of more conventional finite difference schemes for physical modeling. An introduction of the mathematics of this method and several results are given, showing the equivalence of PS methods to finite difference methods on bounded grids. A comparison of the computation time is given at the end.

3.6.1 Finite Difference Grids as Convolution Kernels

There are at least two ways of deriving Pseudo Spectral methods which can be found in literature:

1. A derivation by global interpolation functions.¹¹³
2. A derivation by the equivalence with finite difference grids.¹¹⁴

In this work, the derivation of the method is connected to the second approach, but is developed by using the convolution theorem. We are starting with a discrete, numerical solution method of the PDE of the linear string as presented in section 3.3.2. As shown above, the finite difference approximation for the acceleration of the linear string can be calculated numerically by discretising the second derivative in space with a finite difference approximation and multiplying it with a constant that depends on the wave velocity in the medium and the discretisation step widths in space and time

$$a(t)|_i = c^2 \cdot u_{xx} \approx c^2 \cdot \frac{u(i - \Delta x, t) - 2 \cdot u(i, t) + u(i + \Delta x, t)}{\Delta x^2}. \quad (3.62)$$

For reasons of brevity, the right hand multiplicand is set to $\frac{c^2}{\Delta x^2} \equiv 1$. To solve equation 3.62 numerically, one would at first discretise the string into a number of finite points. The acceleration at every point of the string can now be calculated as follows

arXiv:0809.1320 (2008) besides the authors work published in: Florian Pfeifle: “Multisymplectic Pseudo-Spectral Finite Difference Methods for Physical Models of Musical Instruments”, English, in: *Sound - Perception - Performance*, ed. by Rolf Bader, vol. 1, Current Research in Systematic Musicology, Springer International Publishing, 2013: 351–365. Other work concerned with the applicability of PS methods for musical instrument simulation and synthesis was a research project at the University of Edinburgh. The research team concluded that the method is not suited for musical acoustics but didn’t publish any of their findings.

¹¹³This approach is utilised in works like: L.N. Trefethen: *Spectral methods in MATLAB*, vol. 10, Society for Industrial Mathematics, 2000, pp. 41 ff. or Miguel Hermanns and Juan Antonio Hernandez: “Stable high-order finite-difference methods based on non-uniform grid point distributions”, in: *International Journal for Numerical Methods in Fluids* 56 (2007): 233–255.

¹¹⁴This approach is taken in the works of Bengt Fornberg: B. Fornberg: “High-order finite differences and the pseudospectral method on staggered grids”, in: *SIAM Journal on Numerical Analysis* 27.4 (1990): 904–918 or Fornberg, *A practical guide to pseudospectral methods*.

3 Numerical methods

Listing 3.1: Pseudocode for acceleration calculation

```

1 for ( t=0: SampleLength )
2   for ( i=1: stringPoints -1)
3     Acceleration [ i ] = u [ i -1]-2 u [ i ]+u [ i +1 ];

```

The operation at the right-hand side of line 3 can also be written as a convolution of the vector of deflections \mathbf{u} with a convolution kernel

$$\delta_{xx} = [1 \quad -2 \quad 1],$$

for every timestep

$$\mathbf{a} = \delta_{xx} * \mathbf{u}. \quad (3.63)$$

With the convolution theorem and the properties of the Fourier Transform, we can calculate this time domain convolution (configuration space) as a multiplication in the frequency domain

$$\delta_{xx} * \mathbf{u} \equiv \mathcal{F}^{-1} \{ \mathcal{F} \{ \delta_{xx} \} \cdot \mathcal{F} \{ \mathbf{u} \} \}. \quad (3.64)$$

Equation 3.64 states that both calculations (time domain and frequency domain) are equivalent. But at this point, the computational cost of the Fourier transform is higher than the formulation in the time domain and there is no real advantage in transferring the convolution operation to the frequency domain. This changes if the order of the finite difference approximation is increased. As we have seen in section 3.2, the error of the second order central finite difference approximation is dependant on $\mathcal{O}(\Delta x^2)$, so to minimise this error, we can use higher order approximations for the spatial finite differences. A fourth order finite difference approximation of the second derivative can be written as

$$u_{xx}|_i \approx \frac{1}{12\Delta x^2} (- u(i - 2\Delta x) + 16u(i - \Delta x) - 30u_i \dots \\ + 16u(i + \Delta x) - u(i + 2\Delta x)) + \mathcal{O}(\Delta x^4), \quad (3.65)$$

The order can be increased to the maximal number of discrete node points N on the string, minimising the spatial discretisation error to order $\mathcal{O}(\Delta x^N - 1)$. This means, if a finite difference interpolation function for the whole string is used as a convolution kernel, this error is only dependant on the discrete step-width Δx .¹¹⁵ As stated before, the convolution with the resulting kernel can be computed in the time or in the frequency domain which gets computationally more efficient when simulating higher order geometries or large problems

¹¹⁵Again, if $\Delta x \rightarrow 0$ one gets an expression for the analytical, continuous case.

with a high number of grid-points.

An equivalent formulation can be achieved by regarding basic equalities of the Fourier-Transform which state that a derivative in the time domain can be calculated in the frequency domain as¹¹⁶

$$u_x \equiv \mathcal{F}^{-1} \{i \cdot \omega \cdot \mathcal{F} \{u\}\}. \quad (3.66)$$

If the Fourier transform of the vector \mathbf{u} is known, one can calculate the analytical derivative of the vector in frequency domain and transform the result back to the time domain to get u_x . Extending this to a second order differentiation, we can write

$$u_{xx} \equiv \mathcal{F}^{-1} \{-\omega^2 \cdot \mathcal{F} \{u\}\}. \quad (3.67)$$

With this equivalence one can either perform the differentiation directly in the frequency domain or calculate high order finite difference weights δ_{xx} and transform the calculated weights of the differentiation function to the time domain. Because both approaches yield identical results, choosing the appropriate approach depends only on the respective problem and geometry and on the performance of the Fourier-Transform on the computation platform.

3.7 Final High Level Algorithm

In this section, the final algorithms for the high level (HL) and the low level (LL) models are presented. In their basic formulation, they are identical, but the HL models are discretised in the spatial domain with pseudo-spectral weights, whereas the LL model utilises second order central differences.

3.7.1 Introduction

To complete the analysis of the presented algorithm, and to substantiate the decision for the method applied in this work, the central findings regarding our set of rules developed in the introduction of this chapter, are summarised up front:

- The most straight-forward way of implementing physical models with finite difference approximations is achieved, when the Newtonian equations of motion are discretised and solved.
- For audio applications, the minimum temporal sampling rate of 44100 Hz is so high that *basic* second order time discretisation yields sufficiently accurate results.

¹¹⁶Mallat, *A Wavelet Tour of Signal Processing The Sparse Way*, p. 38.

3 Numerical methods

- The spatial discretisation introduces larger error than the temporal discretisation, so a high order method spatial discretisation benefits the accuracy of the models.
- Symplectic methods are capable of computing stable long-term simulations.
- Explicitness of all physical quantities is given when applying the *Explicit Euler* or similar algorithms.

These main findings lead to the conclusion that explicit symplectic/multi-symplectic methods with high order spatial discretisation are well suited to describe the acoustic-mechanical vibrations of musical instruments. Even though, other methods have advantages in several domains¹¹⁷. The only algorithm that incorporates all of the mentioned requirements is the *Explicit Euler* or similar higher order algorithms, like the Velocity-Verlet or the PERFL method.

3.7.2 Basic Formulation

The basic features of the final algorithm can best be illustrated by a finite difference solution to a 0-dimensional oscillating mass point. As presented in section 3.5, the algorithm solving the ODE of a mass point, coupled to a spring can be written as

$$\begin{aligned}
 a(t) &= -k \cdot x(t) \\
 v(t + \Delta t) &= v(t) + a(t) \cdot \Delta t \\
 x(t + \Delta t) &= x(t) + v(t + \Delta t) \cdot \Delta t.
 \end{aligned} \tag{3.68}$$

The equation system can be formulated in one line as

$$x(t + \Delta t) = x(t) + [v(t) - k \cdot x(t) \cdot \Delta t] \cdot \Delta t = x(t) + [v(t) \cdot \Delta t - \kappa \cdot x(t)] \tag{3.69}$$

with $\kappa = k \cdot \Delta t^2$. Because Δt is constant for all time steps, a normalised velocity is proposed here

$$\tilde{v} = \frac{v}{\Delta t} \tag{3.70}$$

as well as a normalised acceleration

$$\tilde{a} = \frac{a}{\Delta t^2}. \tag{3.71}$$

Rearranging 3.69 using 3.70 and 3.71 into the three step formulation we get

$$\begin{aligned}
 \tilde{a}(t) &= -\kappa \cdot x(t) \\
 \tilde{v}(t + \Delta t) &= \tilde{v}(t) + \tilde{a}(t) \\
 x(t + \Delta t) &= x(t) + \hat{v}(t + \Delta t)
 \end{aligned} \tag{3.72}$$

¹¹⁷ The unconditional stability of implicit methods for instance.

3 Numerical methods

with $\kappa = \frac{k}{\Delta t^2}$.

Now we can rewrite equation 3.72 to a global form with $\tau =$ the discrete time-shift operator, as introduced before and \bigcup the Hutchinson operator¹¹⁸ we obtain

$$\begin{bmatrix} \mathcal{A} \\ \mathcal{V} \\ \mathcal{U} \end{bmatrix} = \bigcup_{t=1}^T \begin{bmatrix} -\kappa\tau_{t-}u \\ \tau_{t-}v + a \\ \tau_{t-}u + v \end{bmatrix}. \quad (3.73)$$

With $\mathcal{A}, \mathcal{V}, \mathcal{U}$, the acceleration, velocity and deflection over the complete time range, a, v, u In this form, one has an explicit formulation for the acceleration, the velocity and the deflection of an oscillating mass-point. Extending this to higher dimensions and including the multi-symplectic Euler-box scheme and pseudo-spectral approximation of the spatial discretisation as shown in section 3.6, we can rewrite equation 3.72 to

$$\begin{bmatrix} \mathcal{A} \\ \mathcal{V} \\ \mathcal{U} \end{bmatrix} = \bigcup_{t=1}^T \begin{bmatrix} \mathcal{F}^{-1} \left[\kappa \cdot \hat{\delta}_{xx} \cdot \mathcal{F} [\tau_{t-}\mathbf{u}] \right] \\ \tau_{t-}\mathbf{v} + \mathbf{a} \\ \tau_{t-}\mathbf{u} + \mathbf{v} \end{bmatrix}. \quad (3.74)$$

In equation 4.34 the pseudo-spectral FD operator and grid constant Δx , timing constant Δt , as well as the material dependent wave velocity c are written in condensed form as

$$\delta_{xx} = \delta_{xx} \cdot \text{frac} \Delta t^2 \cdot c^2 \Delta x^2, \quad (3.75)$$

combining several multiplicands into one.

3.8 Final Low Level Algorithm

In this section, the basic optimisations for the presented algorithm as well as the modification for the implementation on the parallel hardware platform are described. After a short overview on the basic steps, more specific details of the implementation follow in chapter 6, specifically the sections about the layer model and the complete instrument geometries. The starting point is a simple formulation to exemplify the basic properties of the algorithm and all applied optimisations for the hardware model. The LL algorithm implemented in VHDL is different from the HL algorithm in several regards. First, and most importantly, the pseudo-spectral discretisation in space is not implemented directly. Second, all multiplications by two or powers of two are performed as shift operations. And third, the multiplication with damping terms is implemented by rewriting the damping constant multiplication by a finite sum of shift operations.

¹¹⁸This operator is adapted from John E. Hutchinson: "Fractals and Self Similarity", in: *Indiana Mathematics Journal* 30 (1981): 713-747 and denotes a for loop from $t = 1$ to $t = T$ with $t \in N$.

3.8.1 Model of a Linear String

With equation 3.73 and a formulation for the 1-dimensional string, we have developed in section 3.3.2, the time stepping algorithm for an elastic linear string can be approximated with a symplectic time integrator and a finite difference in space formulation in the following form

$$\begin{aligned} \mathbf{a}^t &= k \cdot \delta_{xx} * \mathbf{u}^t \\ \mathbf{v}^{t+\Delta t} &= \mathbf{v}^t + \mathbf{a}^t \\ \mathbf{u}^{t+\Delta t} &= \mathbf{u}^t + \mathbf{v}^{t+\Delta t}. \end{aligned} \quad (3.76)$$

If we now use a sample rate (SR) with the properties $SR = 2^N$ with $N = 1, 2, 3, \dots$, meaning SR is power of two, the multiplication with $\Delta t^2 = \frac{1}{SR^2}$ can be implemented as rightshifts¹¹⁹, and the multiplication by two as leftshifts at the respective position of the string i

$$a^t|_i = ((k) \gg 16) * (-(((u) \ll 2)|_i + (u|_{i+1} + u|_{i-1})) \gg 16) \quad (3.77)$$

$$v^{t+1}|_i = v^t|_i + a^t|_i \quad (3.78)$$

$$u^{t+1}|_i = u^t|_i + v^{t+1}|_i \quad (3.79)$$

with $((\cdot) \gg C)$ indicating a rightshift¹²⁰ by a constant C and $((\cdot) \ll C)$ indicating a left shift by a constant. The shift operation can only be applied if we use a fixed point or an integer data type¹²¹. As one can see, the final formulation is similar to the version of the algorithm derived in section 3.7.

3.8.2 Approximating Damping Parameters

Damping of physical systems, expressed in mathematical form, whether velocity or internal (force dependant) damping, has the following structure

$$\xi_{damped} = \xi - \alpha \cdot \xi, \quad (3.80)$$

with ξ an arbitrary damped value and $0 \leq \alpha < 1$, a damping constant, we can reformulate the same equation as follows

$$\xi_{damped} = \xi - \sum_{n=1}^N \beta \xi, \quad (3.81)$$

where $\beta = \nu \cdot \frac{1}{2^n}$ and $\nu \in [-1, 0, 1]$. With this *sequence*, every arbitrary constant can be approximated. Because of the fixed point data type applied for the real-time models on the

¹¹⁹This enables us to write the division, which is a very resource consuming operation in hardware, as a shift operation, which is easier to implement and has a lesser resource utilisation.

¹²⁰For the data type applied in this work with the most significant bit at the left-side of an vector, this represents a downshift.

¹²¹A more thorough explanation of this is presented in section 6 of this work.

FPGA, we can express every operation of the form $\lambda * 2^x$ as shift operations, depending on the sign of x . This allows us to perform multiplications with constants smaller than one or divisions, with constants larger than one, as shift operations. This technique can be extended to machine precision. The only drawback of this approximation is that at this point, values have to be approximated manually. This is only a minor flaw of this technique because *exact* damping parameters are unknown for most materials, and manual a approximation (*Ad hoc*) is common practice in many works.

3.8.3 Linear Velocity Damped String

As an example for the aforementioned optimisation techniques, a linear velocity damped string is implemented on hardware. A fixed point data-type with a bit depth of 32 bit for the deflection, velocity and 64 bit for the acceleration is used here. The calculation for the equations of motion for one point can be written as

$$\begin{aligned}
 A^t|_i &= (CQ \gg 16) * (-(S \ll 2)|_i + (S|_{i+1} + S|_{i-1}) \gg 16) \\
 V^{t+1}|_i &= V^t|_i + A^{t+1}|_i - (V^t|_i \gg 13) + (V^t|_i \gg 15) \\
 S^{t+1}|_i &= U^t|_i + V^{t+1}|_i
 \end{aligned} \tag{3.82}$$

with S the deflection, V the velocity and A the acceleration of a discrete node-point and CQ the normalised and squared wave velocity. The resulting time series of a velocity damped string calculated on hardware is presented in chapter 6.

3.9 Error and Stability Analysis

This section gives an overview on the possible errors of numerical methods as well as stability considerations regarding the time integration schemes applied in this thesis. Due to the fact that all numerical methods are only approximations of continuous differential equations, they are susceptible to various kinds of errors when compared to the analytical, continuous solution of a given problem. The most palpable error influencing the stability properties of the numerical solution is the discretisation error, which directly depends on the applied discretisation of the independent variables, in this thesis space and time. As shown in section 3.2.1, these errors are quantifiable by an error estimate of the truncated Taylor series term indicated by $\mathcal{O}(\cdot)$.¹²²

¹²²In explicit finite difference implementations, without algorithmic optimisations, the computational cost depends on the step width of the discretisation, hence this error was of great concern in the beginning of computational finite difference methods in the 1950s, see: Thom e, "Short history of finite differences". But even on modern computers, with their high data throughput and larger instruction-sets, the spatial grid size and temporal stride width is the main limiting factor. The computational complexity of an explicit 1-dimensional finite difference solution, comparable to the method presented here, scales with $(FS)^2$, with FS the sample rate. See: Bilbao, *Numerical Sound Synthesis*. P. 146.

3 Numerical methods

A second class of errors is introduced by truncation and rounding errors due to finite length number representation in the digital domain. These errors are not as easily assessable upfront compared with the discretisation errors. When using a floating point number representation, a rounding error can become as large as the data bit-width itself¹²³. This class of error is known to cause instabilities when implementing signal processing algorithms with IIR filters¹²⁴ or by implicit methods,¹²⁵ but is not as critical for the algorithm and specific data type applied in this work, as will be shown in chapter 6.

A third class of errors can be present in a physical model from incomplete or wrongfully modeled physical behaviour or missing information regarding the modeled problem, like for instance an inaccurate modeling of boundary conditions of membranes or strings, unrealistic damping parameters or false coupling parameters. Because the last error is harder to assess in a mathematical sense, only the first two errors are discussed here¹²⁶.

Because all of the mentioned errors can lead to instabilities in the numerical schemes, it is indispensable to have a sound error prediction for these problems before implementing the models on a dedicated hardware platform to perform in real-time.

A sound error prediction makes it possible to establishing bounds in which a numerical method yields accurate and stable results. Several sources of errors can be ruled out at the beginning, simplifying the debugging procedure in later stages of the implementation. For most basic finite difference schemes, stability analyses can be found in literature, starting with the fundamental works of Courant, Friedrichs, and Lewy,¹²⁷ to the works of Neumann and Richtmyer,¹²⁸ Lax and R.D.,¹²⁹ Lax¹³⁰ or Kreiss,¹³¹ to more recent publications like Strikwerda and Wade,¹³² Moore and Reich¹³³ or Ehlers, Zinatbakhsh, and Markert.¹³⁴ In the following sections, an overview on the mathematical tools for error prediction and stability analysis is given and the applicability of the respective method for the whole geometry

¹²³An exacter analysis of this error can be found in chapter 5.

¹²⁴See for instance: Uwe Meyer-Baese: *Digital Signal Processing with Field Programmable Gate Arrays*, 2nd ed., Berlin, Heidelberg: Springer, 2007 or K.-D. Kammeyer, *Digitale Signalverarbeitung*. Pp. 109-136.

¹²⁵Here, the solution of a system of linear equations depends on matrix inversion operations, an operation highly susceptible to numerical noise produced by rounding errors.

¹²⁶More thoughts on the error introduced through wrongful physical assumptions can be found in section 4.

¹²⁷Courant, Friedrichs, and Lewy, "Über die partiellen Differenzgleichungen der mathematischen Physik".

¹²⁸John von Neumann and R. D. Richtmyer: "A Method for the Numerical Calculation of Hydrodynamic Shocks", in: *Journal of Applied Physics* 21 (1950).

¹²⁹Lax and R.D., "Survey of the stability of linear finite difference equations."

¹³⁰Peter D. Lax: "On the stability of difference approximations to solutions of hyperbolic equations with variable coefficients", in: *Communications on Pure and Applied Mathematics* 14.3 (1961): 497-520.

¹³¹Heinz-Otto Kreiss: "Über die Stabilitätsdefinition für Differenzgleichungen die Partielle Differentialgleichungen approximieren", in: *Nord. Tidskr. Inf. (BIT)* 2 (1962): 153-181.

¹³²John Strikwerda and Bruce Wade: "A survey of the Kreiss matrix theorem for power bounded families of matrices and its extensions", in: *Banach Center Publications* 38.1 (1997): 339-360.

¹³³Brian Moore and Sebastian Reich: "Backward error analysis for multi-symplectic integration methods", in: *Numerische Mathematik* 95.4 (2003): 625-652.

¹³⁴W. Ehlers, S. Zinatbakhsh, and B. Markert: "Stability analysis of finite difference schemes revisited: A study of decoupled solution strategies for coupled multifield problems", in: *International Journal for Numerical Methods in Engineering* 94.8 (2013): 758-786.

models of musical instruments, implemented in this work, is discussed.

3.9.1 Discretisation Error

Before several methodologies for error and stability analysis are presented, there are two prerequisites of the method which must be considered upfront. On the assumption that we are only interested in explicit algorithms with directly accessible calculation parameters, the error and stability conditions are directly dependant on the spatial and temporal discretisation step-width.

Two restraining factors regarding the step width, when modeling applications for sound synthesis, are the human hearing range and the fundamental spatial frequency as well as the highest spatial frequency of the modeled instrument geometries. In practice, this means that one has to have a temporal sampling rate that is twice the highest humanly perceptible frequency¹³⁵ and a spatial sampling rate that must be able to represent the full spectral informations from the lowest to the highest partial inside this frequency range.

In most modern audio applications, the minimal temporal sampling rate is 44,100 Hz¹³⁶. Because the hardware implementation of the real-time algorithm requires the sampling rate to be a power of two, the sampling rate for all model parts is at least 2^{16} , for some geometries 2^{17} or 2^{18} . The minimum spatial sampling frequency¹³⁷ can best be illustrated at the discretisation of a linear string. The speed of sound c on a low banjo string, a D_3 with the fundamental frequency $f \approx 147$ Hertz, can be calculated by the simple equivalence

$$c = f \cdot \lambda, \tag{3.83}$$

with $\lambda =$ the wave length. From classical mechanics we know that the fundamental frequency on a string vibrates with a wave length of $\frac{\lambda}{2}$. Inserting the length of the banjo string, which is approximately 0.67 meters, into equation 3.83 we obtain

$$c = f \cdot \lambda \approx 147 \cdot 0.67 \cdot 2 \approx 199 \left[\frac{m}{s} \right], \tag{3.84}$$

If we now propose a maximal spatial frequency of $f_{max} = 20$ kHz that must be representable by a grid, and reinsert the values into equation 3.83 we get a λ_{min} of

$$\lambda_{min} = \frac{c}{f_{max}} \approx \frac{199}{20000} \approx .01 [m]. \tag{3.85}$$

If one wants to model a banjo string with a correct λ , we have to take into account that a

¹³⁵Because of the Nyquist sampling theorem.

¹³⁶ Sampling rate of the Red Book Compact Disc standard.

¹³⁷Spatial sampling frequency = $\frac{1}{\text{discrete spatial step width}}$.

3 Numerical methods

sine wave of an arbitrary λ must be discretised with two points at least¹³⁸, we have a $\lambda_{min} = 0.005m$. The discrete number of points N on the banjo string can now be calculated by

$$N = \frac{length}{\lambda_{min}} \approx \frac{0.67}{0.005} = 134. \quad (3.86)$$

A discretised string with this N is capable of capturing all spatial frequency features on the string. With these quantities, the CFL condition can be estimated with the spatial and temporal step widths. Including the wave velocity c , we obtain

$$K_{CFLstring} = \frac{c \cdot \Delta x}{\Delta t} \approx \frac{199 * 0.005}{2^{16}} = 1.5182E - 5, \quad (3.87)$$

which is almost five magnitudes smaller than the theoretical CFL-number¹³⁹ of 1 for an explicit numerical scheme like FDTD or the symplectic Euler scheme. Hence, choosing viable psychoacoustic requirements leads to an inherently low CFL¹⁴⁰ number for most geometries.

3.9.2 Stability and Error Measures

In this section, we present methods that can be utilised to check the stability conditions for numerical schemes and algorithms.

All final models in this work are whole geometry formulations of the musical instruments implemented as coupled problems. Hence, these models can not be described easily as monolithic systems with only one governing differential equation. Therefore, several of the presented stability measurements are not applicable for the whole system, but yield assessments for stability conditions of the uncoupled problems. In some cases, the uncoupled stability analysis can be extended to the coupled problems.

Even though the error analysis in this work is not aimed at comparing the numerical solution to the analytical solution, we are interested in a robust measure of errors which could lead to an instable numerical simulation of an instrument model.

CFL Stability Condition

The Courant-Friedrichs-Lewy condition formulated in Courant, Friedrichs, and Lewy,¹⁴¹ poses a basic stability condition for explicit as well as implicit difference schemes. In its generalized form for n dimensions and with c the maximal group-velocity of information

¹³⁸ For a reasonably good representation a discretisation step width between 6 and 10 points is practical. But due to the fact that the higher frequencies of strings are often damped and only important in the first milliseconds of the sound, a coarser discretisation is viable.

¹³⁹ see section 3.9.2.

¹⁴⁰ The CFL number gives a necessary condition for stability.

¹⁴¹ Courant, Friedrichs, and Lewy, "Über die partiellen Differenzgleichungen der mathematischen Physik".

3 Numerical methods

transport in the medium, it can be written as

$$K = \Delta t \sum_{i=1}^n \frac{c_i}{\Delta x} \leq K_{CFL}. \quad (3.88)$$

Even though the CFL-condition was developed as an upper limit for convergence of a numerical method at first, it was shown by Lax and Richtmyer that the convergence criterion can be extended to a necessary stability criterion. A fact that is formulated in the basic Lax equivalence theorem which states that

*(G)given a linear hyperbolic partial differential equation. Then a consistent finite difference scheme is stable if and only if it is convergent.*¹⁴²

This means, a scheme is stable, if it converges to the analytical solution. Unfortunately, we can only use this measure, if an analytical solution exists and the problem is linear, well posed and consistent. For other cases, like coupled problems or PDEs with non-constant coefficients, we need to facilitate other stability measures. In addition to that, the CFL number K_{CFL} depends on the numerical method but for most explicit schemes we utilise in this work it is 1.

Expressed in a more intuitive form, the CFL-condition states that the velocity of information that can travel on a given discrete grid in space and time, has to be equal or greater than the maximal *physical* velocity of the respective differential equation it represents. This conditions is necessary but not sufficient.¹⁴³

Von Neumann Stability Analysis

The *Von Neumann* stability analysis was proposed by the American physicist John von Neumann in the 1950s. It was developed to analyze the stability of early finite difference schemes on the first computers in the research facilities of Los Alamos.¹⁴⁴ The Von Neumann stability criterion for finite difference schemes researches the stability of a scheme that iterates the variable \mathcal{U} in time, by introducing an amplification matrix G in the frequency domain as

$$\hat{\mathcal{U}}^{t+1} = G(\Delta t, \Delta x)\hat{\mathcal{U}}^t. \quad (3.89)$$

The hat symbol ($\hat{}$) indicates a Fourier transform. The von Neumann stability criterion states that if the spectral radius ρ ¹⁴⁵ of the amplification matrix G is bounded by a constant $C \in \mathbb{R}$, the scheme is stable. This criterion is necessary and sufficient for stability. As shown by

¹⁴² Lax and R.D., “Survey of the stabiity of linear finite difference equations.”

¹⁴³ *ibid.*

¹⁴⁴ Thomée, “Short history of finite differences”.

¹⁴⁵The spectral radius of a matrix is defined as the maximum absolute value of its *eigenvalues*.

Kreiss, this form it is only applicable for differential equations with constant coefficients.¹⁴⁶ An extension of the spectral stability analysis¹⁴⁷ to problems with variable coefficients¹⁴⁸ can be formulated by using properties of the Kreiss matrix theorem¹⁴⁹. This theorem can be summarized as follows: For finite difference problems with variable coefficients, the Von Neumann stability or the Lax/Richtmyer stability criterion can be satisfied at every discrete point, but the global difference scheme can produce unstable solutions nonetheless. A sufficient stability criterion for a finite difference scheme with variable coefficients is given by

Theorem 1. Kreiss Matrix Theorem. *There exists a real number $C > 0$ such that $\|G^n\| \leq C$ for all G with $n \in \mathcal{N}$.*

Compared to the von Neumann stability criterion, this means that the amplification matrix G must to be power-bound for all simulation time-steps. This means, if all values of the variable constants are known, the amplification matrix can be calculated for these respective values.

Stability Analysis Using Energy Methods

Energy methods estimate the total energy of a continuous system that can be expressed in the form of $\mathcal{H}_t = [\mathcal{T} - \mathcal{V}]_t = 0$. With \mathcal{H} the Hamiltonian, \mathcal{T} the kinetic, and \mathcal{V} the potential energy of the system. The conservation of energy in finite difference schemes can be calculated via the same relation by employing a discrete version of the kinetic and the potential energy of a vibrating system.¹⁵⁰ This energy analysis is based on the Hamiltonian formalism that is based on the law of conservation of energy, which states that energy is not lost, but transferred from one form to another.¹⁵¹ Because musical instruments are always subjected to energy loss, in the form of sound radiation, internal damping¹⁵² and damping due to friction losses at interaction points between different geometries, this method can only be applied to investigate a energy gain or loss in a numerical scheme, and artificial losses (numerical damping) that a scheme adds to an otherwise lossless system. A variational formulation for physical

¹⁴⁶Kreiss, “Über die Stabilitätsdefinition für Differenzgleichungen die Partielle Differentialgleichungen approximieren”.

¹⁴⁷Also known as energy analysis Peter D. Lax: “The scope of the energy method”, in: *Bulletin of the American Mathematical Society* 66.1 (1960): 32–35.

¹⁴⁸Kreiss, “Über die Stabilitätsdefinition für Differenzgleichungen die Partielle Differentialgleichungen approximieren” showed that local stability is not synonymous with global stability in variable coefficients problems.

¹⁴⁹Strikwerda and Wade, “A survey of the Kreiss matrix theorem for power bounded families of matrices and its extensions”.

¹⁵⁰Bilbao, *Numerical Sound Synthesis*. pp. 38-40.

¹⁵¹ An interesting side-note is the historic fact that Hermann von Helmholtz was the first to give a formalised description and a proof for the conservation of energy presented in a work from 1843. <http://www-history.mcs.st-and.ac.uk/Biographies/Helmholtz.html>.

¹⁵²Transfer of mechanical energy to thermal energy in the material.

systems with losses is cumbersome to formulate with a Hamiltonian formalism,¹⁵³ but by researching an idealised system without loss, this method can be applied successfully to find stability conditions for finite difference time stepping schemes or to find formulations for new, stable finite difference schemes, as shown for instance in works of Stefan Bilbao¹⁵⁴.

Stability Analysis of Coupled Problems

The models presented in this work are all coupled problems, which have a non-linear excitation mechanism in the form of time varying excitation, changing boundary conditions due to interaction with the structure and variable coupling constants.

For these sorts of problems, analytical stability conditions are impossible to formulate by the mentioned stability measures.

A methodology for coupled dynamical systems, as presented in Ehlers, Zinatbakhsh, and Markert¹⁵⁵ can be applied to coupled problems of differential equations. In this publication, an algorithm for the stability analysis of coupled problems is developed. It makes use of the Neumann stability criterion, using the amplification matrix \mathbf{G} and the appertaining amplification polynomial $G_a(\phi)$ of the numerical scheme. The amplification polynomial is analyzed using the Schur-Cohn stability criterion, the Roth-Hurwitz criterion and finally the Liénart-Chipart criterion to analyze the algorithm.

A final remark on the stability analysis of coupled PDEs stresses the intricacy of finding explicit stability conditions for arbitrary schemes:

It is worth mentioning that to achieve an analytical critical value for the time-step size is not always feasible. In fact, the complexity of the coefficients of the Hurwitz polynomial may hinder establishing the conditions under which all the corresponding parameters of the Liénart-Chipart criterion are positive. In such cases, a numerical experiment can be used in order to find the critical size of the time step (...)

3.9.3 Stability Analysis Used in this Thesis

Because of the mentioned problems regarding the stability analysis for coupled numerical schemes used in this thesis, analytical stability conditions are not formulated for whole geometry physical models of the musical instruments. Hence, the stability conditions of the coupled models could only be gained by a numerical simulation of the problems. Nonetheless, an initial stability measure was applied for the uncoupled problems, as they could be

¹⁵³ One can apply an extended Hamiltonian or Lagrangian formulation Vikas Rastogi, Amalendu Mukherjee, and Anirban Dasgupta: “A Review on Extension of Lagrangian-Hamiltonian Mechanics”, in: *Journal of the Brazilian Society of Mechanical Science and Engineering* 18.1 (2011): 22–33.

¹⁵⁴ Bilbao, *Numerical Sound Synthesis*. Bilbao, “Conservative numerical methods for nonlinear strings”.

¹⁵⁵ Ehlers, Zinatbakhsh, and Markert, “Stability analysis of finite difference schemes revisited: A study of decoupled solution strategies for coupled multifield problems”.

3 Numerical methods

analyzed by the mentioned techniques. For the single geometries, the CFL condition was the most applicable stability measure, and an analysis of the undamped system yielded a clear stability range.

In this chapter, MATLAB and C programming language implementations of the modelled instruments are presented. These non-real-time versions of the physical models are developed to be compared to the real-time implementations described in section 6.

Another motivation for implementing the instrument models in C/MATLAB before porting them to a hardware programming language was the possibility to examine the significance of particular physical parameters, like for instance coupling strength between two geometries, non-linearities in material properties and the influence of those parameters on the synthesized sound as well as the overall simulation results. In many cases, this helped deciding which parameters were deemed important and which parameters could be left out of a model without noticeably impacting the simulation results regarding the physical accuracy and synthesis quality.

Besides characteristic, instrument specific features like a special excitation mechanism of the string (violin-bow) or a special sound-radiation (orifices of the *ruan*), the coupling between the singular instrument parts and the external excitation of the models are of special interest here.

Therefore, the high level models are developed to act as benchmark and test implementations for the final low level implementations and to validate the aptness of the underlying physical assumptions. This includes an examination regarding:

1. the stability of the numerical models,
2. the resource utilisation (computational cost) of the methods and
3. quality of the synthesis results,

the *high level* code is translated to low level hardware description language VHDL¹.

¹Very Large Scale Integrated Circuit Hardware Description Language. Properties of VHDL are discussed in

All following sections start with basic formulations of the singular instrument parts, before more complex geometries and coupled systems are introduced. The models of the singular parts of the instruments act as building blocks for the final instrument models. At the end of each section, the simulation results for the implemented models are presented.

As shown in chapter 3, the mathematical algorithm used for all modelled instruments as well as their structural parts is comparable. For 0-dimensional problems, coupled or uncoupled, the symplectic Euler integration scheme is applied. For higher dimensions, the multi-symplectic Euler box scheme is utilised. In the latter case, pseudo-spectral finite difference (PSFD) approximations for the spatial discretisation are applied.

4.1 1-dimensional wave equation models

The 1-dimensional wave equation, in all its subsets, is of fundamental importance in instrument acoustics. All important modes of vibrations of strings can be modelled by applying the 1-dimensional wave equation as the governing PDE. Transversal, longitudinal and torsional motion of strings are the basic modes of musical string vibrations. All three can be described by the 1-dimensional wave equation.²

In the following subsections, model equations for vibrating strings with different material properties and boundary conditions are presented. In all instances, the underlying PDE is the wave equation in one dimension.

There are two general assumptions regarding the attributes of vibrating strings in musical instruments which are used in this thesis:

1. Strings are fastened under very high tension, sometimes near the maximal tensile strength.
2. The transverse motion of the string is the principal sound generating effect.

By applying these two fundamental principles, a focus is put on the transverse motion of the string initially, leaving longitudinal and torsional motion out of the consideration until later. Furthermore, focussing the attention to strings under high tension permits it to leave non-linear effects, that can arise in freely hanging wires for instance aside.³

Research history

The research of the vibrating string supposedly began with Pythagoras who

more detail in section 5.

² See: Fletcher and Rossing, *Physics of Instruments*, pp. 35-68 or Morse and Ingard, *Theoretical Acoustics*, pp. 95-143.

³ For a consideration of freely hanging wires see: Herb Bailey: "Motion of a hanging chain after the free end is given an initial velocity", in: *American Journal of Physics* 68.8 (2000): 764-767.

4 Physical models

” ...is said to have observed how the divisions of a stretched string into two segments gave pleasing sounds when the length of this two segments had a simple ratio (2:1,3:1 ,3:2, etc.).⁴

There still is an ongoing debate amongst scholars about whether Pythagoras made his findings systematically, as suggested by the legend of the *Pythagorean hammer*⁵, or if he reached his conclusions empirically. It is very likely that:

(..) Pythagoras von den Erfahrungen an Instrumenten ausgegangen sein [wird].⁶

An accepted historic fact is that the

(...)ratios of pitches, which are inversely as the ratios of the lengths of the strings(...)⁷

were denominated as such by scholars following the Pythagorean school.⁸

During the year 1625, Marin Mersenne⁹ published the observation that there is a correlation between the frequency: f , the tension T , the length L , and the cross-sectional area A of a string, and formulated the law $f \sim \frac{1}{L} \sqrt{\frac{T}{A}}$. A rule that was generalised by Galileo in 1638 by replacing the cross-sectional area A with the weight per unit length as $\rho \cdot g$ ¹⁰. Brooke Taylor extended this formula and arrived at a formulation for the fundamental frequency of a string using the aforementioned properties

$$f_0 = \frac{1}{2 \cdot L} \sqrt{\frac{T}{\rho}}.^{11} \quad (4.1)$$

A mathematical derivation of the 1-dimensional wave equation and the motion of a string was proposed by Jean-Baptiste le Rond d'Alembert in 1747 (section 4.1)¹²

Lagrange derived a differential equation of the string by starting from a sonorous line model, known today as a coupled mass-spring system.¹³ In that manner, he developed a solution of

⁴Neville H. Fletcher and Thomas D. Rossing: *The Physics of Musical Instruments*, Springer Verlag, 1998, p. 36.

⁵The Pythagorean hammer legend was refuted by many researchers as it is founded on non-physical assumptions. It is most likely due to false translation of ancient sources by medieval scholars. See: Barbara Münxelhaus: *Pythagoras musicus: Zur Rezeption der pythagoreischen Musiktheorie als quadriviale Wissenschaft im lateinischen Mittelalter*, Verlag für Systematische Musikwissenschaft Bonn-Bad Godesberg, 1976, pp. 36-42.

⁶Ibid., p. 54.

⁷C. Truesdell: “Outline of the History of Flexible or Elastic Bodies to 1788”, in: *The Journal of the Acoustical Society of America* 32.12 (1960): 1647–1656.

⁸ibid.

⁹Marin Mersenne: *Harmonie universelle: Contenant la théorie et la pratique de la musique. (Paris 1636)*, Reprint Centre nat. de la recherche scientifique, Paris: Springer, 1965.

¹⁰Truesdell, “Outline of the History of Flexible or Elastic Bodies to 1788”.

¹¹ibid.

¹²In honour of d'Alembert, the one-dimensional wave equation is also known as the d'Alembert equation. See: G. F. Wheeler and W. P. Crummett: “The vibrating string controversy”, in: *American Journal of Physics* 55 (Jan. 1987): 33–37.

¹³Pierce, *Acoustics*.

as sum of sinus-functions. When taking the limit, Lagrange's solution is similar to an (odd) Fourier series.¹⁴ The solution methods proposed by d'Alembert on the one hand, and Lagrange's on the other are the most commonly applied solution methods for the 1-dimensional wave equation for linear strings.¹⁵ Even though the findings of Euler, Lagrange, or Daniel Bernoulli were based on meditations on real strings, some important physical properties eluded those early models. The bending stiffness of a string was included to the description of the string not until the laws of elasticity and flexibility were formulated.¹⁶ Non-linear effects arising from high amplitude deflection, leading to a *pitch glide* were described by Kirchhoff¹⁷. A comparable integro-differential equation for high string deflection was formulated by Carrier.¹⁸ Over the last years, several treatises suggest extensions for the accepted models including further physical properties of strings. In Rowland and Pask¹⁹ the presence of a second longitudinal wave motion in the string that is not included in the model of earlier linear strings is shown. Other findings include systems of coupled strings²⁰. Modern acoustic research of strings often focusses on effects distinct to the respective instrument and type of string. See for instance: Bader²¹ for guitar strings, Cremer²² for violin strings or Askenfelt²³ for piano strings.

Mathematical description of a linear string

A linear string without damping, losses or stiffness is a canonical example for showing basic properties of the 1-dimensional wave equation²⁴. A derivation of the PDE of the string can be achieved by using a Hamiltonian formalism²⁵, approximating the equations of motion using the action principle. A more *classical* way of derivation is a geometrical approach, taken for instance by Fletcher and Rossing.²⁶

Consider a linear string²⁷ under tension T , fixed at two points x_0 and x_L . At both points (the boundary), the displacement of the string is set to zero $u(x) = 0$ for $\{x \in 0 \vee L\}$. Suppose

¹⁴Wheeler and Crummett, "The vibrating string controversy".

¹⁵The Lagrange solution method is also known as the Bernoulli solution. See: Kuypers, *Klassische Mechanik*, pp. 250-252.

¹⁶Truesdell, "Outline of the History of Flexible or Elastic Bodies to 1788".

¹⁷Li-Qun Chen and Hu Ding: "Two nonlinear models of a transversely vibrating string", English, in: *Archive of Applied Mechanics* 78.5 (2008): 321-328.

¹⁸G.F. Carrier: "On the non-linear vibration problem of the elastic string", in: *Quarterly of Applied Mathematics* 3 (1945): 157-165.

¹⁹Rowland and Pask, "The missing wave momentum mystery".

²⁰Chabassier and Chaigne, "Modeling and numerical simulation of a nonlinear system of piano strings coupled to a soundboard".

²¹Bader, "Complete Geometric Computer Simulation of a Classical Guitar".

²²Cremer, *Physik der Geige*, pp. 29-170.

²³A. Askenfelt: *Five Lectures on the Acoustics of the Piano*, Publications issued by the Royal Swedish Academy of Music, Kungl. Musikaliska Akademien, 1990.

²⁴Kuypers, *Klassische Mechanik*, pp. 237-261.

²⁵Michael E. Taylor: *Partial Differential Equations I*, Berlin and Heidelberg: Springer, 1996, p. 116.

²⁶Fletcher and Rossing, *Physics of Instruments*, p. 22.

²⁷Linear material properties and total elasticity is assumed.

4 Physical models

we take a small part of the string from x to $x + \Delta x$ in the domain $x \in [0, L]$. If this small part is displaced from equilibrium then the force, acting on this segment, can be written as the deflection difference between two points x and $x + \Delta x$. See figure 4.1.

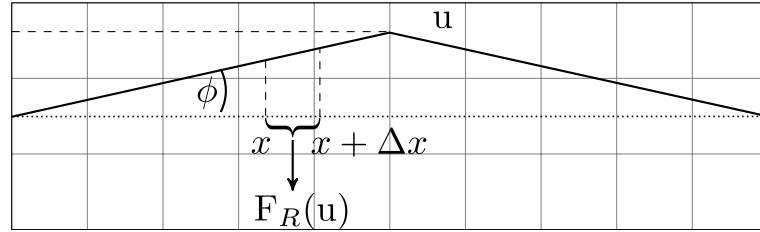


Figure 4.1: String segment displaced from equilibrium.

The restoring force acting on the small portion of the string, is the difference

$$F_R = T \sin(\phi_{x+\Delta x}) - T \sin(\phi_x). \quad (4.2)$$

By applying the Taylor's formula

$$f(x + \Delta x) = f(x) + \frac{\partial f(x)}{\partial x} dx + \dots \quad (4.3)$$

to the first term on the right-hand side, keeping only the linear terms we can rewrite equation 4.2 to

$$F_R = T \sin(\phi_x) + T \frac{\partial \sin(\phi_x)}{\partial x} dx - T \sin(\phi_x) = T \frac{\partial \sin(\phi_x)}{\partial x}. \quad (4.4)$$

For a small displacement of the string we can state that: $\sin(\phi_x) \approx \tan(\phi_x)$ ²⁸. The tangent of an angle can be rewritten as

$$\tan(\phi_x) = \frac{\partial \mathbf{u}}{\partial x}. \quad (4.5)$$

Using equation 4.4 and 4.5 we can state

$$F_R = T \frac{\partial \sin(\phi_x)}{\partial x} dx = T \frac{\partial \tan(\phi_x)}{\partial x} dx = T \frac{\partial \frac{\partial \mathbf{u}}{\partial x}}{\partial x} dx = T \frac{\partial^2 \mathbf{u}}{\partial x^2} dx. \quad (4.6)$$

With Newtons second law of motion

$$F = ma = m \frac{\partial^2 \mathbf{u}}{\partial t^2}, \quad (4.7)$$

²⁸A significant difference between the *tangent* and sinus starts at angles \geq than 40 degrees. As is depicted in the first image in Appendix 2, the angle between the banjo string and the bridge when initially deflected is about 30 degree.

4 Physical models

we can say

$$\begin{aligned} F_R &= T \frac{\partial^2 \mathbf{u}}{\partial x^2} dx \\ m \frac{\partial^2 \mathbf{u}}{\partial t^2} &= T \frac{\partial^2 \mathbf{u}}{\partial x^2} dx. \end{aligned} \quad (4.8)$$

The mass m is given as $m = \rho \Delta x^{29}$ with ρ is the density of the string. When we let $dx \rightarrow 0$ we can set $dx = \Delta x$. This results in the well known formulation of the 1-dimensional wave equation

$$\frac{\partial^2 u}{\partial t^2} = \frac{T}{\rho} \frac{\partial^2 u}{\partial x^2}. \quad (4.9)$$

Numerical Model of a Linear String

In this model only the transversal motion in one polarisation of the string is regarded here. The time integrator, as presented in section 3.7, based on the PDE, presented in chapter 2 using equation 4.9 can be written as

$$\begin{bmatrix} \mathcal{A} \\ \mathcal{V} \\ \mathcal{U} \end{bmatrix} = \bigcup_{t=1}^T \left\{ \begin{array}{l} \mathcal{F}^{-1} \left[\hat{\delta}_{xx} \cdot \mathcal{F} [\tau_{t-} \mathbf{u}] \right] \\ \tau_{t-} \mathbf{v} + \mathbf{a} \\ \tau_{t-} \mathbf{u} + \mathbf{v} \end{array} \right\}, \quad (4.10)$$

with $\mathcal{A}, \mathcal{V}, \mathcal{U}$ the total acceleration, velocity and deflection over the spatial domain $0, \dots, L$ and the time interval $1 < t \leq T$. τ is the time shift operator, $\hat{\delta}_{xx}$ the Fourier transformed, weighted central differences operator of order $N = \frac{L}{\Delta x}$ defined in equation 3.75, and $\mathbf{a}, \mathbf{v}, \mathbf{u}$ the acceleration, velocity and deflection in vector representation over the spatial domain.

Simulation Parameters:

The following model of the linear string is simulated with the parameters given in Table 4.1.

Parameters	Values
Sample frequency	2^{17} Hz
Δt	2^{-17} Hz
Discrete points N	128
Length of the string in meters	0.65
Δx	$\frac{0.65}{127}$
Wave propagation speed c	$\frac{1}{\frac{\Delta x}{\Delta t}}$

Table 4.1: Values for the linear string model.

²⁹This can be assumed if we neglect the changing length of the string and work under the assumption that the deflection is small.

Simulation Results

The numerical results of the linear string model are depicted in 4.2, which depicts the motion of the whole string over time resulting from a symmetric triangular excitation. In the next series of figures, one can see the movement of a string excited by a Gaussian pulse with Neumann boundary conditions. In figure 4.4, the spectrum of the string with a triangular deflection is depicted.

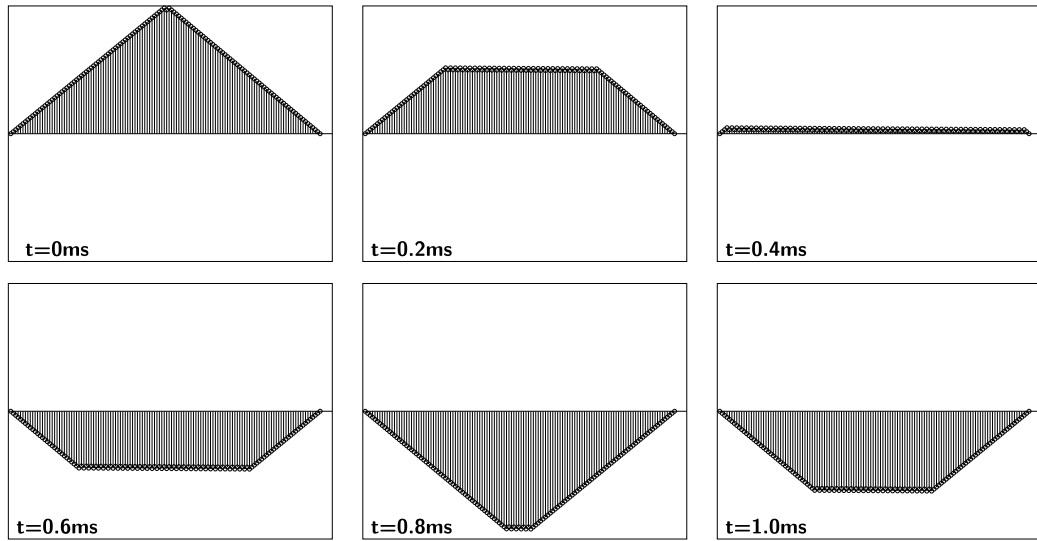


Figure 4.2: Time series of a linear string, deflected in triangular shape at $t = 0$.

Figure 4.3 shows the deflection of a point on the string with a shifted triangular deflection as initial condition.,

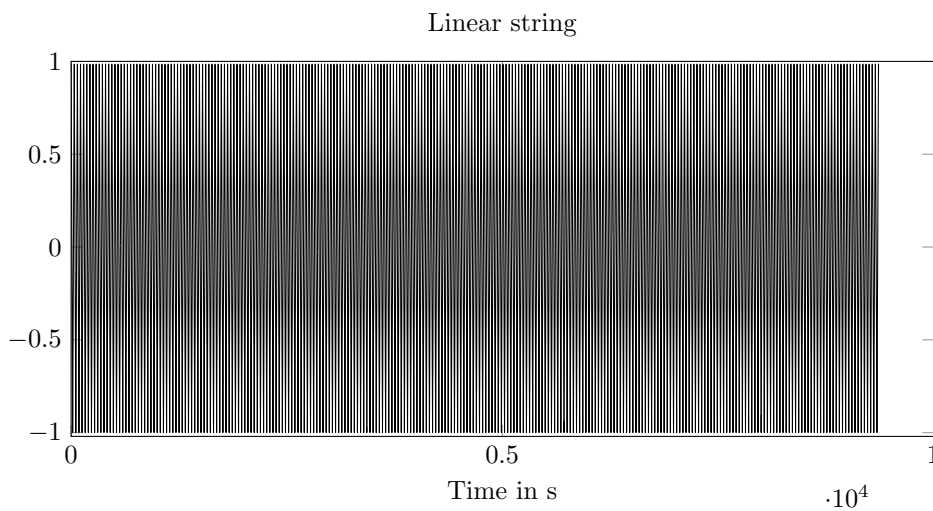


Figure 4.3: Simulation of linear string with triangular deflection.

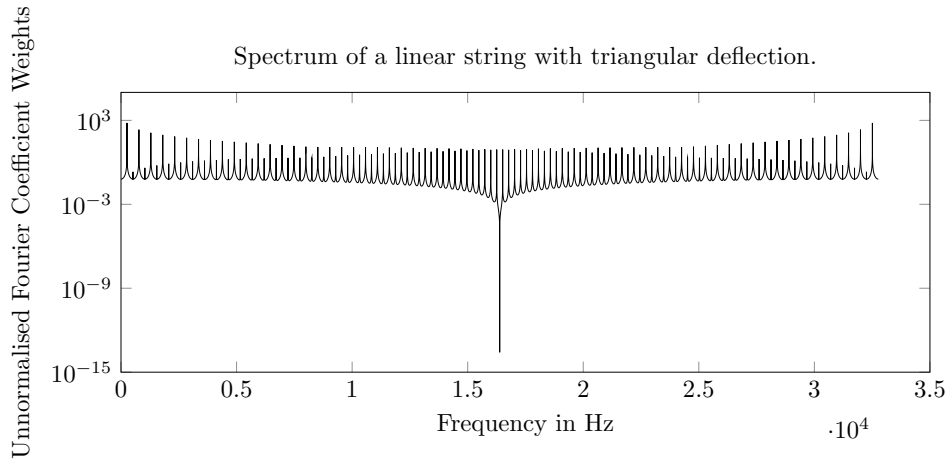


Figure 4.4: Spectrum of the string vibration shown in Figure 4.3.

Boundary conditions

The 1-dimensional wave equation, used to model the motion of an instrument string, can exhibit different boundary conditions. For a completely rigid string fixation Dirichlet boundary conditions can be applied. They are defined as $u(0) = u(L) = 0$.

Even though the derivation of equation 4.9 assumes fixed boundary conditions, realistic strings are never completely fixed at their boundaries. Especially in lute instruments, there is an considerable amount of energy transfer at the coupling points between strings, bridge, and soundboard.

Depending on the rigidity of the fixation, the string boundaries exhibit a finite impedance when attached to an instrument body or other kind of resonator. A first approximation for this effect can be developed by supposing that the bridge acts as a mass, connected to the boundary point of the string. For small deflections and a bridge mass that is large compared to the mass of the string point, the slope of the string at the boundary B exerts the force $F_B = T u_x|_B$.³⁰ In this assumption, only the restoring force due to the tension T is taken into account. To extend this model by including more realistic conditions, the force resulting from the bending stiffness of the string can be added. Taking the same point at the interaction between string and bridge, the shear force exerted by the string can be written as $F_{B_s} = EI u_{xxx}|_B$.

Combining both forces results in an approximation of the transversally acting force at the coupling point

$$F_B = B \cdot \frac{\partial^3 u_b}{\partial x^3} + T \cdot \frac{\partial u}{\partial x} \quad (4.11)$$

³⁰This expression can be derived by using Taylor's formula similar to the derivation of equation 4.9.

4 Physical models

with B the bending stiffness³¹ and T the tension of the string. This consideration only holds if the deflection of the string is small, which is usually the case for the instruments under consideration.

A second boundary condition that can be used in the model of a linear strings is the Neumann boundary conditions, named after the German mathematician Carl Gottfried Neumann.³² Using finite differences, the Neumann boundary condition can be approximated as

$$u_x|_i = 0 \approx \frac{-u_{i-1} + u_i}{2 * \Delta x} = 0 \rightarrow u_i = u_{i-1}. \quad (4.12)$$

A temporal evolution of a string excited by a Gaussian pulse at time-step $t = 0$ is depicted in Figure 4.5.

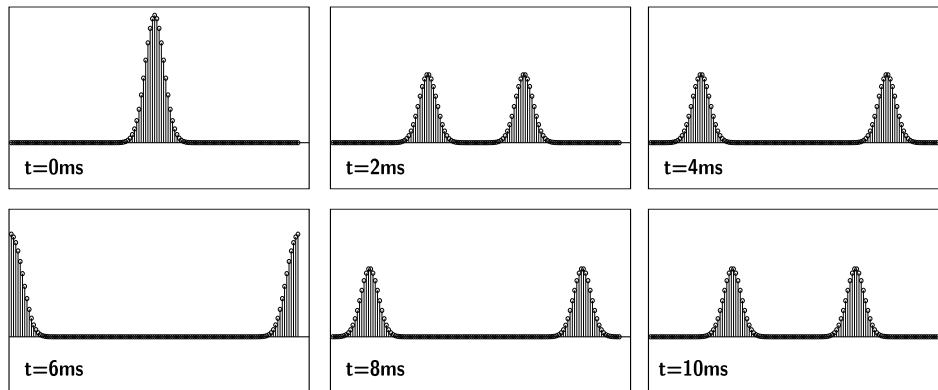


Figure 4.5: Time series of a linear string with Neumann boundary conditions, deflected with a Gaussian bell shape at $t = 0$.

Along with these boundary conditions there are Robin boundary conditions which use the proposition that the strings are fixed at an elastic boundary modelled as a spring. They can be written as

$$a \cdot u + b \frac{\partial u}{\partial n} = C, \quad (4.13)$$

with a, b constants depending on the boundary, u the deflection, $\frac{\partial}{\partial n}$ a first derivative in the normal direction, and C a constant boundary value. Other boundary conditions, implemented in later models of whole geometry simulations are described in the following subsections.

³¹The bending stiffness is defined as before $B = EI = ESK^2$ with E the Young's modulus, S the cross-sectional area and K the radius of gyration.

³² They are not named after the American mathematician John von Neumann. In some publications they are called *von Neumann* boundary conditions. See for instance: Francisco M Fernández and Eduardo A Castro: "Hypervirial analysis of enclosed quantum mechanical systems. II. von Neumann boundary conditions and periodic potentials", in: *International Journal of Quantum Chemistry* 19.4 (1981): 533–543.

Discussion

As one can see from figure 4.3 and 4.4, if one chooses the right ratio for Δx and Δt , the simulation yields analytic results of the wave equation. There is no visible dispersion or losses, and the spectrum shows an ideal $\frac{N}{1}$ for $N \in 1, \dots$, Number of partials. The influence of an different ratio of Δt and Δx is shown by Bilbao,³³ and he develops a methodology for approximating an ideal ratio to build schemes with a small numerical error.

4.1.1 Linear string with damping

To model a vibrating string more realistically, losses can be added to the linear non-dispersive 1-dimensional string. Dispersion, or energy losses, can be modelled by different means, and as the result of the following physical parameters:

- Velocity damping due to external (air) friction.
- Internal damping due to losses in the material because of non-linearities³⁴.
- Damping due to losses at the boundaries.³⁵

Velocity damping

Velocity damping can be modelled by adding a damping term with the dimensionless constant $\alpha \in (0 \dots 1)$ to the linear wave equation. In real strings the acting air friction is negligibly small in most cases because of the small circumference and the resulting small surface of the string. Nevertheless, of It is one of the standard techniques to model losses in strings³⁶ by adding a friction damping term, resulting in an exponential decay of a string. The linear DE with an additional velocity damping term can be written as

$$\mathbf{u}_{tt} - c^2 \cdot \mathbf{u}_{xx} + \alpha \cdot \mathbf{u}_t = 0. \quad (4.14)$$

With $\mathbf{v} = \mathbf{u}_t$, the time stepping scheme can be rewritten to

$$\begin{bmatrix} \mathcal{A} \\ \mathcal{V} \\ \mathcal{U} \end{bmatrix} = \bigcup_{t=1}^T \left\{ \begin{array}{l} \mathcal{F}^{-1} \left[\hat{\delta}_{xx} \cdot \mathcal{F} [\tau_t - \mathbf{u}] \right] - \alpha \cdot \tau_t - \mathbf{v} \\ \tau_t - \mathbf{v} + \mathbf{a} \\ \tau_t - \mathbf{u} + \mathbf{v} \end{array} \right\}. \quad (4.15)$$

³³Bilbao, *Numerical Sound Synthesis*. Pp. 135-136.

³⁴This exact mechanism of internal damping is still under heavy research in various fields of nano-mechanics.

³⁵Numerical damping, or numerical viscosity, as used in fluid dynamic simulations is not mentioned here because there is only partial physical reasoning behind this technique. It goes back to the work of Neumann and Richtmyer (Neumann and Richtmyer, "A Method for the Numerical Calculation of Hydrodynamic Shocks") and is applied in computational fluid dynamics since that time. See: E.J. Caramana, M.J. Shashkov, and P.P. Whalen: "Formulations of Artificial Viscosity for Multi-dimensional Shock Wave Computations", in: *Journal of Computational Physics* 144 (1998): 70-97.

³⁶Bilbao, *Numerical Sound Synthesis*. pp. 153 ff.

All other constant and variable names are inherited from equation 4.34.

Simulation Results

Figure 4.6 and Figure 4.7 show the time evolution of a simulated string with different values of velocity damping factor β . Figure 4.8 shows the spectrum of a linear string with different velocity damping factors.

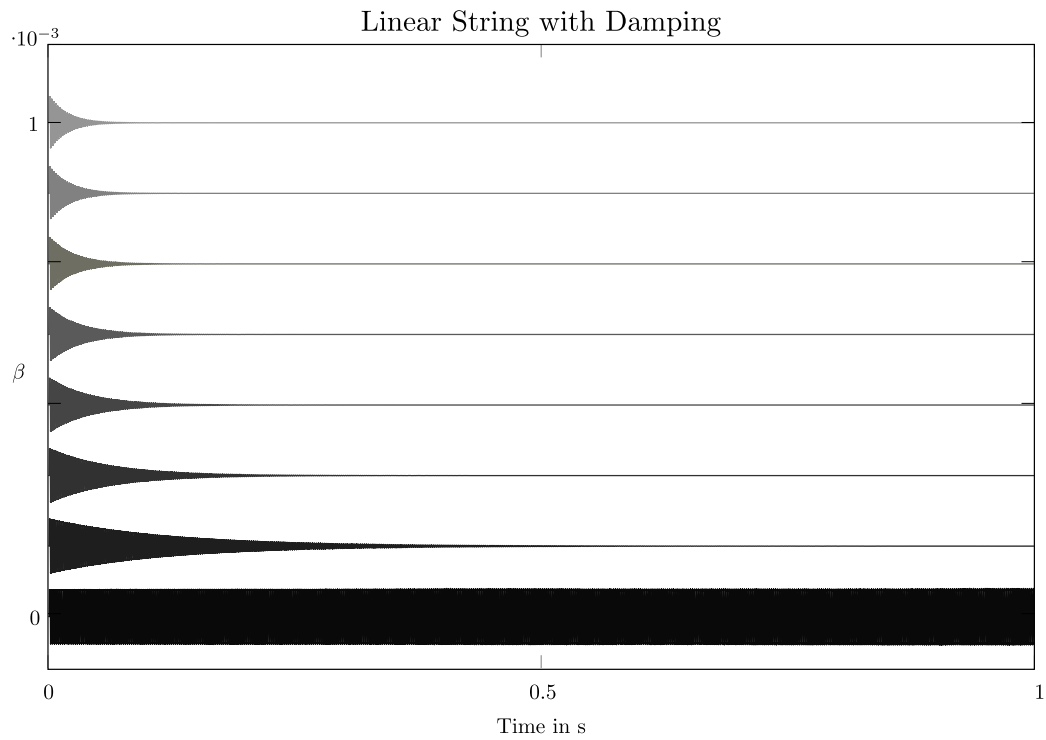


Figure 4.6: String with different damping factors β from undamped to highly damped.

4 Physical models

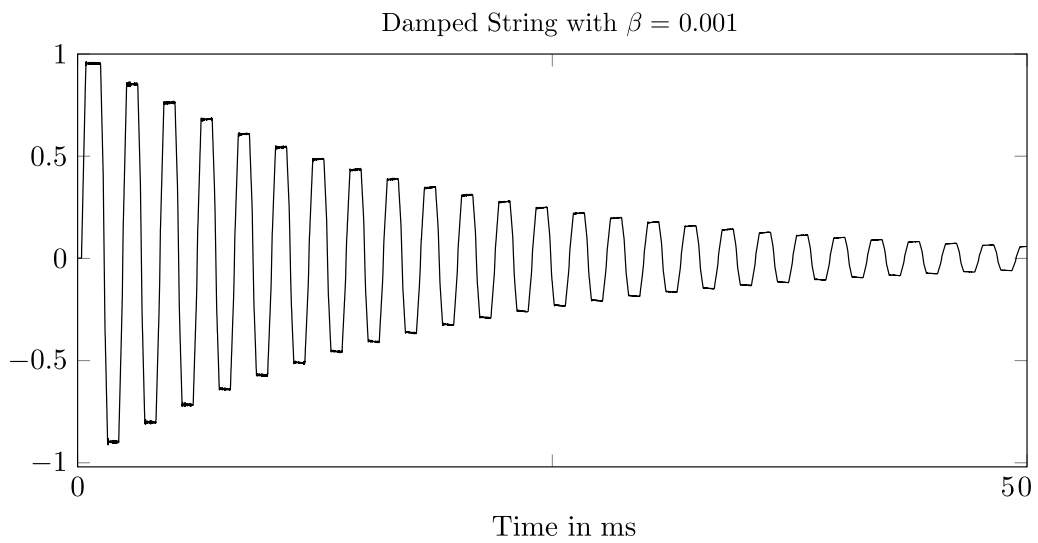


Figure 4.7: Enlarged part of damped string with $\beta = 0.001$.

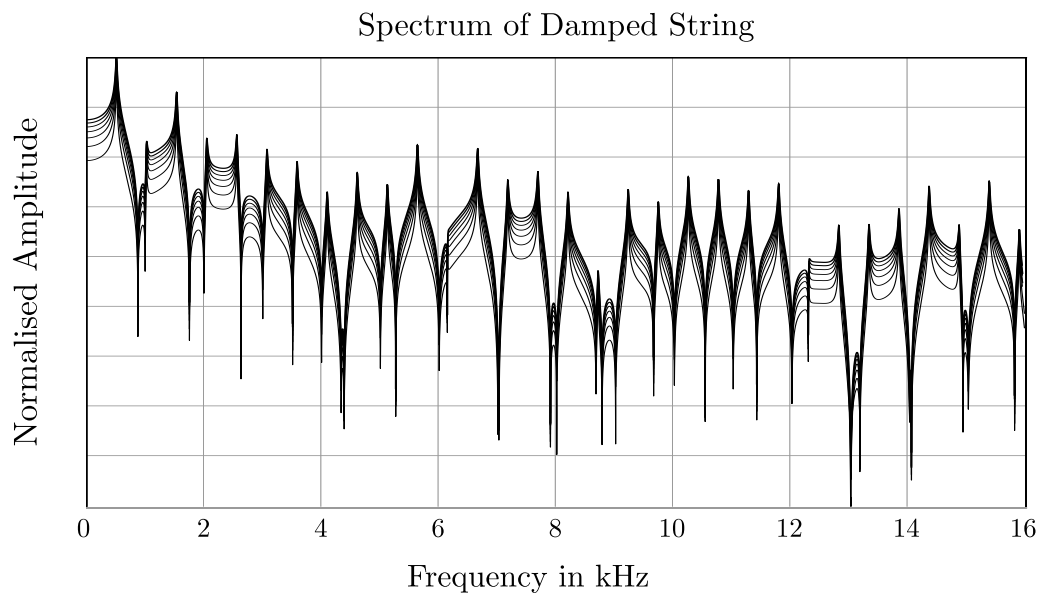


Figure 4.8: Spectrum of a string with different damping factors β from undamped to highly damped.

Review

Figure 4.6 to Figure 4.7 show the influence of velocity damping on the vibration of a linear string model. The exponential decay does not influence the peaks of the strings' partials. Thus, its initial shape remains unchanged only the strings amplitude decreases exponentially.

Internal damping

The exact physical mechanisms of internal damping of acoustic materials are not as well understood as the mechanisms of velocity dependent damping. But to simulate internal damping one can propose a damping that is dependant on the acceleration of the string at the respective point³⁷. It is proposed that internal losses account for frequency dependent losses of the string. Based on this preliminary assumption, one can use the method presented by Hong and Lee³⁸ and extended by Bavu³⁹, to find values for internal damping coefficients. The DE for a string with frequency dependent losses can be written as

$$\mathbf{u}_{tt} = c^2 \cdot \mathbf{u}_{xx} + \alpha \cdot \mathbf{u}_{xxt} = 0. \quad (4.16)$$

The third order term on the right side can be interpreted as a time derivative of the acceleration of the linear string. So one can rewrite equation 4.16 into the following time stepping form

$$\begin{bmatrix} \mathcal{A} \\ \mathcal{V} \\ \mathcal{U} \end{bmatrix} = \bigcup_{t=1}^T \left\{ \begin{array}{l} \mathcal{F}^{-1} \left[\hat{\delta}_{xx} \cdot \mathcal{F} [\tau_{t-} \mathbf{u}] (1 - \alpha \cdot \delta_t) \right] \\ \tau_{t-} \mathbf{v} + \mathbf{a} \\ \tau_{t-} \mathbf{u} + \mathbf{v} \end{array} \right\}. \quad (4.17)$$

Simulation Results

Figure 4.9 shows two sections of the time evolution of a simulated string with different values of internal damping factor α . Figure 4.9 **a** shows the first 15 milliseconds of the simulated string, Figure 4.9 **b** shows the deflection of the string at around 5 seconds simulation time.

³⁷This kind of damping was proposed for physical models of strings by: Chaigne and Askenfelt, “Numerical simulations of piano strings. I. A physical model for a struck string using finite difference methods”.

³⁸(S.-W. Hong and C.-W. Lee: “Frequency and time domain analysis of linear systems with frequency dependent parameters”, in: *Journal of Sound and Vibration* 127.2 [1988]: 365–378).

³⁹Julien Bensa et al.: “The simulation of piano string vibration: From physical models to finite difference schemes and digital waveguides”, in: *The Journal of the Acoustical Society of America* 114.2 (2003): 1095–1107.

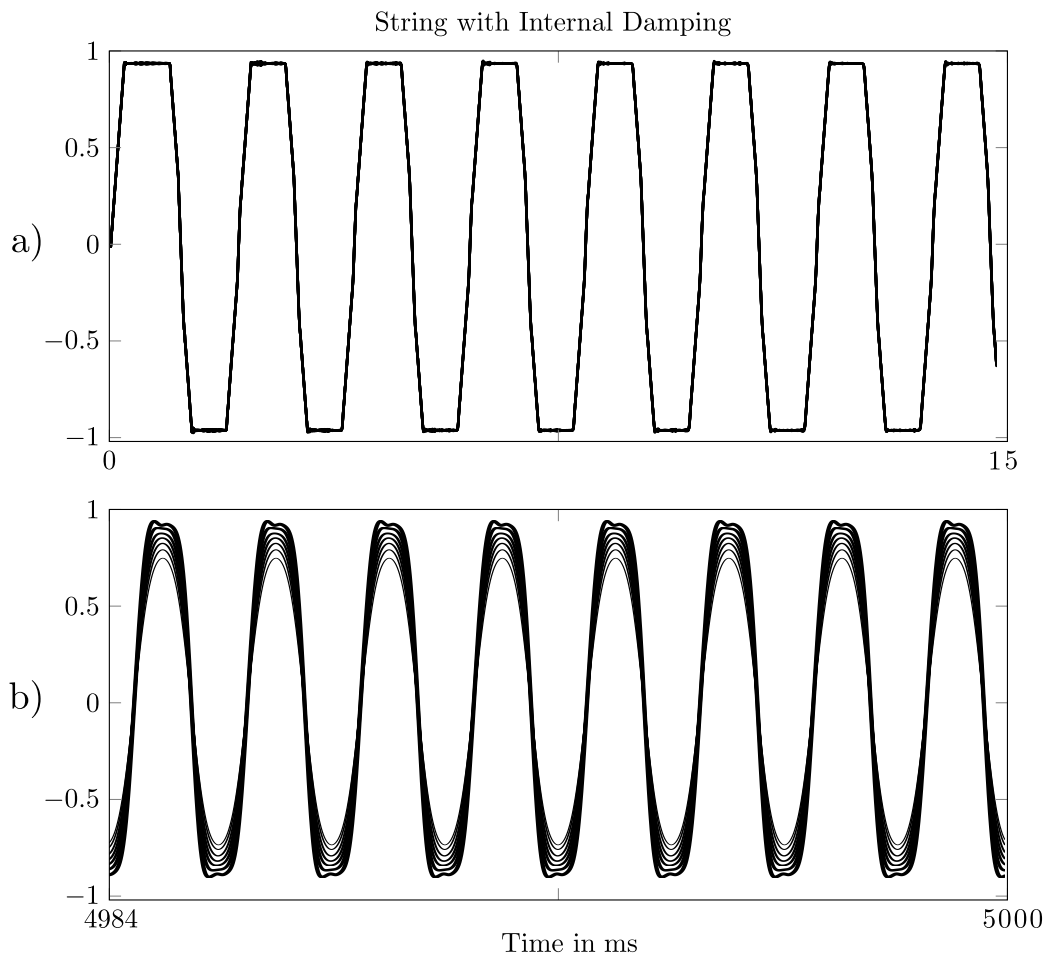


Figure 4.9: String with different internal damping factors α from undamped to highly damped.

Review

As visible in figure

Damping at the boundaries

Damping due to losses at the boundaries can be modelled by either adding a virtual impedance at one end point of the string⁴⁰, by increasing the velocity damping at the boundary or simulating a moving endpoint. A virtual impedance at point L of the string is proposed, leading to a formulation of the force at the end point

$$F_L = Z \cdot v \rightarrow a = \frac{Z \cdot v}{m_L} \quad (4.18)$$

⁴⁰This is an easy formulation for moving string adjustments (Fletcher and Rossing, *Physics of Instruments*).

with m_L the mass of the string portion and the virtual mass attached at point L . A higher velocity damping is straight-forward to implement by applying open boundary conditions and changing the damping coefficients at the respective points 0 and L . A moving end-point can be modelled by adding either a mass or a spring with a higher stiffness at the end points. A simplified version of a slightly loose endpoint can be modelled by setting the deflection at the boundary points of the string to a value between free and fixed boundary conditions.

4.1.2 High Deflection String

Instrument strings can be subject to various non-linear effects, like for instance the special boundary conditions of sitar strings⁴¹ or the non-linear excitation of violin strings. A non-linear effect that directly influences physical properties of the string is a changing length, due to high amplitude vibrations or *in situ* tuning of the string. There are several ways to model these effects with physical methods. A commonly utilised approach for including non-linear effects due to large amplitudes can be described by adding a non-linear duffing term to the linear wave equation. This yields

$$\mathbf{u}_{tt} - c^2 \cdot \mathbf{u}_{xx} - \alpha \cdot \mathbf{u}^3 = 0. \quad (4.19)$$

The Duffing equation, developed by the German engineer Georg Duffing and named after him, can be applied to model non-linear stiffness effects in varying fields, as shown in Brennan and Kovacic.⁴² By analysing equation 4.19, one finds that the non-linear *Duffing*-term adds a deflection dependent restoring force, which can be reasoned as a higher stiffness in the extremal ranges of the string deflection. By adding this term to a time stepping method, one can simulate pitch glides in strings and membranes⁴³. A second method of modelling a deflection dependent tension modulation, is by integrating over the length of the string

$$\rho \mathbf{u}_{tt} - \frac{1}{\rho A} \cdot \left(T_0 + \frac{k}{2L} \int_{x=1}^L \mathbf{u}_x^2 \right) \mathbf{u}_{xx} = 0, \quad (4.20)$$

with T_0 the tension in the rest position of the string, ρ the density, E the Young's modulus and A the cross section respectively. This equation is also known as the Kirchhoff equation.⁴⁴

⁴¹Chandrika P. Vyasarayani, Stephen Birkett, and John McPhee: "Modeling the dynamics of a vibrating string with a finite distributed unilateral constraint: Application to the sitar", in: *The Journal of the Acoustical Society of America* 125.6 (2009): 3673–3682.

⁴²Michael J. Brennan and Ivana Kovacic: "Examples of Physical Systems Described by the Duffing Equation", in: *The Duffing Equation*, John Wiley & Sons, Ltd, 2011: 25–53.

⁴³For membranes see section 4.2.2.

⁴⁴It was first derived by: Gustav Kirchhoff: *Vorlesungen über mathematische Physik. Mechanik*, H. G. Treubner, 1876, p. 446.

4 Physical models

Later, Carrier⁴⁵ derived a similar equation that can be written in the form

$$\rho \mathbf{u}_{tt} - T_0 \cdot \left(1 + \frac{Er}{LT_0} \int_{x=1}^L \mathbf{u}^2\right) \mathbf{u}_{xx} = 0, \quad (4.21)$$

with r the diameter of the cross-section.

Another way of including the influence of changing length of a string that is applied in several works concerned with non-linear string motion, can be derived by using the general 1-dimensional wave equation of the form

$$u_{tt} = [c(x) \cdot u_x]_x, \quad (4.22)$$

with $c = \frac{T}{\rho}$. With the proposition that the tension is time dependent⁴⁶, one can rewrite equation 4.22 to

$$u_{tt} = \left[\frac{T(x, t)}{\rho} \cdot u_x\right]_x. \quad (4.23)$$

In equation 4.23, one directly sees how the changing deflection (curvature) has an immediate influence on the tension of the string.

Another way to take the changing length of the string into account, as proposed by Vargas-Jarillo and Gonzalez-Santos⁴⁷ or Bader,⁴⁸ is to formulate a non-static finite difference grid. In these works, this method is described as a straight-forward way of coupling the longitudinal motion of the string to the transversal motion, and vice versa. If one takes a finite point on a string, one can include the longitudinal deflection of the finite points directly in the formulation of the finite differences terms. Equation 3.50 gives a formulation for the exact force acting on a quasi-particle in transversal direction. The longitudinal movement can be added to the string by rewriting equation 3.50 to

$$\begin{aligned} F_{left} &= -F_0 \cdot \left(1 - \sqrt{l_0 + (u[m2]_{lo} - u[m1]_{lo})^2 + (u[m2]_{tr} - u[m1]_{tr})^2}\right) \\ &\quad \cdot \frac{u[m2]_{tr} - u[m1]_{tr}}{\sqrt{l_0 + (u[m2]_{lo} - u[m1]_{lo})^2 + (u[m2]_{tr} - u[m1]_{tr})^2}} \\ F_{right} &= -F_0 \cdot \left(1 - \sqrt{l_0 + (u[m2]_{lo} - u[m1]_{lo})^2 + (u[m2]_{tr} - u[m1]_{tr})^2}\right) \\ &\quad \cdot \frac{-u[m3]_{tr} + u[m2]_{tr}}{\sqrt{l_0 + (u[m2]_{lo} + u[m3]_{lo})^2 + (u[m2]_{tr} - u[m3]_{tr})^2}} \end{aligned} \quad (4.24)$$

49

⁴⁵Carrier, "On the non-linear vibration problem of the elastic string".

⁴⁶It depends on the change of deflection over time or the changing in curvature.

⁴⁷C. Vargas-Jarillo and G. Gonzalez-Santos: "A Numerical Study of Discrete Nonlinear Elastic Strings in Two Dimensions", in: *Proceedings of the CCE 2010* (2010): 400-405.

⁴⁸Bader, *Computational Mechanics of the Classical Guitar*.

⁴⁹Similar formulations can be found in several works like for instance: Rowland and Pask, "The missing wave

4 Physical models

An analysis of equation 4.24 shows that this formulation leads to paradoxical results. If the string is deflected and thus has a high extension, Δx gets larger, but, as Δx gets larger, the pitch of the modelled string must go down because the pitch is inversely proportional to Δx in the formulation of finite differences. Hence, this scheme can not be applied to model non-linear effects due to longitudinal – transversal coupling with satisfactory, realistic results.

Numerical results

The following figure depicts the spectrum of a non-linear restoring force, modelled by adding a Duffing term to the linear wave equation.

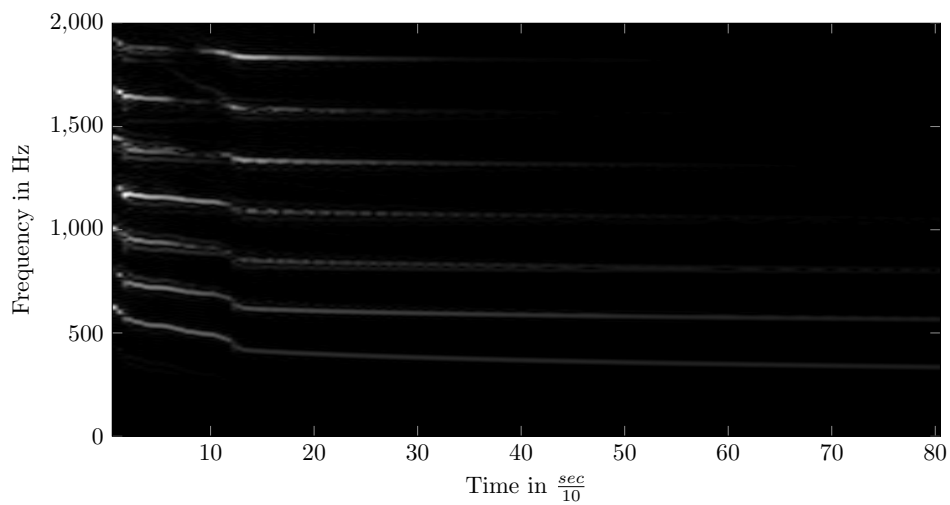


Figure 4.10: Spectrogram of string with non-linear Duffing-term. $\alpha = 0.001$

Figure 4.11 show the spectrum of a simulations using equation 4.24.

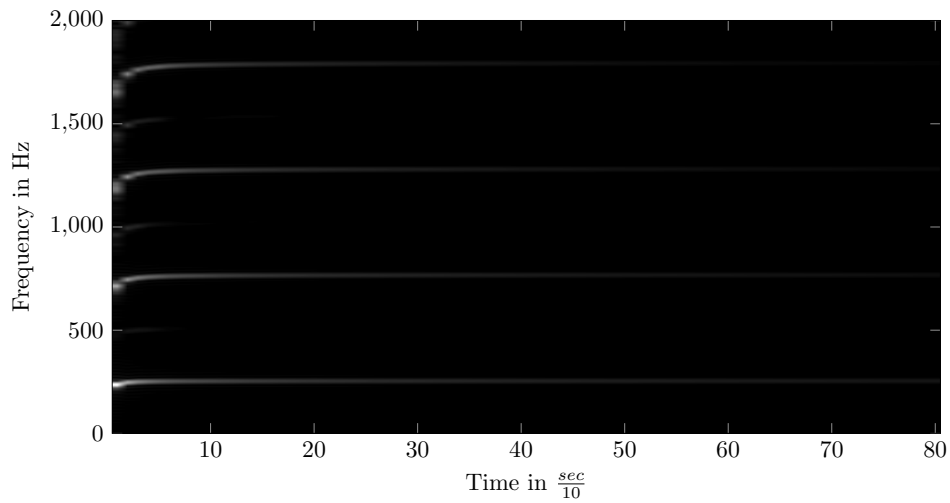


Figure 4.11: Spectrogram of string with non-linear geometric coupling.

The next figure shows the spectrum of a string with Kirchhoff-Carrier term added to model the effects of high-deflection pitch glides.

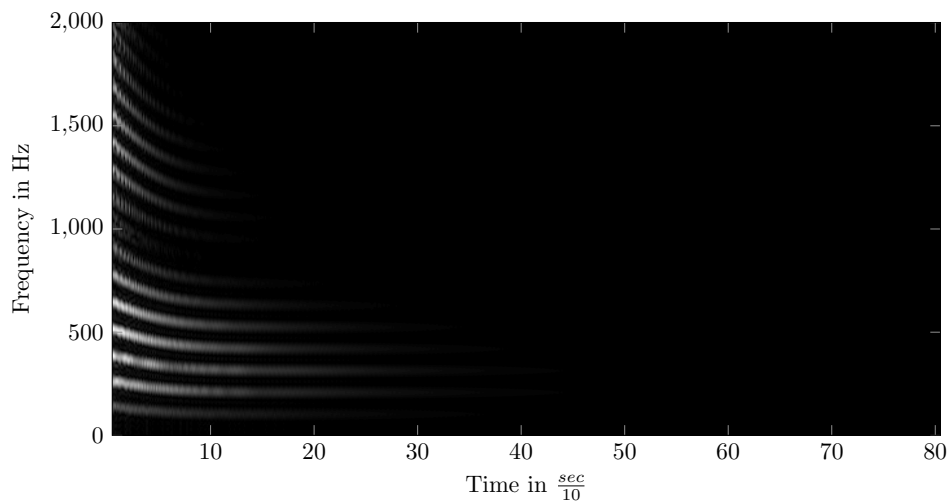


Figure 4.12: Spectrogram of string with Kirchhoff-Carrier-type term.

Discussion

An analysis of pitch glides found in real strings shows that a changing length has a greater influence on the tension T of the string, but not as much on the density ρ ⁵⁰. A question that arises is: Does the changing length of the string act locally or globally on the tension? If one analyses PDE 4.22 one finds that the tension should act globally and only due to the

⁵⁰The changing density can be neglected only for metal strings and maybe nylon strings. For rubber strings made of polyisoprene, it must be taken into consideration.

effects of the strings overall deflection. But if the difference equation is analysed, one can ask how the information of the changing length should be propagated instantaneously over the whole domain of the string without violating the speed of information transport in a string. The proposed models of the wave equation for a taut string reveal that the longitudinal movement could transport this kind of information. But then again, how is the changing length transferred to all segments of the string immediately, and why does the longitudinal motion, which also has a wave like characteristic, and thus should travel up and down the string, transport the changing length instantaneously?

When modelling the influence of the changing length, as proposed in equation 4.24, one is confronted with a paradox: If the longitudinal interval of two adjacent quasi-particles gets smaller, the pitch of the modelled string rises because of the inversely quadratic influence of the step width on the pitch. In a real string, the exact opposite is the truth: If a string is relaxed, the pitch is lowered. This means, in a physical model of the string, the influence of a changing length onto the tension must be much stronger than the local influence of changing quasi-particle distance. In conclusion: With this knowledge the only reasonable way of modelling the effect of changing length is by including a Kirchhoff-Carrier like term to the wave equation.

It is supposed that the changing tension is not transported via an acoustical longitudinal wave, but a different material property not coupled to the acoustical transversal motion of the string.

4.1.3 String with Bending Stiffness

Equation 4.9 describes the transverse motion of strings accurately if all assumptions, made in the derivation are met to a certain degree. The hypothesis of total elasticity, used in derivation of the PDE is a simplification of physical properties of real strings used in banjos and most other lute instruments as they have an inherent stiffness. Even nylon strings, used in classical guitars, have a finite bending stiffness which is considerably smaller than that of metal strings but influences the strings vibration nonetheless. The effects of bending stiffness can be included into the mathematical formulation of a string by adding beam like term to equation 4.9. It can be modelled as

$$\rho \frac{\partial^2 \mathbf{u}}{\partial t^2} = T \frac{\partial^2 \mathbf{u}}{\partial x^2} - EI \frac{\partial^4 \mathbf{u}}{\partial x^4}, \quad (4.25)$$

with E the Young's modulus and I the second moment of area, which is $\frac{\pi^2}{4} r^4$, with r the circumference of the string, for round strings. The inclusion of bending stiffness into the PDE of a string influences its spectral properties, because the additional beam-like characteristics of a stiff string has an influence on the position of the partials in the spectrum and, depending on the circumference of the string in relation to its length, adds frequencies to the spectrum of

4 Physical models

the string. The perceptual importance of bending stiffness for the lower tones of a piano was shown in Anderson and Strong.⁵¹ In violin strings, bending stiffness influences the rounding of the *Helmholtz* motion corners.⁵²

Up to this point of the work, the presented string models were based on the (linear) 1-dimensional wave equation that is valid for completely elastic strings and motion in one direction. In real strings, however, one finds that the larger the circumference compared to the length of the string is, the more important the influence of bending stiffness on the vibration and the resulting sound of the string is. The inharmonicity in piano strings, especially important in the lower register⁵³ of the piano or large bowed instruments, as cellos or contrabasses, can be modelled by adding beam-like characteristics to the model of the string. The physical motivation for the inclusion of bending stiffness into the model of a string is explained in section 4.1.3. As shown there, adding a beam-like term⁵⁴ to the linear 1-dimensional wave equation⁵⁵, we obtain the following PDE

$$\mathbf{u}_{tt} - c^2 \cdot \mathbf{u}_{xx} - \xi \cdot \mathbf{u}_{4x} = 0, \quad (4.26)$$

with $\xi = \frac{EI}{m\mu}$. The time stepping algorithm can be extended to

$$\begin{bmatrix} \mathcal{A} \\ \mathcal{V} \\ \mathcal{U} \end{bmatrix} = \bigcup_{t=1}^T \left\{ \begin{array}{l} \mathcal{F}^{-1} \left[(\hat{\delta}_{xx} - \hat{\delta}_{4x}) \cdot \mathcal{F} [\tau_{t-\mathbf{u}}] \right] \\ \tau_{t-\mathbf{v}} + \mathbf{a} \\ \tau_{t-\mathbf{u}} + \mathbf{v} \end{array} \right\}. \quad (4.27)$$

Simulation Results

Figure 4.13 shows a string with added bending stiffness modelled as an Euler-Bernoulli-like beam-like term.

⁵¹Brian E. Anderson and William J. Strong: “The effect of inharmonic partials on pitch of piano tones”, in: *The Journal of the Acoustical Society of America* 117.5 (2005): 3268–3272.

⁵²Cremer, *Physik der Geige*, p. 38.

⁵³Balazs Bank and Heidi-Maria Lehtonen: “Perception of longitudinal components in piano string vibrations”, in: *The Journal of the Acoustical Society of America* 128.3 (2010): EL117–EL123.

⁵⁴A fourth order differential term from the Euler-Bernoulli beam equation.

⁵⁵Fletcher and Rossing, *Physics of Instruments*, p. 43.

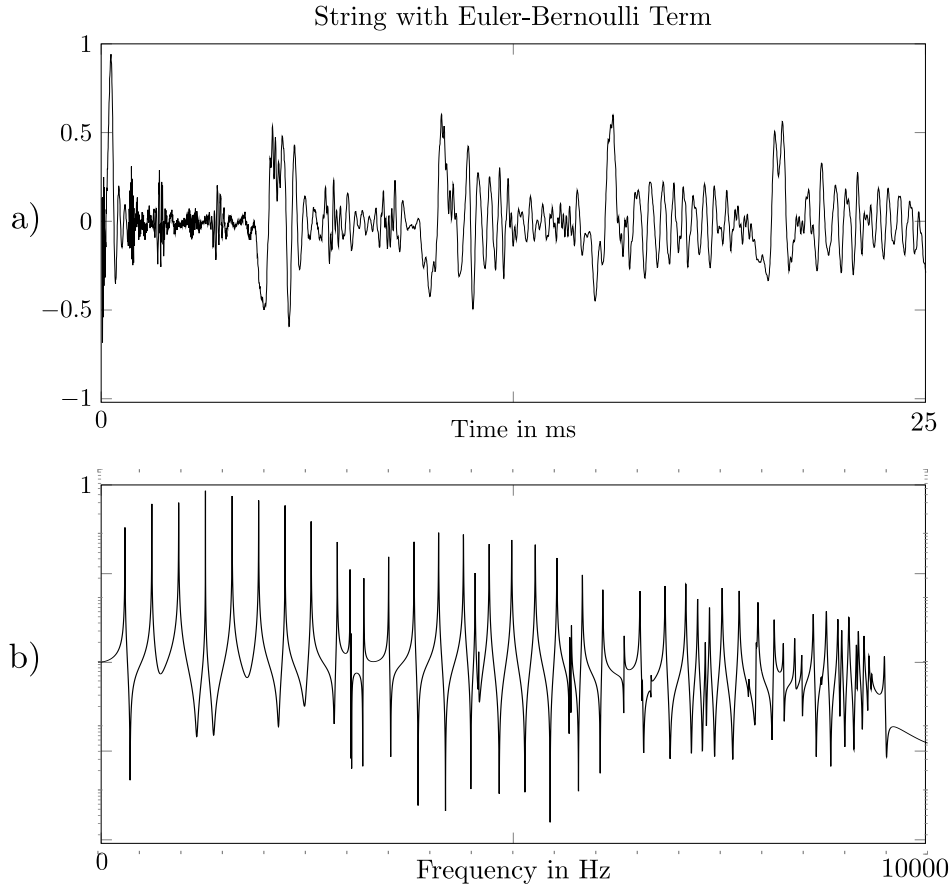


Figure 4.13: Time series and spectrogram of stiff string with Euler-Bernoulli term.

Timoshenko beam

Besides the presented Euler-Bernoulli beam, there are other formulations for beams that can be used for modelling the dynamic behaviour of stiff strings. One example is the Timoshenko beam, successfully applied to model lower piano strings⁵⁶. The Timoshenko beam theory adds a deflection dependent shearing and rotational inertia to the Euler-Bernoulli beam theory. The coupled differential equations can be written as

$$\begin{aligned}\rho A \rho I \phi_{tt} &= (E \cdot I \phi_x)_x + \kappa A G (u_x - \phi) \\ \rho A u_{tt} &= (\kappa A G (u_x - \phi))_x.\end{aligned}\tag{4.28}$$

As before, velocity dependent and frequency dependent damping can be added to equation 4.28, to yield a more realistic decay characteristic.

⁵⁶Juliette Chabassier: “Modélisation et simulation numérique d’un piano par modèles physiques”, PhD thesis, 2012.

Simulation Results

Figure 4.14 shows a string with added bending stiffness modelled with a Timoshenko beam-like term.

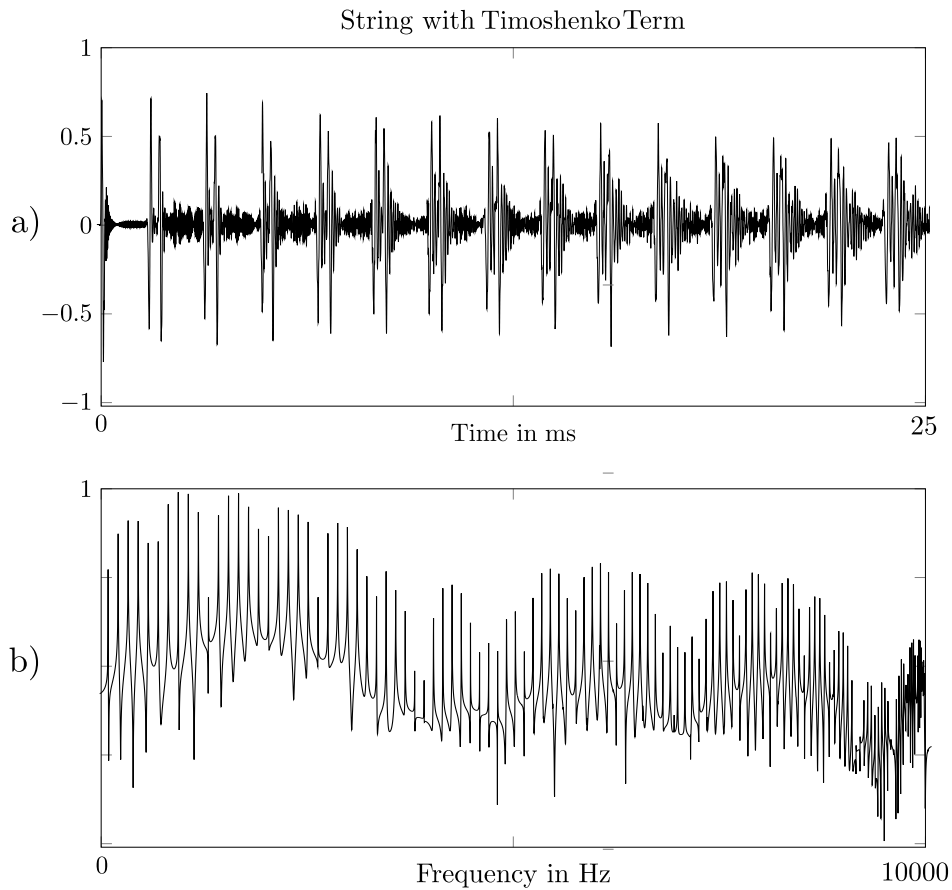


Figure 4.14: Time series and spectrogram of stiff string with Timoshenko term.

4.1.4 Stiff string with damping and end support losses

The final string model incorporates all of the presented features. The end support losses are modelled by an additional mass, attached at the boundary points, for the model of a singular string. When more than one strings, coupled to a resonator are modelled, the end support loss are modelled by the impedance relation developed in 4.4.

Numerical results

Figure 4.15 shows the modelled time series of a string with bending stiffness, velocity and acceleration damping and losses at the boundaries. The figure shows the simulated deflection of one point near the middle of the string over the first four seconds.

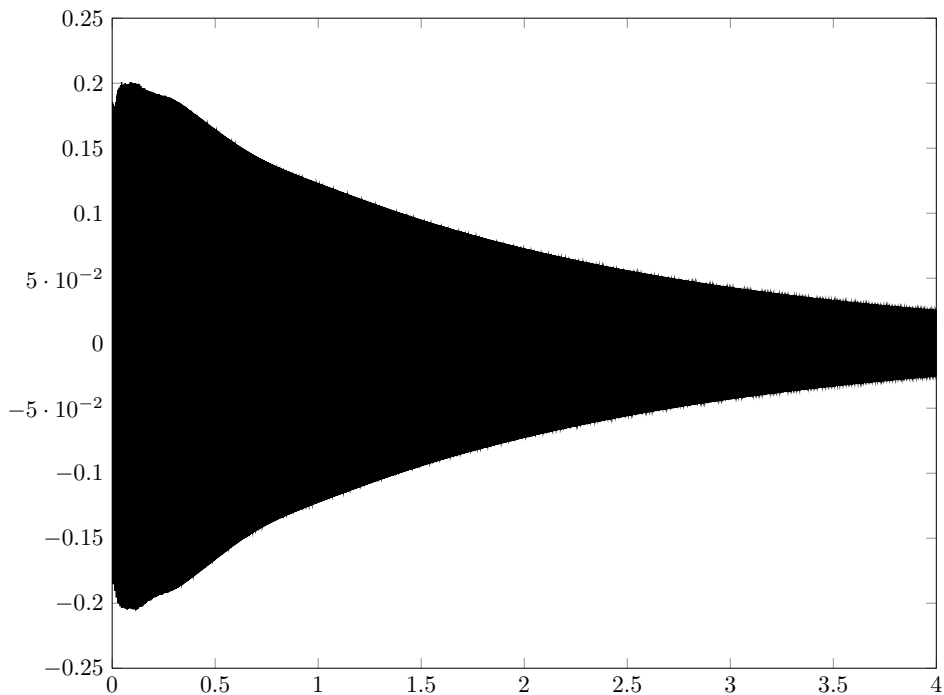


Figure 4.15: Deflection over time of single point.

4.1.5 Discussion

As shown in chapter 3, choosing the right values for Δt and Δx leads to a numerical solution which yields analytical results for the linear wave equation. Choosing both constants differently adds dispersion to the string that rises with simulation time. As shown in chapter 2, this effect is present in real strings. Hence, an analytic solution to the wave equation on the string is not necessary because it does not reproduce the physical reality. The addition of losses, stiffness and changing length results in a model of the string that exhibits realistic motion when compared with the measured strings, presented in section 2.

4.2 2-dimensional wave equation models

To model acoustical phenomena in higher dimensions, the 1-dimensional wave equation can be extended to the 2-dimensional wave equation. Besides the linear case of elastic membranes or plates, even more complex geometrical structures, like plates with buckling and orthotropic material properties or plates with orifices can be described with the 2-dimensional wave equation. All plate-like and membrane-like components of the musical instruments modelled in this work are described with the 2-dimensional wave equation⁵⁷. At first, linear cases of the 2-dimensional wave equation are presented and used as the foundation for models of more intricate geometrical problems.

Research history

Analogue to the string, the membrane is a thoroughly researched object in physics and in mathematics. Research can be found in such various fields as classical mechanics⁵⁸, acoustics⁵⁹ or topology in mathematics⁶⁰. The equations of motion of an ideal membrane can be described by the two dimensional wave equation. A solution to this equation on the surface of the membrane is the Bessel function⁶¹. In many traditional skin covered lute instruments, the membrane acts as an amplification device for the sound of the plucked or bowed string coupled to the membrane⁶². In some Brazilian percussion instruments like the *cuica* or the *chicken*, the membrane amplifies the sound of a scrubbing sound produced by a stick-slip motion of fingers or a rosin covered cloth moved over a rough surface.

Because of the vast distribution of membrane covered string instruments an exhaustive organologic research history of membrane covered instruments is far beyond the scope of this work.⁶³

Mathematical description of the linear membrane.

The motion of a round membrane can be described by the solution of the 2-dimensional wave equation. The 2-dimensional wave equation can be deduced in a purely mathematical

⁵⁷ The formulation of a 3-dimensional geometry as a 2-dimensional problem is feasible for most instruments, because the sound producing or sound radiating plates or membranes have small heights compared to their extent in the other two spatial dimensions.

⁵⁸ Kuypers, *Klassische Mechanik*, p. 254.

⁵⁹ Fletcher and Rossing, *Physics of Instruments*, pp. 70-99

⁶⁰ Taylor, *Partial Differential Equations I*, 126ff

⁶¹ Developed By Friedrich Wilhelm Bessel as a mathematical tool for geodesic problems. *ibid.*

⁶² Among countless others, some illustrative examples are the Afghan *rabob*, the Mali *ginbri* or the Chinese *sanxian*.

⁶³ One interesting trivia can be noted, there are vanishingly few accounts of European string instrument with a membrane covered body. An European string instrument with a membrane as a resonator is the *bumbass*, also known as the *devils-violin* or *buhai* in Romania. Another skin covered instruments is the Georgian *chuniri* found in remote mountain regions of Svenetia.

4 Physical models

manner or by a physically motivated point of view similar to the derivation of the first order wave equation on a string. Again, the basic assumption is that the forces acting on a linear membrane, due to the tension at the boundaries and a deflection at a specific point lead to an acceleration in the opposite direction of the curvature of the membrane.

In a Cartesian coordinate system in the membrane plane, the forces in the x- and y-directions acting on a 2-dimensional section with the edges dy , dx and the deflection u can be written as:

$$Tdy\left[\left(\frac{\partial u}{\partial x}\right)_{x+dx} - \left(\frac{\partial u}{\partial x}\right)_x\right], \quad (4.29)$$

$$Tdx\left[\left(\frac{\partial u}{\partial y}\right)_{y+dy} - \left(\frac{\partial u}{\partial y}\right)_y\right] \quad (4.30)$$

or more conveniently as:

$$T \frac{\partial^2 u}{\partial x^2} dx dy, \quad (4.31)$$

$$T \frac{\partial^2 u}{\partial y^2} dx dy. \quad (4.32)$$

Following Newton's second law, the sum of these forces is equal to the acceleration times the elements mass $m = dx dy \rho$, with ρ the density.⁶⁴ Thus, the governing differential equation of a linear membrane can be written as:

$$\frac{\partial^2 \mathbf{u}}{\partial t^2} = c^2 \cdot \left[\frac{\partial^2 \mathbf{u}}{\partial x^2} + \frac{\partial^2 \mathbf{u}}{\partial y^2} \right], \quad (4.33)$$

with $c = \sqrt{\frac{T}{\rho}}$.

4.2.1 Linear membranes

A linear, elastic membrane can be modelled by the 2-dimensional wave equation in a straightforward manner. The numerical integration scheme for the 2-dimensional wave equation for transient motion (equation 4.33) can be written as

$$\begin{bmatrix} \mathcal{A} \\ \mathcal{V} \\ \mathcal{U} \end{bmatrix} = \bigcup_{t=1}^T \left\{ \begin{array}{l} \mathcal{F}^{-1} \left[\widehat{\delta}_{2x2y} \cdot \mathcal{F} [\tau_{t-\mathbf{u}}] \right] \\ \tau_{t-\mathbf{v}} + \mathbf{a} \\ \tau_{t-\mathbf{u}} + \mathbf{v} \end{array} \right\}. \quad (4.34)$$

Boundary conditions

Boundary conditions for membranes are a highly delicate matter influencing the vibration of the membrane substantially. As shown in chapter 2, the radiated mode shapes are qualitatively comparable to the analytical solution of the membrane. But quantitatively they dif-

⁶⁴Morse and Ingard, *Theoretical Acoustics*.

4 Physical models

fer considerably. Among other influencing variables, the boundary conditions are known to have a huge impact on the radiated mode shapes and the acoustical spectrum of membranes.⁶⁵ In this initial model of the membrane, two standard boundary conditions are utilised, Dirichlet and Neumann boundary conditions, as presented in section 4.1. The Dirichlet boundary can be implemented in the same way as before, by setting the deflections of points on the boundary to zero. The Neumann boundary condition can again be modelled by a virtual node outside the domain of the membrane. The calculation for the acceleration at the boundary Ω thus gives

$$\mathcal{A}|_{xy\Omega} = c^2 \cdot (-4 \cdot u(x; y) + u(x + 1; y) + u(x - 1; y) + 2 * u(x; y - 1)). \quad (4.35)$$

Geometrical shape

The shape of any 2-dimensional structure can be formulated by applying the boundary conditions at designated points. The implementation of the resulting mesh grid can be formulated by a conditional statement. If the values are defined as:

Inside Domain	I
Dirichlet boundary	D
Neumann boundary	N

Table 4.2: Mesh grid values for arbitrary shapes.

they can be used to model a rectangular membrane with Dirichlet boundary conditions on the rim and a circular orifice in the middle. This leads to a grid dependent acceleration calculation of

$$\mathcal{A} = \bigcup_{t=1}^T \begin{cases} \mathcal{F}^{-1} \left[\hat{\delta}_{2x2y} \cdot \mathcal{F} [\tau_{t-\mathbf{u}}] \right] & \text{for } I \\ 0 & \text{for } D \\ \mathcal{F}^{-1} \left[\hat{\delta}_{x\bar{x}y\bar{y}} \cdot \mathcal{F} [\tau_{t-\mathbf{u}}] \right] & \text{for } N \end{cases} . \quad (4.36)$$

The values for the acceleration at the boundaries can be calculated either in the time domain or in the frequency domain.

Numerical results

In the following membrane models, damping is included in the calculation because real membranes, just like real strings, are always subject to losses. The fundamental frequency of the membrane can be calculated by The simulation parameters are given in table 4.3.

The first figure depicts the transient motion of a linear membrane due to an excitation with a stiff hammer force.

⁶⁵Fletcher and Rossing, *Physics of Instruments*, pp. 602-615.

4 Physical models

Membrane radius	15 cm
Grid size	64x64 points
Fundamental frequency	200 Hz

Table 4.3: Simulation parameters for the round membrane.

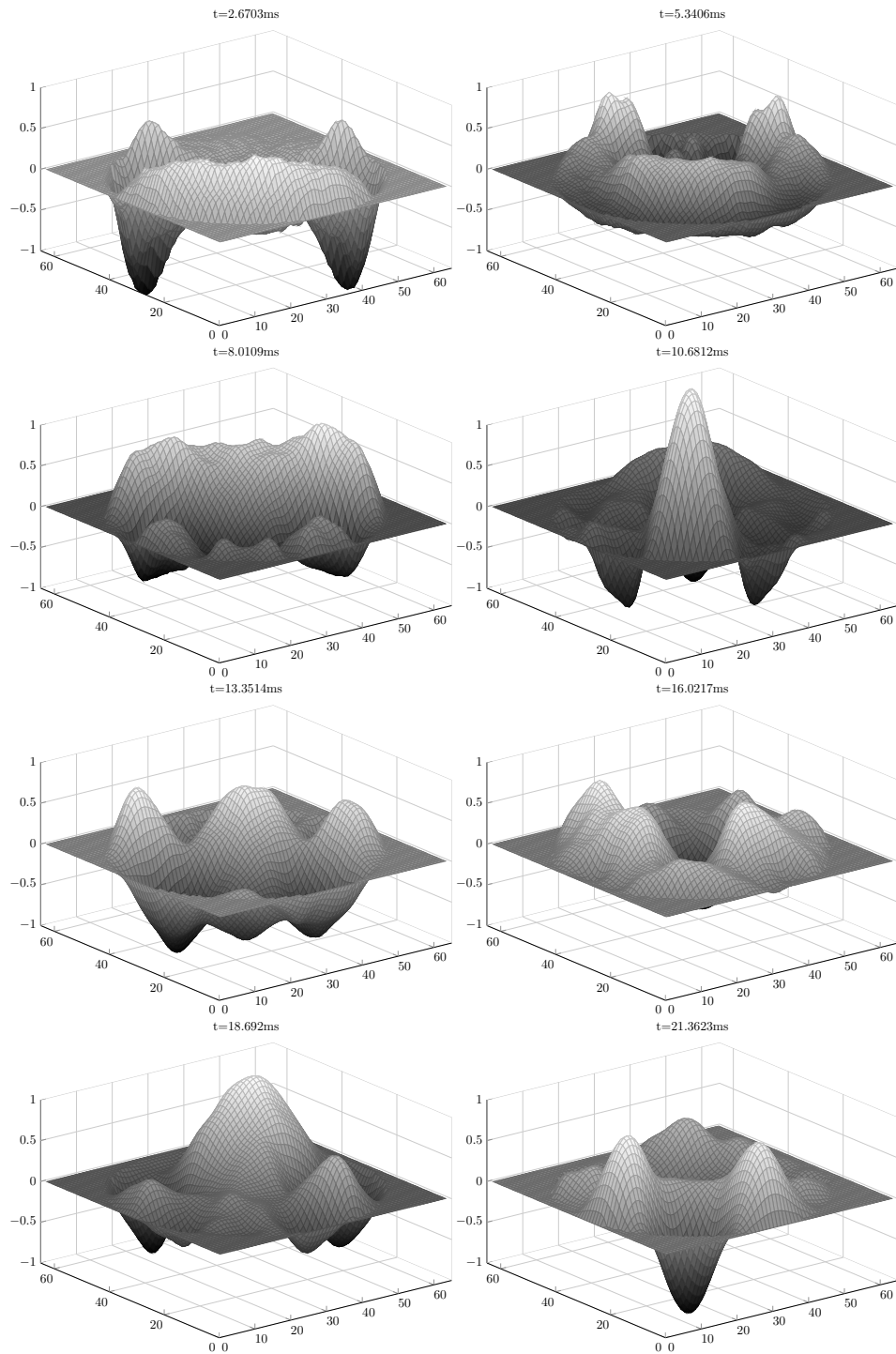


Figure 4.16: Deflection of a linear damped membrane over time.

4 Physical models

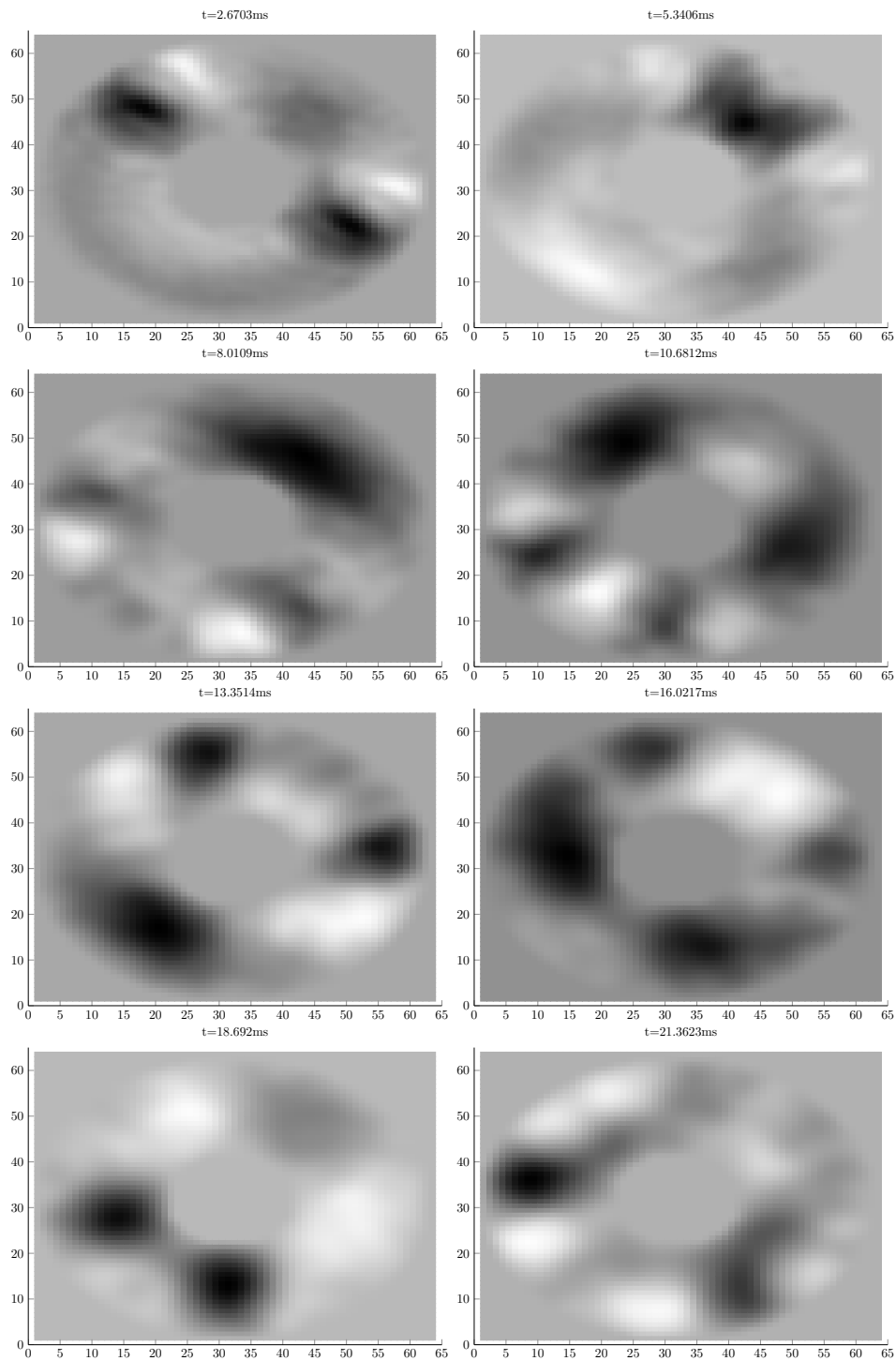


Figure 4.17: Deflection of a linear membrane with opening.

Figure 4.17 shows the same membrane with Dirichlet boundary conditions applied in the centre of the membrane.

4.2.2 Tension modulated membranes

Tension modulation in membranes is used as a musical effect or stylistic device, comparable to pitch bend effects in string instruments⁶⁶. An illustrative example of such playing techniques is the pitch bend drumming technique for snare drums and tom toms. Another example of a musical instrument that utilises tension modulation is the West-African *talking drum*⁶⁷. In accordance with the three models for 1-dimensional tension modulated strings, it is possible to use different approaches for modelling the effects of changing tension in membranes. Similar to the 1-dimensional case, a non-linear *Duffing* term can be included, to add a deflection dependent, non-linear spring stiffness constant. A deflection dependent pitch modulation, due to changing tension in a membrane can also be modelled via 2-dimensional version of a Kirchhoff-Carrier equation. The deflection dependant tension can be computed in the form of a 2-dimensional tension distribution summation over the domain of the membrane

$$\mathbf{T}_{nl} = T_0 + \sum_{i=1}^{NX} \sum_{j=1}^{NY} \mathbf{u}^2, \quad (4.37)$$

with \mathbf{u} the deflection of the membrane, NX, NY the number of grid points in the x and y direction respectively, and T_{nl} the non-linear tension on the membrane. The geometrical approach proposed in section 4.1.2 can be extended to the 2-dimensional case, but also leads to unphysical simulation results as shown in figure 4.19.

Numerical results

The effect of the pitch-glide effects in a simulated membrane is shown in the next figures. Figure 4.18 shows the spectrum of a Kirchhoff-Carrier-like modelled membrane. Figure 4.19 shows the spectrum of a pitch glide, modelled by geometrical longitudinal transversal coupling.

⁶⁶The pitch bend is often used as an expressive effect in blues guitar playing. One fundamental playing technique of the Chinese zither *ghu-zheng* is based on bended strings.

⁶⁷Gerhard Kubik: "Theory of African Music", in: *Intercultural Music Studies 7*, ed. by Max Peter Baumann, Wilhelmshafen: Florian Noetzel Verlag, 1994.

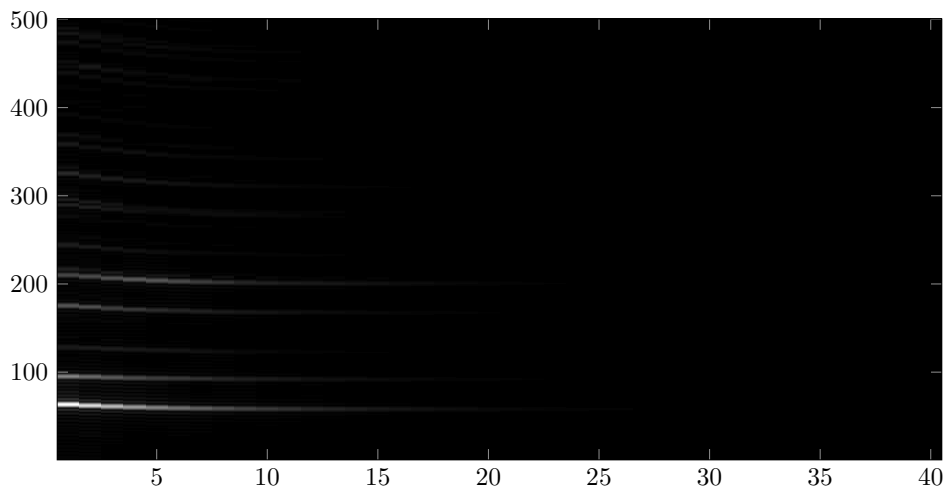


Figure 4.18: Spectrogram of membrane with Kirchhoff-Carrier like tension change.

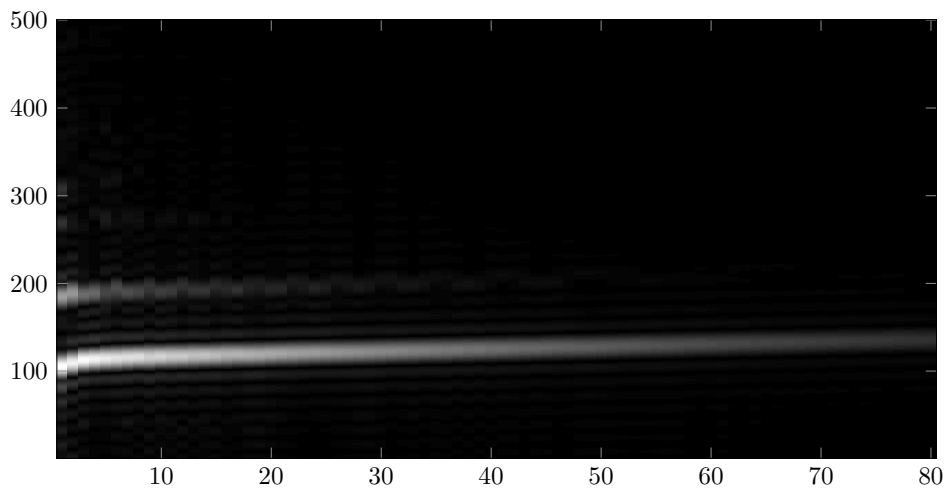


Figure 4.19: Spectrogram of membrane with geometrical coupling between longitudinal and transversal motion.

Discussion

As one can see in figures 4.18 and 4.19, the Kirchhoff-Carrier-like tension modulation yields plausible results. Whereas the geometrical coupling between longitudinal and transversal motion leads to a paradoxical simulation results: The larger the deflection, the lower the pitch [sic!]. Similar to the 1-dimensional case, this result is not physical.

4.2.3 Plates

The time stepping algorithm for a vibrating plate with fixed boundary conditions is similar to the time stepping algorithm of other 2-dimensional structures, like the model of the linear

4 Physical models

membrane. The difference between both algorithms is the form of the difference operator. The fourth order difference operator for the spatial discretisation of a plate can be written as

$$\delta_p = D(\cdot\delta_{4x} + \delta_{4y} + 2 \cdot \delta_{2x2y}). \quad (4.38)$$

A central difference approximation yields a 2-dimensional operator with the following weights

$$\delta_p = \begin{vmatrix} 0 & 0 & 1 & 0 & 0 \\ 0 & 2 & -8 & 2 & 0 \\ 1 & -8 & 20 & -8 & 1 \\ 0 & 2 & -8 & 2 & 0 \\ 0 & 0 & 1 & 0 & 0 \end{vmatrix}.^{68} \quad (4.39)$$

Higher order operators can be found by approximating the grid values with spectral methods or by a Taylor series approximation as presented in chapter 3.

Boundary conditions

Boundary conditions for plates are more intricate to model than boundary conditions for membranes or strings. This is mainly because of the higher order of the differential equation. In the models applied here, either fixed boundary conditions⁶⁹, or free boundary conditions⁷⁰ are applied. As before, free boundary conditions can be modelled by relation 4.12 and fixed can be implemented by setting $x \in \Omega = 0$ with Ω the boundary points of the plate.

Numerical results

A modelled time series of a clamped plate, excited by an elastic hammer impact can be seen in figure 4.20

⁶⁸Bathe, *Finite-Element Methoden*, p. 159.

⁶⁹The *ruan* or the *yueqin* for instance

⁷⁰The boundaries at the orifices on the top-plate of the *ruan* are modelled with free boundary conditions.

4 Physical models

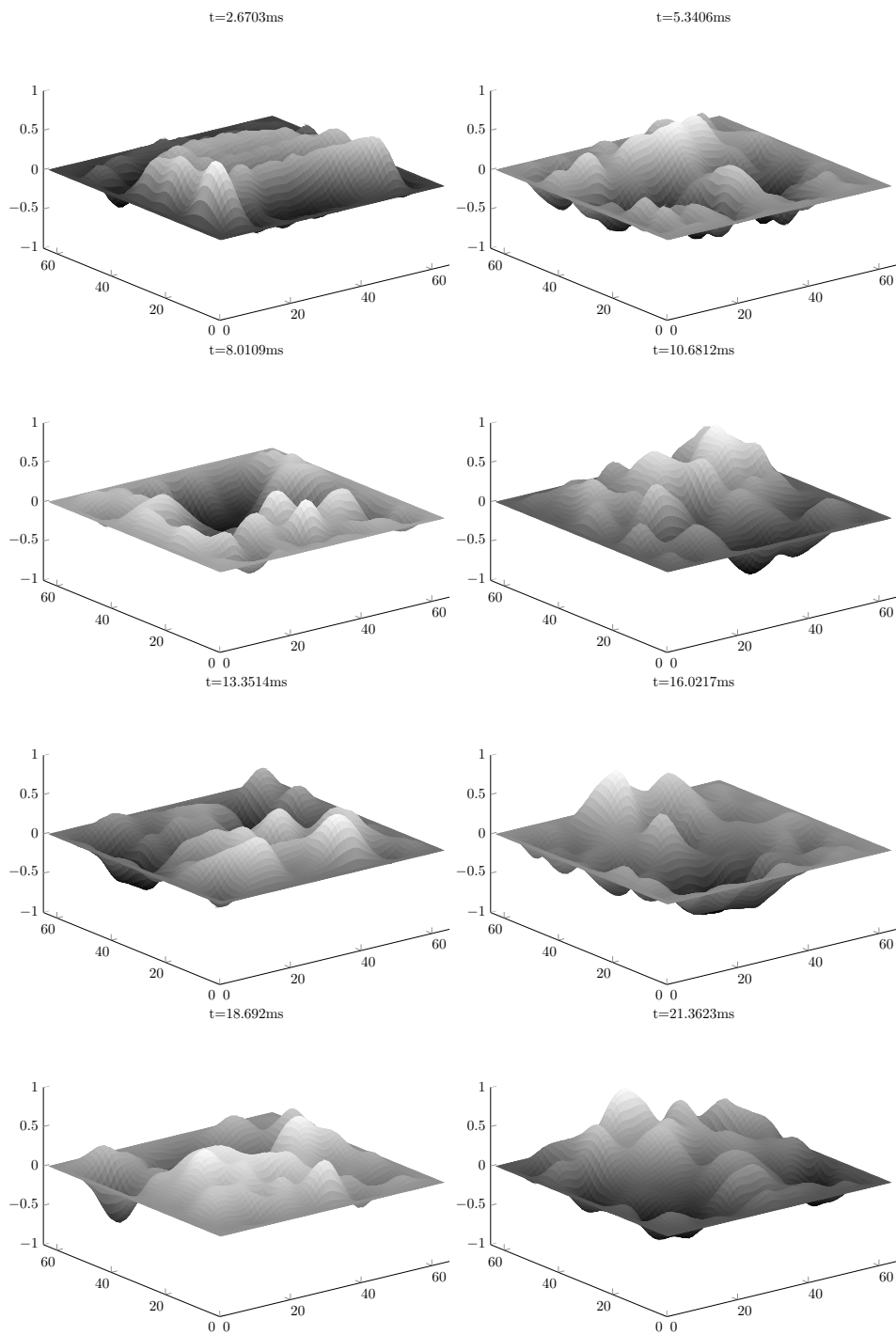


Figure 4.20: Time series of plate model excited by elastic hammer.

4.2.4 Stiff membranes

Comparable to the string, real membranes used in musical instruments have a finite flexibility, thus have a bending stiffness. In concordance with the model of the stiff string, this effect

can be achieved by adding a plate-like term to the linear and completely elastic membrane. The time stepping scheme can be written as

$$\begin{bmatrix} \mathcal{A} \\ \mathcal{V} \\ \mathcal{U} \end{bmatrix} = \bigcup_{t=1}^T \left\{ \begin{array}{l} \mathcal{F}^{-1} \left[(\widehat{\delta}_{2x2y} + \widehat{\delta}_P) \cdot \mathcal{F} [\tau_{t-\mathbf{u}}] \right] \\ \tau_{t-\mathbf{v}} + \mathbf{a} \\ \tau_{t-\mathbf{u}} + \mathbf{v} \end{array} \right\}. \quad (4.40)$$

Numerical examples

In figure 4.21 the deflection for several time steps of a round membrane with the inclusion of stiffness is shown.

4 Physical models

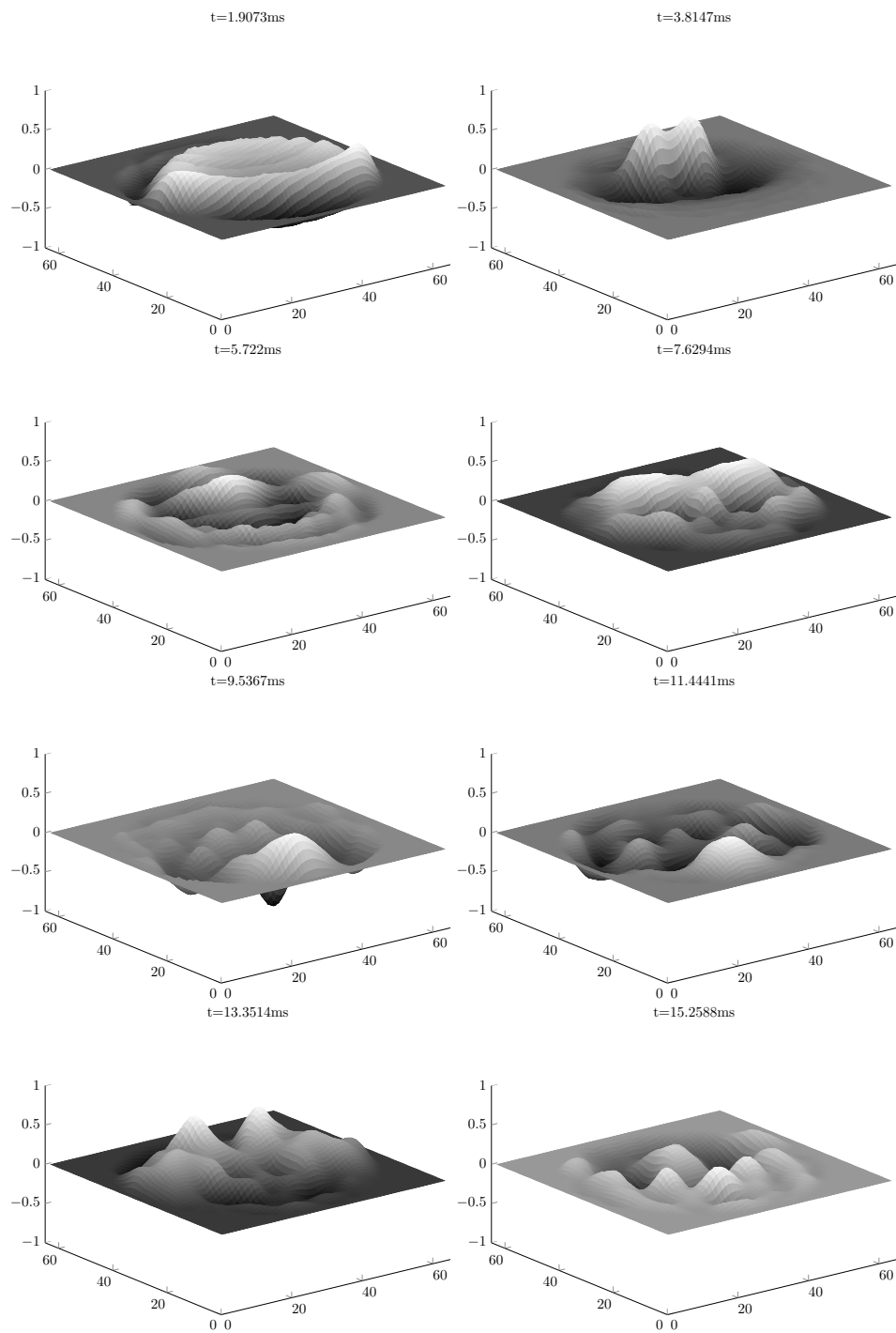


Figure 4.21: Deflection for several time steps of a membrane with stiffness excited by an elastic hammer.

4.2.5 Frequency dependent damping

To model a wooden plate with realistic decay characteristics, velocity dependent damping as well as frequency dependant damping must be added to the model of a wooden sound board. The damping can be implemented by adding a two terms to the plate equation, similar to the damping terms added to the PDE of the string. The complete equation can be written as

$$u_{tt} - \nabla^2 \nabla^2 u + \beta \cdot u_t + \alpha \cdot u_{xxt} = 0. \quad (4.41)$$

For reasons of brevity we have set $\nabla^2 \nabla^2 = u_{4x} + u_{4y} + 2 \cdot u_{2x2y}$. α and β are dimensionless damping coefficients.

4.2.6 Wooden orthotropic plates

As mentioned in section 4.2.6, most resonance wood used for soundboards have orthotropic material properties and as a consequence different wave speeds in the respective grain directions⁷¹.

Mathematical description

The theory of plate and shells is used in many fields of structural mechanics and numerical simulation techniques. Fundamental concepts of free vibrating thin plates were formulated by Euler and extended by Bernoulli⁷². After several attempts to find a formulation for bending in plates, Kirchhoff proposed a consistent formulation.⁷³ Important additions to the plate theory were developed by Timoshenko at the beginning of the 20th century, mainly driven by changing material utilisation in the shipbuilding industry.⁷⁴ This thesis is mainly concerned with plates that can be described by the *classical* Kirchhoff plate theory.

The differential equation for the transversal deflection u as a result to bending waves⁷⁵ on a 2-dimensional, isotropic plate in x, y is given as:

$$D \left[\frac{\partial^4 u}{\partial x^4} + 2 \frac{\partial^4 u}{\partial x^2 \partial y^2} + \frac{\partial^4 u}{\partial y^4} \right] = \frac{\partial^2 u}{\partial t^2}, \quad (4.42)$$

with $D = \frac{Eh^3}{2(1-\nu^2)}$. The variables are:

⁷¹Ulrike G. K. Wegst: "Wood for sound", in: *Am. J. Bot.* 93.10 (2006).

⁷²Eduard Ventsel and Theodor Krauthammer: *Thin Plates and Shells: Theory, Analysis and Applications*, Marcel Dekker, 2001, p. 16.

⁷³G. Kirchhoff: "Über das Gleichgewicht und die Bewegung einer elastischen Scheibe.", in: *Journal für die reine und angewandte Mathematik* 40 (1850): 51–88.

⁷⁴Ventsel and Krauthammer, *Thin Plates and Shells: Theory, Analysis and Applications*, p. 17.

⁷⁵The bending waves are the main cause of sound radiation on plates.

4 Physical models

E :	Young's modulus in $[\frac{N}{m^2}]$.
h :	Height of the plate in $[m]$.
ν :	Poisson's ratio.

Table 4.4: Isotropic plate theory constants.

Because most wood used in instrument making has orthotropic material properties⁷⁶, the PDE for the plate can be extended to incorporate these features. Following the laws of elasticity, wood has three different Young's moduli, three shear moduli as well as six Poisson ratios, for the respective grain directions: longitudinal, transversal and radial and their cross terms.⁷⁷

The wood, used for front- and back plates of violins is in most instruments a longitudinal-radial cut of the tree. Hence, the parameters of interest are:

E_L :	The Young's modulus in the longitudinal grain direction.
E_R :	The Young's modulus in the radial grain direction.
ν_{LR} :	The Poisson ratio in the longitudinal/radial grain direction.
ν_{RL} :	The Poisson ratio in the radial/longitudinal grain direction.

Table 4.5: Orthotropic constants for wood plate.

Using these parameters, we can apply the PDE for orthotropic plates⁷⁸:

$$D_x \frac{\partial^4 u}{\partial x^4} + \left(\frac{D_{xy} + D_{yx}}{2} + D_{sh} \right) \frac{\partial^4 u}{\partial x^2 \partial y^2} + D_y \frac{\partial^4 u}{\partial y^4} = \frac{\partial^2 u}{\partial t^2}, \quad (4.43)$$

with the following material dependent constants:

$$\left| \begin{array}{l} D_x = \frac{E_L}{1 - \nu_{LR}\nu_{RL}} \frac{h^3}{12} \\ D_y = \frac{E_R}{1 - \nu_{RL}\nu_{LR}} \frac{h^3}{12} \\ D_{xy} = \frac{E_L \nu_{RL}}{1 - \nu_{LL}\nu_{RR}} \frac{h^3}{12} \\ D_{yx} = \frac{E_R \nu_{LR}}{1 - \nu_{LL}\nu_{RR}} \frac{h^3}{12} \\ D_{sh} = \frac{Gh^3}{12}, \end{array} \right|$$

Table 4.6: Constants for orthotropic plates.

with G the shear modulus and h the height of the plate orthogonal to the $x - y$ plane. For Sitka spruce, those values are:

⁷⁶Wegst, "Wood for sound".

⁷⁷Voichita Bucur: "Springer Series in Wood Science", in: *Acoustics of Wood*, 2nd ed., Springer, 2006, p. 47.

⁷⁸See equation 7.31 in: Ventsel and Krauthammer, *Thin Plates and Shells: Theory, Analysis and Applications*, p. 210.

4 Physical models

$$\begin{aligned}
 E_L &= 13.5\text{E}09 \\
 E_R &= 1.3\text{E}09 \\
 \nu_L &= 0.33 \\
 \nu_R &= 0.029 \\
 G &= \frac{\sqrt{(E_{LL} * E_{RR})}}{2 * (1 + \sqrt{\nu_{LL} * \nu_{RR}})}
 \end{aligned}$$

Table 4.7: Material properties for Sitka spruce. Values from table 7.2 in: Bucur.⁷⁹ And table 4.1B in: Bucur.⁸⁰

The PDE for an orthotropic plate is given as

$$D_x \cdot u_{4x} + 2\left(\frac{D_{xy} + D_{yx}}{2} + D_{sh}\right)u_{2x2y} + D_y \cdot u_{4y} = 0. \quad (4.44)$$

Numerical examples

In figure 4.23, the spectrum of an orthotropic wooden plate in comparison to the spectrum of an isotropic wooden plate is shown.

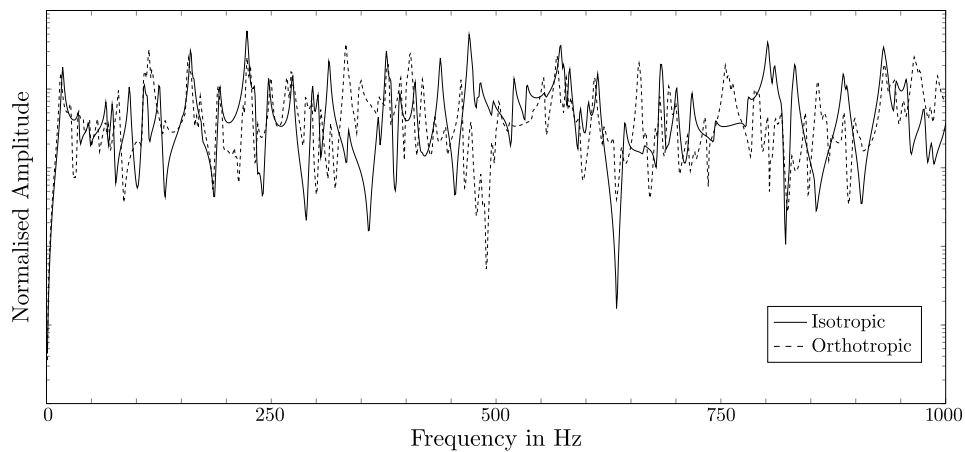


Figure 4.22: Simulated spectrum of a wood plate with orthotropic and isotropic material properties.

4.2.7 Wooden orthotropic plate with buckling

In several instruments, the resonance boards are subject to in-plane tension leading to a buckling of the plate. Some examples include: The back-plate of a classical guitar⁸¹, front- and back plates of violins and the sound board of grand pianos⁸² The PDE of plates with

⁸¹This depends on the quality of the instrument.

⁸²In grand pianos this is known as crowning.

buckling can be written as

$$D_x \cdot u_{4x} + 2\left(\frac{D_{xy} + D_{yx}}{2} + D_{sh}\right)u_{2x2y} + D_y \cdot u_{4y} + N_x u_{xx} + 2N_{xy}u_{xy} + N_y u_{yy} = 0, \quad (4.45)$$

with constants depending on the internal forces due to an in-plane load:

$$\left| \begin{array}{l} N_x = \text{External force acting in the } x\text{-direction} \\ N_y = \text{External force acting in the } y\text{-direction} \\ N_{xy} = \text{Combination of both forces.} \end{array} \right|$$

Table 4.8: Force constants for plates under buckling.

Numerical examples

Figure 4.23 depicts the spectrum of an wooden plate with and without buckling.

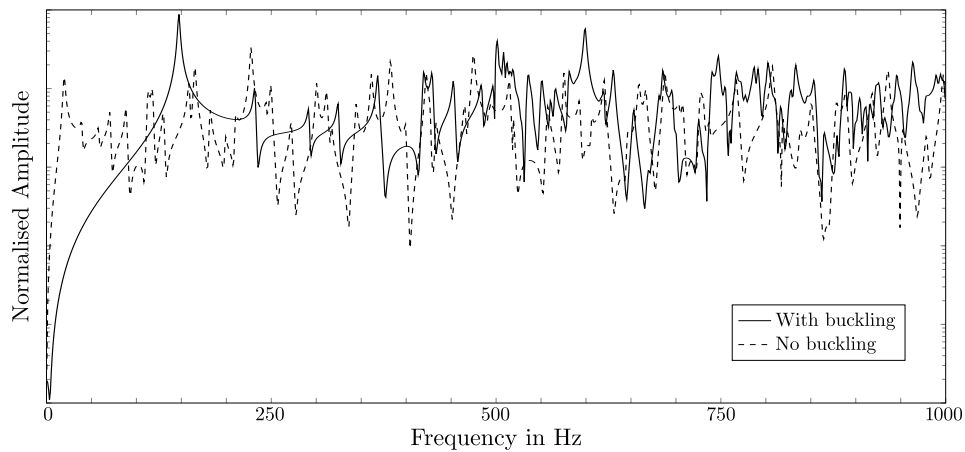


Figure 4.23: Simulated spectrum of a wood plate with orthotropic and isotropic material properties.

4.3 3-dimensional wave equation models

Finite difference methods for modelling the wave equation in three spatial dimensions are commonly utilised in room acoustics⁸³ or electromagnetic field calculations⁸⁴. In this section, two models for 3-dimensional air volumes are presented.

⁸³Carlos Spa, Adan Garriga, and Jose Escolano: “Impedance boundary conditions for pseudo-spectral time-domain methods in room acoustics”, in: *Applied Acoustics* 71.5 (2010): 402–410.

⁸⁴Yee, “Numerical solution of initial boundary value problems involving maxwell’s equations in isotropic media”.

4.3.1 Closed air cavities

Finite difference methods have one drawback: The computational cost rises with $\mathcal{O}^{Dimension}$ with the grid size. Hence, for large numerical room acoustic problems, like concert halls, these methods are impracticable when utilising un-optimised explicit finite difference formulations and real-time simulations are striven for. Air cavities in musical instruments, like the air volume in the banjos resonator for instance, are considerably smaller, and the resulting mesh grid of discrete points are several orders of magnitude smaller than mesh grid sizes used in room acoustics. The 3-dimensional wave equation is a straight-forward extension of the lower-dimensional wave equations and can be written as

$$p_{tt} = c^2 \cdot p_{XYZ}, \quad (4.46)$$

with p the pressure, XYZ the second derivatives in the respective directions x, y, z , and $c^2 = \frac{1}{\rho \cdot \kappa}$ ⁸⁵, with $\rho =$ the density of air, $\kappa = \frac{1}{\gamma \cdot P}$ ⁸⁶ with $\gamma =$ the adiabatic index of air and $P =$ the normal pressure. In many works concerned with finite difference methods for room acoustic, this equation is solved numerically using a FDTD approach, based on the Yee discretisation scheme⁸⁷. In this work, the symplectic Euler scheme, utilised for the other geometries presented in this work, can be applied for 3-dimensional schemes as well, and the time stepping algorithm can be written in the known form as

$$\begin{bmatrix} \mathcal{A} \\ \mathcal{V} \\ \mathcal{P} \end{bmatrix} = \bigcup_{t=1}^T \left\{ \begin{array}{l} \mathcal{F}^{-1} \left[\hat{\delta}_{XYZ} \cdot \mathcal{F} [\tau_{t-\mathbf{P}}] \right] \\ \tau_{t-\mathbf{P}} + \ddot{\mathbf{p}} \\ \tau_{t-\mathbf{P}} + \dot{\mathbf{p}} \end{array} \right\}. \quad (4.47)$$

\mathcal{A} and \mathcal{V} are the second and first derivative of the pressure by time respectively. Similar to the formulation of the solid structure time integrators, both variables comprise the simulation results for the entire spatial- and time domain.

Boundary conditions

Boundary conditions for all closed surfaces Ω are implemented as Neumann boundary conditions by setting: $\frac{\partial p}{\partial x} = 0$; $\frac{\partial p}{\partial y} = 0$; $\frac{\partial p}{\partial z} = 0$ for boundaries in the x, y, z direction. These boundary conditions can be implemented by using a mirror point, as presented before. For the basic case of a centred second order finite difference stencil, the boundary values of the

⁸⁵Morse and Ingard, *Theoretical Acoustics*, p. 233

⁸⁶(ibid., p. 230)

⁸⁷(Yee, "Numerical solution of initial boundary value problems involving maxwell's equations in isotropic media").

acceleration at point $x \in \Omega$ can be computed by

$$\mathcal{A}|_{ijk\Omega} = c^2 \cdot (5 \cdot p_{ijk} + p_{i+1jk} + p_{i-1jk} + p_{ij+1k} + p_{ij-1k} + p_{ijk-1}). \quad (4.48)$$

These boundary conditions can be applied for all back- and front plate boundaries in the presented instrument models.

4.3.2 Air cavities with orifices

The wooden resonators of three of the modelled instruments have air filled cavities with orifices. The openings change the boundary conditions of the air volume at the respective position of the air volume mesh grid. Instead of an air-structure interaction, the air is connected to the surrounding free field, enabling the air to radiate into the normal direction of the orifice. Hence, Sommerfeld radiation conditions can be applied for the orifices extending to a virtual room.⁸⁸ The boundary conditions at the respective points can be implemented by applying the Sommerfeld radiation condition in the z -direction of the domain. For the 1-dimensional case, the Sommerfeld radiation conditions can be expressed by following relation

$$\left(\frac{\partial u}{\partial t} + c \cdot \frac{\partial u}{\partial x}\right)|_{x=\infty} = 0. \quad (4.49)$$

This leads to the following condition for the first time derivative of the pressure at the openings Ω in the z -direction

$$p_t|_{\Omega 0} = -c \cdot p_x, \quad (4.50)$$

the right side of equation 4.50 can then be discretised with one-sided finite differences.

⁸⁸The virtual room around the instruments is not modelled in this thesis. The acoustical near-field of the instruments is assumed to be free of reflections from a virtual room, meaning free-field conditions are implied.

4.4 Coupled geometries

In this section, the singular geometry models presented before are coupled, resulting in instrument geometries consisting of their constituent acoustical parts. As will be shown below, coupling between singular vibrating geometries can be modelled in different ways, depending on the interacting parts and the physical properties at the interaction point between the geometries.

4.4.1 Elastic spring coupling

A point-blank way to model interactions of linearly coupled vibrating systems can be achieved by implementing the coupling as an elastic spring between two interacting points on the respective geometries. If one point of one geometry $u1$ is coupled with another point on a second geometry $u2$, one can write the equation of motion for the coupled point as a set of ODEs as

$$\begin{aligned} u1_{tt} - \kappa f_{\nabla}(u1) - k_{12} \cdot u2 &= 0 \\ u2_{tt} - \kappa f_{\nabla}(u2) - k_{12} \cdot u1 &= 0, \end{aligned} \tag{4.51}$$

with κ a constant depending on the respective geometry, f_{∇} a potential function depending on the geometry and the interaction point, and $*$ a coupling constant depending on the interaction strength and the respective geometry at the coupling point. This results in an interaction between both geometries, depending on the respective deflections at the coupling point and the spring constant (stiffness) of the virtual spring. Similar coupling is often applied in vibrational analysis of coupled structural mechanics.⁸⁹

4.4.2 Impedance coupling

Another way of coupling geometries implemented in this work is modelled by a coupling via the impedances at the interaction point. This can be achieved by following the relation⁹⁰

$$Z = \frac{F}{v}, \tag{4.52}$$

with Z the real impedance, F the acting force and v the velocity at the interaction point. With the proposition that the impedance is constant and purely real during one time step,

⁸⁹L. Cremer, M. Heckl, and B.A.T. Petersson: *Structure Borne Sound*, 3rd ed., Springer, 2010, pp. 434-437.

⁹⁰Fletcher and Rossing, *Physics of Instruments*, p. 52.

equation 4.52 can be rewritten to

$$\begin{aligned}
 F &= v \cdot Z = \\
 m \cdot a &= v \cdot Z = \\
 a &= \frac{v}{m} \cdot Z
 \end{aligned} \tag{4.53}$$

for the acceleration at the interaction point. To calculate the acting force at a coupling point F_{CP} between to geometries G_1 and G_2 , one can express this as the sum of the force F_{G_1} and the external force that acts on this point $F_{EXT_{G_2}}$. To calculate the force for a finite time step, this can be rewritten into following equations

$$\begin{aligned}
 F_{CP} &= F_{G_1} + \frac{1}{\Delta t} \int_{t_1}^{t_2} F_{EXT_{G_2}} dt \\
 &= -\nabla V + m \cdot \frac{1}{\Delta t} \int_{t_1}^{t_2} a dt \\
 &= -\nabla V + m \cdot (v + c)
 \end{aligned} \tag{4.54}$$

with V = potential energy and v, c the velocity and an integration constant, which is proportional to the acceleration at the beginning of the integration time. This method of coupling is applied in several sections of the instrument models, for instance the coupling between an air volume and an adjacent radiating surface or the coupling between the membrane and the resonator of the banjo.

4.4.3 Structural coupling

A coupling of strings and a resonating body is achieved by regarding the acting forces at the bridge. With the proposition that the string is attached at the interaction point, the bridge, the acting force is equal to the shear force of the string giving the following formulation for the force⁹¹

$$F_{tr} = B u_{3x} + T u_x, \tag{4.55}$$

with B the bending stiffness and T the tension of the string. The bending stiffness B is defined as

$$B = E \cdot A \cdot K^2 \tag{4.56}$$

⁹¹Matthew David Tuttle: "Plucked Instrument Strings: A Combined Frequency - Time Domain Wave Approach to Investigate Longitudinal forces at the Bridge Support", Master's Thesis, Chalmers University of Technology, 2007, pp. 29-30.

4 Physical models

with the elastic modulus E , the area of the string cross section and K the radius of gyration defined as $r/2$ for a cylindrical string. As shown by Bank and Sujbert,⁹² the acting force at the bridge due to the longitudinal motion of the string can be written as⁹³

$$F_{lo} = -[T + EA\xi_x|_{Br} + \frac{1}{2}EAy_x|_{Br}r^2] \quad (4.57)$$

with ξ the longitudinal displacement of the string. The coupling of the resonance body's motion back to the string depends on the attachment of the string. If the string is fastened at the bridge, like the strings of the yueqin, the motion of the bridge has a direct influence in the longitudinal direction of the string, i.e. making the string shorter and longer while in motion.⁹⁴ If the strings run over a bridge, and are not fastened there otherwise, as is the case in the banjo, the violin, and the ruan, the influence of a moving bridge acts more in the transversal polarisations of the string.

⁹²Balázs Bank and László Sujbert: "Generation of longitudinal vibrations in piano strings: From physics to sound synthesis", in: *The Journal of the Acoustical Society of America* 117.4 (2005): 2268–2278.

⁹³Here, an uniform tension distribution over the string is proposed.

⁹⁴This is similar to the effects found in the Finnish *Kantele*. See: C. Erkut et al.: "Acoustical Analysis and model-based sound synthesis of the kantele", in: *J. Acoust. Soc. Am.* 112.4 (2002): 1681–1691.

4.5 American 5-string banjo model

In this section, an overview on the physical model of the North-American 5-string banjo, implemented in this thesis, is presented.

The first model incorporates two parts of the banjo, which are of fundamental importance for the distinct timbre of the instrument and are the basic parts responsible for the sound production: A string coupled to a membrane.⁹⁵ An archaic prototype of a banjo could be constructed, using only a string coupled to a membrane. Hence, at first, the focus is put on an accurate model for a banjo-string, a membrane and the coupling between both geometries. In an additional step, this basic model is extended in several ways to include all five strings, a wooden bridge, more realistic boundary conditions of the membrane, the air volume beneath the membrane and a model for the finger-pick string interaction. One of the differences of both models is the coupling between the banjo string and the membrane. It is implemented as:

1. Type I: One string is coupled directly to the membrane, and the influence of the bridge is only approximated linearly.
2. Type II: Five strings are coupled to a model of a wooden banjo bridge which is coupled to the membrane.

For the type I model, the coupling between the end-point L of the string and the membrane is approximated by an impedance coupling as shown in section 4.4. Due to the fact that the bridge of the banjo moves when excited by string pulses, it can be approximated as a moving end support.⁹⁶ With the relations developed in section 4.4, the acting force at the interaction point can be written as

$$F = Z * v_L. \quad (4.58)$$

Hence, the acting force at the coupling point can be written as

$$F_{CP} = F_M + F_{SEP}. \quad (4.59)$$

Another approach of modelling two coupled geometries can be achieved by following the assumption that the sum of the forces, acting at the bridge must be zero. The force that acts at the contact point of the string (S) and the membrane (M) can be written via a Newtonian force relation

$$F_{CP} = f(u_M + u_S) \quad (4.60)$$

⁹⁵The other components of the banjo also influence the acoustical vibrations as well, but are not as fundamentally crucial for the timbre of the banjo as the string and the membrane.

⁹⁶Fletcher and Rossing, *Physics of Instruments*, p. 52.

4 Physical models

The membrane is modelled utilising a finite difference approximation for the spatial differential as before. This yields following conditions at the coupling points

$$\mathcal{A}_{CP} = \delta_{2x2y}u + \frac{1}{\Delta t}v_L\kappa. \quad (4.61)$$

It is presumed that the coupling constant κ depends on the mass ratio between the string, the bridge and the membrane.

4.5.1 Banjo string model

The material properties, like the thickness of the string and the applied tension are listed in table 2.1. Exact material properties regarding the internal damping of the strings are not quantifiable exactly for the used strings. Hence, in this work, the material properties, influencing the internal damping, like the Young's modulus are approximated with values taken from literature initially and modified *Ad hoc* to improve the model of the strings and add more variability to the sound. The spatial domain is discretised with a pseudo spectral grid approximation, taking the stiffness of the string into account. The equations of motion for the string are discretised in time and solved with a multi-symplectic time integrator as presented in chapter 3. For practical reasons, only first order integrators are used for the whole geometry models because they are applied in the real-time models as well. As already shown, the error introduced by the time discretisation is small compared to the spatial discretisation. The time stepping algorithm for the model of the banjo string with velocity and internal, frequency dependant damping, changing length and coupling at the end point of the string is shown in equation 4.62

$$\begin{bmatrix} \mathcal{A} \\ \mathcal{V} \\ \mathcal{U} \end{bmatrix} = \bigcup_{t=1}^T \dots$$

$$\left[\begin{array}{l} \left\{ \begin{array}{ll} \mathcal{F}^{-1} \left[(1 + \kappa \sum \tau_{t-\mathbf{u}^2}) \hat{\delta}_{xx} \cdot \mathcal{F} [\tau_{t-\mathbf{u}}] (1 - \alpha \cdot \delta_t) - \beta \cdot \tau_{t-\mathbf{v}} \right] & x \neq 0 \vee L \\ 0 & x = 0 \vee L \\ \mathcal{F}^{-1} \left[\hat{\delta}_{xx} \cdot \mathcal{F} [\tau_{t-\mathbf{u}}] (1 - \alpha \cdot \delta_t) - \beta \cdot \tau_{t-\mathbf{v}} \right] - \mathcal{Z}\mathbf{v}_M & x = x_B \\ \tau_{t-\mathbf{v}} + \mathbf{a} \\ \tau_{t-\mathbf{u}} + \mathbf{v} \end{array} \right. & \end{array} \right]. \quad (4.62)$$

To start the time stepping algorithm, the initial deflection and velocity of the string is needed to calculate the acceleration at $t = 1$. A simple triangular deflection for the string is used as starting condition for the string. The velocity is zero.⁹⁷ As mentioned in section 2, the strings

⁹⁷The triangular shape of the excitation function is a feasible approximation for most plucked string instru-

of the banjo can be subject to non-linear effects, due to high amplitude deflection. These effects are included in equation 4.62 with the *Kirchhoff-Carrier*-like term and the constant $\kappa = \frac{k \cdot A}{2 \cdot L}$. The coupling of the acoustical vibrations from the membrane back to the string is modelled by an impedance formulation presented in section 4.4 and denoted by the term \mathcal{Z}_{v_M} , with v_M the velocity of the membrane at the virtual coupling point.

4.5.2 Banjo membrane model

The membrane of the banjo is modelled as a round membrane with stiffness and non-linear tension distribution. The banjo membrane presented in section 2 are used as a guide line for the physical parameters applied in this model. The material properties are given in table 2.2. The membrane is approximated by a rectangular $64 \cdot 64$ grid with a round sub grid of a 30 grid points radius. The boundary conditions are realised by a higher velocity damping at the respective points.

$$\begin{bmatrix} \mathcal{A} \\ \mathcal{V} \\ \mathcal{U} \end{bmatrix} = \bigcup_{t=1}^T \dots$$

$$\left\{ \begin{array}{l} \left\{ \begin{array}{ll} \mathcal{F}^{-1} \left[\hat{\delta}_{XY} \cdot \mathcal{F} [\tau_{t-} \mathbf{u}] (1 - \alpha \cdot \delta_t) \right] - \tau_{t-} (\beta \cdot \mathbf{v} + \gamma \cdot \mathbf{u}) & \mathbf{u} \neq \Omega \vee \mathbf{x}_{cp} \\ \mathcal{F}^{-1} \left[\hat{\delta}_{XY}^{\Omega} \cdot \mathcal{F} [\tau_{t-} \mathbf{u}] (1 - \alpha \cdot \delta_t) \right] - \tau_{t-} (\beta_{\Omega} \cdot \mathbf{v}) & \mathbf{u} = \Omega \\ \mathcal{F}^{-1} \left[\hat{\delta}_{XY} \cdot \mathcal{F} [\tau_{t-} \mathbf{u}] (1 - \alpha \cdot \delta_t) \right] - \tau_{t-} (\beta \cdot \mathbf{v} + \gamma \cdot \mathbf{u}) - \mathcal{A}_{St} & \mathbf{u} = x_{CPS} \end{array} \right. \\ \tau_{t-} \mathbf{v} + \mathbf{a} \\ \tau_{t-} \mathbf{u} + \mathbf{v} \end{array} \right. \quad (4.63)$$

The impedance interaction at the coupling point is indicated by the term \mathcal{Z}_{v_S} . The boundary conditions of the membrane are modelled by applying different damping at the boundary points $\mathbf{u} = u(x, y) \in \Omega$. For reasons of brevity, the difference operator of the membrane is condensed to $\delta_{XY} = \delta^2 x^2 y - D \delta_{4x4y}$, adding a plate-like stiffness to the membrane with $D = \frac{E 2 h^3}{3 \cdot (1 - \nu^2)}$ (E= Young's Modulus and ν the Poisson ratio). The term $\gamma \cdot \mathbf{u}$ is added to simulate the effects of a Winkler bed, as described in section 4.5.4. The type II model of the banjo does not include the formulation for the Winkler bed. Hence, in the type II model membrane the value $\gamma = 0$.

Membrane boundary conditions

The boundary conditions of the membrane were initially set to Dirichlet boundary conditions. During the work with the banjo model, the boundary conditions were extended

ments because it approximates the shape of the string before its release from a finger or plectrum.

4 Physical models

to boundary conditions that influence the damping at the boundary points as well as the impedance of the membrane at these specific points. To this end, the membrane was implemented with Neumann boundary conditions. To fix the membrane at the rim, a virtual weight, indicated by Ω in equation 4.63, was added to the grid points at the boundary, as well as specific velocity damping, indicated by β_Ω in equation 4.63. By changing the weight at the rim of the membrane, the pitch of membrane could be tuned, by changing the damping, the mode shapes of the membrane could be tuned. Only by applying these measures, the simulated membrane yielded a spectrum that is comparable to the measurements presented in section 2.3.4.

4.5.3 Model of the bridge

The bridge of the banjo is modelled as a two-dimensional plate with forces acting only in the in-plane direction. The PDE⁹⁸ can be written as

$$u_{tt} = N_x \cdot u_{xx} + N_y \cdot u_{yy} + 2N_{xy} \cdot u_{xy} \quad (4.64)$$

The coupling at the interaction point between the membrane and the bridge is modelled by the interacting impedance relations, as presented in section 4.4.

$$\begin{bmatrix} \mathcal{A} \\ \mathcal{V} \\ \mathcal{U} \end{bmatrix} = \bigcup_{t=1}^T \dots \left[\begin{array}{l} \left\{ \begin{array}{ll} \mathcal{F}^{-1} [(\hat{\delta}_{xx} + \hat{\delta}_{yy} + \hat{\delta}_{xy}) \cdot \mathcal{F} [\tau_{t-} \mathbf{u}] (1 - \alpha \cdot \delta_t) - \beta \cdot \tau_{t-} \mathbf{v}] & \mathbf{y} \neq \Omega_M \vee \mathbf{x}_{cp} \\ \mathcal{F}^{-1} [(\hat{\delta}_{xx} + \hat{\delta}_{yy} + \hat{\delta}_{xy})^\Omega \cdot \mathcal{F} [\tau_{t-} \mathbf{u}] (1 - \alpha \cdot \delta_t) - \beta_\Omega \cdot \tau_{t-} \mathbf{v}] - \mathcal{Z} \mathbf{v}_M & \mathbf{u} = \Omega_M \\ \mathcal{F}^{-1} [(\hat{\delta}_{xx} + \hat{\delta}_{yy} + \hat{\delta}_{xy}) \cdot \mathcal{F} [\tau_{t-} \mathbf{u}] (1 - \alpha \cdot \delta_t) - \beta \cdot \tau_{t-} \mathbf{v}] - \mathcal{Z} \mathbf{v}_S & \mathbf{x} = x_{CP} \end{array} \right. \\ \tau_{t-} \mathbf{v} + \mathbf{a} \\ \tau_{t-} \mathbf{u} + \mathbf{v} \end{array} \right] \quad (4.65)$$

The coupling between the string and the bridge is modelled in three ways following equations 4.54, 4.51 and 4.55.

4.5.4 Model of the air cavity

In the type I model of the banjo, the influence of the air volume was realised by incorporating a *Winkler bed*⁹⁹ to the formulation of the membrane. The influence of a Winkler bed can be

⁹⁸This equation is taken from: Ventsel and Krauthammer, *Thin Plates and Shells: Theory, Analysis and Applications*, p. 98. Omitting the load in the normal direction of the plate.

⁹⁹Cremer, Heckl, and Petersson, *Structure Borne Sound*, pp. 119-120.

included to the formulation of a membrane by adding an amplitude dependant stiffness. Figure 4.24 give a schematic overview of the mechanical principle of the Winkler bed.

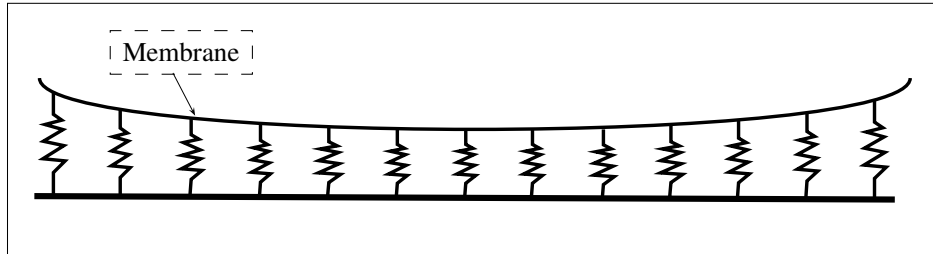


Figure 4.24: Mechanical principle of Winkler bed.

To include the Winkler bed into the formulation of the banjo membrane, a deflection dependant term with can be added to equation 4.33

$$\frac{\partial^2 \mathbf{u}}{\partial t^2} = c^2 \cdot \left[\frac{\partial^2 \mathbf{u}}{\partial x^2} + \frac{\partial^2 \mathbf{u}}{\partial y^2} - \gamma \cdot \mathbf{u} \right], \quad (4.66)$$

with γ a uniform stiffness per area coefficient. Applying this extension to the membrane model, the lower membrane modes can be tuned to approximate the spectrum of a real banjo membrane more precisely, as shown in figure 4.27. The membrane equation for the type I model is given in equation 4.63.

In the type II model, the air under the membrane is modelled as a 3-dimensional air volume coupled to the membrane. Modern 5-string banjos have a detachable back. Therefore, the boundary conditions of the air volume changes from Neumann boundary conditions to Sommerfeld radiation conditions, when the back is removed.¹⁰⁰ The boundary conditions of the air at the contact point with the resonator are modelled as Neumann boundary

¹⁰⁰ Because the banjo is pressed against the torso when played, the back of the banjo is never really open in a realistic playing setting. Hence, the effect of the open back is diminished. In the model of the banjo presented here, the open open back is modelled for comparison of the banjo measurements, presented in chapter 2.

conditions. The time stepping algorithm can be written as

$$\begin{bmatrix} \mathcal{A} \\ \mathcal{V} \\ \mathcal{P} \end{bmatrix} = \bigcup_{t=1}^T \dots$$

$$\left[\begin{array}{l} \left\{ \begin{array}{l} \mathcal{F}^{-1} \left[\hat{\delta}_{XYZ} \cdot \mathcal{F} [\tau_{t-\mathbf{p}}] (1 - \alpha \cdot \delta_t) \right] \\ \mathcal{F}^{-1} \left[\hat{\delta}_{XYZ}^{\Omega} \cdot \mathcal{F} [\tau_{t-\mathbf{p}}] (1 - \alpha \cdot \delta_t) \right] \\ \mathcal{F}^{-1} \left[\hat{\delta}_{XY} \cdot \mathcal{F} [\tau_{t-\mathbf{p}}] (1 - \alpha \cdot \delta_t) \right] - \mathcal{Z} \mathbf{v}_M \\ \mathcal{F}^{-1} \left[\hat{\delta}_{XY}^N \cdot \mathcal{F} [\tau_{t-\mathbf{p}}] (1 - \alpha \cdot \delta_t) \right] \end{array} \right. \\ \tau_{t-\dot{\mathbf{p}}} + \ddot{\mathbf{p}} \\ \tau_{t-\mathbf{p}} + \dot{\mathbf{p}} \end{array} \right. \begin{array}{l} \mathbf{p} \neq \Omega \vee \mathbf{p}|_{z=0} \vee \mathbf{p}|_{z=H} \\ \mathbf{p} = \Omega \\ \mathbf{p} = \mathbf{p}|_{z=0} \\ \mathbf{p} = \mathbf{p}|_{z=H} \end{array} \right] \quad (4.67)$$

4.5.5 Numerical results

Simulation results for the type I banjo model are depicted in figure 4.25.

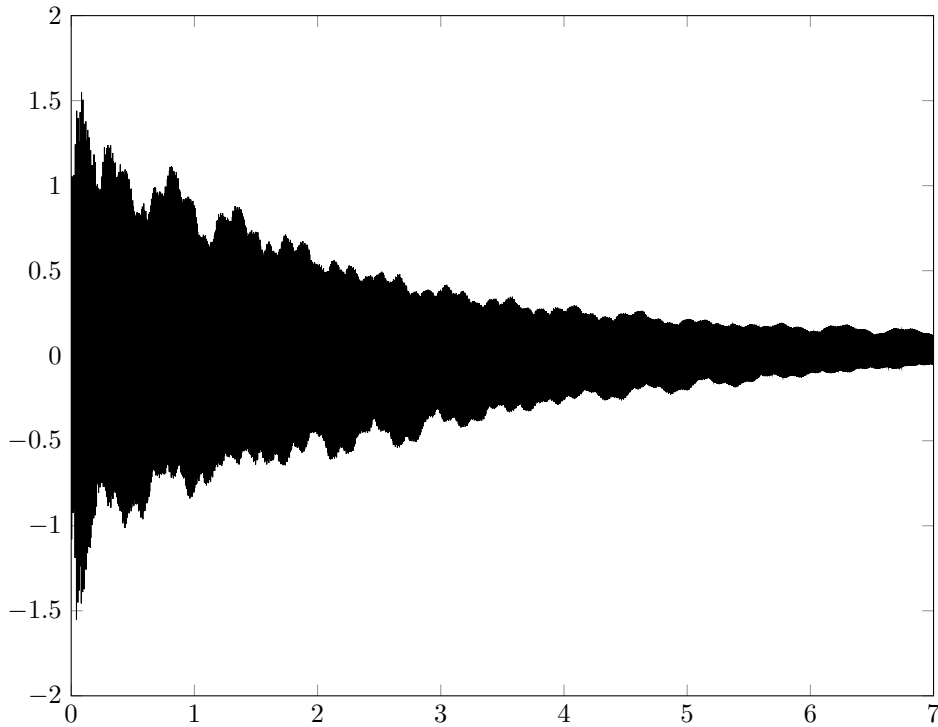


Figure 4.25: Single string coupled to membrane.

Figure 4.27 depicts the simulated mode shapes of an open back banjo membrane, excited by an elastic hammer impact.

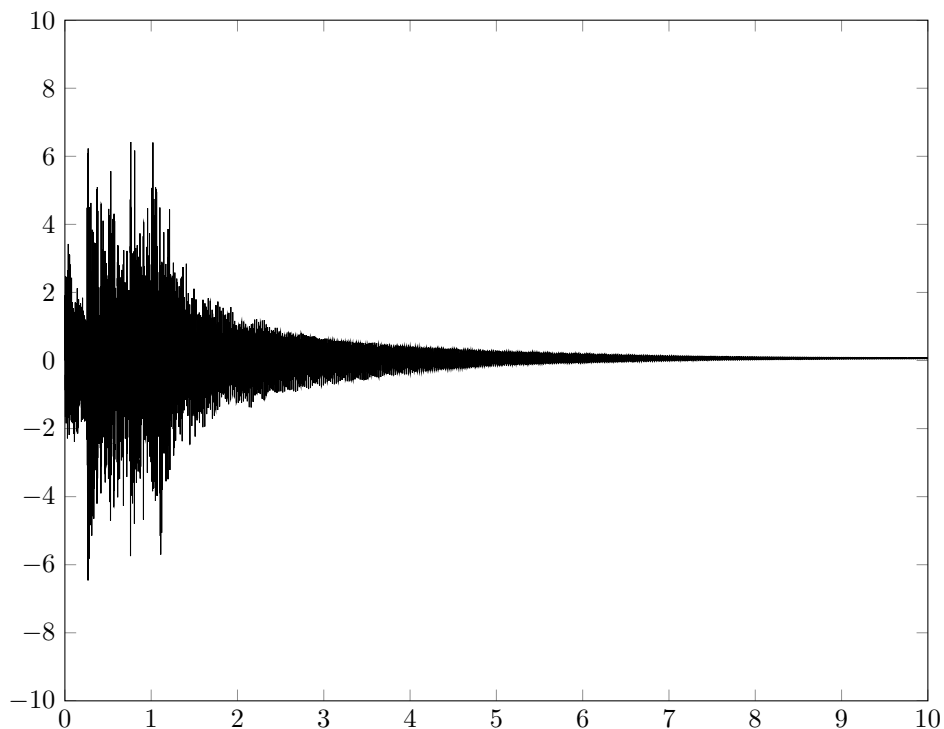


Figure 4.26: Model II five strings plucked consecutively.

Figure 4.28 shows the time series of a banjo resulting from a knock on the membrane near the bridge.

4.5.6 Discussion

The steady comparison with the measurements led to a model of the banjos membrane including the air volume under the membrane, a non-linear tension distribution across the membranes surface and specially matched boundary conditions. The simulations of the banjo model show that the air volume under the membrane can be approximated by a Winkler bed, yielding good results for frequencies under 1kHz. Including all proposed modifications in the model of the membrane resulted in comparable spectral information in the sub 1 kHz range. The final membrane, modified to approximate the measurements more correctly, includes:

- A non-linear tension distribution over the membrane, taking the net-force of the banjo bridge acting in the normal direction of the membrane into account.
- Boundary conditions that act on the damping and the impedance at the rim.
- A Winkler bed formulation for an initial model of the membrane.

4 Physical models

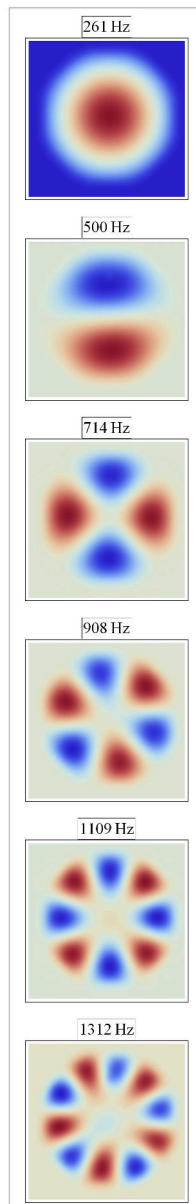


Figure 4.27: Model II knock on membrane. No strings/open back.

- The air volume inside the banjo, modelled by 3-dimensional finite differences.

The mode shapes of the simulated banjo membrane shown in figure 4.27 exhibits following ratios.

The frequency ratios of the simulated type I banjo membrane are in good concordance with the ratios of the measured banjo membrane.

4 Physical models

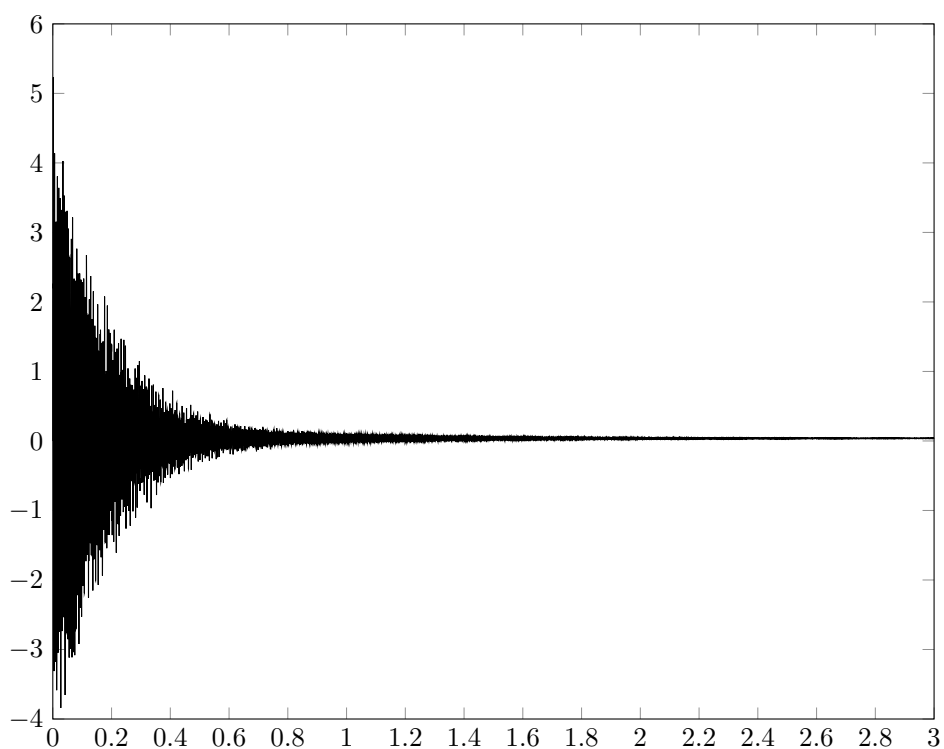


Figure 4.28: Model II knock on membrane. Resonating strings.

Mode	Ratio _{Meas}	Ratio _{Sim}
(0,1)	1	1
(1,1)	1.88	1.91
(2,1)	2.73	2.74
(0,2)	—	—
(3,1)	3.52	3.48
(1,2)	—	—
(4,1)	4.27	4.25
(2,2)	—	—
(0,3)	—	—
(5,1)	5.03	5.03

Table 4.9: Measured vs. simulated frequency ratios of a round banjo membrane without strings. The mode numbers indicate (axial, radial) nodal lines.

4.6 Yueqin model

The model of the *yueqin* consists of the following parts:

- Four linear strings with velocity and frequency dependent damping.
- A wooden front- and back-plate.
- An enclosed air volume.
- A model for the pluck string interaction.

This models extends the banjo model in two areas. The front plate, which is now a round, orthotropic wood plate, and the attachment of the strings. As already mentioned in chapter 2, the strings of the *yueqin* transmit the vibration energy directly at their fixation. Due to this, there is no bridge and no additional end fixture of the string.

4.6.1 String model

The string model of the *yueqin* is comparable to the model of the banjo string, with different boundary conditions and different damping parameters. Because modern instruments have strings made of nylon, the internal damping of the string is higher compared to the metal strings of the banjo. The simulated *yueqin* string includes a model for tension modulation, Dirichlet boundary conditions at the head, impedance boundary conditions at the fixture, velocity damping and internal damping. The time integrator for the string of the *yueqin* can be written as

$$\begin{bmatrix} \mathcal{A} \\ \mathcal{V} \\ \mathcal{U} \end{bmatrix} = \bigcup_{t=1}^T \left\{ \begin{array}{ll} \mathcal{F}^{-1} \left[\hat{\delta}_{xx} \cdot \mathcal{F} [\tau_{t-\mathbf{u}}] (1 - \alpha \cdot \delta_t) - \beta \cdot \tau_{t-\mathbf{v}} \right] & \text{for } x \neq 0 \vee L \\ 0 & \text{for } x = L \\ \mathcal{F}^{-1} \left[\hat{\delta}_{xx} \cdot \mathcal{F} [\tau_{t-\mathbf{u}}] (1 - \alpha \cdot \delta_t) - \beta \cdot \tau_{t-\mathbf{v}} \right] - \mathcal{Z}_{\mathbf{v}FP} & \text{for } x = 0 \\ \tau_{t-\mathbf{v}} + \mathbf{a} & \\ \tau_{t-\mathbf{u}} + \mathbf{v} & \end{array} \right. , \quad (4.68)$$

with the already known damping constants α , β and the characteristic impedance at the coupling point of the string.

String fixture

The string fixture is modelled by the coupling relations presented in section 4.4. The static force due to the tension of the strings, acting at the bridge, is not included into the model of

the yueqin because the force does not act in the normal direction of the front plate. Additionally, the bridge is glued onto the sound-board of the yueqin, which leads to a coupling, acting on the sheer moment of the wooden front plate. This coupling is approximated by an impedance coupling at the fixation points of the string, acting on several node points on the front plate in contact with the affixed bridge.

4.6.2 Model of the front- and back-plate

The front- and back plate of the yueqin are modelled as 2-dimensional, orthotropic Kirchhoff plates with velocity and frequency dependent damping. The boundary conditions of both plates are modelled as Dirichlet boundary conditions.

$$\begin{bmatrix} \mathcal{A} \\ \mathcal{V} \\ \mathcal{U} \end{bmatrix} = \bigcup_{t=1}^T \left\{ \begin{array}{l} \mathcal{F}^{-1} \left[\hat{\delta}_{XY} \cdot \mathcal{F} [\tau_{t-\mathbf{u}}] (1 - \alpha \cdot \delta_t) - \beta \cdot \tau_{t-\mathbf{v}} \right] \text{ for } \mathbf{x} \neq \Omega \vee \mathbf{x}_{CP} \\ 0 \text{ for } x = \Omega_B \\ \mathcal{F}^{-1} \left[\hat{\delta}_{XY}^{\Omega_N} \cdot \mathcal{F} [\tau_{t-\mathbf{u}}] (1 - \alpha \cdot \delta_t) - \beta \cdot \tau_{t-\mathbf{v}} \right] \text{ for } \mathbf{u} = \Omega_O \\ \mathcal{F}^{-1} \left[\hat{\delta}_{XY} \cdot \mathcal{F} [\tau_{t-\mathbf{u}}] (1 - \alpha \cdot \delta_t) - \beta \cdot \tau_{t-\mathbf{v}} \right] - \mathcal{Z}_{\mathbf{v}FS} \text{ for } \mathbf{x} = x_{CP} \\ \tau_{t-\mathbf{v}} + \mathbf{a} \\ \tau_{t-\mathbf{u}} + \mathbf{v} \end{array} \right. \quad (4.69)$$

The front and back plate are modelled with finite differences on a rectangular grid of 64×64 points. The round geometry is approximated by computing the vibrations on a round sub-grid with a 15 point radius. Thus, at the boundaries two points of the grid remain, to represent the boundary conditions.

4.6.3 Model of the enclosed air

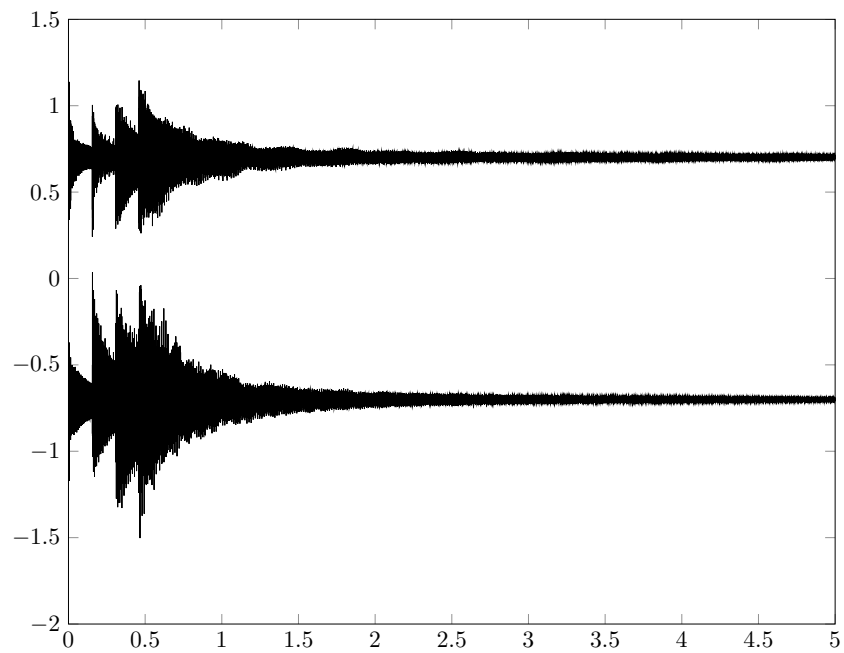
The enclosed air volume of the yueqin is modelled as a 3-dimensional air volume with a grid of $64 \times 64 \times 15$ in the x, y, z directions respectively. The coupling of the air volume to the front plate and the back plate is modelled by the impedance relation given in equation 4.53. The boundaries in x and y plane are modelled as Neumann boundary conditions. The time integrator of the air volume can be written as:

$$\begin{bmatrix} \mathcal{A} \\ \mathcal{V} \\ \mathcal{P} \end{bmatrix} = \bigcup_{t=1}^T \dots$$

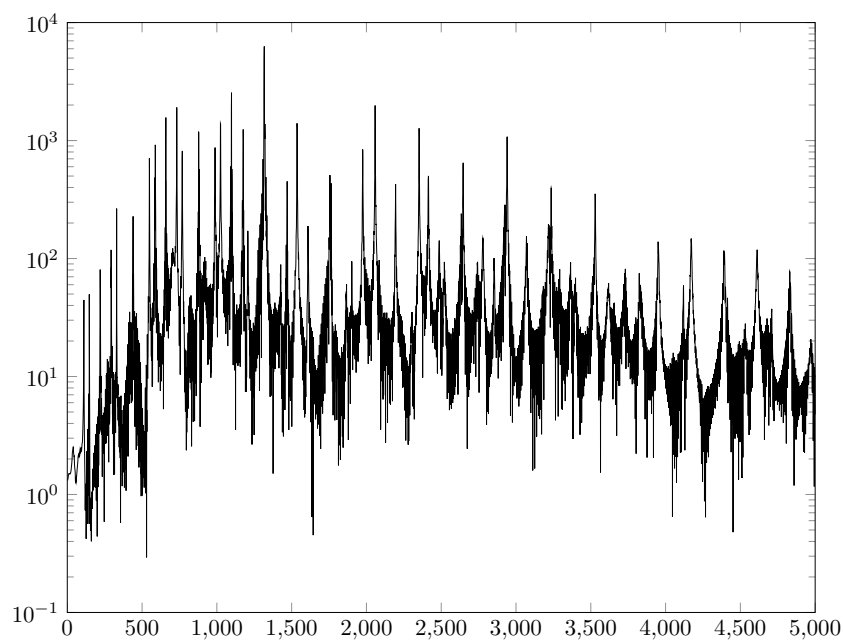
$$\left\{ \begin{array}{ll} \mathcal{F}^{-1} \left[\hat{\delta}_{XYZ} \cdot \mathcal{F} [\tau_{t-\mathbf{p}}] (1 - \alpha \cdot \delta_t) \right] & \mathbf{p} \neq \Omega \vee \mathbf{p}|_{z=0} \vee \mathbf{p}|_{z=H} \\ \mathcal{F}^{-1} \left[\hat{\delta}_{XYZ}^{\Omega} \cdot \mathcal{F} [\tau_{t-\mathbf{p}}] (1 - \alpha \cdot \delta_t) \right] & \mathbf{p} = \Omega \\ \mathcal{F}^{-1} \left[\hat{\delta}_{XY} \cdot \mathcal{F} [\tau_{t-\mathbf{p}}] (1 - \alpha \cdot \delta_t) \right] - \mathcal{Z} \mathbf{v}_{FP} & \mathbf{p} = \mathbf{p}|_{z=0} \\ \mathcal{F}^{-1} \left[\hat{\delta}_{XY} \cdot \mathcal{F} [\tau_{t-\mathbf{p}}] (1 - \alpha \cdot \delta_t) \right] - \mathcal{Z} \mathbf{v}_{BP} & \mathbf{p} = \mathbf{p}|_{z=H} \\ \tau_{t-\dot{\mathbf{p}}} + \ddot{\mathbf{p}} & \\ \tau_{t-\mathbf{p}} + \dot{\mathbf{p}} & \end{array} \right. \quad (4.70)$$

4.6.4 Numerical results

Figure 4.29 shows a time series of the yueqin model and the spectrum of the same recording.



(a)



(b)

Figure 4.29: Simulation results of the yueqin. Four consecutively plucked strings. 4.29a: Time series, left and right channel. 4.29b: Spectrum.

4.7 Ruan model

The model of the ruan consists of the following parts:

- Four strings with velocity and frequency dependent damping.
- A wooden front plate and back plate.
- An enclosed air volume.
- A model for a wooden bridge.
- A model for the pluck string interaction.

This model extends the banjo and yueqin model in two ways. The front plate has two orifices, the attachment of the strings and a wooden bridge that is larger than the bridge of the banjo model. Another feature of the ruan model is the tremolo excitation of the string, realised by a plectrum-string interaction model.

4.7.1 String model

The string model of the ruan is comparable to the model of the banjo string with different damping parameters and slightly altered boundary conditions because of the larger bridge. Comparable to the strings of the yueqin, ruan strings are made of nylon, thus having other internal damping characteristics compared to the banjos metal strings. The time integrator for the string of the ruan looks like

$$\begin{bmatrix} \mathcal{A} \\ \mathcal{V} \\ \mathcal{U} \end{bmatrix} = \begin{bmatrix} \mathcal{F}^{-1} \left[\hat{\delta}_{xx} \cdot \mathcal{F} [\tau_{t-\mathbf{u}}] (1 - \alpha \cdot \delta_t) - \beta \cdot \tau_{t-\mathbf{v}} \right] & \text{for } x \neq 0 \vee L \\ 0 & \text{for } x = L \\ \mathcal{F}^{-1} \left[\hat{\delta}_{xx} \cdot \mathcal{F} [\tau_{t-\mathbf{u}}] (1 - \alpha \cdot \delta_t) - \beta \cdot \tau_{t-\mathbf{v}} \right] - \mathcal{Z}\mathbf{v}_B & \text{for } x = 0 \\ \tau_{t-\mathbf{v}} + \mathbf{a} \\ \tau_{t-\mathbf{u}} + \mathbf{v} \end{bmatrix}, \quad (4.71)$$

with the already introduced damping constants α, β and the characteristic impedance at the coupling point of the string with the bridge.

String fixture

The string fixture of the ruan is modelled like the string fixture of the banjo. The coupling to the bridge is implemented as presented in section 4.4.

4.7.2 Model of the front- and back plate

Analogous to the yueqin, the front plate of the ruan is modelled as a 2-dimensional, orthotropic Kirchhoff plate with velocity and frequency dependent damping. The boundary conditions of both plates are modelled as Dirichlet boundary conditions. The only difference are the two orifices on the front plate of the ruan. Here, Neumann boundary conditions are applied at the edge of the opening.

$$\begin{bmatrix} \mathcal{A} \\ \mathcal{V} \\ \mathcal{U} \end{bmatrix} = \bigcup_{t=1}^T \left\{ \begin{array}{l} \mathcal{F}^{-1} \left[\hat{\delta}_{XY} \cdot \mathcal{F} [\tau_{t-}\mathbf{u}] (1 - \alpha \cdot \delta_t) - \beta \cdot \tau_{t-}\mathbf{v} \right] \text{ for } \mathbf{x} \neq \Omega \vee \mathbf{x}_{cp} \\ 0 \text{ for } x = \Omega_B \\ \mathcal{F}^{-1} \left[\hat{\delta}_{XY}^{\Omega_N} \cdot \mathcal{F} [\tau_{t-}\mathbf{u}] (1 - \alpha \cdot \delta_t) - \beta \cdot \tau_{t-}\mathbf{v} \right] \text{ for } \mathbf{u} = \Omega_O \\ \mathcal{F}^{-1} \left[\hat{\delta}_{XY} \cdot \mathcal{F} [\tau_{t-}\mathbf{u}] (1 - \alpha \cdot \delta_t) - \beta \cdot \tau_{t-}\mathbf{v} \right] - \mathcal{Z}_{\mathbf{v}FS} \text{ for } \mathbf{x} = x_{CP} \\ \tau_{t-}\mathbf{v} + \mathbf{a} \\ \tau_{t-}\mathbf{u} + \mathbf{v} \end{array} \right. \quad (4.72)$$

The same rectangular 64x64 grid with a round sub-grid, as applied in the yueqin model, is used here.

4.7.3 Model of the bridge

In the model of the ruan, the bridge approximated with the same scheme as the bridge of the banjo. In contrast to the bridge of the banjo, the ruan is modelled with two feet and different material properties, resulting in different wave propagation speeds in the x and y directions.

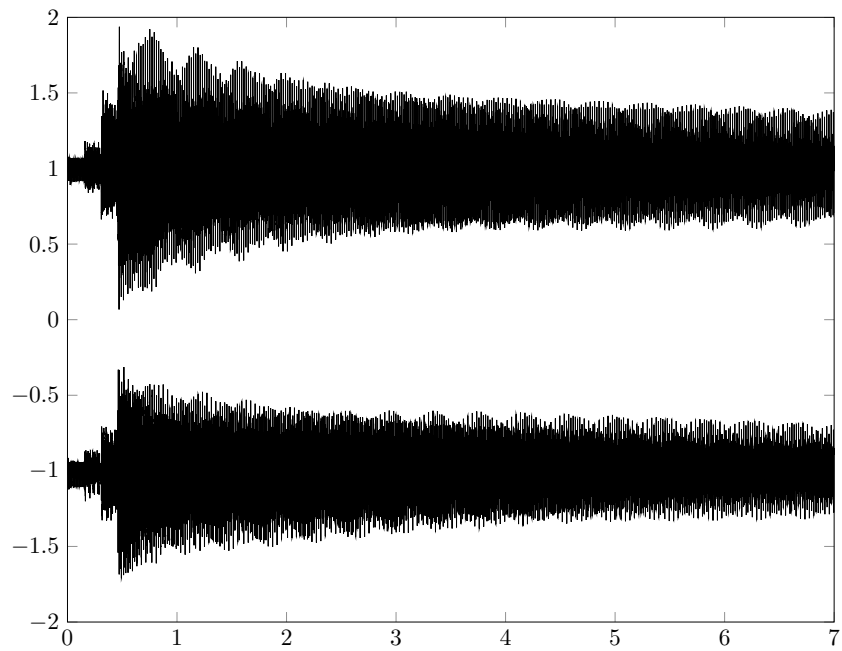
4.7.4 Model of the enclosed air

The enclosed air is modelled as a 3-dimensional air volume with a grid of 64x64x15 in the x, y, z directions respectively. The coupling of the air volume to the front plate is modelled by the impedance relations presented in section 4.4. The boundaries in x and y plane are Neumann boundary conditions. The boundary condition at the orifice is implemented as a Sommerfeld radiation condition in the z direction. The time stepping method of the air volume can be written as:

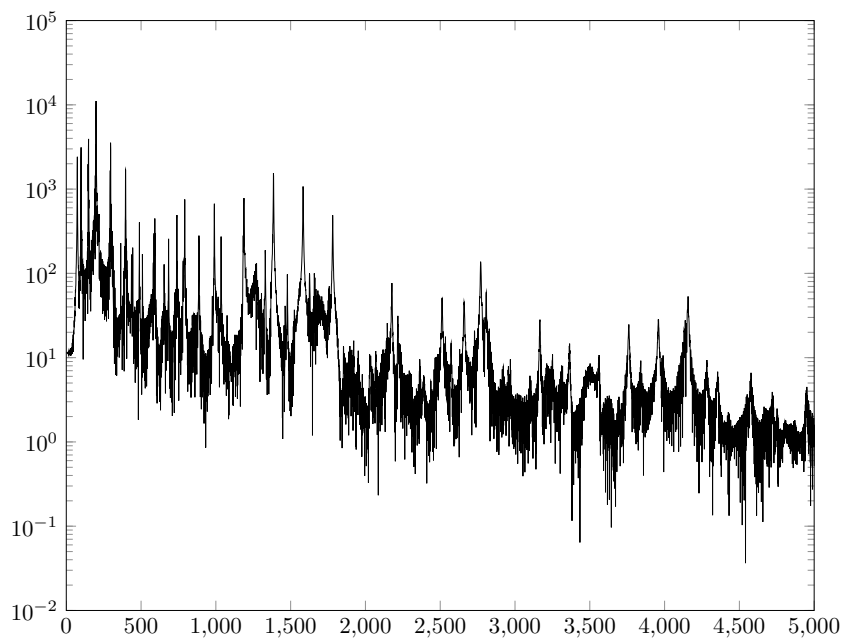
$$\begin{aligned}
 \begin{bmatrix} \mathcal{A} \\ \mathcal{V} \\ \mathcal{P} \end{bmatrix} &= \bigcup_{t=1}^T \dots \\
 \left\{ \begin{array}{l} \mathcal{F}^{-1} \left[\hat{\delta}_{XYZ} \cdot \mathcal{F} [\tau_{t-\mathbf{p}}] (1 - \alpha \cdot \delta_t) \right] \quad \mathbf{p} \neq \Omega \vee \mathbf{p}|_{z=0} \vee \mathbf{p}|_{z=H} \\ \mathcal{F}^{-1} \left[\hat{\delta}_{XYZ}^{\Omega} \cdot \mathcal{F} [\tau_{t-\mathbf{p}}] (1 - \alpha \cdot \delta_t) \right] \quad \mathbf{p} = \Omega \\ \mathcal{F}^{-1} \left[\hat{\delta}_{XY} \cdot \mathcal{F} [\tau_{t-\mathbf{p}}] (1 - \alpha \cdot \delta_t) \right] - \mathcal{Z} \mathbf{v}_{FP} \quad \mathbf{p} = \mathbf{p}|_{z=0} \\ \mathcal{F}^{-1} \left[\hat{\delta}_{XY} \cdot \mathcal{F} [\tau_{t-\mathbf{p}}] (1 - \alpha \cdot \delta_t) \right] - \mathcal{Z} \mathbf{v}_{BP} \quad \mathbf{p} = \mathbf{p}|_{z=H} \\ \left\{ \begin{array}{l} \delta_{x-\mathbf{p}} \quad \mathbf{p} = \mathbf{p}|_{z=0} \wedge \Omega_O \\ \tau_{t-\dot{\mathbf{p}}} + \ddot{\mathbf{p}} \quad \mathbf{p} \neq \mathbf{p}|_{z=0} \wedge \Omega_O \end{array} \right. \\ \tau_{t-\mathbf{p}} + \dot{\mathbf{v}} \end{array} \right. \end{array} \right. \quad (4.73)
 \end{aligned}$$

4.7.5 Numerical results

Figure 4.30 shows a time series of the ruan model and the appertaining spectrum of the same recording.



(a)



(b)

Figure 4.30: Simulation results of the ruan. Four consecutively plucked strings. 4.30a: Time series, left and right channel. 4.30b: Spectrum.

4.8 Violin model

A finite difference physical model of a complete violin geometry was presented by Bader¹⁰¹. The string/bow, model implemented in this thesis is loosely based on the same model. It consists of:

- Four strings with velocity and frequency dependent damping.
- A wooden bridge.
- A wooden front- and back-plate with orifices.
- The enclosed air volume.
- A model for the bow string interaction.

At this point, it is necessary to point out that a complete and exhausting physical model of the violin is not the aim of this work and the model presented here is valid up to a certain point of accuracy. None the less, this model shows the feasibility of the approach even for more subtle, intricate instruments compared to the banjo.

4.8.1 Violin string model

The time stepping method for the four violin strings is a composite of equation 4.15 and equation 4.17. The fixation of the string at the nut is modelled as Dirichlet boundary conditions. The coupling between the string and the bridge is modelled by relation 4.52. As already discussed in chapter 2, open strings and pressed strings of the violin have differing boundary conditions. The interaction between the finger and the string depends on the rigidity of the finger tip and the applied finger force at that point. The changing boundary conditions can be modelled as a change in damping characteristics at the interaction point and the neighbouring points. A boundary dependent damping coefficient of the string α_B acting at the boundary can be expressed as

$$\alpha_B|_{i=L} = \begin{cases} 0.999 & \text{if string open,} \\ 0.993 & \text{if string pressed.} \end{cases} \quad (4.74)$$

4.8.2 Violin bridge model

As argued in section 2.3.3, the bridge of the banjo has such high *eigen-frequencies* that it is reasonable to omit it in a model of a complete banjo and approximate the force transmission

¹⁰¹Rolf Bader: “Whole geometry Finite-Difference modeling of the violin”, in: *Proceedings of the Forum Acusticum 2005* (2005): 629–634.

from the string to the membrane with relation 4.53¹⁰². The bridge of a violin on the other hand, has an impact on the vibration of the string and the radiated sound as well. Woodhouse¹⁰³ identified a distinct bridge hill in the spectrum of the violin between 3 and 5 kHz. Hence, a finite difference model of the violin bridge is implemented in this work. There are several modes of motion for violin bridges¹⁰⁴ in the horizontal and vertical directions orthogonal to the string. Comparable to the model of the banjo bridge, the violin bridge is approximated by a 2-dimensional plate model with in-plane forces.¹⁰⁵

4.8.3 Violin top plate model

The front plate and back plate of the violin are fixed under tension and exhibit buckling. Hence, the front- and back plate are modelled as plates with buckling, and velocity as well as frequency dependent losses. The front- and back plates are coupled at the rim, simulating the presence of ribs. The orifices on the front plate of the violin are modelled as rhombus-like openings¹⁰⁶. Free boundary conditions are applied at the points on the plate surrounding the orifices.

$$\begin{bmatrix} \mathcal{A} \\ \mathcal{V} \\ \mathcal{U} \end{bmatrix} = \bigcup_{t=1}^T \left\{ \begin{array}{l} \mathcal{F}^{-1} \left[\hat{\delta}_{XY} \cdot \mathcal{F} [\tau_{t-\mathbf{u}}] (1 - \alpha \cdot \delta_t) - \beta \cdot \tau_{t-\mathbf{v}} \right] \text{ for } \mathbf{x} \neq \Omega \vee \mathbf{x}_{cp} \\ 0 \text{ for } x = \Omega_B \\ \mathcal{F}^{-1} \left[\hat{\delta}_{XY}^{\Omega_N} \cdot \mathcal{F} [\tau_{t-\mathbf{u}}] (1 - \alpha \cdot \delta_t) - \beta \cdot \tau_{t-\mathbf{v}} \right] \text{ for } \mathbf{u} = \Omega_O \\ \mathcal{F}^{-1} \left[\hat{\delta}_{XY} \cdot \mathcal{F} [\tau_{t-\mathbf{u}}] (1 - \alpha \cdot \delta_t) - \beta \cdot \tau_{t-\mathbf{v}} \right] - Z_{\mathbf{v}FS} \text{ for } \mathbf{x} = x_{CP} \\ \tau_{t-\mathbf{v}} + \mathbf{a} \\ \tau_{t-\mathbf{u}} + \mathbf{v} \end{array} \right. \quad (4.75)$$

4.8.4 Air cavity

The air filled cavity is modelled as a three dimensional air volume coupled to the front and backplate via relation 4.53. At the orifices, Sommerfeld radiation conditions are utilised. The time integration scheme is similar to the scheme of the ruan given in equation 4.73. The only difference are the material parameters of the wood and the different geometry of the instrument.

¹⁰²This was implemented in the first model of the banjo.(F. Pfeifle and R. Bader: "Real-time virtual banjo model and measurements using a microphone array", in: *J. Acoust. Soc. Am.* 125.4 [2009]: 2515–2515)

¹⁰³Woodhouse, "On the "Bridge Hill" of the Violin".

¹⁰⁴See the figures in (Cremer, *Physik der Geige*, 184ff.)

¹⁰⁵A structural description on the bridge forces is presented in: *ibid.*, p. 193.

¹⁰⁶The shape of the orifices does not influence the cavity frequency if an equivalent area of the openings is used. A technique applied in: *ibid.*, p. 216.

4.8.5 Bow string model

The bow string interaction model is based on the model presented in Bader¹⁰⁷ and the assumptions presented in section 2.4.4. It is extended in several regards and includes the following controllable parameters:

- The number of contact points.
- The bow-velocity.
- The bow-pressure.
- The position of the bow on the string.
- The amount of rosin on the bow.

The iterative process of the model can be described in pseudo-code as¹⁰⁸:

Listing 4.1: Pseudo-code of bow/string model.

```
1 state = glue :
2   if deflectionContactPoint+1 > deflectionContactpoint
3     state = glide
4   else if netForceString > bowPressure
5     state = glide
6   end
7
8 state = slip :
9   if abs(velocityContactPoint) < velocityBow
10    state = glue
11  end
12 if state == glue
13   velocityContactPoint = velocityBow
14 else
15   Normal string calculation with friction damping
16   at bow/string interaction point.
17 end
```

A schematic block diagram is shown in figure 4.31.

¹⁰⁷Bader, “Whole geometry Finite-Difference modeling of the violin”.

¹⁰⁸ Stick/slip is denoted as glue/glide.

4 Physical models

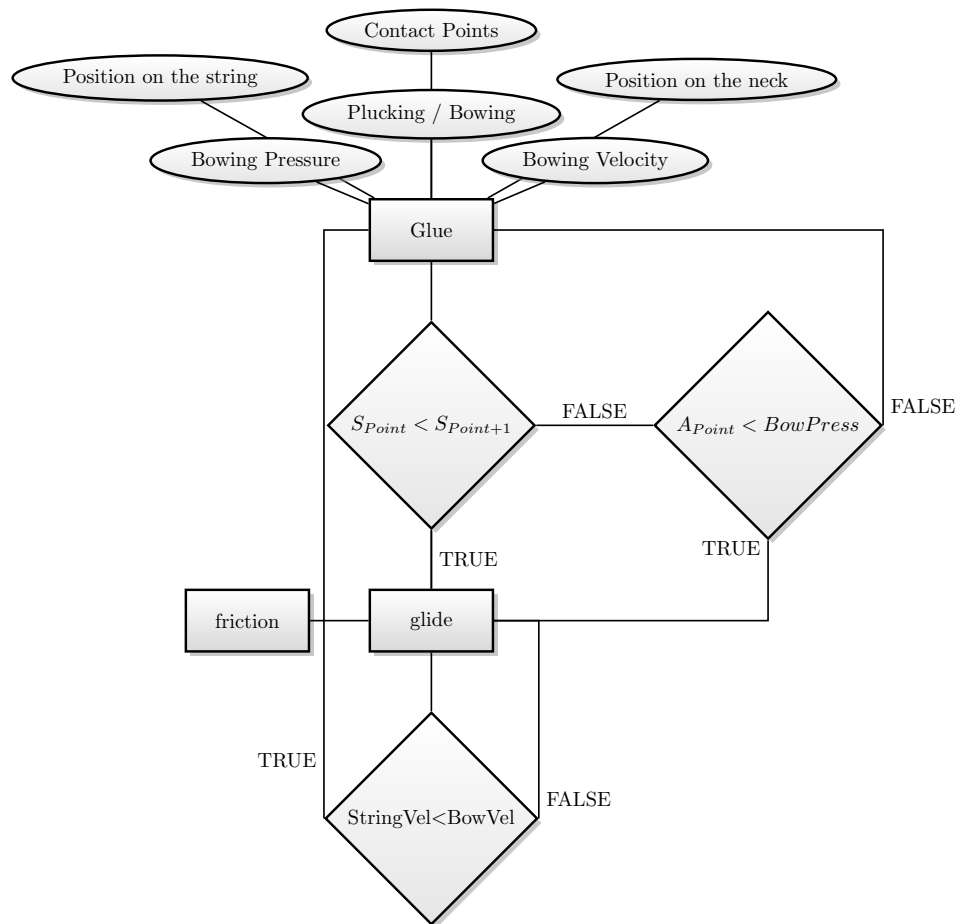


Figure 4.31: Bow string interaction model.

Mathematical formulation

Figure 4.32 illustrates the basic principle of an idealised interaction between a violin bow and a violin string. The mathematical description of the bow/string interaction formulates the relation between the stick-slip cycle of the bow/string interaction and the motion of the string.

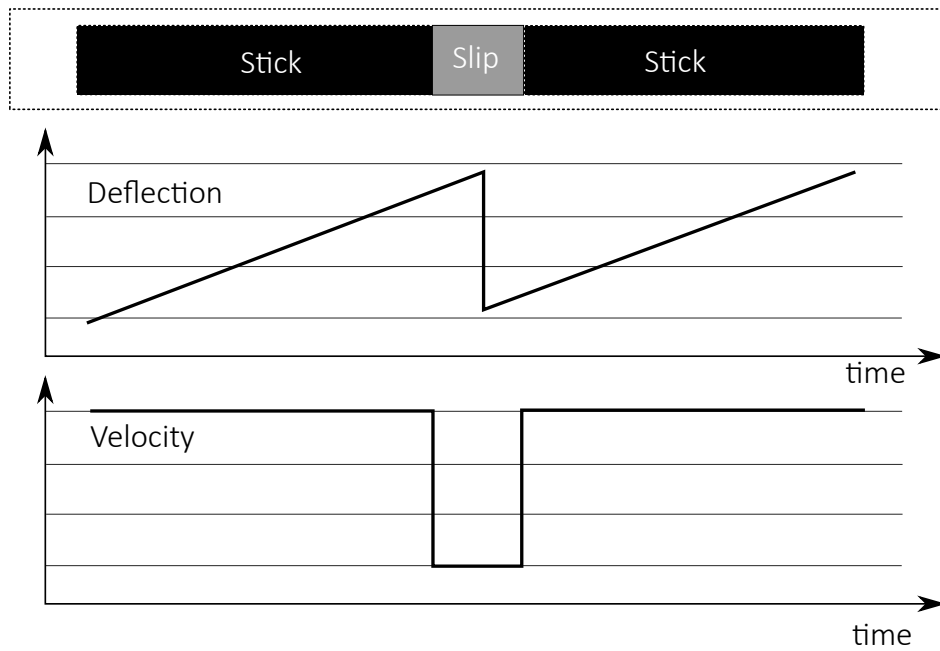


Figure 4.32: Idealised Helmholtz motion of a bowed string.

The process of the idealised stick-slip model can be summarized as follows:

- The bow, which is in contact with the string at a certain point has a certain velocity v_b . Due to the friction of the bow, the string starts to stick to the bow, thus having the same velocity as the bow.
- If the bowing pressure p_b is too small, or the net force of the string acting in the opposite direction of the string extension, or a reflected wave exerts a force larger than the force of the bow. The string starts to slip.
- This leads to a condition where the string oscillates back to its neutral position. The friction between the bow and the string leads to a large damping at the bow point.
- If the string velocity is smaller than a certain value, the string sticks to the string again, repeating the cycle.

This model leads to the following requirements: When the string sticks to the bow the condition at the contact point CP must be:

$$v_{CP} = v_B, \quad (4.76)$$

When the model is in the slipping phase the PDE of the string can be extended to:

$$\rho \frac{\partial^2 u}{\partial t^2} = T \frac{\partial^2 u}{\partial x^2} - EI \frac{\partial^4 u}{\partial x^4} - \beta(x) \cdot \frac{\partial u}{\partial t}, \quad (4.77)$$

with $\beta(x)$ a position dependent damping coefficient that has a large value at the contact point between bow and string due to the friction between both.

Discussion

The model described above is able to simulate various effects of a bow/string interaction with satisfactory results. In the real-time implementation, this model is modified in one central point: If the bow sticks to the string the velocity of the interaction point is not strictly set to the bow velocity, but the bow velocity is added to the string velocity at that point. At this moment, I don't have a reasonable, physically justifiable explanation for this modification of the standard model, but the simulation results of the violin are more realistic when the bow/string model is implemented in this way. Further research will be conducted at the Institute of Systematic Musicology to elucidate the possibility of such an effect in real violin strings.

4.9 Sound integration over surfaces

Because this work is mainly concerned with acoustical parameters of instruments, all models are calculated as autonomous geometries, omitting influences of room acoustic parameters and the influence of air movement in the far field. For auralisation of the acoustical vibrations of the instruments, the sound radiation is integrated to two points into a virtual room above the instrument. The radiating points are weighted depending on the distance to the respective sound radiating parts. Additionally, the difference in arriving sound due to the finite speed of sound in air is also taken into account. A certain distance to a sound radiating surface leads to a specific delay that rises with the distance from the sound radiating surface. A short outline shall exemplify the applied method: If we have a sound receivers in a centred position 1 meter in front of a banjo, which has a membrane diameter of approximately 30 cm, the distance of the receiver to a point on the rim of the membrane can be calculated using Pythagoras' theorem by the equation

$$\Delta z_{Rim} = \sqrt{\Delta z_{Center}^2 + \Delta y_{max_{Membrane}}^2} = \sqrt{1^2 + .15^2}[m] = 1.0112[m] \quad (4.78)$$

Hence, the difference between the centre-point and a point on the rim is 1.12 cm. With a sample rate of 2^{17} Hz and a velocity of sound of $343 \frac{m}{s}$, we get a maximal spatially representable delay of approximately $343/2^{17}[m] \approx 2.27mm$. Thus, the membrane sound, radiated from node-points near the boundary are approximately 4 sample steps behind the sound produced at the membrane centre.

This effect can be included by implementing a sample delay, depending on the position of the virtual listener. This sample delay can be included in the sound integration model straight-

forward.

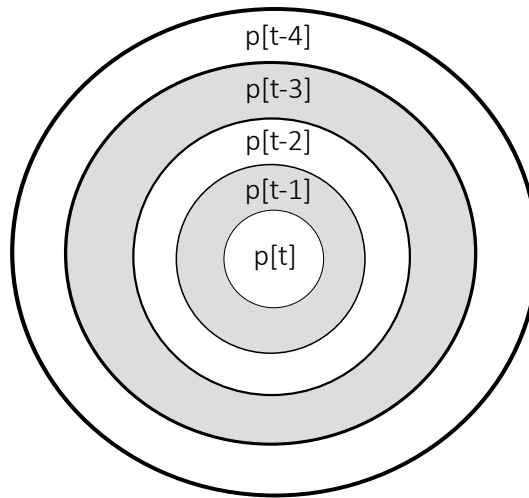


Figure 4.33: Integration delays for round membrane and centred receiver.

CHAPTER 5

FPGA - A STRUCTURAL OVERVIEW

Metal on Metal...

(Anvil,1982)

In this chapter, a structural overview on the FPGA devices used in this thesis is given. After an overview of several features of the specific hardware, used for all hardware designs, an introduction to two FPGA boards used as development platforms for the designs, is given. In the following sections concerned with structural properties, a focus is put on specific features of FPGA devices that sets them apart from CPUs of standard PCs and the advantages and disadvantages of an FPGA for implementing numerical methods in general and the physical modeling problems regarded in this thesis in special.

To this end, the parallel hardware properties and the input/output structure are of special interest in this chapter. Furthermore, particular features like the on-board AC-97 AD/DA converter on the Virtex-2 development board, as well as special functional blocks like the DSP-48 block on the development board consisting of the Virtex-6, that are used for the real-time models are explained in more detail.

All on-board communication protocols, which are utilised in the final models presented in chapter 6, are explained and exemplified with a data transmission instance.

This chapter ends with a short introduction to the PCIe communication protocol that is used for data transfer in 2nd generation design models. This includes a basic example of a host-device data transport and communication is presented.

5.1 History of FPGAs

The historic development of FPGA devices is closely linked to the evolution of integrated digital circuits in the late 1960s, the 1970s and early 1980s. The development of logic devices of that time period was mainly driven by the manifold advances in transistor and integrated circuit technology, or in the words of C. Maxfield:

*The late 1960s and 1970s were rampant with new developments in the digital IC arena.*¹

Custom logic devices of that time period can roughly be divided into two categories:

1. Programmable Logic Devices (PLDs).
2. Non-programmable devices like Application Specific Integrated Circuits (ASICs) or Application Specific Standard Parts (ASSPs).

The main difference between both device classes can be found in their basic structure. PLDs are only partially wired to perform certain binary logic functions, whereas ASICs are hard-wired during the initial production state. This means, a specific function of an ASIC is *fixed* and can not be altered by an end-user after the production state, a PLD on the other hand can.

These fundamental differences lead to differing design and implementation practices and thus to differing fields of applications. In comparison to PLDs, ASICs have a higher logic gate count and are mainly used to implement highly specialised functions, but have the drawback of long production cycles for implementation, prototyping and debugging. If an ASIC has inherent design errors, they often surface *after* a first prototype is manufactured and the appliance is running under realistic conditions in the respective field of application. PLDs and Programmable Read Only Memory (PROMS) devices can be programmed after the production state, which has the advantage that a faulty chip design does not lead to an complete erroneous production charge. Still, compared to most ASICs, PLDs have considerably smaller logic capabilities.

The first programmable devices had a transistor array structure that could be flashed with different logic circuit designs by adding connections (anti-fuse technology) Clive Maxfield: *The Design Warriors Guide to FPGAs*, Elsevier, 2004, p. 12, or removing connections (fusible link technology) *ibid.*, p. 10. The added or removed links were permanent, so the devices could only be programmed once. Due to that, they were capable of performing specially designed tasks with very high clock rates but they could not be reconfigured after a design was implemented on the device.

¹Clive Maxfield: *The Design Warriors Guide to FPGAs*, Elsevier, 2004, p. 28.

Further advances in the field of programmable integrated circuits lead to technologies that made it possible to erase an initial design and re-program the device. The most prominent technology among these devices are Erasable Programmable Read Only Memory (EPROM) or the Electrically Erasable PROM (EEPROM). Devices incorporating these technologies could be programmed and reprogrammed multiple times by removing the connections of the design on the metal layer by exposing it to ultra-violet light or a certain voltage respectively. Up to this point of programmable hardware evolution, there always existed a gap between the two clusters of hardware device classes. On the one hand there were PLDs, which were highly configurable but only consisted of a small amount of logic facilities, and ASICs on the other hand that could perform highly complex logic circuits but were not (re-)configurable and were expensive and elaborate to develop for.

The next large leap in the evolution of freely programmable hardware was sparked by research done by Ross Freeman and Bernard Vonderschmitt, the founders of XILINX, who were the first to develop and produce freely programmable hardware-gate logic on a large scale.²

In 1985, the first commercially available programmable logic chip was the XC2064, called a Field Programmable Gate Array (FPGA)³. The first FPGA device had 64 programmable and freely connectible Logic Blocks (CLB's) and an aggregate gate count of 1200 logic gates⁴. FPGAs were developed as a device to combine programmability of PLD's, reconfigurability of EEPROMS and high logic gate count of ASICs Maxfield, *The Design Warriors Guide to FPGAs*, pp. 49ff. This period of time is often regarded as the starting point for the development of more advanced FPGA devices by XILINX and other vendors. At the present day, the biggest FPGA chip vendors are XILINX and Altera among other smaller companies as Lattice Semiconductor or Microsemi *ibid.*, pp. 161 ff.

In this work, XILINX hardware is used exclusively, but the presented models could be are not bound to a specific vendor and could be implemented on other FPGA devices as well.

² <http://www.edn.com/electronics-blogs/fpga-gurus/4306558/Remembering-Ross-Freeman>.

³Field Programmable literally means, programmable in the field, outside of the laboratory, where a logic function is programmed onto the device. The name FPGA is still used today for logic devices of similar design structure and logic capabilities.

⁴Modern FPGAs like the Virtex-7 have around 2 Million logic gates.

5.2 Features and properties of FPGAs

In the following section, features and properties of the FPGA devices used in this work are presented. On a fundamental level, modern FPGAs are comparable to earlier FPGA chips, but special device features can change from generation to generation. Hence, only a portion of the capabilities of FPGAs are presented here and a focus is put on structural parts used during this thesis.

5.2.1 Structure of FPGAs

As stated before, the hardware structure of FPGAs are influenced by PLDs, EEPROMs and ASICs. Depending on the device generation, basic logic gates are realised by different techniques.

In a large fraction of older FPGAs, the basic logic functions are implemented with logical gates comparable to SRAM-cells.⁵

In modern FPGA devices logic gate functionality is realized by look-up tables (LUTs)⁶ which are, in a sense, addressable function generators. This means that they can be programmed to perform different logic functions on a set of inputs.

These basic logic cells are part of a larger logic conjunction which is called a *slice* in Xilinx devices. All slices contain one LUT, eight storage elements, multiplexers and carry logic *Virtex-6 FPGA Configurable Logic Block User Guide*, version 1.2, Xilinx, 2012. Some Xilinx slices, called *slicemibid.*, additionally contain functions to store data as distributed RAM⁷ and have 32-bit wide shift registers.

Two slices form a configurable logic block (CLBs), as is depicted in Figure 5.1. It depicts a (LUT)-based CLB, as commonly found in XILINX FPGAs. Earlier Xilinx FPGAs, as the Virtex-II pro, contained LUTs with 4 inputs. Newer Virtex-7 devices have configurable 6-input LUTs. LUT-based CLBs are used in all the XILINX FPGAs applied in this work, therefore only LUT-based CLBs are considered here.

⁵Maxfield, *The Design Warriors Guide to FPGAs*, 57 ff.

⁶LUTs are also called Logic Function Generators XILINX: *Configurable Logic Block User Guide*, XILINX, 2010, p. 2 ff.

⁷Random Access Memory.

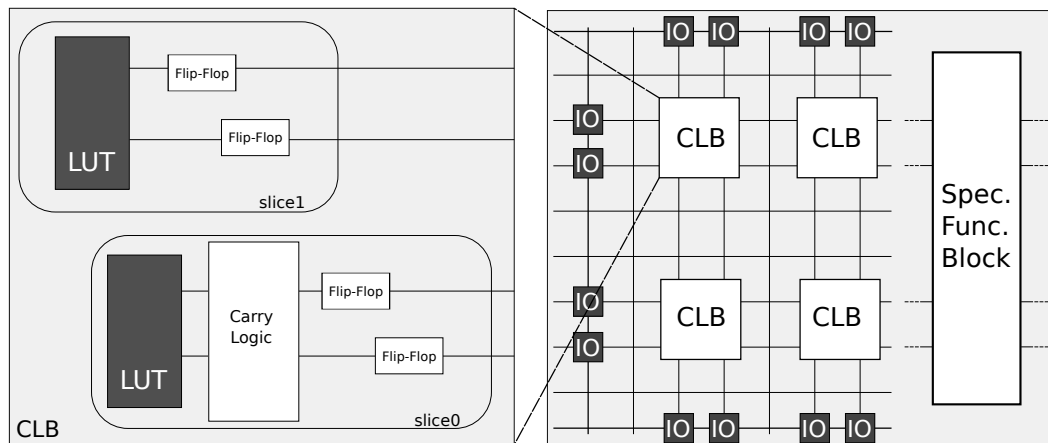


Figure 5.1: Schematic overview of a Virtex-6 CLB, the programmable interconnect network and a special function block.

The LUTs inside a CLB can operate in several different input/output modes depending on the device class and generation. In addition to being connectible as 6-input 2-output LUTs, they can be configured as shift registers, RAM blocks or first-in/first-out memory. In some CLBs there are additional latches, in other are Flip-Flop cells *Virtex-6 FPGA Configurable Logic Block User Guide* which can be used as asynchronous or synchronous registers.

The outputs of the single CLBs are connected to a programmable interconnection network, which is attached to a multiplexer on the output stages, multiplexing output signals to input stages of other CLBs. This cascading of CLBs allows for more complex logic functions, larger RAM blocks or longer shift register.

A structural overview of a SLICEM is shown in figure 5.2.

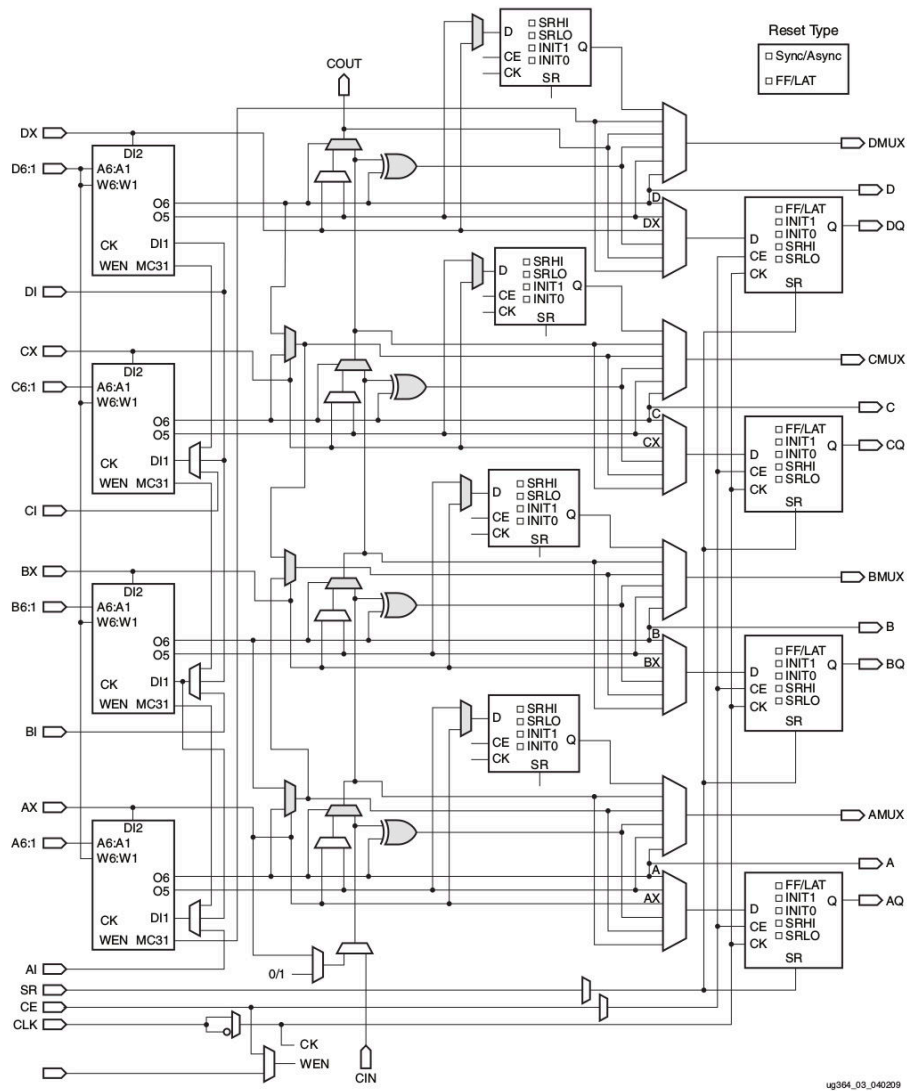


Figure 5.2: Schematic overview of a *slicem* with additional shift and distributed RAM capabilities. Taken from *Virtex-6 FPGA Configurable Logic Block User Guide*.⁸

The single CLBs are connected with an interconnection network, which is attached to a multiplexer on the output stages, multiplexing output signals to input stages of other CLBs.

5.2.2 Special function blocks

Besides basic logic cells, XILINX FPGAs contain other functional logic blocks, that can differ from device generation to device generation. Some additional logic blocks which are used in the presented designs, are memory blocks in the form of random access memory (RAM) and first in/first out (FIFO) memory blocks. A logic blocks that extends basic FPGA logic

by an integrated circuit implementation of arithmetic function is the DSP48e1 block with integrated Multiply-and-Accumulate (MAC) circuitry. All special function blocks are on the FPGA die close to the logic gate resources and can be connected to the same high-speed interconnection network the core logic is connected to as is shown in Figure 5.1.

In modern Xilinx FPGAs the CLBs and the special function blocks are arranged in a column layout. Figure 5.3 depicts a schematic overview of the arrangement of DSP48e1, BRAM and logic slices.

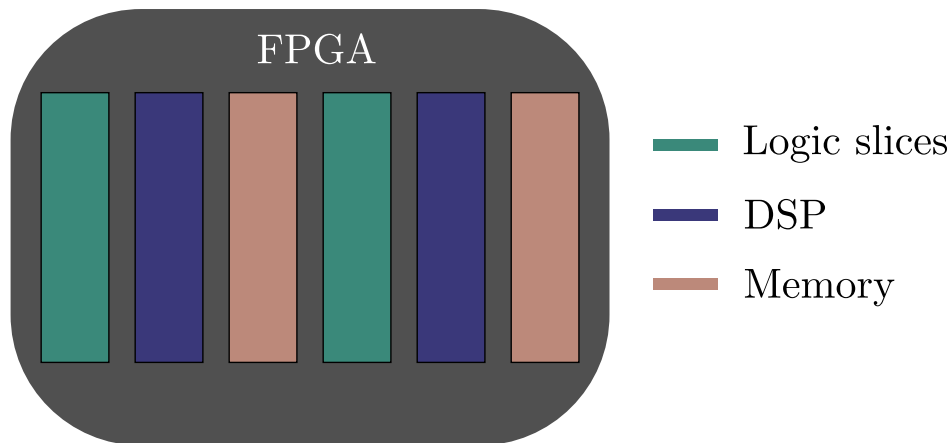


Figure 5.3: Schematic overview of Xilinx column design.

DSP blocks

Most modern FPGAs by the vendors Xilinx or Altera have special logic blocks that are designed to perform DSP typical operations. They are implemented on the same structural level as CLBs, this means that the data transfer between gate based logic and DSP cores can be realised by the high-speed interconnect network.

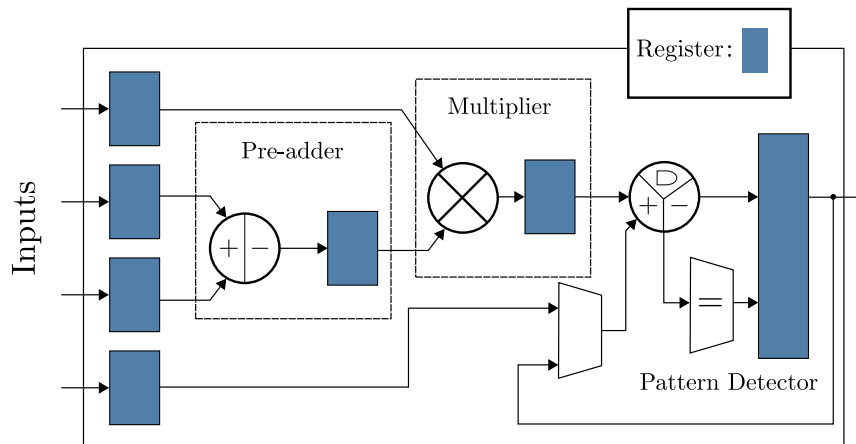


Figure 5.4: Schematic overview of a Virtex-6 DSP48e1. Blue blocks are registers.

Figure 5.4 depicts a schematic overview of a DSP48e1 slice which is part of most modern Xilinx FPGAs. It consists of four inputs, a pre-adder, a 25bit x 18bit multiplier, a 48bit accumulator and a pattern detector that can be used to efficiently compare values.

RAM blocks

In the Xilinx devices used for this thesis RAM can either be implemented by combining several CLBs, this is called distributed RAM or DisRAM. Another sort of dedicated RAM on Virtex FPGAs is called block RAM (BRAM). It can be configured to different sizes and different function modes. Every BRAM block can perform in dual-port mode facilitating 36Kb of memory.

Both memory blocks can be used as memory of variable bit width and depth. Similar to the DSP blocks, the special RAM blocks are located on the FPGA chip and are connected to the CLBs via the internal routing network, which makes the communication and data transfer faster, when compared to a communication with a peripheral RAM which can be implemented on a hardware board connected to the FPGAs IOs, see Figure 5.3. The resources of the Virtex-6 VLX240T FPGA are listed in table 5.4.

5.2.3 Hardware Description Language

A common trait of modern programmable logic devices is that functional logic is designed using a Hardware Description Language (HDL). In the early days of hardware design, the commonly used method was paper and pencil based, drawing schematics of connected logic

registers, a technique comparable to modern CAD⁹ based RTL¹⁰ design tools. To overcome limitations of this design practice for growingly large ASIC designs the first HDLs were introduced during the 1960s to describe functional parts of logic devices on a abstraction level higher than the gate level¹¹. In the late 1980s, the use of HDLs started to replace the process of the schematic based design methodology.¹² During the first years of its development, HDLs were not standardised, and most functions were vendor- and application-specific. Today, there are two HDLs commonly used to program FPGAs, Verilog and VHDL¹³. Both languages incorporate similar concepts, which can be categorised into *low-level* features like:

- bitwise declaration of signals,
- control over electronic signal levels,
- a direct access to signals via physical input and output ports of the hardware development board

and *high-level* constructs like for instance:

- object oriented programming techniques,
- pointer data types
- and procedural programming

among other features.¹⁴

A central difference of a HDL, compared to other programming languages is that it enables the developer to directly design hardware functionality using software statements. This means that every logical instruction must be representable by an equivalent formulation in gate logic.

A second difference is the fact that all code written in a HDL instruction file is evaluated concurrently. This means that instead of sequential code evaluation like in a compiled high-level language (C,C++ or Java ...) all code that is translated into a hardware function is evaluated at the same time, if not specifically designed otherwise. Sequential code can be implemented by designing a finite state machine (FSM).

⁹Computer Aided Design.

¹⁰Register Transfer Level.

¹¹The gate-level is the level of the underlying transistor logic

¹²Maxfield, *The Design Warriors Guide to FPGAs*, p. 153.

¹³Very Highspeed Integrated Circuit Hardware Description Language.

¹⁴In this work only VHDL is applied.

5.2.4 Finite State Machine

Because all logical statements expressed in VHDL are evaluated concurrently, sequential code must be implemented with a Finite State Machine (FSM), which controls the singular steps of the calculation which need to be evaluated successively and synchronised¹⁵. There are three standard versions of FSMs that are commonly used in various applications. The two most prominent are known as:

1. Moore Finite State Machine
A state machine where the output only depends the state.
2. Mealy Finite State Machine
A state machine where the output depends on the state and the input.¹⁶

The FSM implementation, depicted in figure 6.6, is reused for all models of the musical instruments. Because some state outputs of the FSM implemented in this thesis depend on the input¹⁷, the utilised FSM is a mixed Mealy and Moore state machine.¹⁸ Table 5.1 shows the states of the models and the corresponding assignment. The 6 finite states control the arith-

State	Task
1	Load values
2	Calculation step I
3	Calculation step II
4	Calculation step III
5	Write values to the respective memory position
6	Write stable output data

Table 5.1: States for the harmonic oscillator.

metic flow of the math entity¹⁹ through the control signals as shown in figure 6.8. A Root Transfer Level (RTL) structure the of the model including both entities is shown in figure 6.7 and the simulation results from *Modelsim* can be found in figure 6.8.

Development Environment

The Integrated Development Environment (IDE) applied in this work is ISE, a software IDE supplied by XILINX, the vendor of the utilised FPGA chips. Besides the logical constructs of the VHDL standard, there are additional hardware specific features incorporated into ISE,

¹⁵ This includes the calculation for all values which are dependant on values from previous time steps.
¹⁶ (Peter J. Ashenden: *The Designer's Guide to VHDL*, 2nd, San Francisco, CA, USA: Morgan Kaufmann Publishers Inc., 2002).
¹⁷ Because of the possibility to change values of external variables while the computation is running.
¹⁸ A technical definition of both state machines is given in Ashenden. (ibid.)
¹⁹ It would also be possible to implement the FSM directly in the same entity as the mathematics, but for the sake of brevity, both functional parts are implemented in separate structures.

like hardware specific macros and simulation libraries. To make use of the XILINX simulation primitives, it is necessary to use a VHDL specific data type. The most fundamental data-type in VHDL is a BIT, having two possible values: one or zero. To represent longer numbers several bits can be combined to a BIT_VECTOR with a specific length. An extension to this basic binary number representation, STD_LOGIC or STD_LOGIC_VECTOR can be used. Besides binary one and zero values it can take the following values:

- 'U':= uninitialized. This signal hasn't been set yet.
- 'X':= unknown. Impossible to determine this value/result.
- '0':= logic 0.
- '1':= logic 1.
- 'Z':= High Impedance.
- 'W':= Weak signal, can't tell if it should be 0 or 1.
- 'L':= Weak signal that should probably go to 0.
- 'H':= Weak signal that should probably go to 1.
- '-':= Don't care.

STD_LOGIC is used in most XILINX simulation libraries and thus is needed when using hardware specific XILINX macros. Another VHDL data type utilised in this work is SIGNED. This data type represents numbers from $[-\frac{N}{2} \dots \frac{N}{2} - 1]$ in 2's complement format, with N the number of bits.

Design flow

The design flow for the hardware models can be summed-up in 6 steps:

- Development of the low level model in VHDL.
- Synthesize the model.
- Perform a functional simulation of the synthesized system with a VHDL simulation environment²⁰.
- Debug the code using the simulation tool and the synthesis reports.²¹
- Place and route the code and generate a bit-file.

²⁰Mentor Modelsim is used in this work.

²¹The functional simulation can be extended with a timing simulation of the routed design.

5 FPGA - A structural overview

- Flash the bit-file to the specific hardware.

Besides the functional description of the model, in the VHDL source code, the Place&Route process routes external ports to internal buses via a list of I/O-ports.

The declaration for the signal ports is put into a *.ucf-File, a *User Constraint File*. Here all input and output signals are routed to the respective hardware addresses of the respective FPGA board. The router reads the constraint file and connects the hardware ports to the internal signals. The FPGA devices used in this work can all be programmed from a PC via a programming interface and a hardware-specific flash tool called iMPACT by XILINX.

Logic Cells	30816
Slices	13696
Total Block Ram (KB)	2448
Multiplier Blocks	136

Table 5.2: Logic resources of a Virtex-2 XC2VP30 device.

5.3 XUP Virtex-II Pro Development System

The XUP Virtex-II Pro Development System is an FPGA application development board, which consists of a Virtex-II FPGA Chip surrounded by other hardware components and devices. In this work, four of the on-board components are utilised:

1. The Virtex-II Pro FPGA.
2. The AC '97 Audio CODEC²².
3. User Switches.
4. I/O Ports for transmitting and receiving data via a I2S protocol.

5.3.1 Virtex-2 FPGA

The Virtex-2 FPGA was first released in 1998. The main difference, compared to other devices of that time period, was the possibility of programming the chip via an USB-Port from a standard Personal Computer with an point-to-point flash protocol (JTAG). The logic resources of a Virtex-II are presented in table 5.2

5.3.2 LM4550-AC '97 CODEC

In the first hardware models, the on-board audio CODEC chip LM4550 is used as part of the FPGA hardware design. The data communication is realised with a serial communications protocol, the AC '97 Rev. 2.1 specification protocol. Basic functional properties of the CODEC are depicted in figure 5.5. As is shown there, the converter is build around a 18-bit Sigma-Delta ADC/DAC and has multiple input and output signal lines. For the implemented models, one stereo input without amplification and one stereo output is implemented. Table 5.3 gives an overview over the signals connected to the hardware models.

Interface protocol

A serial data transaction of the AC '97 interface can best be illustrated by showing the different phases of data processing and transmission as standardised in the AC '97 Rev. 2.1

²²CODEC=Coder Decoder.

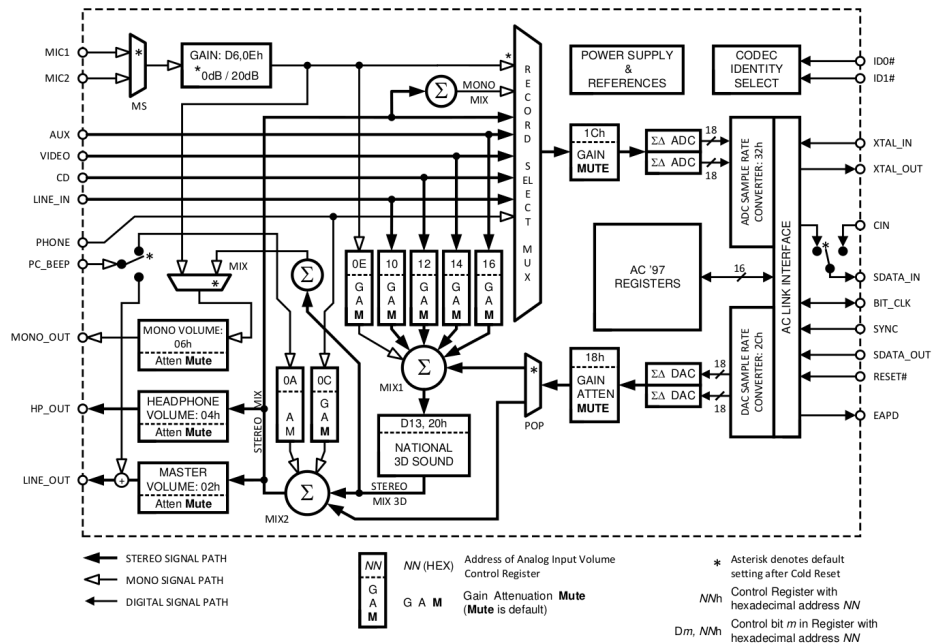


Figure 5.5: Schematic overview of audio CODEC LM4550. Taken from *LM4550 AC '97 Rev 2.1 Multi-Channel Audio Codec with Stereo Headphone Amplifier, sample Rate conversion and National 3D Sound*.²³

SDATA_IN	Signal from the microphone/line input of the converter
BIT_CLK	The clock signal of the serial data
SYNC	Synchronisation bit to synchronise the data frames
SDATA_OUT	Data to the output of the converter
RESET	System wide reset signal for cold and soft reset

Table 5.3: Signals connected to the model.

specification. The AC link serial interface protocol is used as a communication interface to the LM4550 converter. All digital signals are processed in serial with a clock speed of 12,288 Mhz for the link clock signal BIT_CLOCK. The SYNC signal divides the transmission protocol line into frames of $20.8\mu s$ ²⁴ length with one tag slot of 16 bit length and 12 data slots of 20 bit length for every frame. A decomposed serial data frame is depicted in figure 5.6. Depending on the direction of the SDATA signal, slot number 1 and 2 contain command and status signals respectively, the following two slots contain PCM coded data. Depending on the transmission mode and the implementation of the AC '97 protocol, the slots named RSV, which stands for reserved, contain PCM, status or control data.

The serialisation of the parallel data is performed pipelined in the core module of the AC '97

²⁴ $20.8\mu s = \frac{1}{48000} Hz$

5 FPGA - A structural overview

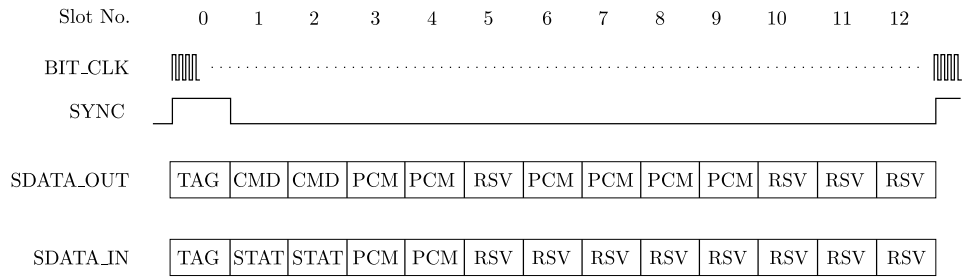


Figure 5.6: AC '97 protocol signal overview.

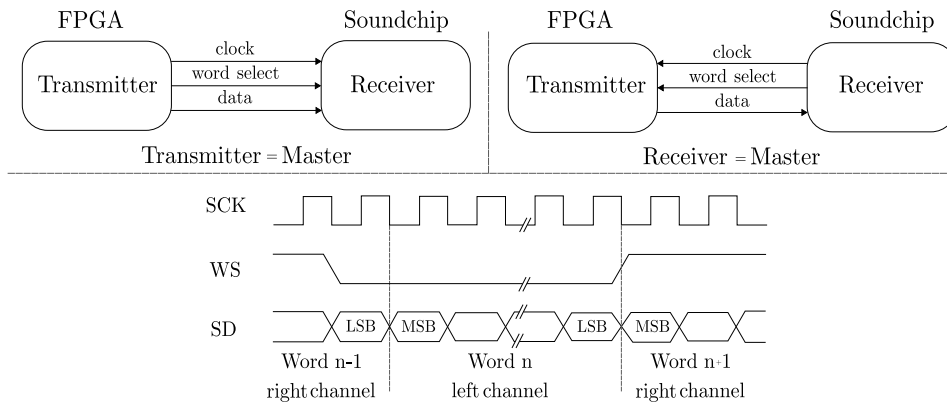


Figure 5.7: I2S system configuration consisting of one transmitter and one receiver. The timing diagram illustrates the serial data transmission of a stereo signal.

interface design. The BIT_CLOCK signal is responsible for the timing of the parallelization, as well as the serialisation of the data.

5.3.3 I2S interface

The first hardware implementations of the violin and the banjo, consists of a Virtex-II Pro and a ML-605 XILINX development board that are connected using an I2S protocol. The strings of the instrument are computed on the Virtex-II board (**B1**), the remaining geometry is computed on the ML-605 board (**B2**). The bidirectional data transmission between **B1** and **B2** contain computed sound data of the strings and calculated sound data from the body of the instrument. Again the AC'97 CODEC on **B1** is used for auralisation of the synthesized sound.²⁵

On each board, a transceiver circuit is implemented to route and process the data stream from one device to the other device. The design of the I2S is implemented following the design specification by Philips Semiconductors as depicted in figure 5.7.

Compared to the AC'97 protocol, the I2S protocol is a more simplistic protocol thus less

²⁵The ML-605 development board does not consist of an audio CODEC.

Logic Cells	241152
Slices	37680
Total Block Ram (KB)	14976
DSP48 Blocks	768

Table 5.4: Logic resources of a Virtex-6 XC6VLX-240t device.

demanding on the hardware resources, because of its smaller protocol overhead. In the implemented designs, the transmitter functions is the master. A schematic overview of a transmitter and receiver interaction can be found in figure 5.7 in the upper left corner with the signal timing at the bottom.

5.4 The ML-605 Evaluation Board

The *ML-605 Evaluation Board* is a development platform for high speed communication and signal processing appliances built around a Virtex-6 chip. The built-in features that are of interest in this work are include:

- The Virtex-6 XC6VLX240T FPGA.
- Two Mezzanin expansion ports.
- A PCIe Gen.1 8x interface / Gen.2 4x interface.
- An IEEE 1394 ethernet IO port.
- Four general purpose IO ports for high speed communication.

5.4.1 Virtex-6 FPGA

As an extension to the instrument models implemented on the Virtex-II chip, a Virtex-6 device was utilised to calculate whole geometry models of instruments, like the model of a violin including the front plate, back plate and the enclosed air in the violin body. The logic resources available on a Virtex-6 VLX-240T device that are utilised in this work, are summarised in table 5.4.

5.5 PCIe interface

Besides multiple other In/Out-ports, which are available on the XILINX ML-605 development board, a host-device communication port, used in this thesis, is the Peripheral Component Interface express (PCIe) interface. In the present stage of the application design, the

PCIe-port is used to transfer data between the interface layer of the instrument model, calculated on the FPGA-Board (Device), and a Graphical User Interface (GUI) running on a Personal Computer (Host). In this section, an introduction to the basic functionalities of the PCIe protocol and a short overview on the implemented model, including the communication protocol, is given.

5.5.1 PCIe fundamentals

In 2002, the PCI interest group, the PCI-Sig consortium²⁶, published the first specifications of the PCIe protocol, as an extension to the, already established PCI and PCI-X protocols.²⁷ To this day, the basic protocol has undergone several revisions and currently has the version number 3.0²⁸. Today, the PCIe interface is a de-facto standard interface for high data throughput communication of peripheral devices, exchanging data with the central processing unit in Personal Computers²⁹. One of the most notable differences of the PCIe interface, compared to the older PCI and PCI-X protocols is the serial structure of the data transfer lanes, instead of the prior parallel structure. Another feature that discerns the protocols is the Point-to-Point communication of PCIe, enabling the bus to handle higher clock rates without protocol overhead of bus arbitration, found for instance in the original PCI protocol specification³⁰. The maximum data transfer rates that can be achieved with a PCIe 3.0 interface are $\approx 16 \frac{GB}{s}$.³¹ In the presented models, the utilised PCIe interface is a version 2.1 revision with a 4x lane interface configuration. The maximal data rate including the 10b/8b protocol overhead is approximately $2 \frac{Gb}{s}$. The communication with the GUI running on the personal computer is achieved by implementing a windows RAM driver writing configuration data to the FPGA board and receiving sound data from the FPGA board.

5.5.2 PCIe layer communication

Following the Open Systems Interconnection (OSI) model³² standard, the PCIe communication protocol implements the three bottommost layers:

1. The Transaction Layer (TL).
2. The Data Link Layer (DLL).

²⁶A consortium of 900 hardware and software companies. A.H. Wilen, J.P. Schade, and R. Thornburg: *Introduction to Pci Express: A Hardware and Software Developer's Guide*, Engineer to Engineer Series, Intel Press, 2003, p. 16.

²⁷ibid.

²⁸Some specifications for Revision 4.0 were published in August 2012. See: http://www.pcisig.com/news_room/Press_Releases/November_29_2011_Press_Release_/.

²⁹Wilen, Schade, and Thornburg, *Introduction to Pci Express: A Hardware and Software Developer's Guide*.

³⁰H. Liebig, Thomas Flik, and M. Menge: *Mikroprozessortechnik und Rechnerstrukturen*, Springer London, Limited, 2005, pp.134.

³¹Wilen, Schade, and Thornburg, *Introduction to Pci Express: A Hardware and Software Developer's Guide*.

³²The ISO number is: ISO/IEC 7498-1.

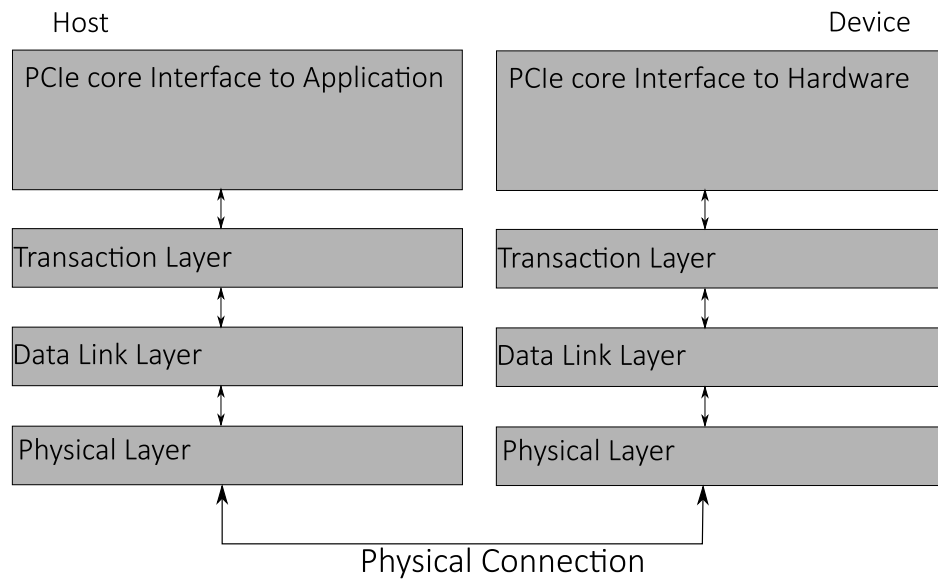


Figure 5.8: PCIe layer model.

3. The Physical Layer (PL).

As depicted in figure 5.8, every layer communicates with the other layer via communication ports. The data is transported in layer specific packets, which have a specific header structure, which is updated for every layer it passes. The topmost layer, viewed from the user application, is the transaction layer. The data presented to the TL is packed into a Transaction Layer Packet (TLP). The TLP consists of the data, also called payload, and TP-header. The TLP is transmitted downstream to the next layer, the Data Link Layer (DLL). In this layer the payload (TLP) is packed into a Data Link Layer Packet (DLLP), adding information to the packet header. The DLLP is then transmitted to the physical layer (PL). In the PL, the logic signal is transferred to an electric signal. Before the physical transmission is realised, the signal is coded to a 8b/10b data protocol to minimize the error-proneness of the physical transmission and enable a better clock recovery.³³

5.5.3 Implemented design

The implemented design is based on a XILINX Core Designer Project for the ML-605 FPGA Development-Board, which utilised four Block-RAM's with 2048 KByte each. The PCIe end-point device implements four addressable RAM-Blocks, that act as *Memory-Spaces*³⁴.

³³The encoding minimizes the DC-offset in the signal. This is achieved by coding the transmitted signal to allow only five consecutive ones or zeros at most. (Liebig, Flik, and Menge, *Mikroprozessortechnik und Rechnerstrukturen*, p. 285).

³⁴The RAM-blocks could also be implemented as IO-Spaces but in this design, the host protocol is crafted to work with *Memory-Spaces*. For the definition of Memory Spaces see: Wilen, Schade, and Thornburg, *Introduction to Pci Express: A Hardware and Software Developer's Guide*, p. 122.

5.6 Final design consideration

Two of the goals of the implemented design is a fast reconfigurability and a fast communication between a front-end and the modelled instrument for a direct interaction and thus good playability in a musical setting. The design methodology for reconfigurable models is presented in chapter 6. The influence of the protocol timing on design considerations is presented in the following section.

5.6.1 PCIe protocol timing

The timing of the PCIe protocol depends on the type of PCIe connection type and the version. The bandwidth for the PCIe 2.0 implementation used in this work has a link speed of approximately $16 \frac{Gb}{s}$ for a 16x connection. The ML605 board has a PCIe 2.0 8x link with a maximal transmission speed of $8 \frac{Gb}{s}$.³⁵ Because the real system has additional overhead added by the operating system driver and PCIe protocol overhead, the raw bit rate considerably smaller. At this point of the work, it is not possible to assess the overhead of the operating system because of the lack of PCIe debug hardware. But at this stage of the development, the synthesised sound from several points are integrated on the hardware, so only one audio sample per time step is transferred from the device to the host.³⁶

In the current design, the control-data from the host to the device is written to the hardware model every 20 milliseconds. Hence, the timing for the upstream data from the host to the device is not critical.

³⁵This means, the protocol could be implemented to transmit the calculated audio data from the model, with a bit depth of 24 bits per sample and a sample rate of 2^{16} with a maximal data transfer rate of ≈ 5080 data points per second.

³⁶An implementation of the newer and more powerful PCIe 3.0 with a 16x link would enhance the data rate to $\approx 32 \frac{Gb}{s}$ which would mean in an ideal case around 20000 data-points of a model on a FPGA could be transferred in real-time.

Il semble que la perfection soit atteinte non quand il n'y a plus rien à ajouter, mais quand il n'y a plus rien à retrancher.

(Antoine de Saint-Exupéry)

This chapter is concerned with FPGA real-time hardware implementation of the physical models presented in chapter 4. It gives a step by step description of optimisations applied in the final hardware models. First, all necessary adoptions for the FPGA implementation are shown with a focus on the data path as well as a classification of used data types. Thereafter, a layer model and a corresponding communication protocol is presented, classifying every block of the implementation according to its functionality and control path. Then, implementations for four complete geometry models are presented.

6.1 Introduction

When using FPGA hardware as a high performance computing platform to enhance existing algorithms in regards to computational speed and throughput there are different strategies that are applicable to improve existing algorithms. When optimizing hardware logic circuits on devices like FPGAs, a central design goal is perfectly summarized by Antoine de Saint-Exupéry's citation in the dictum¹. Applied to hardware design methods it can be translated

¹Translated to English it reads: *Perfection is achieved, not when there is nothing more to add, but when there is nothing left to take away.*

as: The more an algorithm is condensed to its core functionality, the more efficient a hardware model is and the faster and more effective the tasks are performed on the specific hardware.² There are several different techniques typically used to optimised numerical methods on FPGAs,³ but two central techniques which are crucial for FPGA based acceleration of an algorithm are **a)** parallelization and **b)** data-type related optimisations.

6.1.1 Parallelization Considerations

The technique of parallelization has been proven successful for a wide range of different applications, like real-time noise source identification⁴ or high speed direction of- arrival algorithms⁵ or delay-sum beam forming⁶. Other works using the FPGA for Digital Signal Processing (DSP) applications are published by Madanayake et al.,⁷ where 2D/3D Plane Wave Filters are realized by IIR/FIR-Filters or the work by Shuang et al.,⁸ who focuses on converting analog controllers to digital controllers using filter-design techniques. Similar to the mentioned work, there are several papers proposing methods of implementing DSP filter designs (IIR/FIR) on a FPGA chip⁹. The parallel processing capabilities predestine the FPGA to be used in real-time applications. As shown for example for particle track recognition¹⁰, high speed cross correlation¹¹ digital beamforming¹² among other applications. In all mentioned works it was shown that algorithms could be speed-up considerably, or even computed in real-time for the first time, utilising the parallel processing capabilities of modern FPGA chips. Besides the mentioned papers, focussing on highly specialised topics of signal processing, there are several works using FPGAs to calculate various acoustical phenomena

²Andrew B. Kahng et al.: *VLSI Physical Design: From Graph Partitioning to Timing Closure*, Springer, 2011, pp.20ff.

³For a comprehensive list of acceleration strategies see:Herbordt et al. (Martin C. Herbordt et al.: "Achieving high performance with FPGA-based computing", in: *Computer* 40 [2007]: 50–57)

⁴K. Veggeberg and A. Zheng: "Real-time noise source identification using programmable gate array FPGA technology", in: *Proceedings of Meetings on Acoustics* 5 (2009)

⁵C Hao and W. Ping: "The High Speed Implementation of Direction-of-Arrival Estimation Algorithm", in: *International Conference on Communication, Circuits and Systems and West Sino Expositions* 2 (2002): 922–925

⁶P. Chen et al.: "Delay-sum Beamforming on FPGA", in: *ICSP 2008 Proceedings* (2008): 2542–2545

⁷A. Madanayake et al.: "FPGA Architectures for Real-Time 2D/3D FIR/IIR Plane Wave Filters", in: *Proceedings of the 2004 International Symposium on Circuits and Systems ISCAS 2004* 3 (2004).

⁸Kai Shuang et al.: "Converting Analog Controllers to Digital Controllers with FPGA", in: *(ICSP2008) Proceedings* (2008).

⁹O. Maslennikov and A Sergiyenko: "Mapping DSP Algorithms into (FPGA)", in: *Proceedings of the International Symposium on Parallel Computing in Electrical Engineering* (2006); T. Blich et al.: "The Digital Signal Processing Using FPGA", in: *ISSE 2006, 29th International Spring Seminar on Electronics Technology* (2006): 322–324

¹⁰M. Liu et al.: "System-on-an-FPGA Design for Real-Time Particle Track Recognition in Physics Experiments", in: *11th Euromicro Conference on Digital System Design Architectures, Methods and Tools* (2008).

¹¹B. Von Herzen: "Signal Processing at 250 Mhz Using High-Performance FPGAs", in: *IEEE Transactions onvery large scale integration (VLSI) Systems* 6.2 (1998)

¹²Z. Wang et al.: "FPGA implementation of Downlink DBF Calibration", in: *Antennas and Propagation Society International Symposium* (2005)

applying finite differences. Among the earliest publications using an FPGA to solve a 2-dimensional wave equation with a FDTD¹³ method on a FPGA is the work by Chen et al.¹⁴ A physical model of a string implemented on a FPGA was proposed by Gibbons, Howard, and Tyrrell.¹⁵ Other notable publications, regarding numerical computations of the wave equation using finite difference methods, are the works of Erden Motuk as for instance Motuk, Woods, and Bilbao¹⁶ or Motuk et al.¹⁷ Here, as well as in his thesis¹⁸, Motuk utilises a FDTD algorithm to solve the 2-dimensional wave equation for membranes or plates.

6.1.2 Data Type Considerations

As mentioned in section 5, when designing hardware logic, a fundamental design decision is the choice of an appropriate data type for a given algorithm. The most commonly used data types for numerical computations are floating-point and fixed-point. Both data types differ in their effective number representation in the digital domain. Besides a different bit encoded representation of numbers, they have different algebraic rules.

Even though modern DSP applications almost exclusively work with floating-point representation making use of hardware implemented arithmetic units of modern DSPs or CPUs, a fixed-point $Q.X$ data type is used in this work for the central arithmetic functions. In this section, the reasoning for the choice of data type is presented.

There are several important selection criteria influencing the choice of the data type in a hardware design.

- The data type of the input and output signals.
- The flexibility expected from the data type regarding its range and resolution accuracy.
- Applicability of data type dependent benefits and algebraic optimisations.
- Internal algorithmic structure of the design.

In this work, a fixed-point data type is chosen because it has several advantageous features for the presented hardware designs on a FPGA, compared to a floating-point implementation. The final low-level algorithm, as presented in section 3.8, is already tailored versus a fixed-point data type because in its basic form it has only one multiplication compared to at

¹³Finite Differences in the Time Domain.

¹⁴Wang Chen et al.: "An FPGA implementation of the two-dimensional finite-difference time-domain (FDTD) algorithm", in: *Proceedings of the 2004 (ACM/SIGDA) 12th international symposium on Field programmable gate arrays*, New York, USA: ACM, 2004: 213–222.

¹⁵Gibbons, Howard, and Tyrrell, "Real-time FPGA".

¹⁶E. Motuk, R. Woods, and S Bilbao: "Implementation of Finite-Difference Schemes for the Wave Equation on FPGA", in: *IEEE International Acoustics Speech and Signal Processing ICASSP 2005* 3 (2005).

¹⁷E. Motuk et al.: "Design Methodology for Real-Time FPGA-Based Sound Synthesis", in: *IEEE Transactions on signal processing* 55.12 (2007).

¹⁸See: Motuk, "System-On-Chip implementation of real-time finite difference based sound synthesis"

least 4 additions/subtractions. One of the advantages of a floating-point data type is that a multiplication can be realised by a only a few logic instructions if some preliminaries are met, one drawback of floating-point is that additions/subtractions are more costly to implement compared to a fixed-point implementation. Because the core algorithm consists of more additions/subtractions compared to multiplications, it is beneficial to use a data type that is optimised towards these arithmetic operations.

Another important feature of fixed-point data types is that multiplications or divisions by numbers expressible as powers of two can be implemented as left- or right-shift operations. A comparable *trick* is not applicable when using a floating-point data type.¹⁹

A third point that supports the decision for a fixed-point data type is that binary scaling can be applied by normalising the acceleration to the square of the sampling frequency, and the velocity to the sampling frequency, which is a power of two in the presented design. Hence, the scaling can be performed by a shift operation. The final time stepping method, derived in chapter 3, inherently contains this normalisation in the factor Δt^2 or Δt . Hence, no additional scaling must be applied besides the re-normalisation of the velocity and the acceleration when quantitative results are needed.

Another consideration regarding the data type decision is the fact that floating-point is optimised towards a large range of representable values, whereas fixed-point is optimised towards resolution inside a given range. As already argued in chapter 2, if we are interested in physical properties of musical instruments, we need explicit expressions for the deflection, velocity and the acceleration. For all signals one can define a physically reasonable maximum value, including a safety margin and a digital range that is larger than the humanly perceivable signal to noise ratio.²⁰

For the modelled musical instruments, all observable signals are dissipative. This means, all signals have values inside well defined numerical boundaries. Regarding this property, one can state that the resolution inside this range should be as high as possible.²¹ Therefore, a data type optimised towards resolution is suited better than a data type optimised towards range. Finally, the first FPGA implementation used a 20 bit fixed-point DAC²², hence, applying a fixed-point data type was additionally motivated by practical reasons because no additional data type conversion entity had to be implemented.

All mathematical operations are performed using a 2's complement Q0.31 data type with

¹⁹ There exist operations that can be computed by exploiting properties of floating-point bit representation as is shown in J. F. Blinn: "Floating-point tricks", in: *IEEE Computer Graphics and Applications* 17.4 (July 1997): 80–84.

²⁰ A dynamic range higher than the human hearing range of $\approx 130-140[dB]$ can be achieved by implementing an accordingly large bit depth of the signals. The theoretical dynamic range for the 32 bit deep signals used in this work is $DR[dB] = 20 * \log_{10}(2^{31}) \approx 187dB$. This range is larger than needed because most DA-converters are capable of converting with 24 bit using a fixed-point or quasi fixed-point representation.

²¹ This can be achieved by normalisation and re-normalisation of the physical values to the maximal numerical value.

²² Digital Analog Converter.

left aligned MSB²³. The data types in other parts of the hardware design are bit vectors or the IEEE data type *std logic vector*²⁴. Besides these arguments for using a fixed-point data representation, there is one additional factor that supports the decision.

As is shown Goldberg,²⁵ floating-point number representation can be sensitive to rounding errors. In extreme cases, these rounding errors of floating-point computations can lead to unstable solutions of otherwise stable methods.²⁶ As already mentioned in chapter 3, a long-term stability of a real-time synthesis depends on the stability of the underlying algorithm and data type. The maximal rounding error of the presented method using a fixed-point implementation is bound to the least significant bit and averages to zero over time, when implementing the algorithm in the way described in section 6.4.

²³Most Significant Bit.

²⁴This data type incorporates several special signal conditions like high impedance or weak signals. (Ashenden, *The Designer's Guide to VHDL*, pp. 45).

²⁵David Goldberg: "What Every Computer Scientist Should Know About Floating-Point Arithmetic", in: *ACM Computing Surveys* 23 (1991): 5–48.

²⁶R.D. Skeel: "Symplectic integration with floating-point arithmetic and other approximations", in: *Applied numerical mathematics* 29.1 (1999): 3–18 for stability considerations regarding symplectic methods.

6.2 Routing Layer Model

To ensure an inter-model connectivity and transportability of interchangeable design features, and to make the design of the finite difference models more transparent, a layer model is developed to classify each specific functional part of the models and assort them according to their respective functionality. The applied model is inspired by the OSI-layer model and adjusted in several regards to fit the needs of this work.

All functional parts of the FPGA implementations are categorised into five different sub-layers, each encapsulating a specific functionality, specific data types, specific communication protocols as well as data transport signals. An overview on the names, data types and functions for each specific layer is given in table 6.1.

Layer	Function	Signals	I / O ports
1. Arithmetic Layer (AL)	Core calculations of the model	Arithmetic signals	Model algorithm constraint and boundary values, algorithm results
2. Math Routing Layer (MRL)	Routing of parallel AL algorithms	Routing signals; Control Signals	Routing signals / Status signals
3. Control Circuit Layer (CCL)	Internal timing and control signal decoding	Timing signals; Data signals	Control signals/- Data signals
4. Model Routing Layer (MoR)	Global timing / Routing signals between CCL instantiations	Timing signals; Data signals	Control signals/- Timing signals
5. Interface Layer (IL)	I/O communication with external devices	Routing signals/- Control signals	Control data input for model algorithm from external device/ Model algorithm results output

Table 6.1: Layer model signal description.

Applying the proposed layer model approach for real-time hardware implementations of musical instruments on FPGAs results in a data- and communication protocol structure which is incorporated at the core level of the design. One benefit of this approach is the modularity of the implemented designs, whereby all singular instrument parts can be organized, connected and rewired, without a complete re-design of the complete model. This follows a recommended design practice for hardware designs,²⁷ and can be compared to an object oriented design approach, a commonly used approach in high-level languages like C++ or

²⁷ *Synthesis and Simulation Design Guide (UG626)*, version 13.2, Xilinx, 2011, p. 41.

Java to ensure higher re-usability of implemented code²⁸. The singular layers and their functionalities are presented in the following sections.

6.2.1 Arithmetic Layer

All numerical computations of the hardware models are performed on this layer. It is the bottommost layer for all FD implementations because it implements the fundamental functions of all numerical calculations. The arithmetical processing is controlled by a Finite State Machine (FSM), which ensures a signal validity and synchronisation of each time- and computation step. A schematic overview of the arithmetic layer (AL) is given in figure 6.1.

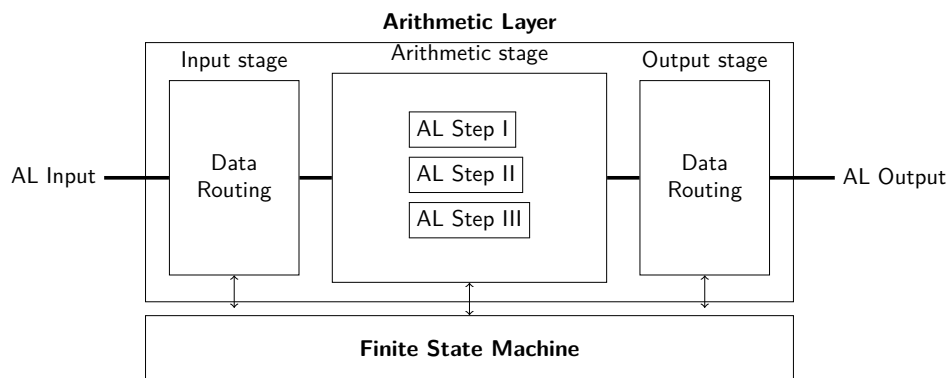


Figure 6.1: Schematic overview of the Arithmetic Layer.

In the first step of the AL, all input variables are routed to their appertaining internal signals. In the following time steps, the specific arithmetic tasks are performed corresponding to the underlying order of the equation and structure of the finite difference algorithm. In the last state of the AL all calculated output signals are routed to their respective output signals.

Input/Output Data Types

The data type of all input- and output signals is *STD_LOGIC_VECTOR*, ensuring a data compatibility to XILINX-simulation and implementation libraries²⁹. In the first stage of the arithmetic layer, all external input signals are converted to the internal Q0.31 data format.

Internal Signals Data Type

All internal signals are signed 2's complement Q0.31 data type. The physical parameters computed in the AL are the deflection, velocity and acceleration for structural mechanics and pressure, particle velocity and the change of the particle velocity in the model of the enclosed air volume.

²⁸Ulla Kirch and Peter Prinz: *C++ Lernen und professionell anwenden*, 5th, mitp, 2010.

²⁹*Synthesis and Simulation Design Guide (UG626)*.

Shared Resources

The AL is designed towards resource sharing functionality with a focus on optimizing the use of multiply and add units. Where applicable, only one multiplier is used per FD grid cell and all remaining arithmetical functions are divided among the FSM states for maximal possible resource sharing.

6.2.2 Math Routing Layer

In the math routing layer (MRL), all processes running in the AL are routed, configured and connected according to their assigned function. All parallelization of mathematical resources is implemented in this layer. The initial and boundary values are routed to their respective calculation kernels in the AL. Additionally, all memory resources for the parallel parts of the calculation are implemented and controlled here. Another function of the MRL is the processing and routing of externally applied physical constraints, like for instance contact point switching between a bow and a string or switching the coupling point between a string and a membrane in the banjo model. A structural overview is depicted in figure 6.2.

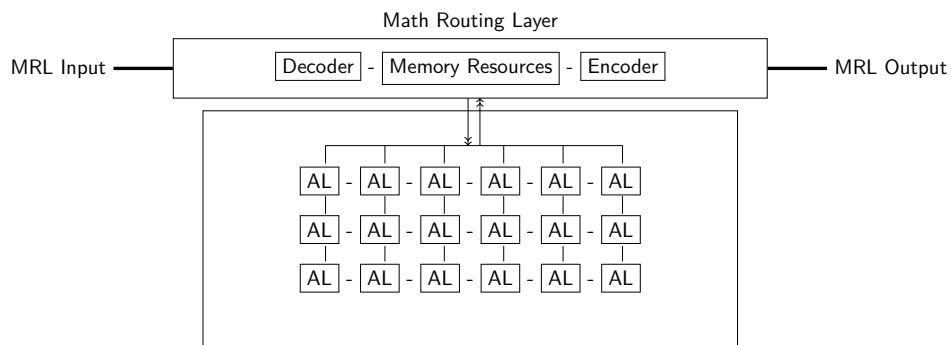


Figure 6.2: Math Routing Layer (MRL).

Data type

The data type used in this layer is exclusively *Std_Logic_Vector*.³⁰ If not noted otherwise, all following layers have a *Std_Logic_Vector* data type.

6.2.3 Control Circuit Layer

In the control circuit layer (CCL) all control data is routed to the respective receiver and the resulting audio data is accumulated and transported to higher and lower layers. Another

³⁰As already mentioned, this is due to constraints posed by Xilinx simulation libraries, which explicitly need *Std_Logic_vector* data types and not *Bit_Vector* signals, which would be sufficient for the communication protocol and internal data transport of all presented models and layers.

functional part of the CLL is the provision of a timing and synchronisation protocol for real-time parameter changes. The CCL-decoder controls the transfer of parameter signals, like for instance the excitation points of the string, or the coupling points between the strings and a front plate. An overview of the CCL is shown in figure 6.3

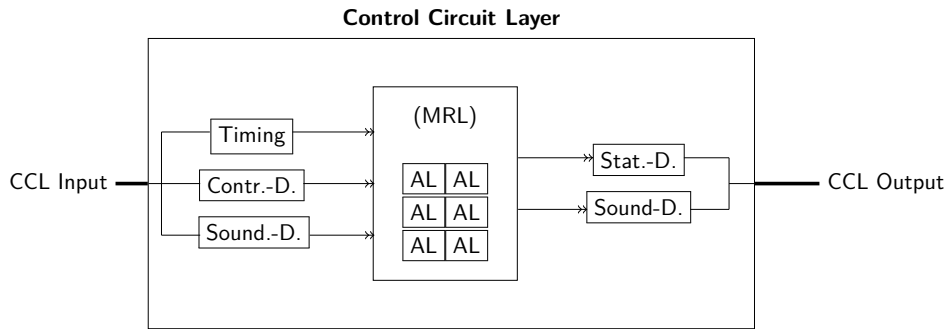


Figure 6.3: Control Circuit Layer (CCL).

6.2.4 Model Routing Layer

In this layer, the actual model of the instrument is routed and all different parts of the modelled geometries are connected to yield the final system. All calculated values that are coupled to other parts of the instrument are routed here. Control data is transferred to the corresponding part of the model, which is indicated by a specific bit code.

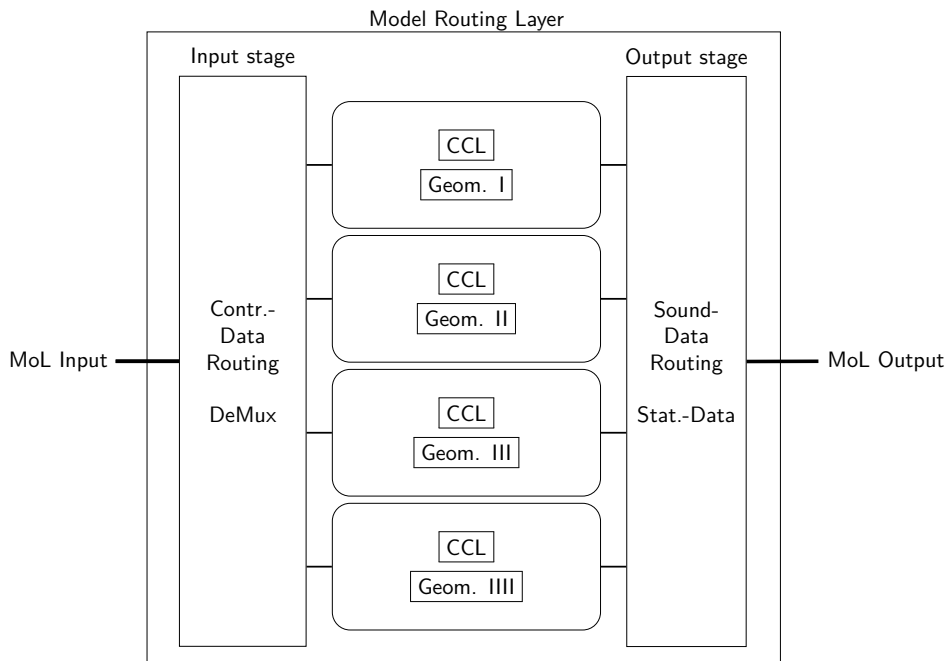


Figure 6.4: Model Routing Layer overview.

6.2.5 Interface Layer

The Interface Layer is the topmost layer in the model. Here, all external data input and output is managed, decoded and routed. It is the interaction layer with all input and output devices, such as the PCIe interface, the AC97 interface or the I2S interface for data transport as described in section 5. A block diagram of the IL is shown in figure 6.5.

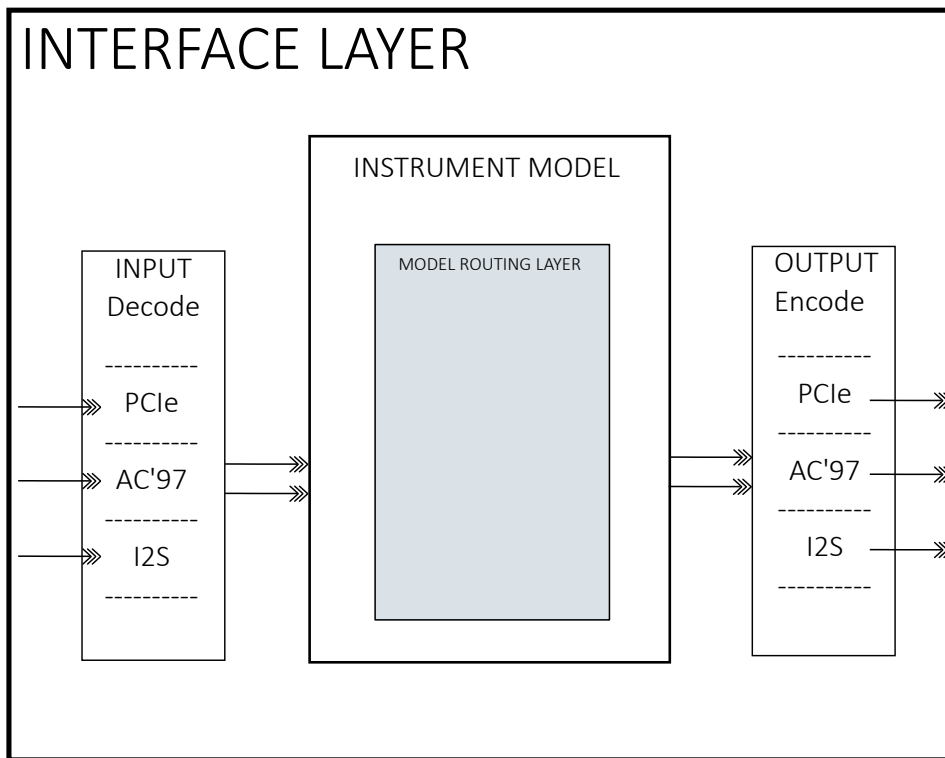


Figure 6.5: Block diagram of the Interface Layer.

Depending on the model either the PCIe, AC'97 or the I2S interface is used for communication and data transfer. Models of singular geometries are implemented with the AC'97 and the I2S protocol. For the complete geometry models the PCIe interface is applied.

In the IL, the data from the respective transmitter is decoded and then routed to the instrument model, the MoR. Status and synthesised data from the MoR is packed into packages of the data transfer type, and send to the receiver.

6.3 Hardware Operator Notation

To facilitate a clear overview on the hardware implementations of proposed models, a set of digital operators are introduced in this section. They are intended to act as an extension to the well-established FD operator notation used in chapter 3 and 4.

Similar to the notation introduced there, the proposed operators allow to abstract several mathematical operation into a simpler notation. In the following, this concept is extended to a lower abstraction level by resolving the underlying mathematical operations to the specific operations assuming a fixed point data-type and a typical binary logic hardware structure.

6.3.1 Operator Definition

As developed in section 3, there are four basic arithmetic operations used for the core algorithm and a number of register read and write operations.

Left/Right Shifts These operations are used to replace divisions or multiplications with base-2 numbers by a left- or right-shift.

A left-shift by integer N bit positions is indicated by $\ll N$, a right shift by $\gg N$.

Addition/Subtraction Both operations are implemented using the arithmetic circuitry of the DSP48e1 circuitry of Xilinx FPGA hardware.

Multiplication A multiplications is implemented using the DSP48e1 multiplication circuitry.

Register Read and Write Both operations are realised using (BRAM) resources on the FPGA hardware chip. The order of the difference equation determines the number of read operations. The number of dependent variables in the difference equation determines the numbers of write operations. A read operation from a register of a value Δx strides away relative to the centred point is written as $\epsilon_{R\Delta x+}/R\Delta x-$, a write operation is written as $\epsilon_W(\mathbf{a})[\mathbf{b}]$, with \mathbf{a} the destination register and \mathbf{b} the source register or function.

6.3.2 Combined Operations

Using the introduced operations, a centred finite difference operator for a first order difference can be written as

$$\bar{\delta}_x = T_\Delta \cdot [\epsilon_{R\Delta x+}, -\epsilon_{R\Delta x-}] \quad (6.1)$$

6 Real-time FPGA models

Operator	Reg. Op.	Shift Op.	Mult.	Add./Sub.
$\bar{\delta}_t$	2	0	1	1
$\bar{\delta}_x$	2	0	1	1
$\bar{\delta}_{xx}$	3	1	1	2
$\bar{\delta}_{4x}$	5	4	1	4
$\bar{\delta}_{2x2y}$	5	1	1	4
$\bar{\delta}_{\nabla^4}$	13	10	1	12
$\bar{\delta}_{2x2y2z}$	7	2	1	6

Table 6.2: Digital operations for FD operators used in this work.

with T_Δ a multiplicand which depends on the stride of the discrete grid in the spatial domain. A second order centred FD operator in vector notation can be written as

$$\bar{\delta}_{xx} = T_\Delta \cdot [(\epsilon_{R\Delta x-}), \epsilon_R (< 1), (\epsilon_{R\Delta x+})] \quad (6.2)$$

with $T_\Delta = \frac{1}{\Delta x}$. A higher order digital FD-operator used for the fourth order differential equation of the beam can be constructed by a convolution of two second order digital FD operators

$$\bar{\delta}_{4x} = \bar{\delta}_{xx} * \bar{\delta}_{xx}. \quad (6.3)$$

This can be extended to higher spatial order difference operators leading to a specific numbers of digital operations for the respective operator given in Table 6.2.

Using the values given in Table 2, approximate the used resources of a model before implementing it in hardware.

6.3.3 Damping Approximation by Shifts

The following assumptions are based on the prerequisite that the damping coefficients are heuristically approximated values. A multiplication with a value β can be approximated by a finite sum of left-/right- shifts using

$$v_d = v \cdot \left(1 - \sum_{k=0}^{deg} \alpha_k \frac{1}{2^k}\right) \quad (6.4)$$

with v_d an arbitrary damped quantity, deg the order of approximation of the damping and a multiplicand $\alpha \in (-1, 0, 1)$. In this way, arbitrary damping coefficients can be approximated by a number of shifts.

6.4 VHDL Translation of the Algorithm

To benefit from the features of FPGA hardware, it is necessary to adopt the algorithm to this specific hardware architecture. The parallel processing capabilities of FPGAs, compared to serial processing hardware, can only be utilised completely when an implementation makes use of parallelism. To this end, it is important to get an in-depth overview of the data path, the data processing structure, the control structure and data dependencies of the numerical method applied. In this section, the algorithm is analysed in these regards and the findings are applied to formulate an optimised version of the hardware implementation. As before, the basic properties of the method are exemplified at a hardware implementation of a simple harmonic oscillator. Following this, the analysis is extended to implementations of more complex structures of whole geometry designs.

6.4.1 0-dimensional Simple Harmonic Oscillator

The numerical methods utilised for the low-level models were tested and analysed regarding their stability and robustness for long time simulations, as presented in chapter 3. The model of the 0-dimensional oscillating mass point does not include geometrical concurrency. Due to this, no geometrical concurrency is utilised in the hardware version of the algorithm. Nonetheless, several properties of the FPGA implementation, which are applied in the other models of musical instruments as well, can be exemplified at this model.

Algorithm Analysis

As shown in section 3.8, the algorithm can be simplified to a three-step time integrator for every discrete point. The dependencies of the variables are:

$$\begin{aligned} a^t &= f(u^t) \\ v^{t+1} &= f(a^t, v^t) \\ u^{t+1} &= f(v^{t+1}, u^t). \end{aligned} \tag{6.5}$$

Equation 6.5 shows, that the velocity and the deflection depend on results of the time-step $t + 1$ as well as time step t . For uncoupled problems, the explicit computation of the acceleration can be included into the calculation of the velocity as $v^{t+1} = f(u^t, v^t)$. For coupled problems, where an explicit formulation of the acceleration can be employed for a straightforward way of coupling two geometries via the interaction forces, it is advantageous to compute the three physical quantities acceleration, velocity and deflection independently. Hence, a direct evaluation of the acceleration, which is related to the force by equation $a = \frac{F}{m}$, is indispensable.

6 Real-time FPGA models

Time step	Reg. Op.	Shift Op.	Mult.	Add./Sub.
1	3	0	1	0
2	3	1	0	1
3	3	0	0	1
Total	9	1	1	2

Table 6.3: Digital operations for SHO implementation.

The arithmetic requirements of algorithm 6.5 in its basic form, as developed in section 3.8 can be assessed by rewriting it using the introduced digital operator notation to

$$\begin{aligned}
 \epsilon_w(a) & [-\epsilon_R(\kappa) \cdot \epsilon_R(u)] \\
 \epsilon_w(v) & [\epsilon_R(a_{>>16}) + \epsilon_{R\Delta t-}(v)] \\
 \epsilon_w(u) & [\epsilon_R(v) + \epsilon_{R\Delta t-}(u)] \cdot
 \end{aligned} \tag{6.6}$$

Hence, for the implementation of a harmonic oscillator, all basic calculations can be performed by one multiplier, two adders and a shift operation. A hardware resource analysis shows that only one instance of the respective hardware function is used per time step. This means, the algorithm can be implemented with only one adder that is used twice: In time step 2 and time step 3. This adds routing overhead to the design, but minimises the area utilization on the FPGA chip because only one binary adder must be implemented.

Arithmetic Layer

Applying the previous analysis, performed to simplify the algorithm, the AL can be implemented as depicted in the ASMD³¹ chart in figure 6.6.

³¹Algorithmic State Machine with Data path (ASMD).

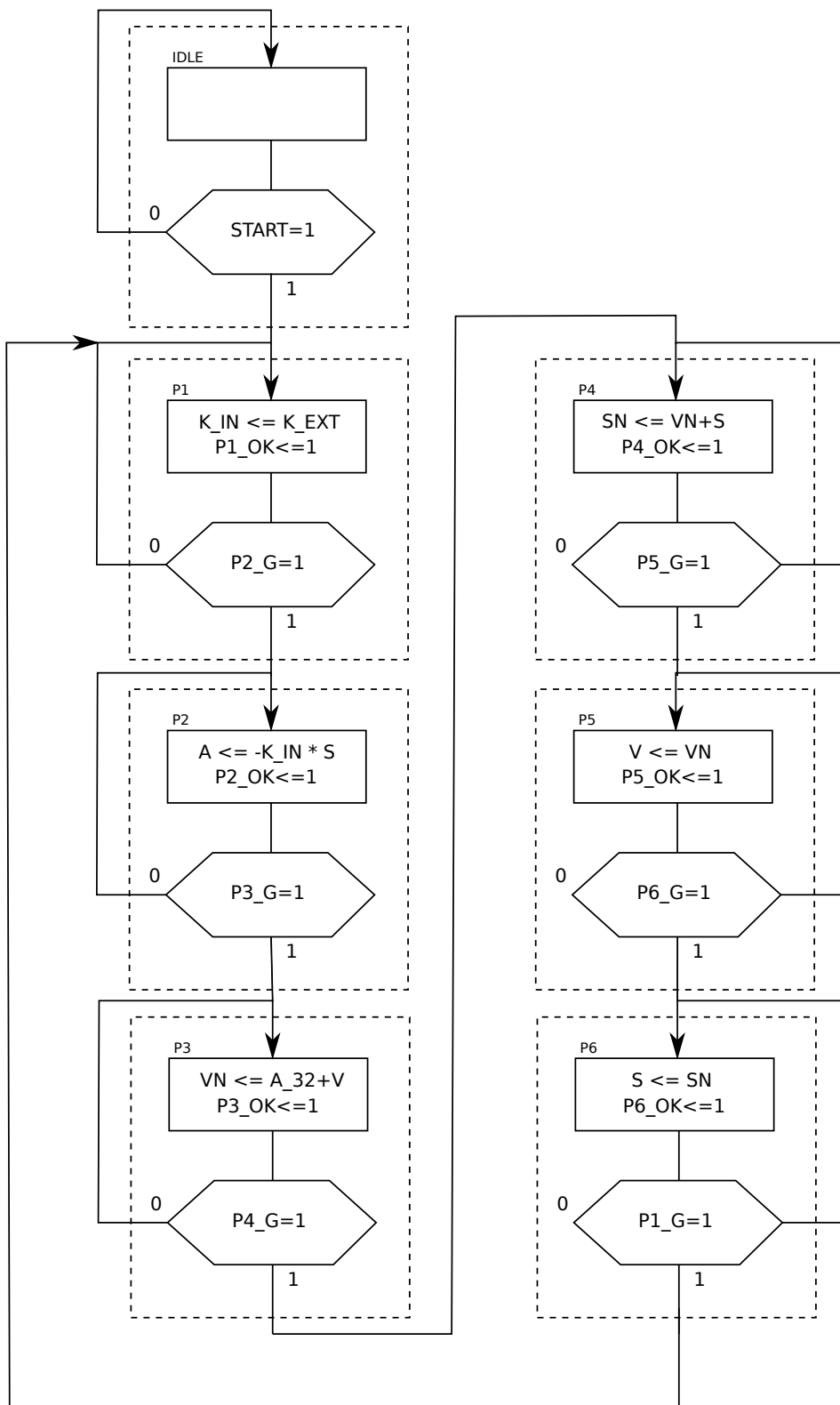


Figure 6.6: ASMD chart of the SHOs AL.

In addition to the physical values a = the acceleration, v = the velocity and u = the deflection, the signal k , a value proportional to the spring stiffness normalised by the sampling frequency, can be changed in real-time while the hardware model is running.

The external value K_{EXT} is routed from an input-port of a push button, implemented as an input-buffer, sending signal changes to the buffered input signal in the AL, to the internal value K_{IN} .

Using the value of K_{IN} and the deflection S the acceleration is computed in state $P2$. The new velocity VN is computed in state $P3$ and the new deflection in state $P4$. State 5 and state 6 are used to overwrite the old the values of the deflection and velocity the new computed values.

Math Routing Layer

As mentioned in chapter 5, to calculate sequential code on a FPGA, it is necessary to implement a Finite State Machine that controls each sequential step of the calculation and guarantees stable signals for the input values and for the output values.

The connection of the AL with the FSM is realised in the MRL, where both entities are declared and instantiated. Here, the coupled signals of both entities are connected and routed as well. The input signal K_{IN} is routed from the IL to the AL, the output signal is routed from the AL to the IL. The register transfer level of the MRL is shown in figure 6.7.

Top entity / IL

In the top entity, all input signals are routed from the physical inputs of the development board to the CM layer. The output signals are routed to the AC97 entity of the board.

AC97 entity

The AC97 entity implements the communication protocol necessary for the data transfer between the hardware model and the on-board AC97 codec, as described in section 5.

Simulation Results

In the following figures, the results of the functional simulation of the SHO are shown. Figure 6.7 shows the Register Transfer Level (RTL) schematic of the Finite State Machine (FSM) and the math kernel of the oscillator. As one can see, both blocks are driven by the same clock signal and have the same reset signal. The start signal only controls the FSM to pause and restart a running calculation without loosing the values of the last calculation step. The control and status signals of the single FSM steps of the calculation are PX_G and PX_OK respectively.

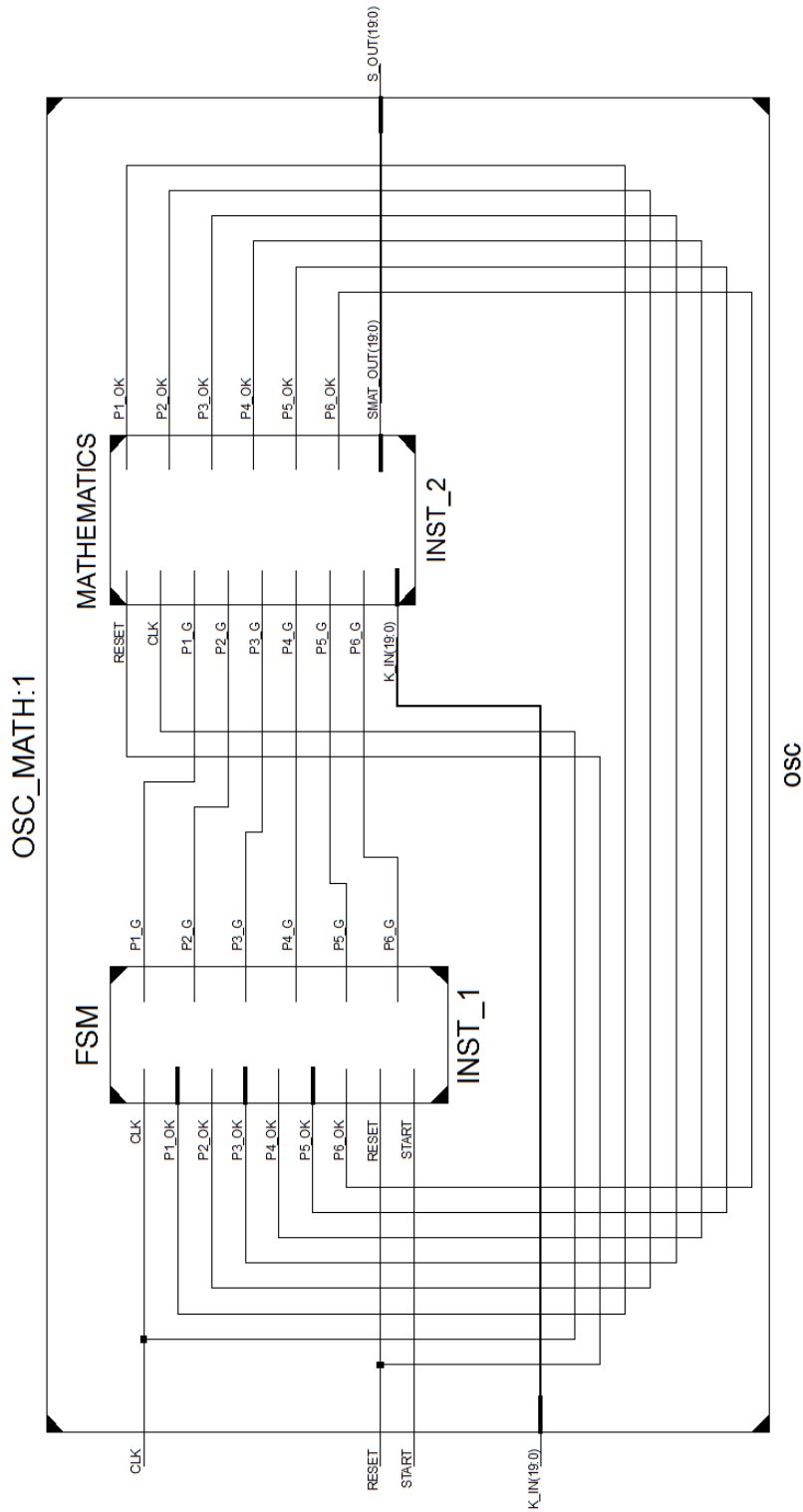


Figure 6.7: RTL view of FSM and Math block.

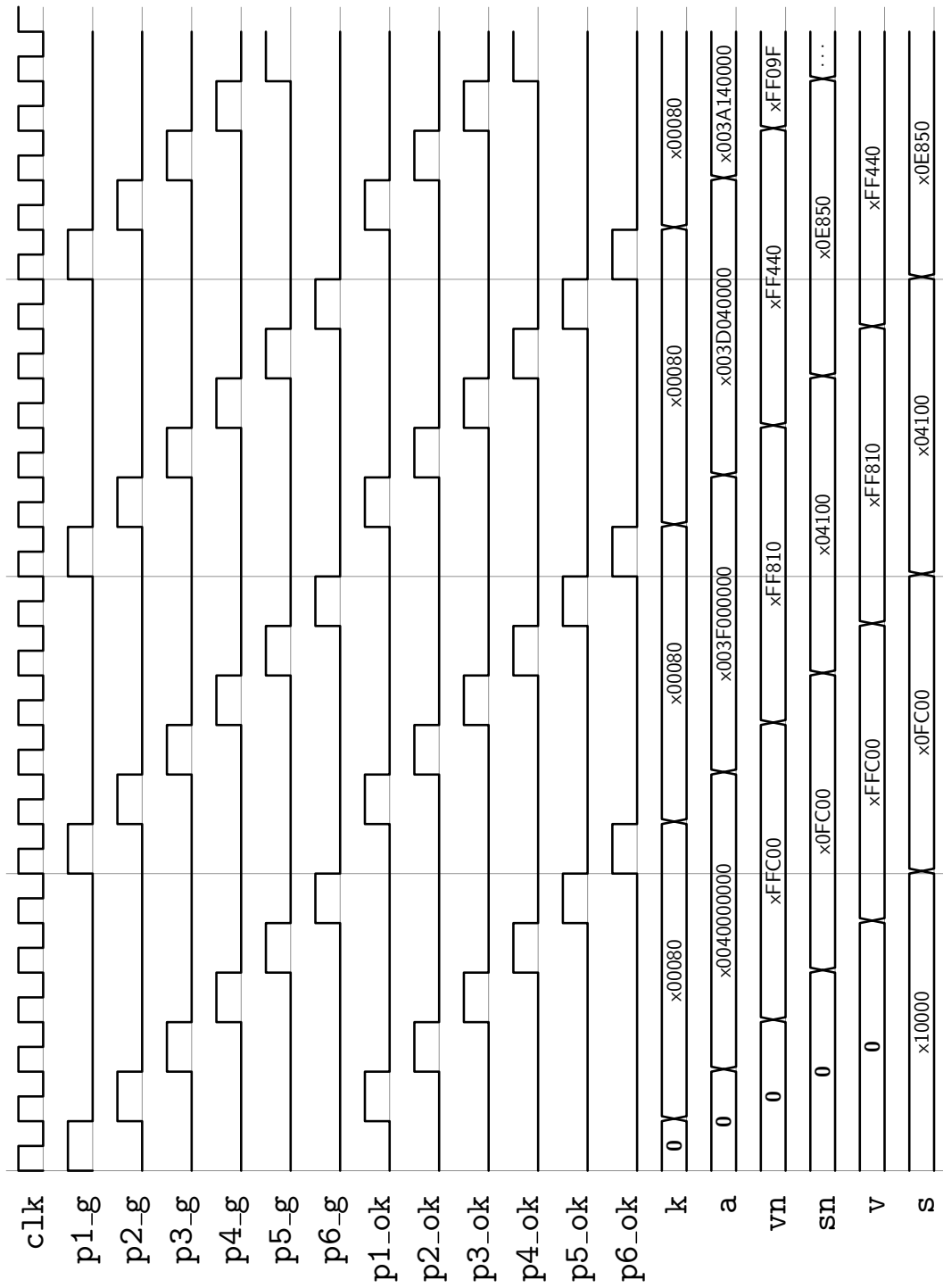


Figure 6.8: Timing diagram of the core functionality of the SHOs AL.

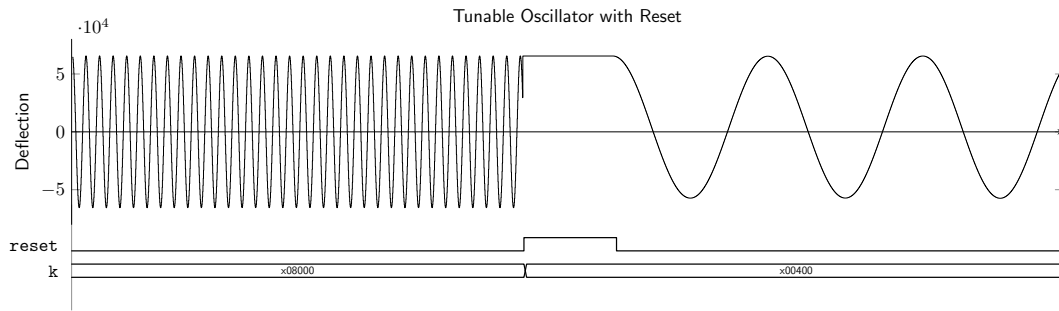


Figure 6.9: Timing diagram with analog output signal.

6.4.2 Structurally Parallel 1-dimensional Wave Equation

In this section, a hardware implementation of the 1-dimensional wave equation is presented. The numerical solution of the linear wave equation used to model a string is translated to VHDL and computed on an FPGA. As is shown in section 3, the local structure of the algorithm is similar to the algorithm of the SHO. Hence, the underlying arithmetic and the control circuit that is used for the SHO is reused for the 1-dimensional string and is extended to account for additional requirements of the string computation. Additional prerequisites arise due to the parallel structure of the string computation. Compared to the SHO, this hardware model utilises the parallel structure of the FPGA hardware based on its geometrical parallelism. Following the presented methodology developed above, the string is implemented as a series of coupled discrete points on the string. The local computations for each time-step and each virtual node-point depend on the values of the velocity and deflection from the previous time step. The calculation of the acceleration additionally depends on the deflection of the adjacent points.

In digital operator notation, equation 4.34 for one time-step can be rewritten to

$$\begin{aligned}
 \epsilon_w(a) & [-\epsilon_R(\kappa) \cdot \bar{\delta}_{xx}(u)] \\
 \epsilon_w(v) & [\epsilon_R(a_{>>16}) + \epsilon_{R\Delta t-}(v)] \\
 \epsilon_w(u) & [\epsilon_R(v) + \epsilon_{R\Delta t-}(u)] .
 \end{aligned} \tag{6.7}$$

Compared to 6.6, equation 6.7 has comparable requirements for the time integration but additional hardware requirements due to the extension to a 1-dimensional problem. A summary of the hardware resources of a linear string is given in Table 6.4.

The parallel implementation of the linear strings uses 10 parallel node-points that are evaluated concurrently. The parallel nodes are instantiated and routed in the MRL. All signals

6 Real-time FPGA models

Time step	Reg. Op.	Shift Op.	Mult.	Add./Sub.
1	6	1	1	2
2	3	1	0	1
3	3	0	0	1
Local Total	12	2	1	4
Parallel Total	120	20	10	40

Table 6.4: Digital operations for linear string implementation.

shared between adjacent mass-points are schematically depicted in figure 6.10 as left/right arrows 6.10.

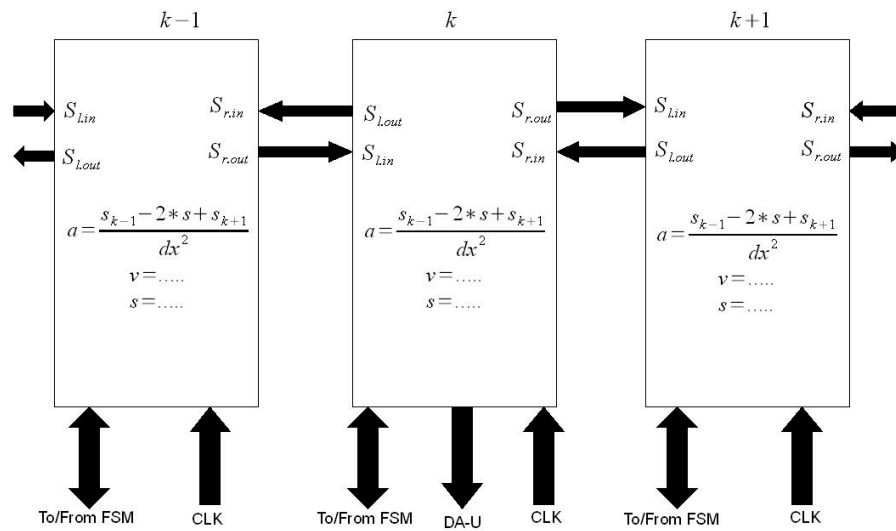


Figure 6.10: Parallel structure of the 1-dimensional wave equation at a random point $k \notin 0 \wedge L$.

Arithmetic Layer

In its fundamental structure, the AL of the linear string is comparable to the structure of the SHO. The ASMD of the linear string AL is depicted in figure 6.11. The only changes in the AL of the string, compared to the SHO, are present in the FSM-states P1 and P2. The remaining calculation steps are similar.

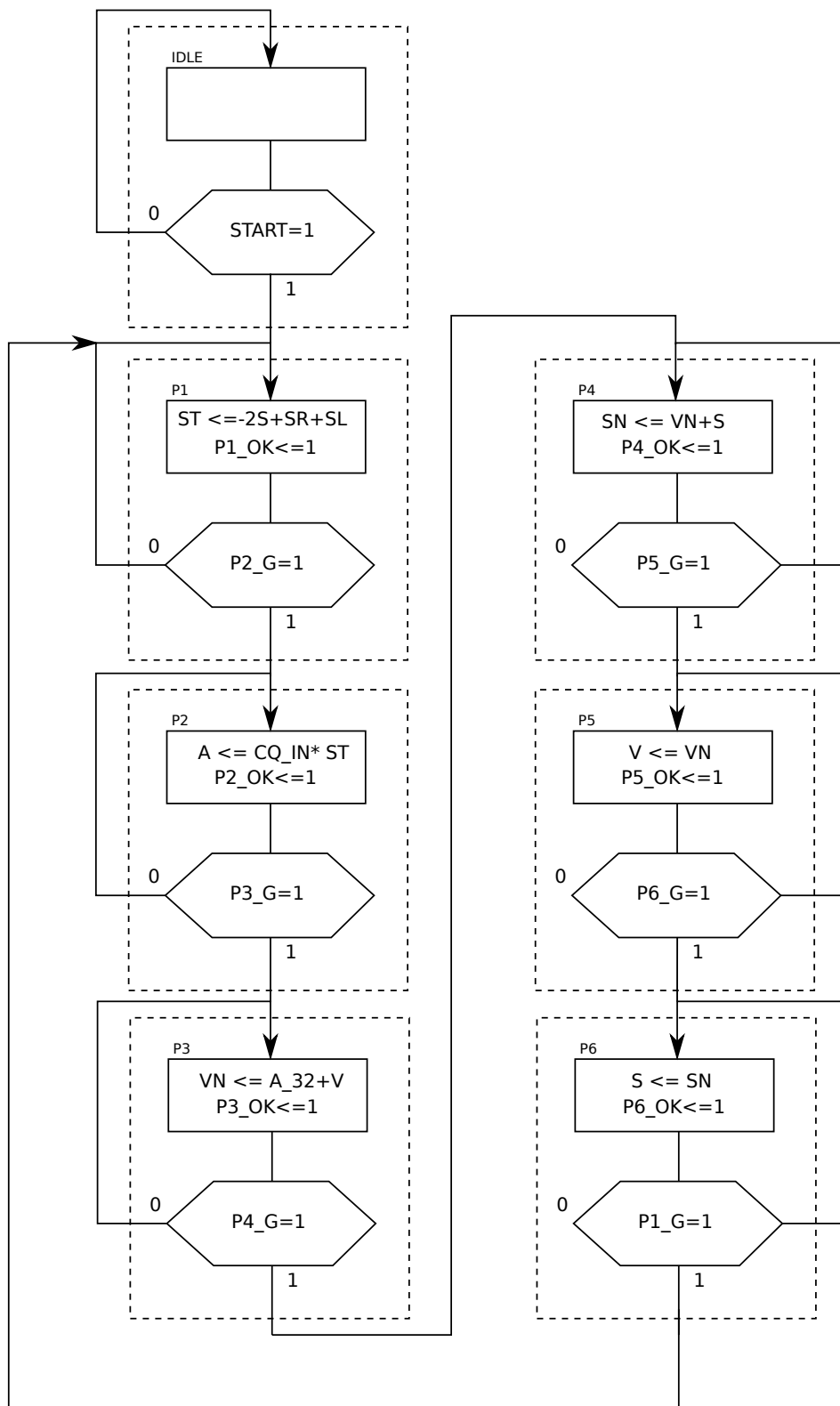


Figure 6.11: ASMD chart of the linear string AL.

Math Routing Layer

The linear string is discretized with 10 node-points, which are calculated in parallel. Besides the signal routing of the connected node points, the initial deflection of one or several points is routed in the MRL implemented in the initial RAM positions. Figure 6.12 shows an extract of the parallel RTL implementation.³²

³² Because of the limited space due to the DIN-A4 format, only four of the ten AL blocks are shown. The functional block of the FSM is the center block.

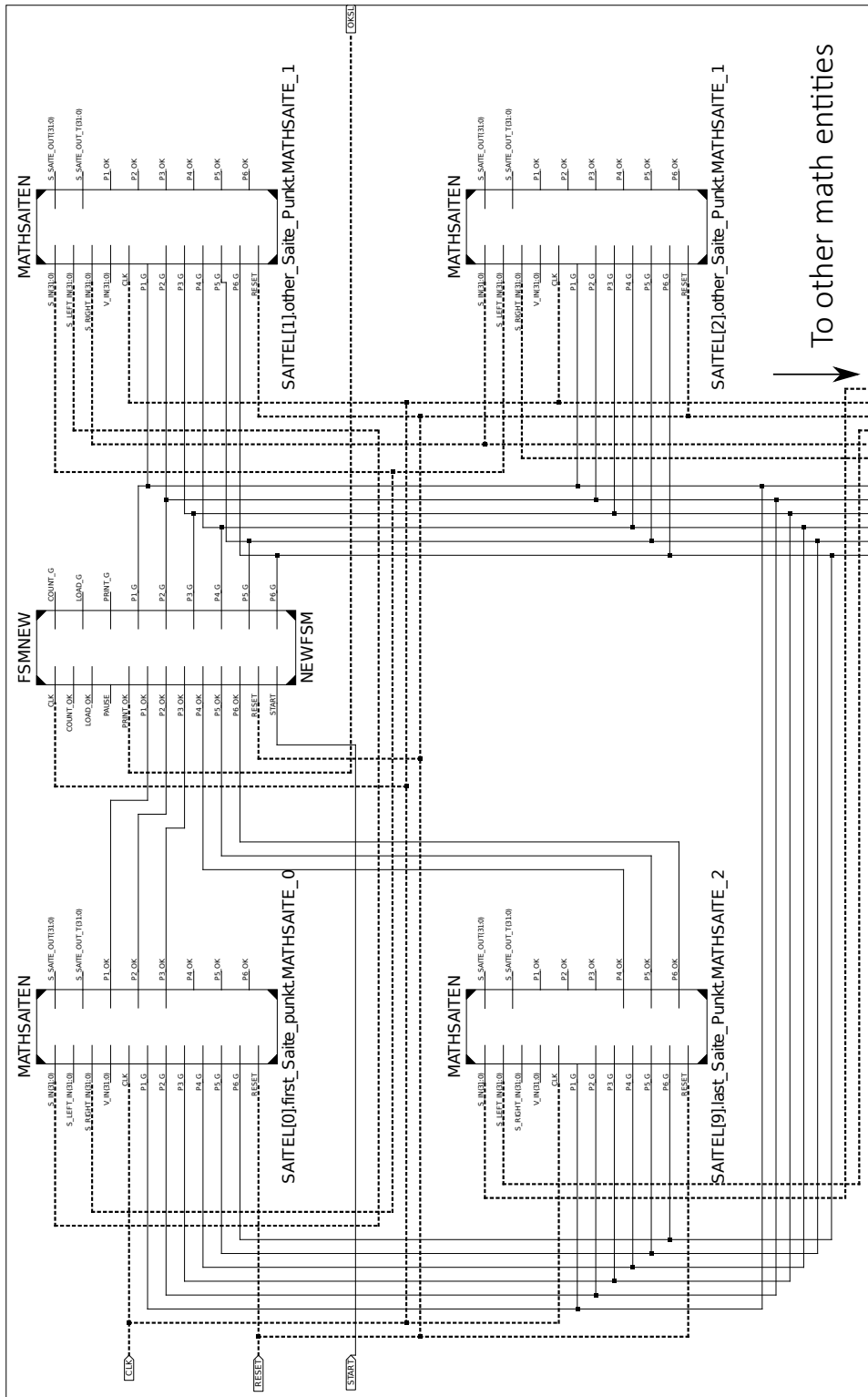


Figure 6.12: CML of the 1-dimensional string showing the FSM and four of the ten AL blocks.

6.4.3 Parallel/Serial 1-dimensional Wave Equation

In the larger model designs of the musical instruments it is not possible to implement all portions of the geometry in parallel because of limited hardware resources. The string model consisting of 10 node-points is extended to the model of a larger string by implementing additional sequential logic in the CCL of the string.

Control Circuit Layer

The fundamental string model, used for all instruments, is composed of a parallel implementation of 10 coupled node-points, which are computed eight times serially, yielding the model of a string with 80 discrete node-points. Hence, for one update of a complete string, the parallel kernels are evaluated eight times sequentially. Because the algorithm requires the evaluation of the velocity and the deflection from the current time step and the preceding time step, it is necessary to save the values for u and v , so they can be accessed at the next time step of the calculation.

The model of the string discretised with 80 node-points instantiates as many memory blocks as parallel kernels (in this case 10) with a bit-width of (32 bit) for both variables and a depth of at least: $\text{RAM-depth} = \frac{N_{\text{String Points}}}{N_{\text{Parallel Points}}}$. Hence, in this example the RAM has a depth of at least 8.

The dynamic memory model is controlled by three additional *outer* states: a write state, a read state and a count state. During the read state, the information from the parallel kernel computation from time-step $t - 1$ is read and routed to the respective values of the kernel. The *calculate* step consists of the six AL states, which calculate the values for time-step t . In the write state, the output values of the parallel computation kernels are written to the associated RAM positions. Figure 6.13 shows an overview in the form of a block diagram.

6.4.4 String with Damping

As shown in section 3.8.2, the force damping can be approximated by a series of shift, additions, and subtraction operations. This property is applied to simulate velocity and acceleration dependent damping without the need to implement an additional multiplication or division circuitry, which would be necessary if the algorithm was implemented with a un-optimised finite difference scheme. In the case of the velocity damped string, the operation is performed directly in the time-step of the velocity calculation. The computation for the velocity from equation 6.7 can now be written as:

$$\epsilon_w(v)[\epsilon_R(a_{>>16}) + \epsilon_{R\Delta t-}((v)(1 + (>> 13) + (>> 15)))] \quad (6.8)$$

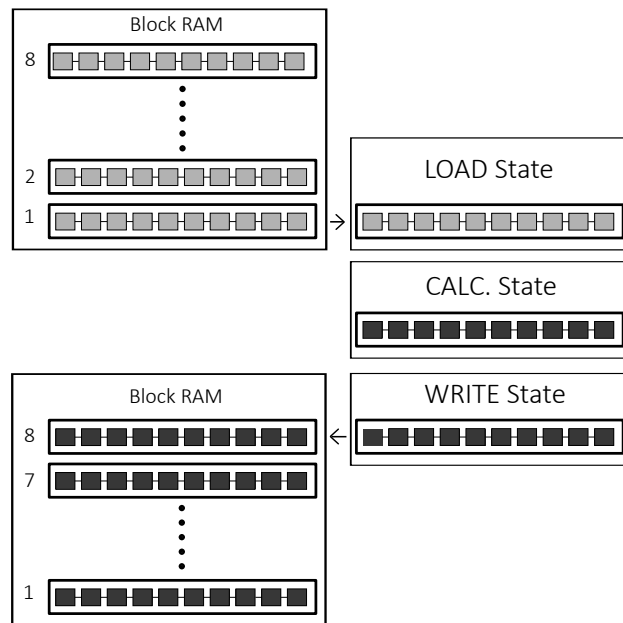


Figure 6.13: Serial/Parallel structure of the 1-dimensional wave equation for 80 node-points.

Compared to the model of linear string without damping, this is the only change in the hardware implementation. The same technique can be applied for acceleration dependent damping and is used in all real-time models.

6.4.5 Bowed String

In this section, the hardware model of a string/bow interaction, as shown in chapter 4, is presented. In the following, a focus is put on the differences compared to the HL model. In addition to the changes for force damping, mentioned in section 6.4.4, the string entity has several other differences compared to the linear string. To control the parameters that guide the bow/string interaction in real-time, it is necessary to route signals from the physical I/O port of the FPGA to the string entity, especially to the math entity. This is realised by adding a controlling and routing circuit to the existing model of the string. There are four global control parameters that guide the behaviour of the string:

1. Bowing - Plucking.
2. Position on the string.
3. Position on the neck.
4. Number of contact points.

When these three parameters are set, there are additional parameter that guide the acoustical vibrations of the string:

1. The bow velocity.
2. The bow force.
3. The amount of rosin.

Implementation

For the implementation of the bow/string interaction, the initial model of the string is extended in several ways. First, a PCIe communication protocol, as presented in chapter 5, is added to the existing model. Using this implementation, it is possible to read data from the model and write parameter changes to the model via a PCIe interface. The implemented communication protocol sends new controller data to the model every 800 sample clock cycles. These are expressed in address and associated data words. For the bow-string interaction, these values are decoded in 8 data words as follows:

Adress	Payload Mask	Controller Value
0h00000001	0h000000ff	String tension
0h00000001	0h0000ff00	Bow Pressure
0h00000001	0h00ff0000	Bow Velocity
0h00000001	0hff000000	Bow/String Interaction Point
0h00000002	0h000000ff	String Length

Table 6.5: Controller data words.

All data words are decoded in the top entity of the model, at the connection between the transaction layer and the top-entity of the FPGA model. After the controller data is decoded, it is transmitted as status signal payload to the next layer of the model, the CCL.

6.4.6 Stiff String

To extend the model of the linear string with velocity and acceleration damping, bending stiffness is added to account for acoustically relevant effects of stiff strings. Therefore, the string model is extended to incorporate two additional I/O signals in the AL, as indicated in equation 6.9.

Arithmetic Layer

The AL of the stiff string with damping is similar to the string without bending stiffness with the inclusion of two additional points on the string. In digital operator notation, the

6 Real-time FPGA models

Time step	Reg. Op.	Shift Op.	Mult.	Add./Sub.
1	11	5	1	6
2	3	1	0	1
3	3	0	0	1
Local Total	17	6	1	8
Parallel Total	176	48	10	80

Table 6.6: Digital operations count for a stiff string implementation.

computation of the acceleration of a stiff string can be written as

$$\epsilon_w(a)[- \epsilon_R(\kappa) \cdot (\bar{\delta}_{xx} - \bar{\delta}_{4x})(u)]$$

The operation count for a stiff string discretised with 80 node points is given in Table 6.6.

6.4.7 2-dimensional Wave Equation

The presented methodology for 1-dimensional problems is extended to higher dimensional problems, like a 2-dimensional wave equation modelling the motion of a membrane. In the following section, a real-time implementation of a membrane, modelled using a linear 2-dimensional differential equation, is presented.

Arithmetic Layer

The basic structure of the AL for the 2-dimensional wave equation is comparable to the already presented models of the 1-dimensional wave equation. The difference of the 2-dimensional AL, in comparison to the 1-dimensional AL, is an additional dependency of the force calculations on four surrounding grid nodes, which can be seen directly in the formulation of the second order 2-dimensional centered FD operator approximation

$$\bar{\delta}_{2x2y} = T_{\Delta}[\epsilon_{R\Delta x-}, \epsilon_{R\Delta y-}, (\ll 2), \epsilon_{R\Delta y+}, \epsilon_{R\Delta x+}]. \quad (6.9)$$

In addition to the deflections from the left and right grid nodes, the deflections from the points above and below the center point³³ are needed for the FD formulation. The multiplications can be performed as shift operations. A graphical representation of a digital FD shift stencil is given in figure 6.14.

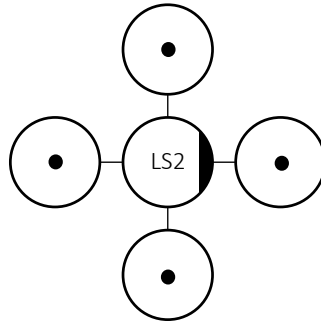


Figure 6.14: FD-shift stencil for the 1-dimensional plate operator. The points indicate that no shift operation is performed at this node. The partial black filling indicates a multiplication by -1 of the respective cell.

Math Routing Layer

The MRL of a 2-dimensional geometry has the same structure as the 1-dimensional MRL of the string with additional BRAM blocks as well as additional signal routing resources. Figure 6.15 shows an extract of the whole 2-dimensional MRL.

³³This is true for Cartesian grids with a five point stencil discretisation. If other grids or higher stencil approximations are used, the operator arithmetic changes.

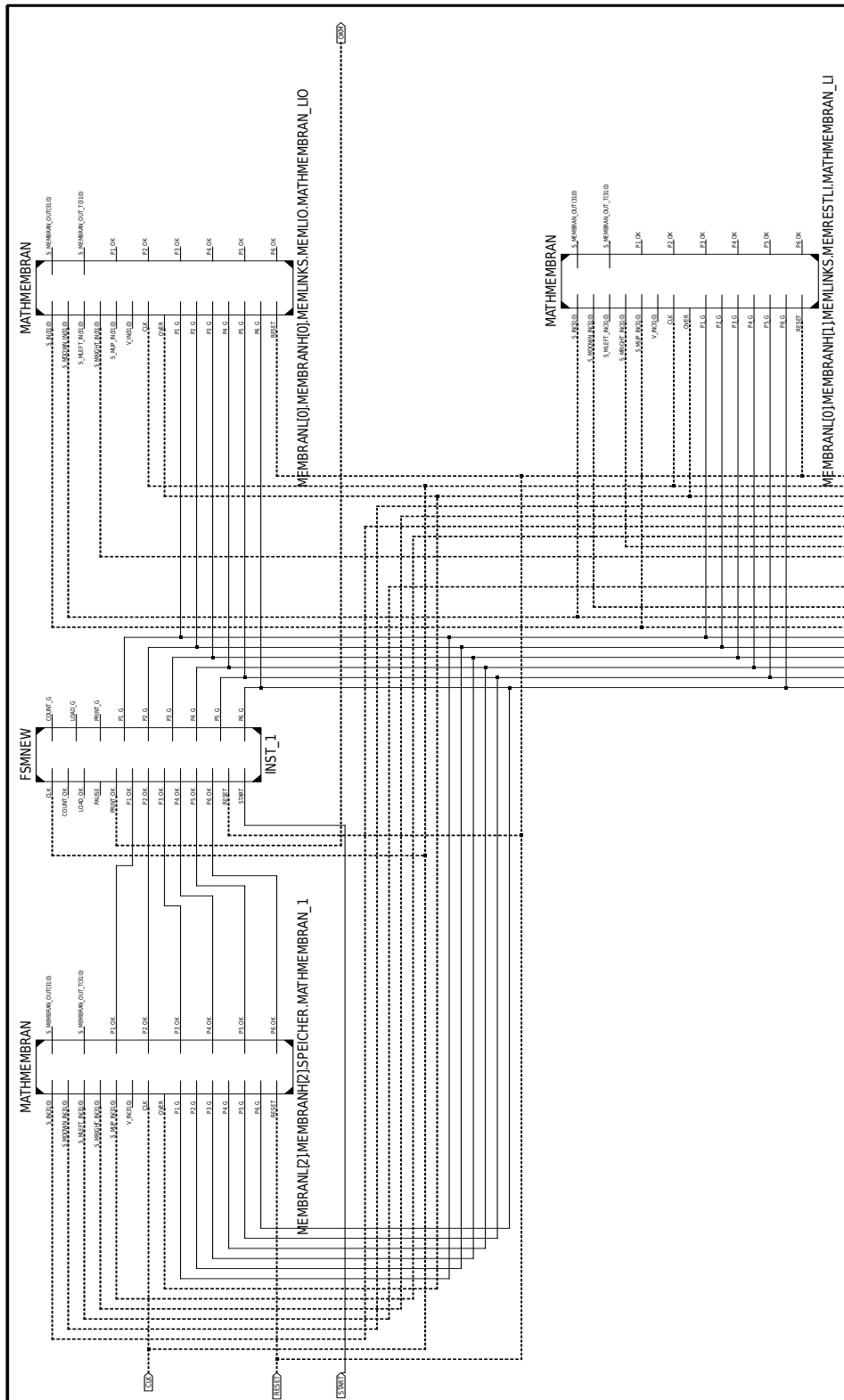


Figure 6.15: MRL of the membrane.

6.4.8 2-dimensional Plate

The 2-dimensional plate equation is used in the model of the violin, the runa and the yueqin. Similar to the HL model, the LL plate equation can be deduced by extending the linear 2-dimensional wave equation of the membrane. In the first case, a linear plate on a Cartesian grid is implemented. As the difference operator of the plate equation shows, the force calculation of one mass point now depends on a 5x5 stencil with values from 12 neighbouring points. In a stencil with weighted points, the plate operator is given in equation 4.39 in chapter 3.

Arithmetic Layer

The structure of the plate AL is similar to the AL of the membrane. There are only a few modifications in the AL for the implementation of a plate. An analysis of the plate stencil³⁴ reveals that all weights can be expressed by multiplications by powers of two or a composition of it³⁵. Hence, the weighting of the stencil can be achieved by taking several left-shifts and additions consecutively. This simplifies the algorithm and saves resources in the final hardware implementation. A shift stencil formulation of the plate hardware implementation is given in figure 6.16.

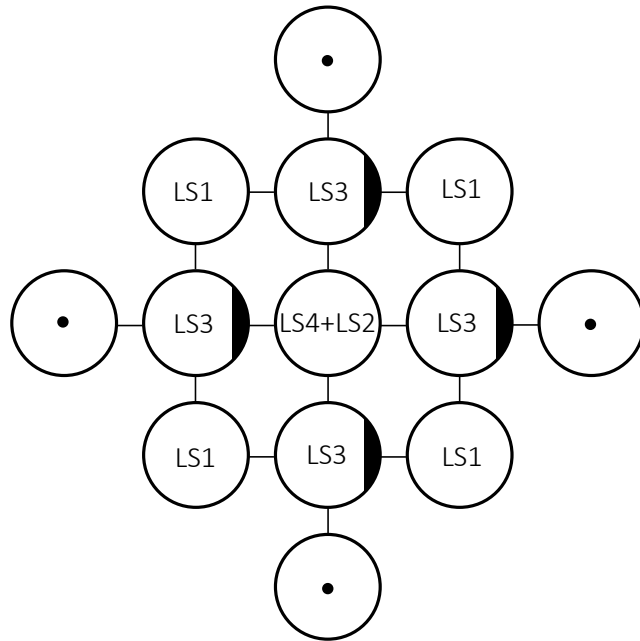


Figure 6.16: FD-shift stencil for the 2-dimensional plate operator. The points indicate that no shift operation is performed at this node. The partial black filling indicates a multiplication by -1 of the respective cell.

³⁴The plate stencil is given in equation 4.39.

³⁵ $20 = 2^4 + 2^2$.

Math Routing Layer

The MRL follows the modifications made in the AL. The acceleration calculation of every discrete node point on a plate requires the values of twelve neighbouring points. Hence, every discrete node point has twelve inputs, receiving the deflections of the node points.

6.4.9 The Violin Bridge

The acoustical relevant vibrations of the violin bridge are modelled by incorporating its geometry as presented in chapter 2. In this formulation, it is necessary to calculate the forces in two directions to include the rocking motion of the violin bridge into the model. Besides changes in the AL, the most prominent difference of the violin bridge implementation is the additional memory requirement. Opposed to the other geometries, every point of the violin bridge needs four memory locations to save the values of:

- the velocity of the discrete point in x direction,
- the velocity of the discrete point in y direction,
- the deflection of the discrete point x direction and
- the deflection of the discrete point y direction.

In addition to that, there are two acceleration computations necessary for every discrete point.

Arithmetic Layer

The AL is similar to the other geometries with the exception, that force calculations in two directions are necessary now.

Math Routing Layer

The MRL incorporates two additional memory blocks, now four in total, to save the values v_x, v_y, u_x and u_y . Besides this change, the routing is not different from the MRLs of the other instruments.

6.4.10 3-dimensional Air Volumes

All final hardware instrument models consist of an air volume enclosed in the resonance body of the respective instrument. As shown in section 2, the air volume plays an important role in the radiated sound of the respective instruments, either influencing the front plate modes or adding independent frequency information to the radiated sound. The air volume is implemented in two ways, first, as an independent entity with the same layers and ports as used for the other geometry models. But as the LL implementations of the musical instruments grew in node size and routing complexity, the transport protocol between the air volume and the other geometry parts lead to a performance bottleneck. A redesign of the 3-dimensional air volume integrated the air entity directly into the model block of the instruments front plate and back plate. The reduction in routing complexity and signal overhead made the model computationally more efficient.

Arithmetic Layer

The finite difference approximation of the 3-dimensional wave equation is an extension of the 2-dimensional wave equation. Because air has no sheering, the movement of sound in air can be approximated by a 7-point stencil as 3-dimensional version of the membrane stencil depicted in figure 6.14. The AL block is depicted in figure 6.17. A description of the functional properties of the signals is given in table 6.7.

Math Routing Layer

The MRL of the air volume is a simple extension of the 2-dimensional models. There are two additional deflection signals that are routed to the AL to calculate the force of each node: S_FRONT and S_BACK, as well as additional BRAMs.

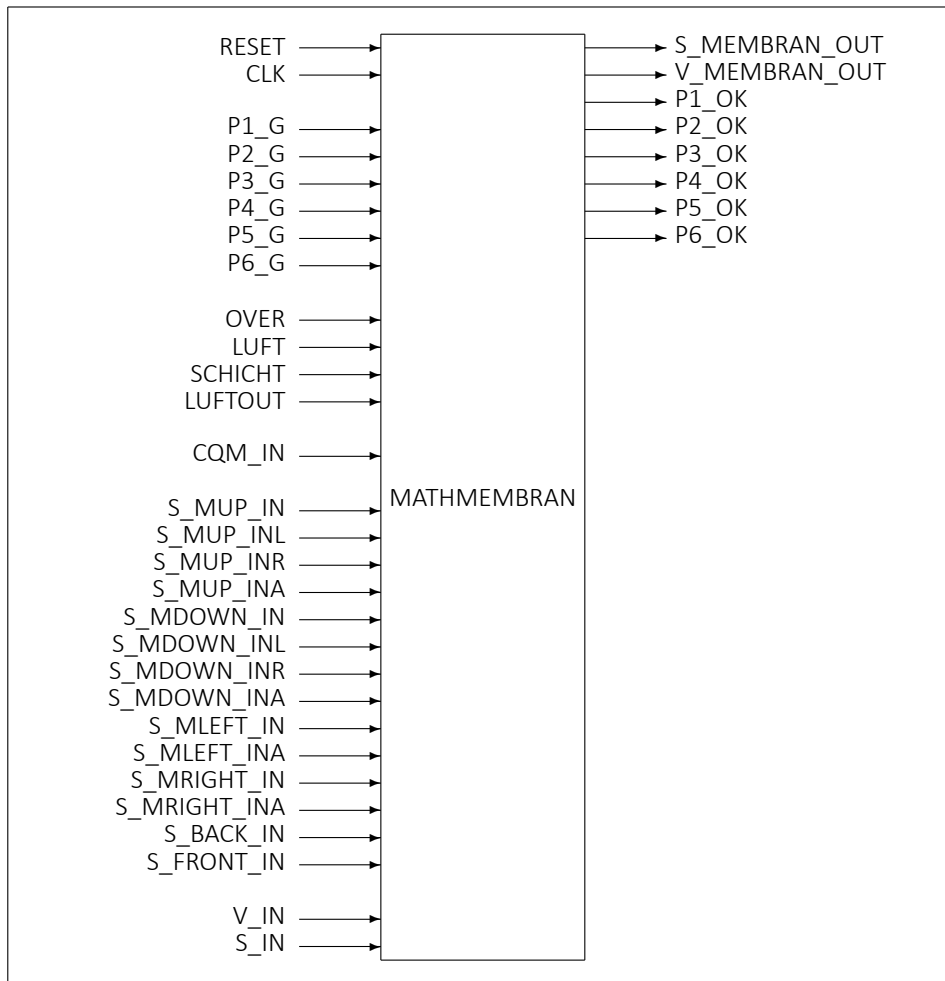


Figure 6.17: Logic block of the air/plate AL.

Signal Name	Function
RESET	Global reset signal
CLK	Global clock signal
PX_G	Status signals from FSM
PX_OK	Status signals to FSM
S_MUP_IN	Upper deflection signal for air/plate/membrane stencil.
S_MUP_INL	Upper-left deflection signal for plate stencil.
S_MUP_INR	Upper-right deflection signal for plate stencil.
S_MUP_INA	Second upper deflection signal for plate stencil.
S_MDOWN_IN	Lower deflection signal for air/plate/membrane stencil.
S_MDOWN_INL	Lower left deflection signal for plate stencil.
S_MDOWN_INR	Lower right deflection signal for plate stencil.
S_MDOWN_INA	Second lower deflection signal for plate stencil.
S_MLEFT_IN	Left deflection signal for air/plate/membrane stencil
S_MLEFT_INA	Second left deflection signal for plate stencil.
S_MRIGHT_IN	Right deflection signal for air/plate/membrane stencil
S_MRIGHT_INA	Second right deflection signal for plate stencil
S_BACK_IN	Back deflection signal for air stencil
S_FRONT_IN	Front deflection signal for air stencil
S_IN	Deflection from prior time step.
V_IN	Velocity from prior time step.
OVER	Coupling point with string (true/false).
LUFT	Air/plate (true/false)
SCHICHT	Index of layer in the instrument body in the orthogonal plate direction.
LUFTOUT	Orifice on the front plate (true/false).
CQM_IN	Tunable wave-velocity factor.
S_MEMBRAN_OUT	Output signal for calculated deflection.
V_MEMBRAN_OUT	Output signal for calculated velocity.

Table 6.7: Air-plate logic block signal description.

6.5 Instrument Models

In this section, the complete FPGA instrument models are presented in detail. All described models are fully functional real-time implementations on FPGA development boards and can be played and modified via pushbuttons, dip-switches or from a personal computer via a control software implemented in C#. All models are constructed from the basic parts presented in the sections above.

6.5.1 Banjo Model

The hardware implementation of the banjo consists of a model for one string, a wooden bridge and a membrane, including the air volume under the membrane. The real-time model of the banjo is implemented utilising the basic building blocks presented in this chapter. The IL receives data words containing information for the position of the plectrum on the string (**BOW_POINT**), the force (**BP_IN**) and the velocity (**BV_IN**) of the plectrum. Additionally, the length (**PR_POINT**) and tune (**CQ_IN**) of the string are transferred from the control software to the hardware board.

Model Routing Layer

The MoR implements three CCLs of the respective geometries, as shown in figure 6.19³⁶. The instance **SAITELNEW** receives the de-serialised values from the IL, the calculated deflection of the string CCL, as a result to the excitation of the string is transferred to the bridge entity called **STEG**. The outputs of the bridge entity are linked to the inputs of the front plate/air entity called **LUFT**. In the **LUFT** entity, the calculated particle velocities are integrated over several points and transferred to the IL as the signal **S_MEM_OUT**.

Banjo String CCL

The string control circuit layer of the banjo is composed of ten parallel ALs, which are calculated eight times to yield a total string node count of eighty points. The math routing layer routes ten parallel 1-dimensional ALs. The AL of the banjo string calculates the model of a string with damping and a non-linear excitation model.

Banjo Bridge CCL

The control circuit layer of the bridge implements the model of a three footed banjo bridge.

³⁶Because of the interchangeable model design, the CCL entities for all models have the same name. Because the violin model supersedes the other instrument models in complexity, all entity names are violin related (in German).

Banjo Membrane CCL

The membrane of the banjo is modelled using a linear 2-dimensional differential equation with velocity and internal damping. The air volume below the membrane is implemented as a three dimensional volume with damping losses at the geometry boundaries.

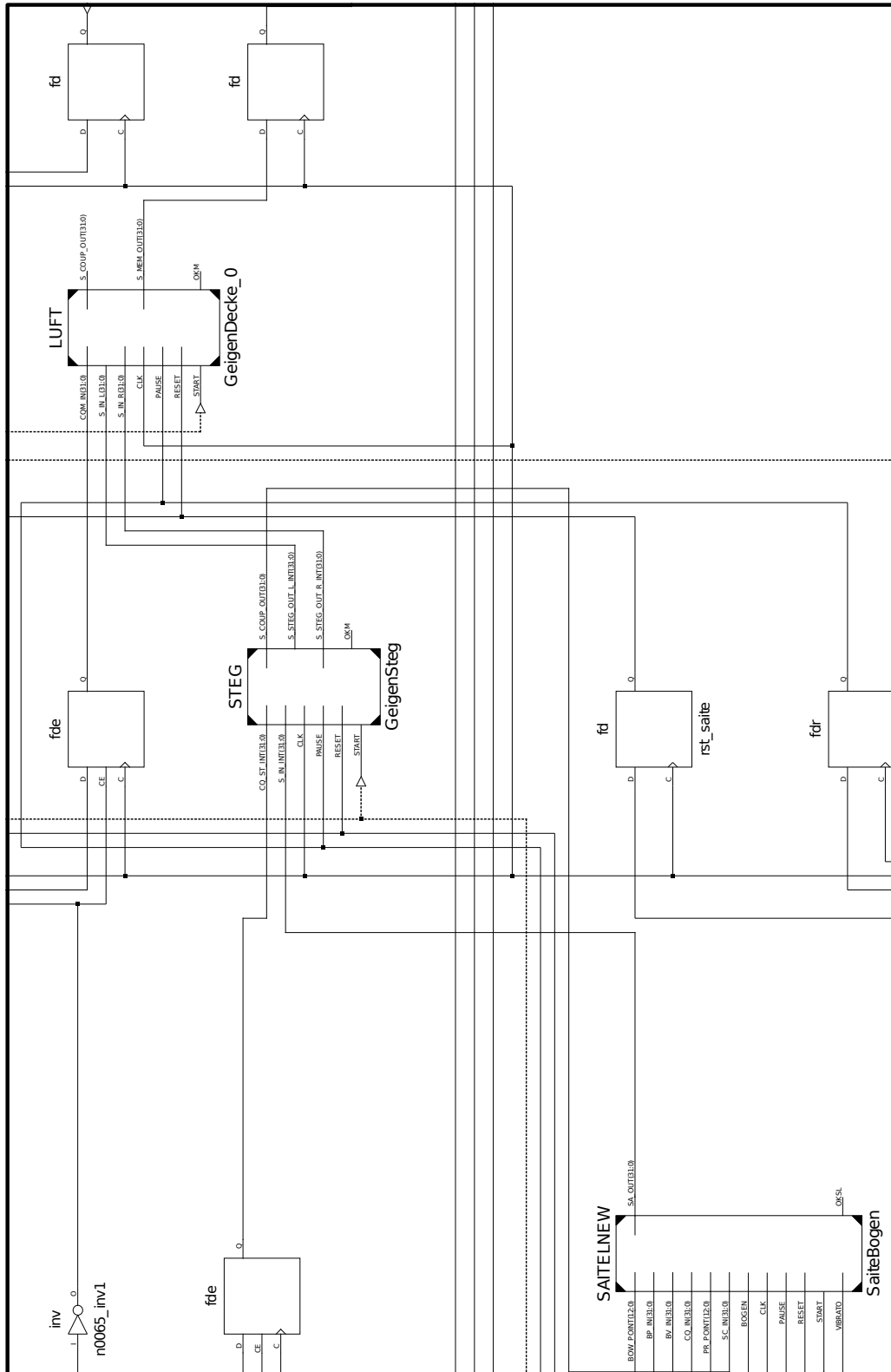


Figure 6.18: Partial CCL of the complete geometry implementations.

6.5.2 Yueqin Model

The model of the yueqin is a direct extension of the banjo model. Among several conjoining geometrical features like the round body there are two very important properties discerning the yueqin from the banjo. First and most importantly, the round body of the yueqin has a wooden soundboard instead of a membrane. And secondly, the strings have a different fastening mechanism. Hence, the model of the wooden bridge is not included in the model of the yueqin. Instead, the strings are fastened at the tailpiece of the instrument, which transmits the acoustical vibrations of the string to the front plate. This mechanism is implemented via an impedance coupling between the last point of the string and the coupling point on the membrane. The communication between the IL and the MoR is similar to the model of the banjo.

Yueqin MoR

In the MoR layer of the yueqin, only the string CCL and the front plate/air CCL are instantiated.

Yueqin String AL

The basic calculations of the strings are similar to the calculations of the banjo string.

Yueqin Front Plate AL

The front plate of the yueqin is modelled in the AL, as described in section 6.4.8, as a plate with velocity and internal damping. The damping parameters for the wood are approximated with *Ad-hoc* values.

6.5.3 Ruan Model

The real-time model of the ruan is a mixture of the model of the yueqin and the model of the banjo. The geometric features of the body are similar to that of the yueqin, the wooden bridge is implemented as in the banjo model. One extension of the yueqin model, is the presence of orifices on the front plate, enabling the enclosed air volume to radiate.

Ruan MoR

The model routing layer is similar to the model routing layer of the banjo.

Ruan front plate MRL

The math routing layer of the front plate implements the orifices as a conditional query, implemented in the **LUFT** entity, and described in table 6.7 via the signal **LUFTOUT**. The initial position of the orifices is saved in a ROM, which is initiated at cold start of the model.

6.5.4 Violin Model

The physical model of the violin supersedes the model of the other instruments because it incorporates all of the mentioned building blocks including several extensions of the basic structures. This is mainly due to the more difficult geometry of the violin, the asymmetric orifices as well as the non-linear bow/string interaction model. In the real-time model of the violin all of these factors are taken into account and are implemented according to the physical model as presented in section 4.8.

The hardware implementation of the violin consists of four strings, a wooden bridge, a wooden front plate, a wooden back plate and an air volume within the body.

As described in section 6.4.5, the IL receives data words containing information for the position of the bow on the string (**BOW_POINT**), the applied force (**BP_IN**), the velocity (**BV_IN**) and the number of contact points of the bow (**SC_IN**). Additionally, the length (**PR_POINT**) and tune (**CQ_IN**) of the string are transferred from the PC host to the hardware board.

Model routing layer

The MoR implements the three CCLs of the respective geometries as shown in figure 6.19³⁷. The instance **SAITELNEW** receives the de-serialised values from the IL, the calculated deflection of the string CCL, due to the excitation of the string is transferred to the bridge entity called **STEG**. The two output signals of the bridge entity are connected to the inputs of the front plate/air/back plate entity called **LUFT**. In the **LUFT** entity, the calculated velocity is integrated from several points on the front plate, and then transferred to the IL via the signal **S_MEM_OUT**.

Violin string CCL

The string control circuit layer of the violin is composed of ten parallel ALs which are calculated eight times. Hence, the string of the real-time violin is discretised by eighty node points. The math routing layer routes ten parallel 1-dimensional ALs. The AL of the violin string calculates the model of a string with damping and the bow/string interaction model.

Violin body CCL

The body of the violin, consisting of a front/back plate and the air volume, is implemented in a single CCL. The AL for the front plate and back plate are described in section 6.4.8, the enclosed air is modelled as shown in section 6.4.10.

³⁷Because of the interchangeable model design, the CCL entities for all models have the same name.

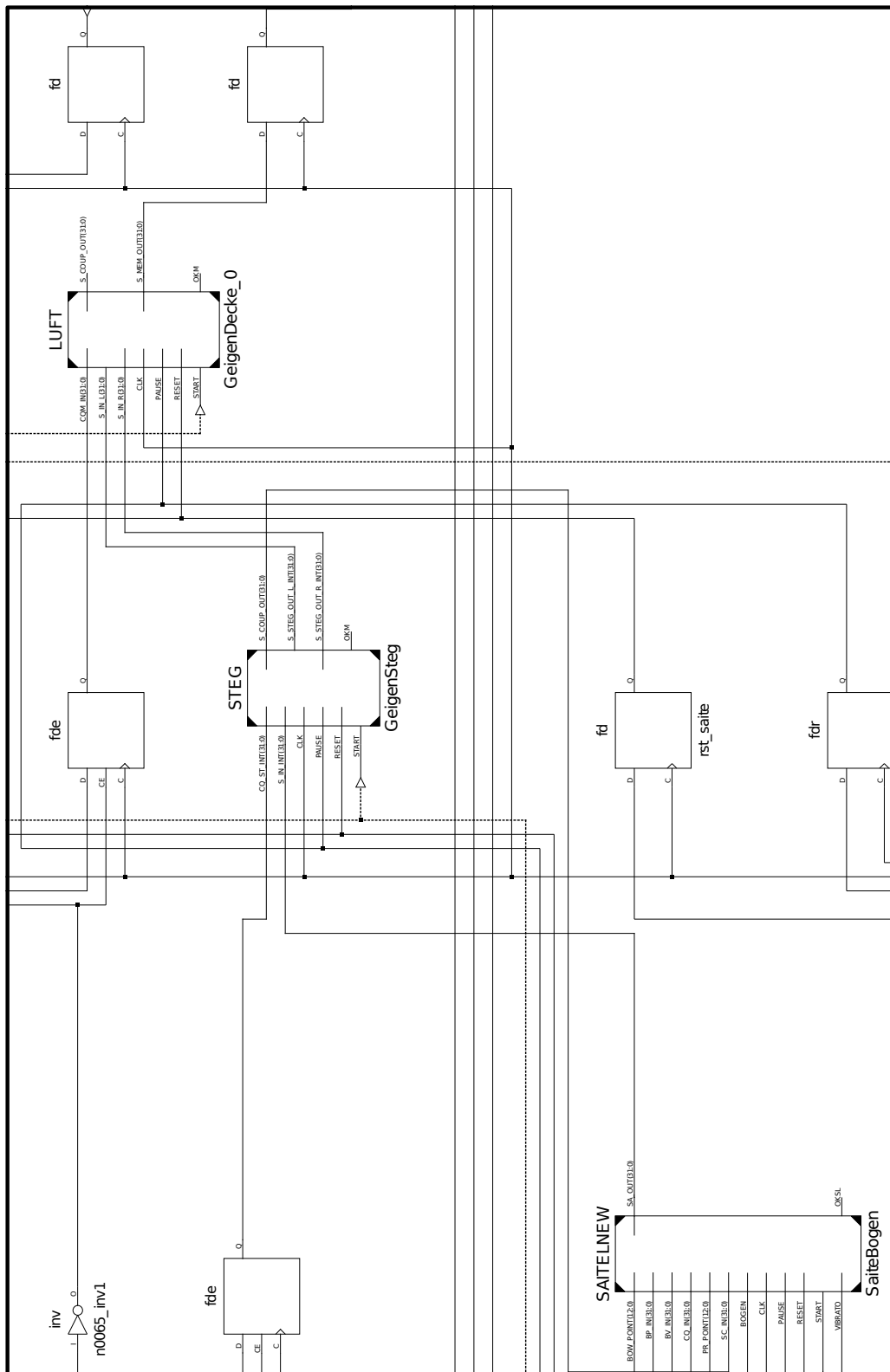


Figure 6.19: MoR of a complete geometry implementations.

6.6 Simulation Results

The following figures show several recordings from the real-time implementation of the instruments. The respective models are controlled via the control GUI described in section 6.7. The synthesised sound of the instruments is transmitted to the host PC via the PCIe interface and recorded there with the audio software *Samplitude*. An wav-File of every sounds can be found on the attached CD in Appendix 5. The bit-Files of the respective models are included on the CD as well.

6.6.1 Banjo

Figure 6.20 shows the detail of a banjo string/finger pick interaction with clearly audible slipping sound of the metal pick over the string. The slipping sounds are indicated in the figure. The complete recording can be found on the CD under the name: *Banjo_Plucked.wav*.

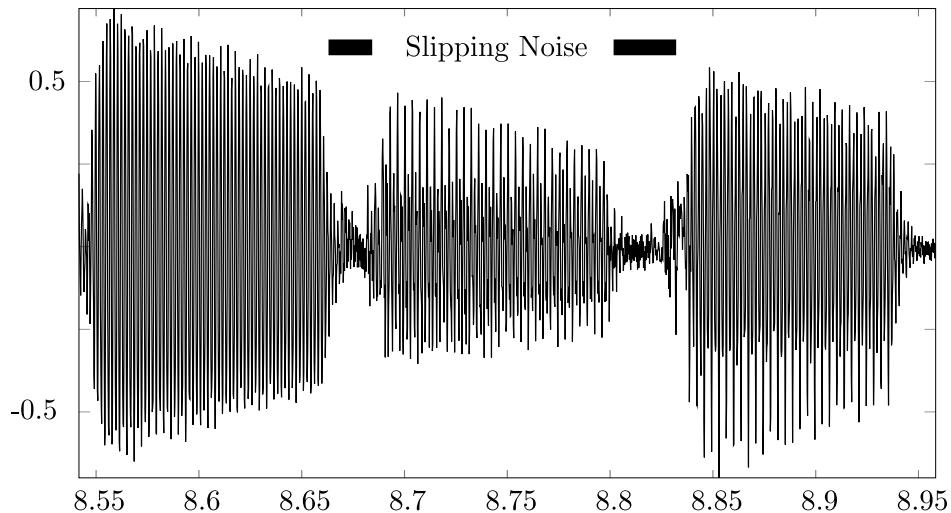


Figure 6.20: Detail of banjo recording.

A sound of some randomly played notes on one string of the banjo model can be found on the CD under the name: *Banjo_Random.wav*.

Discussion

As visible in figure 6.20 and audible on the supplementary sound files, the interaction with the model allows to play expressively on the virtual instrument. At this point of the work, the interaction of the GUI with the FPGA only allows for simple lines, or arbitrary, chaotic playing.

Figure 6.20 shows the effects of the finger pick/string interaction model.

6.6.2 Violin

Figure 6.21 shows the velocity of a bowed violin string. The clearly visible negative *spikes* have a large variance in their minima, pointing to a sound with lots of bow noise.

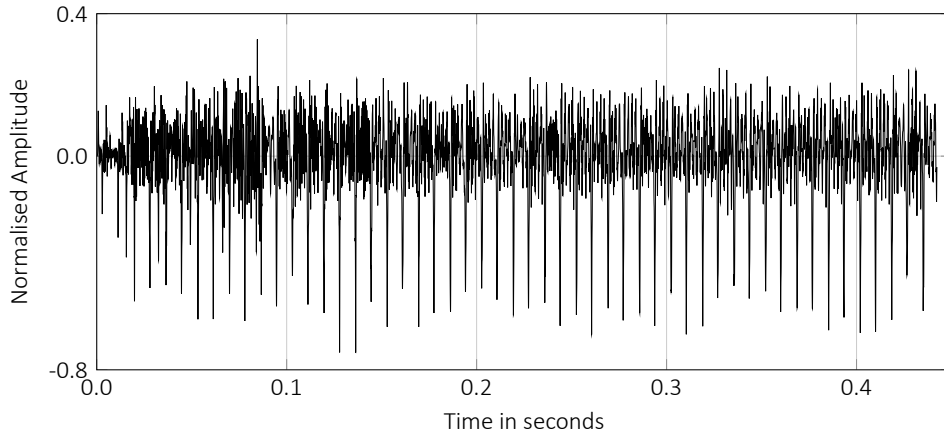


Figure 6.21: Detailed velocity of a bowed violin string.

The next figure (fig. 6.22) shows a single violin note played with varying bow velocity. The recording of the time series can be found on the CD under the name: *Violin_BowVelocity.wav*.

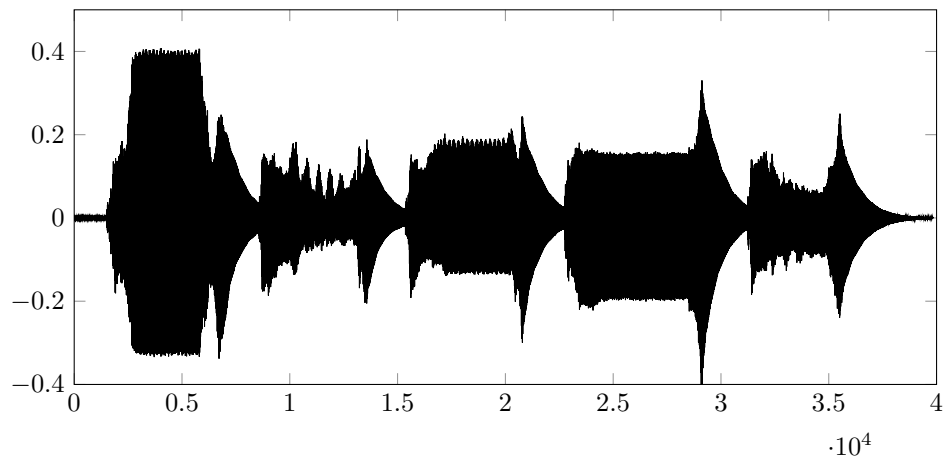


Figure 6.22: Single bowed note with varying bow velocity.

Discussion

The recorded time series show that it is possible to play variable notes on the virtual violin by applying different start values. The depicted velocity on the string is in good accordance with the measured string (see figure 2.10) velocity of a violin.

6.6.3 Ruan

Figure 6.23 shows a fast sequence of notes, played on the virtual ruan. While the notes are playing, the thickness of the front plate is changed, influencing the radiated sound of the instrument. The recording of this time series can be found on the CD under the name: *Ruan_LineTune.wav*.

have a large variance in their minima, pointing to a sound with lots of bow noise.

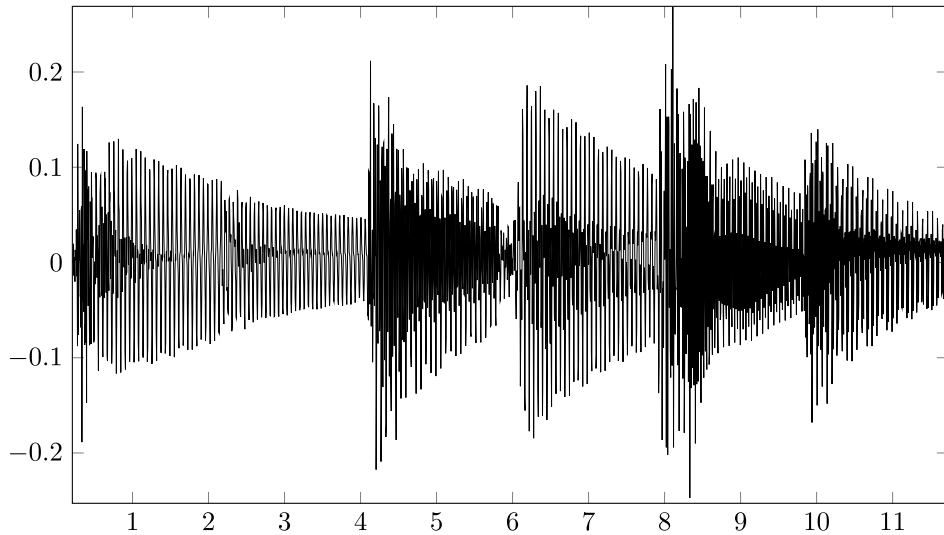


Figure 6.23: Fast sequence of notes, changing the height of the front plate.

The next figure (fig. 6.24) shows an excerpt of a ruan note sequence, played with a tremolo. The figure clearly shows that the tremolo is not static, meaning the vibration on the string influences the shape of the next plucked note. The recording of the time series can be found on the CD under the name: *Ruan_TremoloLine.wav*.

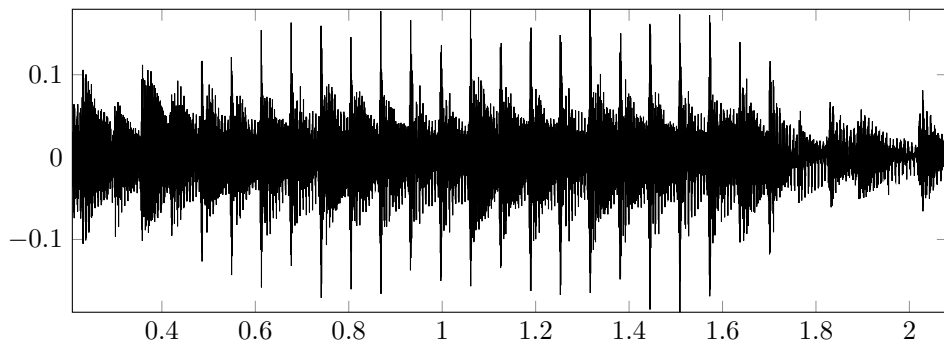


Figure 6.24: Sequence of notes played with a tremolo technique.

Discussion

The first time series of the virtual ruan shows, that it is possible to play with material properties while playing the instrument. Figure 6.24 shows that rapidly plucked notes have a different shape each time because the initial state of the string is different every time due to the fact that it still has vibrational energy stored from the preceding pluck.

6.7 GUI for the Model

The Graphical User Interface (GUI) to control the models is coded in the C#, utilising a memory-write and memory-read driver to communicate with the FPGA board.

The software interface is designed to control parameters of the FPGA models. The number and sort of parameters depends on the implemented hardware model. At boot time, a short handshake configures the FPGA to receive PCIe data from the host PC to interact with the respective model.

At current stage of development, the GUI has basic functionality and is more a proof-of-concept than a readily usable interface. As is shown in figure 6.25, the GUI has several

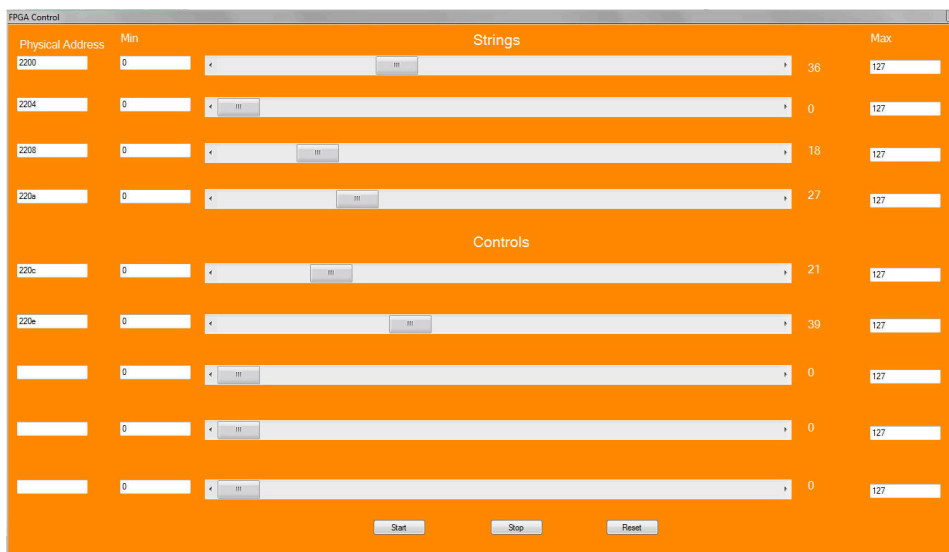


Figure 6.25: Host GUI for controlling the low level models.

assignable linear sliders. Each of the sliders can have a different functionality depending on the device address it writes to. At this moment the GUI can be used to change physical properties of the strings, membrane and soundboards of all instruments in real-time. In addition to that, it is possible to interact with the strings either plucking at a certain position or bowing the strings using one of the presented interaction models, allowing it to play monophonic melodies or single notes.

To conclude this thesis a look back on the work done and a look forward to the work to be done is at place here. In retrospect, this thesis seems unfinished and the author's feeling is that there are more questions that were raised than questions that were answered. This is partially due to the interdisciplinary approach of this thesis focussing on several aspects of acoustics and trying to combine historic research with current research.

There are multiple loose ends that, in the eyes of the author at least, have to be tied up to be finished.

In this thesis, a methodology for modelling and synthesizing physical models of musical instruments, discretised with finite differences computed in real-time on FPGA hardware was presented. A derivation of the underlying algorithm for all models and presented high level models in MATLAB and C as well as real-time models implemented in VHDL and computed on a FPGA.

Additionally, algorithmic properties were researched resulting in a stable and flexible method to auralise physical models of musical instruments for many diverse applications and settings.

7.1 Central Achievements

The central achievement of this work is the development and implementation of a real-time synthesis methodology for physical models of musical instruments. Besides an identification of robust algorithms for real-time physical modelling, the methods were optimised for an implementation on parallel hardware devices.

It was shown that the proposed method is not only applicable for single geometries, but for coupled systems resulting in complete instrument models as well.

Additionally, it was shown that besides linear problems, even highly non-linear problems can

be synthesised and auralised in real-time.

The real-time prototypes for the banjo, violin, ruan, and yueqin are the first complete geometry real-time physical models of their kind.

Besides the possibility of changing physical parameters like internal damping, velocity damping, coupling constants, and radiation properties while playing the instrument in real-time, the FPGA implementation led to several findings of mathematical and numerical nature regarding the implementation of such models.

Additionally, the detailed occupation with mentioned instrument models lead to several insights into vibro-acoustical properties of the instruments that had not been discussed in literature before for the respective instruments.

7.2 Findings of Numerical Nature

The methodology utilising a normalised fixed-point data type to compute real-time representations for the defining physical parameters of the equations of motion was applied for physical modelling and real-time auralisation of musical instruments for the first time.

The importance of an explicit calculation of the acceleration, velocity and deflection was stressed. Related works, regarding the simulation of mechanical and vibro-acoustic problems, most often apply different numerical methods to find an expression only for the deflection¹.

A method to approximate arbitrary terms in the form of $\frac{x}{k}$ with a finite series of terms, expressible as left and right shift operations, is proposed and applied in the real-time models. It is a novel approach to approximate arbitrary divisions when using a fixed point data-type. It is highly applicable to find *ad-hoc*-values for damping parameters, without the effort of implementing a division logic circuit, which is very area- and time expensive in hardware.

The method of coupling pseudo-spectral methods with symplectic and multi-symplectic integrators is proposed here for musicological problems. Even though an exhaustive presentation of the mathematical foundation was beyond the scope of this thesis, important features of both methods could be shown numerically and advantages of the coupled methods were stressed. Their benefits for physical models of musical instruments were exemplified at several high level models.

7.2.1 Layer model

A novel layer model for a convenient implementation of hardware models of musical instruments was developed and implemented in this thesis. Benefits were shown to be the easy

¹The FDTD method, applied in the works of Stefan Bilbao are one example.

scalability and interconnectivity of the singular layers, as well as the interchangeability of core parts of the design.

7.3 Findings Acoustical Nature

7.3.1 Banjo

In this thesis, it was shown that the adjustment of the banjos membrane, leading to specific boundary conditions, is of central importance for the timbre of the instrument. Only when applying exact boundary conditions for the membrane, the characteristic *ringing* sound of the banjo is achieved.

The adjustment of the banjos membrane was always subject to diverse theories among musicians instrument makers and historians. It is widely assumed that the specific boundary conditions are only responsible for the high tension of the membrane, and a there from resulting higher volume of the instrument.

But as presented in section 2.3.4, the fastening of the membrane also influences the spectrum, specifically the positions of the mode shapes of a membrane.

It was shown that the analytical mode shapes can be found in the radiated modes, but at other frequencies as expected. A peculiar finding of the measurements was that there are several equidistant peaks in the frequency range between 500 and 2000 Hz.

This effect is not explained by any theory but has been found in all banjo membranes measured over the course of this thesis. A possible explanation for this effect is the influence of the boundary condition on the radiation patterns of the membrane.

In this thesis, special boundary conditions were applied to model this effect correctly.

modelling an air volume as a Winkler bed

In section 4, it was shown that the influence of the air volume can be approximated by a Winkler bed coupled to the membrane. The influence of the Winkler bed results in a heightened net force acting on the membrane, depending on the deflection of the membrane. It was shown that this is an easy measure to implement the influence of an air volume coupled to a membrane. This method can easily be extended to other instrument models like snares or a timpani.

Influence of the nonlinear tension distribution

The influence of the non-linear tension distribution on the membrane, produced by the force of the bridge, acting in the normal direction to the membrane, was shown in measurements in chapter 2.

It was shown that the modes do not rise uniformly when the bridge is attached to the membrane.

The model of the membrane included the non-linear tension distribution with a varying tension distribution on the membrane. The modeled instrument can be configured with different settings and it was shown that the non-linear effects have an impact on the timbre of the auralised banjo sound.

Non-linear effects due to high deflected strings

The banjo string is deflected comparatively far from its equilibrium position, even under normal playing conditions.

This gives rise to non-linear effects as a result from non-linear restoring forces which can be expressed by adding a Duffing term or a Kirchhoff-Carrier like term to the fundamental partial differential equation of the string.

In this thesis it was argued that the deflection non-linearity can only be modeled by a Duffing term or a Kirchhoff-Carrier-like term.

It was shown that the non-linear term not only accounts for a pitch glide, an effect that is present in loudly played banjo strings, but it also adds non-linear decay characteristic to some higher partials of the banjo, an effect that can be found in real banjo strings as well.

The approach of longitudinal-transversal coupling, as proposed in other works had to be dismissed for the cases of the string and the membrane. It was shown that it leads to unphysical results, at least in the presented cases.

Excitation

The importance of a correct excitation mechanism model for the respective instrument was stressed. It was found that the initial excitation directly influences the overall sound quality of the model and the perceived accuracy of the formulation, hence, it was argued that this is a central part for any physical model.

7.3.2 Ruan

The model of the ruan was developed as an extension to the model of the banjo.

There were two important questions regarding a physical model of the ruan:

1. What role plays the Helmholtz frequency, and how do the air modes influence the overall radiated spectrum of the instrument?
2. How does the back plate of the ruan radiate through the sound holes on the front?
3. How important are these effects for the auralisation of the final model?

As shown in section 2, the air-modes play an important role in the sound radiation properties of the ruan and also the frequencies of the backplate play a role in the radiated sound of the instrument radiating through the orifices.

Importance of the ruan's air cavity

The importance of the Helmholtz frequency for lute-like instruments has been emphasized many times in literature, but the exact behaviour of the interaction of an instrument body with the enclosed air volume has only been described in a few and only simple linear cases, like for instance the ideal Helmholtz resonators or simple cylinders with orifices. In this thesis, the importance of the air volume inside the body of the ruan was emphasized and the influence of the air volume on the radiated sound was shown by simulations and auralisation.

Orthotropic qualities in wood

It was shown that orthotropic material properties in wood plates have to be modeled with great care.

There are still many open questions regarding the exact influences of material properties of non-isotropic material in musical instruments. In this thesis, it was shown that an inclusion of orthotropic material properties had a strong impact on the spectrum of the respective wood plate and the whole instrument.

Hence, besides the internal damping of wood, the exact Young's moduli and Poisson ratios are important for the numerical model of a wooden structure like a front plate or back plate.

7.3.3 Violin

The model of the violin has revealed several interesting properties in the interaction of the bow with the string.

It was proposed that to produce a lively violin sound not only an interface for controlling the bow velocity and the bow pressure is important, but also the form coupling of the violin bow to the strings influences the quality of the synthesised sound.

The *traditional* way to model the interaction between a violin bow and the string, applied in several other publications is implemented by stating the following rules:

- If the bow sticks to the string, the string has the same velocity as the bow at the contact point.
- If the bow does not stick to the string, the string can vibrate with a friction dependent influence at the bow point.

If the violin string is modeled in the way presented in chapter 4, the sound of the model is more realistic and lively, although it is physically not completely clear why this is the case.

Further research on this matter is still in progress at the Institute of Systematic Musicology, at the University of Hamburg.

Internal damping of strings

Modern violin strings are designed with a special focus on their internal damping characteristics because of the playability and the *attack* of the strings. Contrabass players use different sets of strings for different musical settings. When the instrument is played in an orchestral setting, strings with a higher internal damping are preferred. In a musical setting where strings are plucked, the damping is lower because the strings need longer sustain. With the proposed methodology, different damping coefficients can be tested and used, depending on the musical settings and the personal preferences of the player. Changing the internal damping is also possible when playing the virtual instrument in a live setting.

7.4 Future Research

The instrument models, proposed in this work are not strictly bound to the specific hardware used here, but could also be implemented on other hardware devices with some adjustments. To fully benefit fully from the proposed methodology, there are several lines of research that can be performed using the proposed methodology as a foundation. This includes:

- The implementation of larger instrument geometries, like models of a grand-piano or upright bass.
- A solution of other physical problems, like the solution for the Navier-Stokes equation for fluid dynamics to simulate non-linear effects in air present in most wind instruments and that also could play a role in air filled instruments like two-headed drums.
- A refined model for wood and metal plates, like for instance the sound board of a grand piano or a cymbal using non-linear plate equation like the von-Kármán equation would be of interest to extend the simulation capabilities of the proposed method.
- Research of internal damping and a characterisation of different parameters influencing the damping of strings or other complex materials.²
- Another important part in future research will be the development of refined version of the user interface as well as the implementation of an inter-FPGA communication protocol using other high-speed buses.

²This could be achieved by simulating nano-mechanical properties of the materials applied in musical instruments. Because symplectic time integration methods are used for molecular simulations since the 1950s the methodology presented in this work can easily be extended to simulate molecular structures and properties of polymers or wood.

7 Results, Conclusion and Outlook

- The implementation of a more user friendly GUI including the possibility to control the models via MIDI or OSC³.
- In addition to the more technical aspects mentioned above, the quality of synthesised sounds should be confirmed in a larger set of listening tests, performed with musicians, instrument builders as well as non-professional musicians as test subjects. This could help defining a better classification of the influence of certain parameters on the sound quality.

As a final remark regarding the research presented in this thesis is the hope that it can be used as a basis for further research in systematic musicology, aid instrument makers in designing new instrument features and musicians feeling inspired by the possibilities of real-time physical models.

³Open Sound Control.

1 High-speed recordings of banjo pick

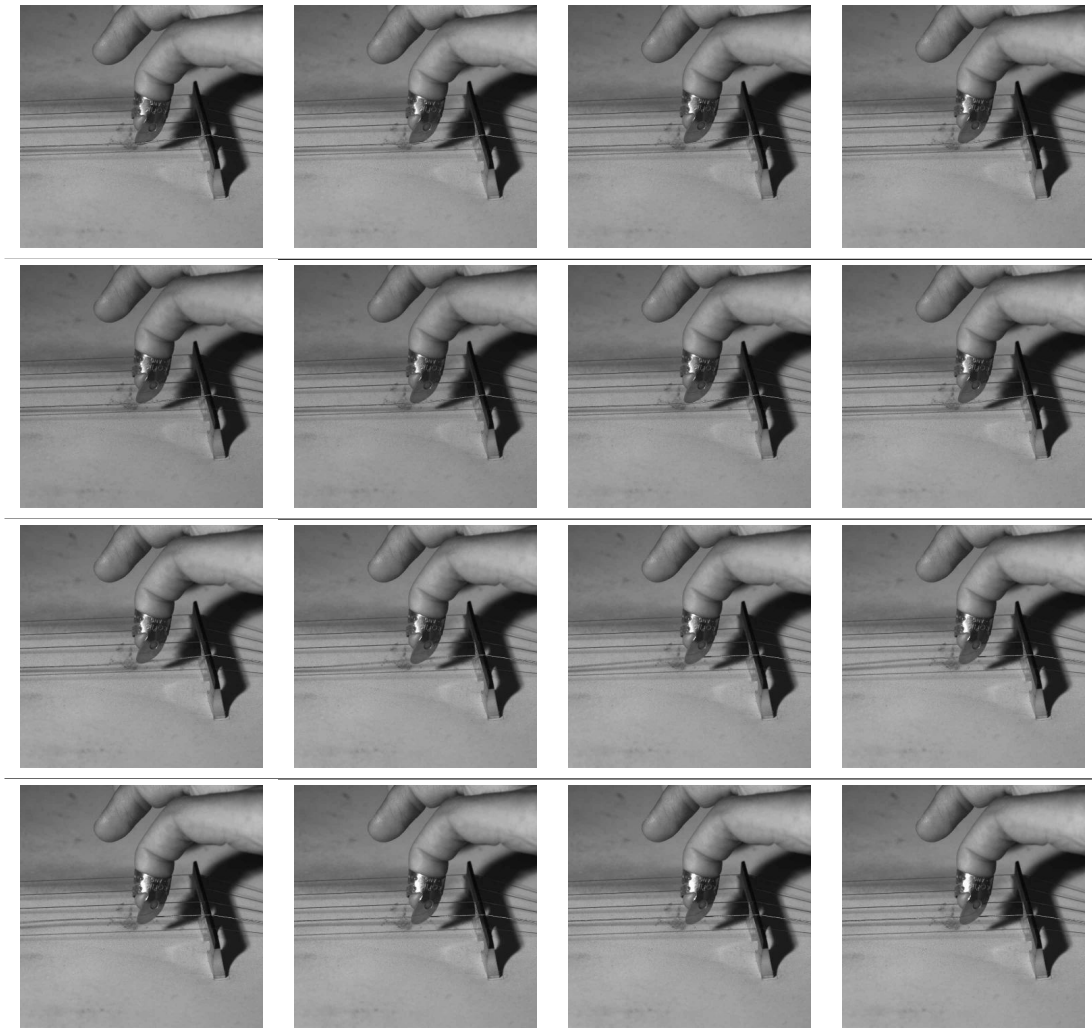


Table 1: Excitation of the string with metal pick I

2 High-speed recordings of banjo bridge

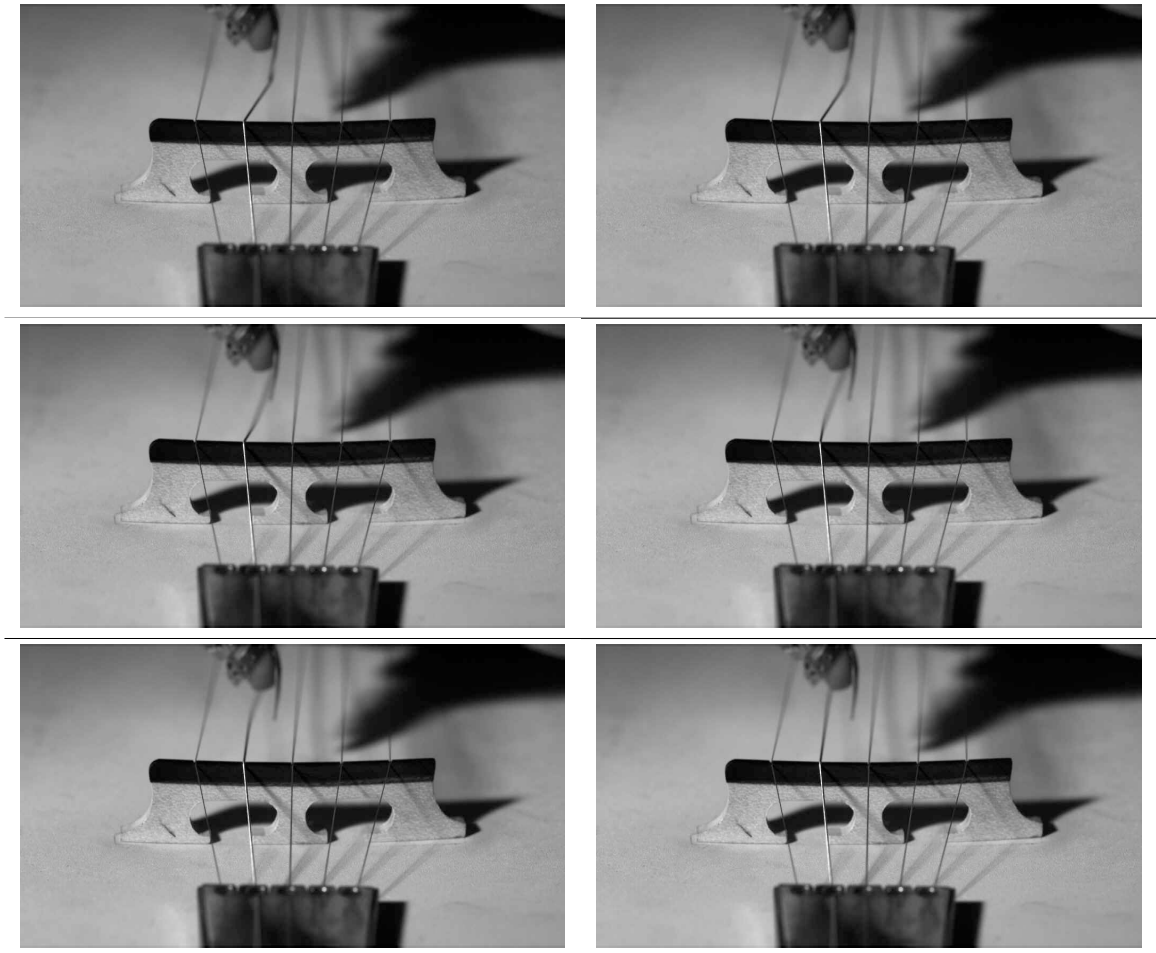


Table 2: Rocking motion of the bridge I

3 High-speed recordings of banjo string

Appendix I

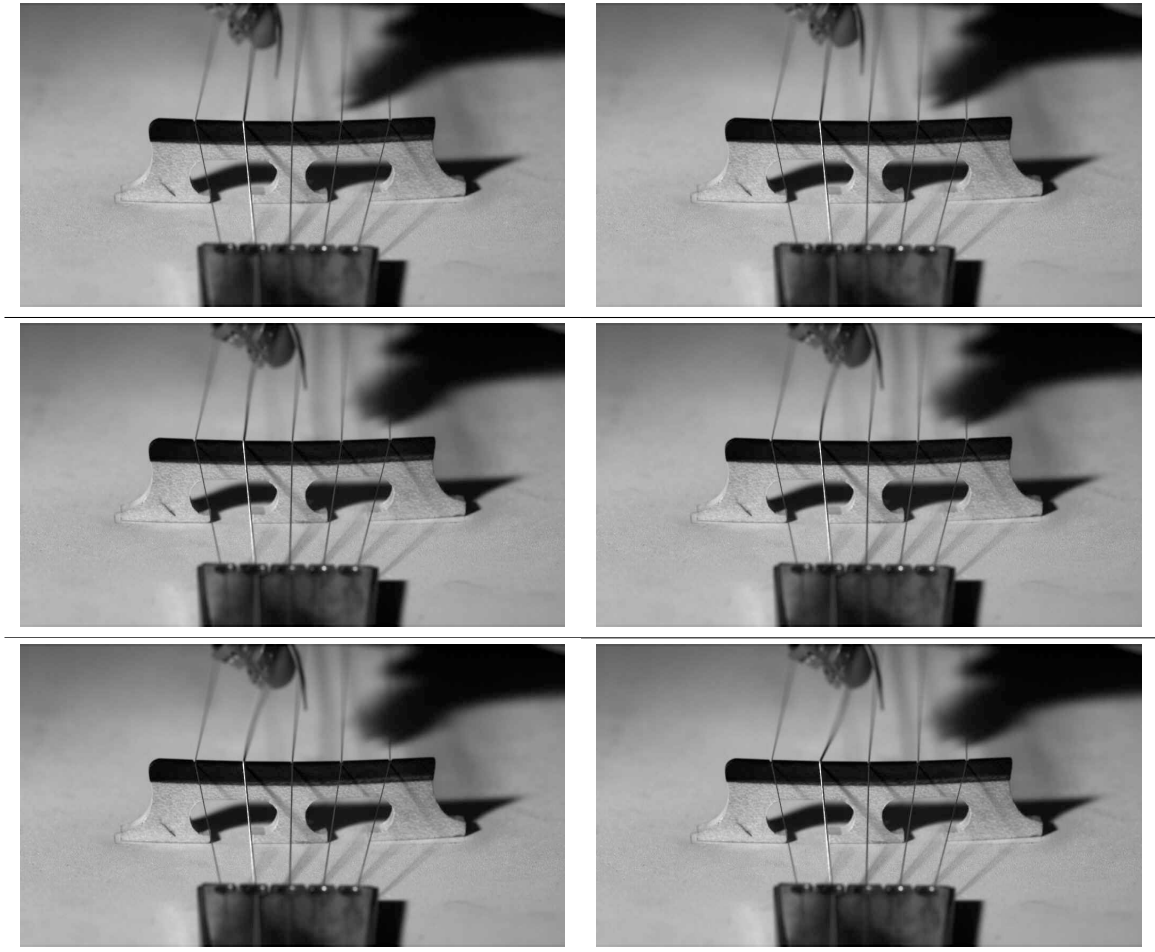


Table 3: Rocking motion of the bridge II

Appendix I

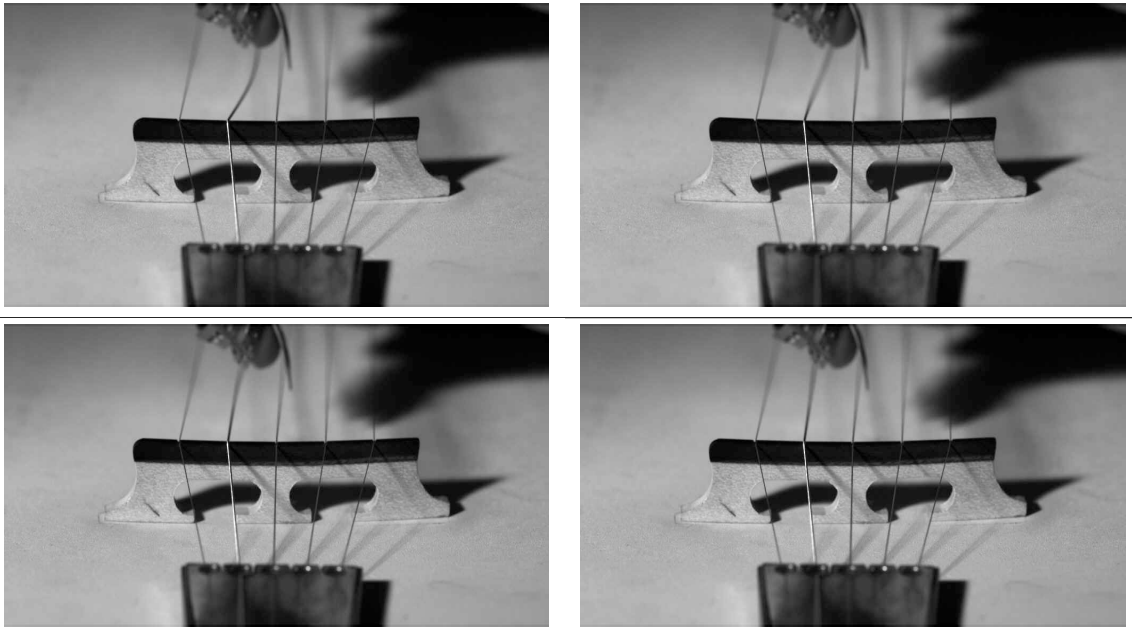


Table 4: Rocking motion of the bridge III

Appendix I

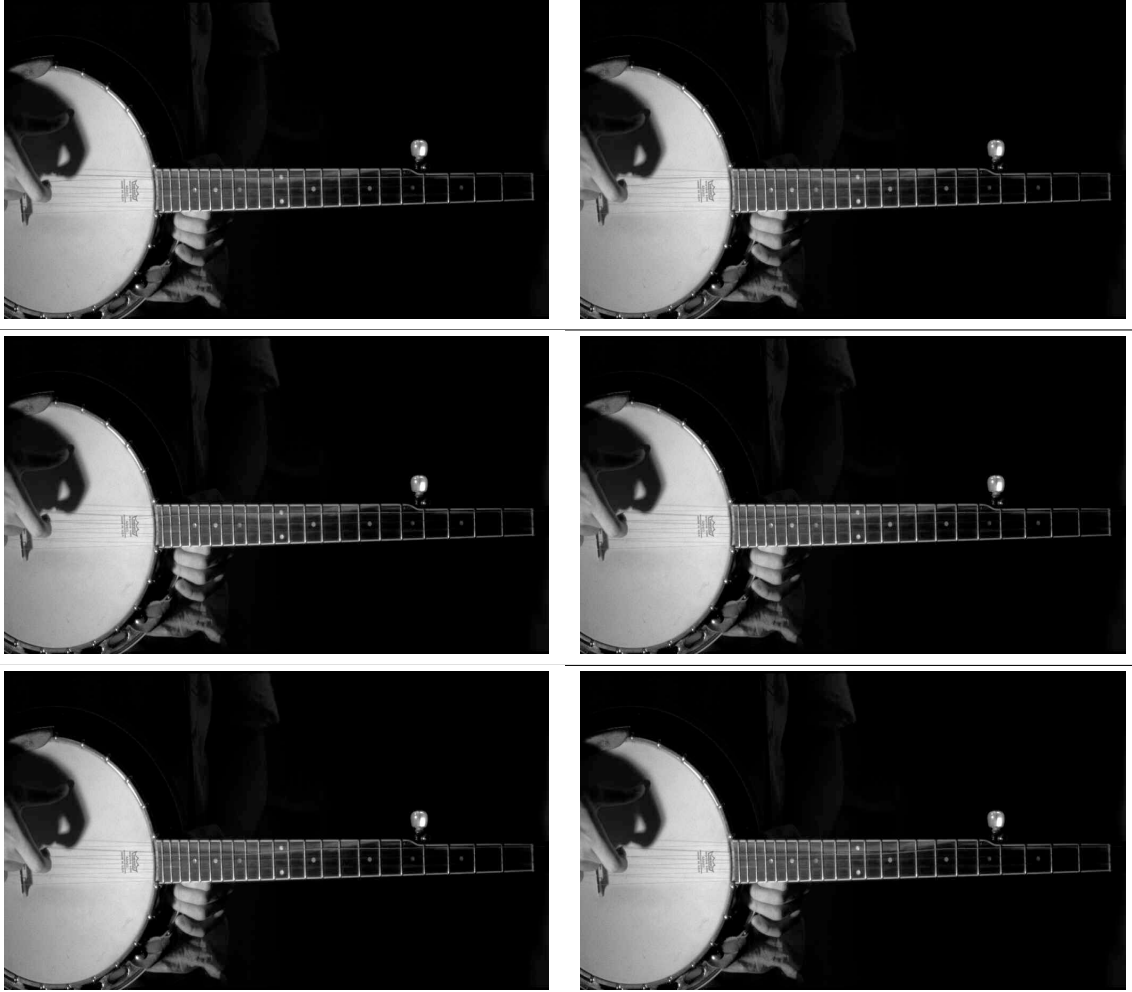


Table 5: String movement I

Appendix I

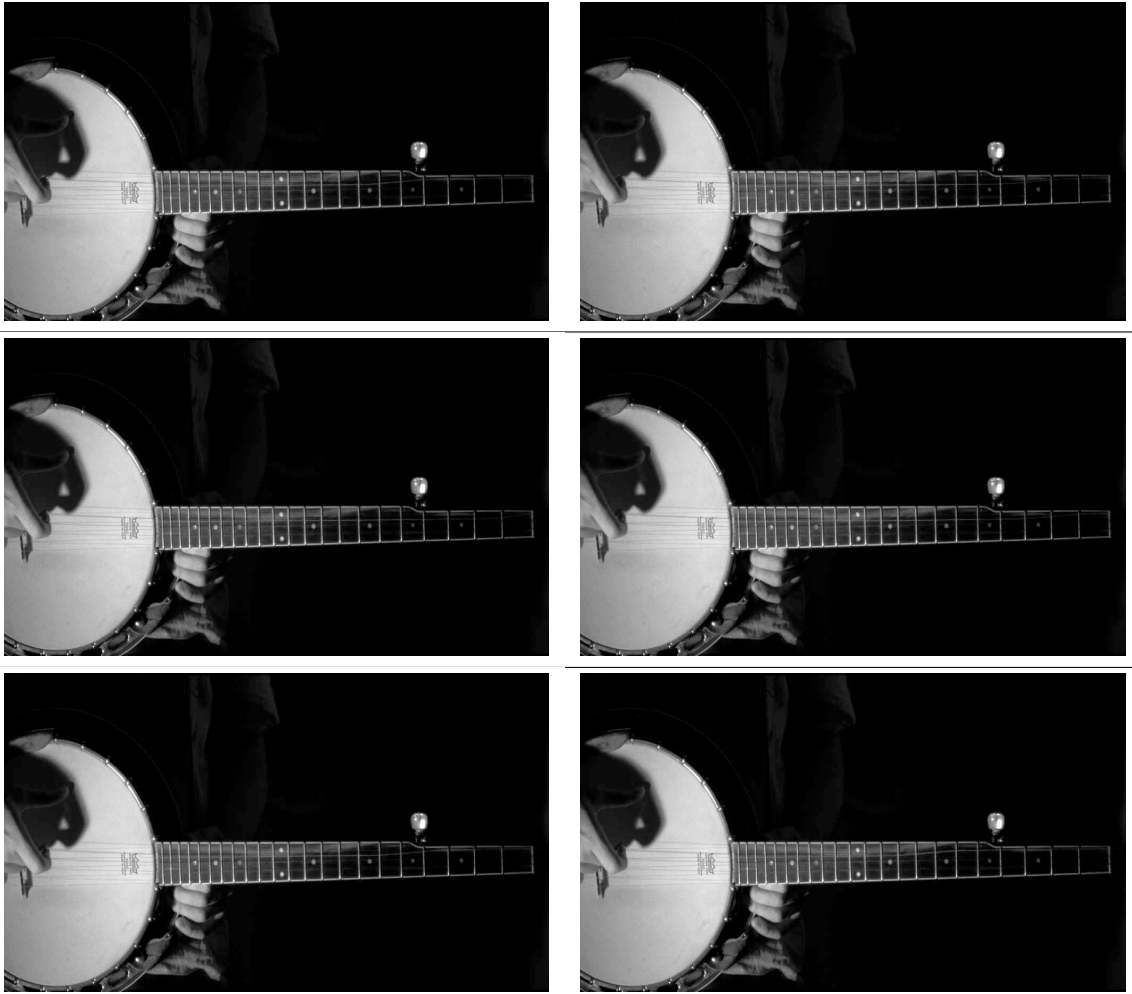


Table 6: String movement II

Appendix I

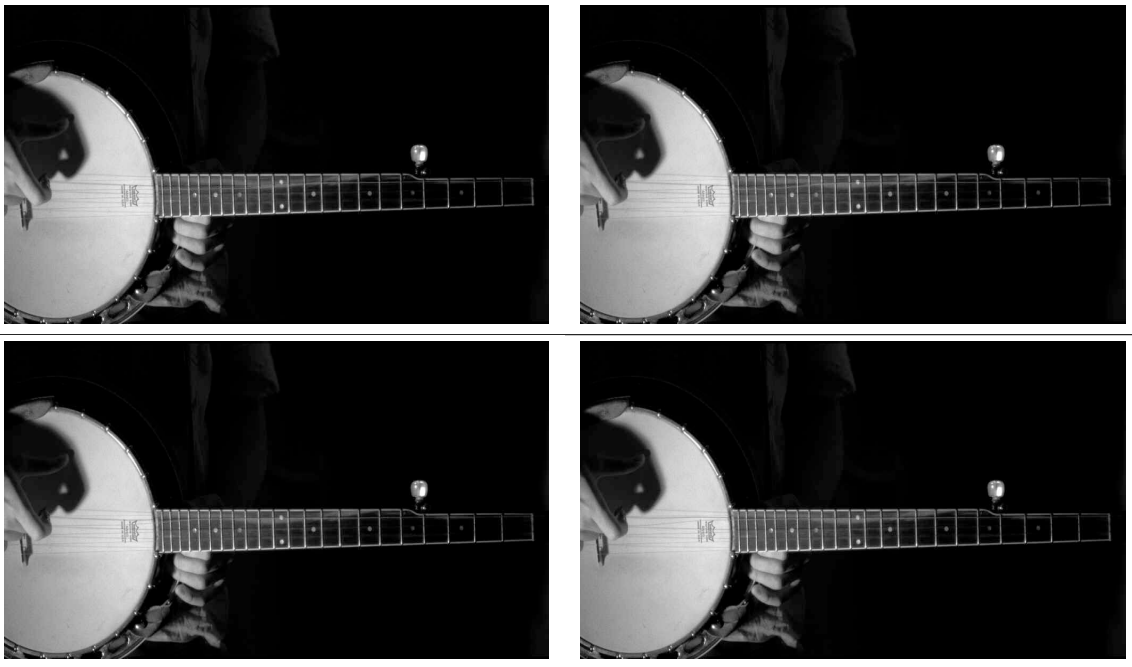


Table 7: String movement II

1 CD contents.

CD File-List

Audiofiles:

1. Banjo_Pluck.wav: Banjo string with finger-pick interaction model. The slipping noise is audible between the single notes.
2. Banjo_Random.wav: Random banjo notes played.
3. Violin_BowVelocity.wav: Changing playing parameters of the extended bow model.
Ruan_LineTune.wav: A simple sequence of notes, real-time change of the ruan's front plate thickness.
4. Ruan_TremoloLine.wav: A line of ruan notes played with a tremolo plectrum technique.
5. RuanNoOrifices.wav: A HL model of the ruan without orifices.
6. RuanOrifices.wav: A HL model of the ruan with orifices.
7. Yueqin.wav: Complete yueqin model.
8. Banjo_Knock.wav: Knock on the membrane of the banjo, resonating strings.

Bit-files. ROM-files for ML605 include *.mcs, *.prm, *.cfi:

1. violin.*
2. banjo.*
3. ruan.*
4. yueqin.*

- Abel, M., S. Bergweiler, and R. Gerhard-Multhaupt: “Synchronization of organ pipes: experimental observations and modeling”, in: *The Journal of the Acoustical Society of America* 119.4 (2006): 2467–2475.
- Anderson, Brian E. and William J. Strong: “The effect of inharmonic partials on pitch of piano tones”, in: *The Journal of the Acoustical Society of America* 117.5 (2005): 3268–3272.
- Anderson, Lois Ann: “The Interrelation of African and Arab Musics: Some Preliminary Considerations”, in: *Music and History in Africa*, ed. by Klaus P. Wachsmann, Evanston: Northwestern University Press, 1971.
- Ascher, Uri M. and Robert I. McLachlan: “Multisymplectic box schemes and the Korteweg-de-Vries equation”, in: *Applied Numerical Mathematics* 48.34 (2004), Workshop on Innovative Time Integrators for PDEs: 255–269.
- Ashenden, Peter J.: *The Designer’s Guide to VHDL*, 2nd, San Francisco, CA, USA: Morgan Kaufmann Publishers Inc., 2002.
- Askenfelt, A.: *Five Lectures on the Acoustics of the Piano*, Publications issued by the Royal Swedish Academy of Music, Kungl. Musikaliska Akademien, 1990.
- Askenfelt, Anders and Erik V. Jansson: “From touch to string vibrations. II: The motion of the key and hammer”, in: *The Journal of the Acoustical Society of America* 90.5 (1991): 2383–2393.
- “From touch to string vibrations. III: String motion and spectra”, in: *The Journal of the Acoustical Society of America* 93.4 (1993): 2181–2196.
- Aydın, A. and B. Karasözen: “Symplectic and multisymplectic Lobatto methods for the ‘good’ Boussinesq equation”, in: *Journal of Mathematical Physics* 49.8 (2008): NA.
- Bacon, R. A. and J. M. Bowsler: “A Discrete Model of a Struck String”, in: *Acta Acustica united with Acustica* 41.1 (1978): 21–27.
- Bader, Rolf: “Complete Geometric Computer Simulation of a Classical Guitar”, in: *Lay-Language paper of the American Acoustical Society* 05 (2005), http://www.aip.org/149th/bader_Guitar.htm.
- *Computational Mechanics of the Classical Guitar*, Springer, Oct. 2005.
- “Finite-element calculation of a bass drum”, in: *J. Acoust. Soc. Am.* 119 (2006): 3290.
- “Reconstruction of radiating sound fields using minimum energy method”, in: *The Journal of the Acoustical Society of America* 127.1 (2010): 300–308.

Bibliography

- Bader, Rolf: “Whole geometry Finite-Difference modeling of the violin”, in: *Proceedings of the Forum Acusticum 2005* (2005): 629–634.
- Bader, Rolf et al.: “Finite-element transient calculation of a bell struck by a clapper”, in: *J. Acoust. Soc. Am.* 119 (2006): 3290.
- Bahill, Terry A., Jeffrey S. Kallman, and Jon E. Liberman: “Frequency Limitations of the Two-Point Central Difference Differentiation Algorithm”, in: *Biological Cybernetics* 45 (1982): 1–4.
- Bailey, Herb: “Motion of a hanging chain after the free end is given an initial velocity”, in: *American Journal of Physics* 68.8 (2000): 764–767.
- Bank, B., S. Zambon, and F. Fontana: “A Modal-Based Real-Time Piano Synthesizer”, in: *Audio, Speech, and Language Processing, IEEE Transactions on* 18.4 (May 2010): 809–821.
- Bank, Balazs and Heidi-Maria Lehtonen: “Perception of longitudinal components in piano string vibrations”, in: *The Journal of the Acoustical Society of America* 128.3 (2010): EL117–EL123.
- Bank, Balázs and László Sujbert: “Generation of longitudinal vibrations in piano strings: From physics to sound synthesis”, in: *The Journal of the Acoustical Society of America* 117.4 (2005): 2268–2278.
- Bargel, Hans-Jürgen: *Werkstoffkunde*, ed. by Günter Schulze, Springer, 2012.
- Bathe, K.J.: *Finite-Element Methoden*, Springer, 2002.
- Bavu, E., J. Smith, and J. Wolfe: “Torsional Waves in a Bowed String”, in: *Acta Acustica united with Acustica* 91.2 (2005): 241–246.
- Beeman, D.: “Some multistep methods for use in molecular dynamics calculations”, in: *Journal of Computational Physics* 20.2 (1976): 130–139.
- Bensa, Julien et al.: “The simulation of piano string vibration: From physical models to finite difference schemes and digital waveguides”, in: *The Journal of the Acoustical Society of America* 114.2 (2003): 1095–1107.
- Berlin, Ira: *Generations of Captivity. A history of African-American Slaves*, Cambridge, Massachusetts and London, England: The Belknap Press of Harvard University Press, 2003.
- Bever, Thomas G and David Poeppel: “Analysis by synthesis: a (re-) emerging program of research for language and vision”, in: *Biolinguistics* 4.2-3 (2010): 174–200.
- Bilbao, S.: “Robust Physical Modeling Sound Synthesis for Nonlinear Systems”, in: *Signal Processing Magazine, IEEE* 24.2 (Mar. 2007): 32–41.
- Bilbao, Stefan: “Conservative numerical methods for nonlinear strings”, in: *The Journal of the Acoustical Society of America* 118.5 (2005): 3316–3327.
- *Numerical Sound Synthesis: Finite Difference Schemes and Simulation in Musical Acoustics*. Chichester, UK: John Wiley and Sons, 2009.
- “Wave and Scattering Methods for the Numerical Integration of Partial Differential Equation”, phd, Stanford, California: Department of Electrical Engineering, Stanford University, May 2001.
- Bissinger, George: “Structural acoustics model of the violin radiativity profile”, in: *J. Acoust. Soc Amer.* 124.6 (Dec. 2008).
- “The Science of String Instruments”, in: ed. by Thomas D. Rossing, Springer, 2010, chap. 18: 317–345.

Bibliography

- Bissinger, George, Earl G. Williams, and Nicolas Valdivia: “Violin f-hole contribution to far-field radiation via patch near-field acoustical holography”, in: *The Journal of the Acoustical Society of America* 121.6 (2007): 3899–3906.
- Blasone, Massimo and Petr Jizba: “Quantum mechanics of the damped harmonic oscillator”, in: *Can. J. Phys.* 80 (2002): 645–660.
- Blinn, J. E.: “Floating-point tricks”, in: *IEEE Computer Graphics and Applications* 17.4 (July 1997): 80–84.
- Boole, George: *A Treatise on the Calculus of Finite Differences* -, 3rd ed., London: MacMillan and Company, 1880.
- Boutillon, Xavier: “Model for piano hammers: Experimental determination and digital simulation”, in: *The Journal of the Acoustical Society of America* 83.2 (1988): 746–754.
- Boyden, D.D.: *The History of Violin Playing from Its Origins to 1761, and Its Relationship to the Violin and Violin Music*, Oxford University Press, 1967.
- Brennan, Michael J. and Ivana Kovacic: “Examples of Physical Systems Described by the Duffing Equation”, in: *The Duffing Equation*, John Wiley & Sons, Ltd, 2011: 25–53.
- Brewster, David M.: *Introduction to Guitar Tone and Effects: A Manual for Getting the Sounds*, Milwaukee: Hal Leonard, 2003.
- Brich, T. et al.: “The Digital Signal Processing Using FPGA”, in: *ISSE 2006, 29th International Spring Seminar on Electronics Technology* (2006): 322–324.
- Bucur, Voichita: “Springer Series in Wood Science”, in: *Acoustics of Wood*, 2nd ed., Springer, 2006.
- Campbell, Murray and Patsy Campbell: “The Science of String Instruments”, in: ed. by Thomas D. Rossing, Springer, 2010, chap. 17: 301–315.
- Caramana, E.J., M.J. Shashkov, and P.P. Whalen: “Formulations of Artificial Viscosity for Multi-dimensional Shock Wave Computations”, in: *Journal of Computational Physics* 144 (1998): 70–97.
- Carlin, Bob: *The Birth of the Banjo. Joel Walker Sweeney an Early Minstrelsy*, Wiesbaden: McFarland & Company, Inc., Publishers, 2007.
- Carrier, G.F.: “On the non-linear vibration problem of the elastic string”, in: *Quarterly of Applied Mathematics* 3 (1945): 157–165.
- Chabassier, Juliette: “Modélisation et simulation numérique d’un piano par modèles physiques”, PhD thesis, 2012.
- Chabassier, Juliette and Antoine Chaigne: “Modeling and numerical simulation of a nonlinear system of piano strings coupled to a soundboard”, in: *Proceedings of 20th International Congress on Acoustics*, 2010.
- Chabassier, Juliette, Antoine Chaigne, and Patrick Joly: “Modeling and simulation of a grand piano”, in: *The Journal of the Acoustical Society of America* 134.1 (2013): 648–665.
- Chadefaux, Delphine et al.: “Experimentally based description of harp plucking”, in: *The Journal of the Acoustical Society of America* 131.1 (2012): 844–855.
- Chaigne, Antoine and Anders Askenfelt: “Numerical simulations of piano strings. I. A physical model for a struck string using finite difference methods”, in: *The Journal of the Acoustical Society of America* 95.2 (1994): 1112–1118.
- “Numerical simulations of piano strings. II. Comparisons with measurements and systematic exploration of some hammer-string parameters”, in: *The Journal of the Acoustical Society of America* 95.3 (1994): 1631–1640.

Bibliography

- Chandio, MS and AG Memon: “Improving the Efficiency of Heun’s Method”, in: *Sindh University Research Journal (Science Series)* 42.2 (2010): 85–88.
- Chen, P. et al.: “Delay-sum Beamforming on FPGA”, in: *ICSP 2008 Proceedings* (2008): 2542–2545.
- Chen, Li-Qun and Hu Ding: “Two nonlinear models of a transversely vibrating string”, English, in: *Archive of Applied Mechanics* 78.5 (2008): 321–328.
- Chen, Wang et al.: “An FPGA implementation of the two-dimensional finite-difference time-domain (FDTD) algorithm”, in: *Proceedings of the 2004 (ACM/SIGDA) 12th international symposium on Field programmable gate arrays*, New York, USA: ACM, 2004: 213–222.
- Conway, Cecelia: *African Banjo Echoes in Appalachia*, Knoxville: The University of Tennessee Press, 1995.
- “Black banjo songsters in Appalachia”, in: *Black music research journal* 23.1-2 (2003).
- Corcoran, Joseph M. and Ricardo A. Burdisso: “A diffusion boundary element method for room acoustics”, in: *12th Pan-American Congress of Applied Mechanics*, Port of Spain, Trinidad, 2012.
- Courant, R., K. Friedrichs, and H. Lewy: “Über die partiellen Differenzgleichungen der mathematischen Physik”, in: *Mathematische Annalen* 100.1 (1928): 32–74.
- Cremer, L., M. Heckl, and B.A.T. Petersson: *Structure Borne Sound*, 3rd ed., Springer, 2010.
- Cremer, Lothar: *Physik der Geige*, Stuttgart, Germany: Hirzel, 1981.
- Curtin, Joseph and Thomas D. Rossing: “The Science of String Instruments”, in: ed. by Thomas D. Rossing, Springer, 2010, chap. 13: 209–244.
- Datadbase, The Wood: *Paulownia*, [Online; accessed 5-October-2013], 2013, URL: <http://www.wood-database.com/lumber-identification/hardwoods/paulownia/>.
- Demoucron, Matthias: “On the control of virtual violins”, PhD thesis, School of Computer Science and Communication, 2008.
- Dessalles, Adrien and Pierre Regis Dessalles: *Histoire general des Antilles*, 3rd ed., Not in copyright, 1847.
- Dias, Frederic and Thomas J Bridges: “The numerical computation of freely propagating time-dependent irrotational water waves”, in: *Fluid Dynamics Research* 38.12 (2006): 803.
- Ehlers, W., S. Zinatbakhsh, and B. Markert: “Stability analysis of finite difference schemes revisited: A study of decoupled solution strategies for coupled multifield problems”, in: *International Journal for Numerical Methods in Engineering* 94.8 (2013): 758–786.
- Elejabarrieta, M. J., A. Ezcurra, and C. Santamaría: “Vibrational behaviour of the guitar soundboard analysed by the Finite Element Method”, in: *Acta Acustica united with Acustica* 87.1 (2001): 128–136.
- Epstein, Dena J.: “The Folk Banjo: A Documentary History”, in: *Ethnomusicology* 3 (1975), ed. by Ann Arbor.
- Erkut, C. et al.: “Acoustical Analysis and model-based sound synthesis of the kantele”, in: *J. Acoust. Soc. Am.* 112.4 (2002): 1681–1691.
- Euler, Leonhard and John D. Balnton: *Foundations of Differential Calculus*, springer verlag, 2000.
- Feng, Quandong et al.: “Implementing arbitrarily high-order symplectic methods via krylov deferred correction technique”, in: *International Journal of Modeling, Simulation, and Scientific Computing* 01.02 (2010): 277–301.

Bibliography

- Fernández, Francisco M and Eduardo A Castro: “Hypervirial analysis of enclosed quantum mechanical systems. II. von Neumann boundary conditions and periodic potentials”, in: *International Journal of Quantum Chemistry* 19.4 (1981): 533–543.
- Fettweis, A.: “Wave digital filters: Theory and practice”, in: *Proceedings of the IEEE* 74.2 (Feb. 1986): 270–327.
- Fletcher, N. and Th. Rossing: *Physics of Musical Instruments*, Springer, 2000.
- Fletcher, Neville H. and Thomas D. Rossing: *The Physics of Musical Instruments*, Springer Verlag, 1998.
- Florens, Jean-Loup: “Expressive Bowing on a Virtual String Instrument”, in: *Gesture-Based Communication in Human-Computer Interaction*, ed. by Antonio Camurri and Gualtiero Volpe, vol. 2915, Lecture Notes in Computer Science, Springer Berlin Heidelberg, 2004: 487–496.
- Fornberg, B.: *A practical guide to pseudospectral methods*, vol. 1, Cambridge university press, 1998.
- “Calculation of weights in finite difference formulas”, in: *SIAM Rev.* 40.3 (1998): 685–691.
- “Generation of finite difference formulas on arbitrarily spaced grids”, in: *Math. Comput* 51.184 (1988): 699–706.
- “High-order finite differences and the pseudospectral method on staggered grids”, in: *SIAM Journal on Numerical Analysis* 27.4 (1990): 904–918.
- Foster, N. and D. Metaxas: “Realistic animation of liquids”, in: *Graph. Models Image Process.* 5.58 (1996): 471–483.
- Friedlander, F.G.: “On the oscillations of a bowed string”, in: *Proceedings of the Cambridge Philosophical Society* 49 (1953): 516–530.
- Fritz, Claudia, Amélie Muslewski, and Danièle Dubois: “A situated and cognitive approach of violin quality”, in: *Proceedings of the 20th international Symposium on Music Acoustics* (2010).
- Geiser, Brigitte: “Studien zur Frühgeschichte der Violine”, in: *Publikationen der Schweizerischen Musikforschenden Gesellschaft : Serie 2*, Bern: Gemeinsamer Bibliotheksverband (GBV) / Verbundzentrale des GBV (VZG), 1974.
- Gibbons, J.A., D.M. Howard, and A.M. Tyrrell: “FPGA implementation of 1D wave equation for real-time audio synthesis”, in: *IEEE Proceedings, Computers and Digital Techniques* 152.5 (2005): 619–631.
- Giordano, N.: “Simple model of a piano soundboard”, in: *The Journal of the Acoustical Society of America* 102.2 (1997): 1159–1168.
- Gödel, Nico: “Numerische Simulation hochfrequenter elektromagnetischer Felder durch die Discontinuous Galerkin Finite elemente Methode”, PhD thesis, Helmut-Schmidt-Universität / Universität der Bundeswehr Hamburg, 2010.
- Goldberg, David: “What Every Computer Scientist Should Know About Floating-Point Arithmetic”, in: *ACM Computing Surveys* 23 (1991): 5–48.
- Gotay, Mark J. and James A. Isenberg: “The symplectization of Science”, in: *Gazette des Mathématiciens* 54 (1992): 59–79.
- Gray, S.K., D.W. Noid, and B.G. Sumpter: “Symplectic integrators for large scale molecular dynamics simulations: A comparison of several explicit methods”, in: *The Journal of chemical physics* 101 (1994): 4062.

Bibliography

- Greenspan, Donald: "Discrete Mathematical Physics and Particle Modeling," in: *IMACS European Simulation Meeting*, 1984: 39–46.
- Gura, Philip F. and James F. Bollman: *America's instrument. The banjo in the Nineteenth Century*, Chapel Hill and London: The University of North Carolina Press, 1999.
- Hairer, Ernst, Christian Lubich, and Gerhard Wanner: "Geometric numerical integration illustrated by the Stoermer-Verlet method", in: *Acta Numerica* 12 (2003): 399–450.
- "Geometric numerical integration illustrated by the Störmer/Verlet method", in: *Acta Numerica* 12 (2003): 399–450.
- *Geometric numerical integration : structure-preserving algorithms for ordinary differential equations*, Springer series in computational mathematics ; 31, Berlin [u.a.]: Springer, 2002.
- Haken, Hermann: *Synergetik*, 2nd ed., Berlin, Heidelberg, New York, Tokio: Springer-Verlag, 1983.
- Hao, C and W. Ping: "The High Speed Implementation of Direction-of-Arrival Estimation Algorithm", in: *International Conference on Communication, Circuits and Systems and West Sino Expositions 2* (2002): 922–925.
- Helmholtz, Hermann von: *Die Lehre von den Tonempfindungen als psychologische Grundlage für die Theorie der Musik*, Vieweg, 1870.
- Hendler, Maximilian: "Banjo. Altweltliche Wurzeln eines neuweltlichen Musikinstrumentes. Verschüttete Spuren zur Vor- und Frühgeschichte der Saiteninstrumente", in: *Afro-Amerikanische Schriften*, ed. by Alfons Michael Dauer, vol. 1, Goettingen: Edition RE, 1995.
- Herbordt, Martin C. et al.: "Achieving high performance with FPGA-based computing", in: *Computer* 40 (2007): 50–57.
- Hermanns, Miguel and Juan Antonio Hernandez: "Stable high-order finite-difference methods based on non-uniform grid point distributions", in: *International Journal for Numerical Methods in Fluids* 56 (2007): 233–255.
- Hiller, Lejaren and Pierre Ruiz: "Synthesizing Musical Sounds by Solving the Wave Equation for Vibrating Objects: Part 1", in: *J. Audio Eng. Soc* 19.6 (1971): 462–470.
- "Synthesizing Musical Sounds by Solving the Wave Equation for Vibrating Objects: Part 2", in: *J. Audio Eng. Soc* 19.7 (1971): 542–551.
- Hong, S.-W. and C.-W. Lee: "Frequency and time domain analysis of linear systems with frequency dependent parameters", in: *Journal of Sound and Vibration* 127.2 (1988): 365–378.
- Hutchings, C.M.: "Klang und Akustik der Geige", in: *Spektrum der Wissenschaft* 2 (1981), original: *Scientific American*, October 1981: 112–122.
- Hutchins, C.N., Stetson K.A., and Taylor P.A.: "Clarification of free plate tap tones by holographic interferometry.", in: *Catgut Acoust. Soc. Newsletter* 16.15 (1971).
- Hutchinson, John E.: "Fractals and Self Similarity", in: *Indiana Mathematics Journal* 30 (1981): 713–747.
- Introduction to Mylar Polyester Films*, DuPont Teijin Films, 2003.
- Jackiewicz, Z., B. Zubik-Kowal, and B. Basse: "Finite-Difference and Pseudo-Spectral Methods for the Numerical Simulations of In Vitro Human Tumor Cell Population Kinetics", in: *Mathematical Biosciences and Engineering* 6.3 (2009): 561–572.
- Jansson, Erik: "On the Prominence of the Violin Bridge Hill in Notes of Played Music", in: *Journal of the Violin Society of America* 22.1 (2009): 169–176.

Bibliography

- Jian, Teng Wei: "Piano Sounds Synthesis with an emphasis on the modeling of the hammer and the piano wire.", MA thesis, University of Edinburgh, 2012.
- Jordan, Charles: *Calculus of Finite Differences*, new york, n.y.: Chelsea Publishing Company, 1950.
- Kahng, Andrew B. et al.: *VLSI Physical Design: From Graph Partitioning to Timing Closure*, Springer, 2011.
- Karjalainen, Matti, Vesa Välimäki, and Zoltan Janosy: "Towards High-Quality Sound synthesis of the Guitar and String Instruments", in: *International Computer Music Conference*, Tokyo, Japan, 1993.
- Kartomi, M.J.: *On Concepts and Classifications of Musical Instruments*, Chicago Studies in Ethnomusicology, University of Chicago Press, 1990.
- K.-D. Kammeyer, K. Kroschel: *Digitale Signalverarbeitung - Filterung und Spektralanalyse mit MATLAB-Übungen*, 6th ed., Wiesbaden, Germany: Vieweg+Teubner-Verlag, Apr. 2006: 587.
- Kirby, Percival Robson: *The Musical Instruments of the Native Races of South Africa*, second, Johannesburg: Witwatersrand University Press, 1965.
- Kirch, Ulla and Peter Prinz: *C++ Lernen und professionell anwenden*, 5th, mitp, 2010.
- Kirchhoff, G.: "Über das Gleichgewicht und die Bewegung einer elastischen Scheibe.", in: *Journal für die reine und angewandte Mathematik* 40 (1850): 51–88.
- Kirchhoff, Gustav: *Vorlesungen über mathematische Physik. Mechanik*, H. G. Treubner, 1876.
- Kirn, Ron: *Paulownia research*, [Online; accessed 5-October-2013], 2013, URL: <http://www.tdpri.com/forum/tele-home-depot/173208-paulownia-research.html>.
- Kreiss, Heinz-Otto: "Über die Stabilitätsdefinition für Differenzgleichungen die Partielle Differentialgleichungen approximieren", in: *Nord. Tidskr. Inf. (BIT)* 2 (1962): 153–181.
- Kubik, Gerhard: *Africa and the Blues*, Jackson: University Press of Mississippi, 1999.
- "Theory of African Music", in: *Intercultural Music Studies* 7, ed. by Max Peter Baumann, Wilhelmshafen: Florian Noetzel Verlag, 1994.
- Kuypers, F.: *Klassische Mechanik*, 8th ed., Weinheim: Viley-VHC, 2008.
- Lax, P.D. and Richtmyer R.D.: "Survey of the stability of linear finite difference equations.", in: *Communications on Pure and Applied Mathematics* 9 (1956): 267–293.
- Lax, Peter D.: "On the stability of difference approximations to solutions of hyperbolic equations with variable coefficients", in: *Communications on Pure and Applied Mathematics* 14.3 (1961): 497–520.
- "The scope of the energy method", in: *Bulletin of the American Mathematical Society* 66.1 (1960): 32–35.
- Lean, M.H. and A. Wexler: "Application of the boundary element method to electromagnetic scattering problems", in: *Antennas and Propagation Society International Symposium, 1981*, vol. 19, 1981: 326–330.
- Levenson, Dan: *Clawhammer Banjo From Scratch A Guide for the Claw-less!*, MELBAY, 2003.
- Liebig, H., Thomas Flik, and M. Menge: *Mikroprozessortechnik und Rechnerstrukturen*, Springer London, Limited, 2005.
- Linn, Karen: *That Half-Barbaric Twang*, 5th ed., Urbana and Chicago: University of Illinois Press, 1994.

Bibliography

- Liu, M. et al.: “System-on-an-FPGA Design for Real-Time Particle Track Recognition in Physics Experiments”, in: *11th Euromicro Conference on Digital System Design Architectures, Methods and Tools* (2008).
- LM4550 AC '97 Rev 2.1 Multi-Channel Audio Codec with Stereo Headphone Amplifier, sample Rate conversion and National 3D Sound, version SNAS032F, Texas Instruments, 2013.
- Madanayake, A. et al.: “FPGA Architectures for Real-Time 2D/3D FIR/IIR Plane Wave Filters”, in: *Proceedings of the 2004 International Symposium on Circuits and Systems ISCAS 2004 3* (2004).
- Maestre, Esteban: “Analysis/synthesis of bowing control applied to violin sound rendering via physical models”, in: *Proceedings of Meetings on Acoustics 19.1* (2013).
- Mallat, Stephan: *A Wavelet Tour of Signal Processing The Sparse Way*, Elsevier, 2009.
- Mamou-Mani, Adrien, Joel Frelat, and Charles Besnainou: “Numerical simulation of a piano soundboard under downbearing”, in: *The Journal of the Acoustical Society of America* 123.4 (2008): 2401–2406.
- Markiewicz, D.W.: “Survey on symplectic integrators”, in: *Preprint Univ. California at Berkeley, Spring* (1999).
- Maslennikow, O. and A Sergiyenko: “Mapping DSP Algorithms into (FPGA)”, in: *Proceedings of the International Symposium on Parallel Computing in Electrical Engineering* (2006).
- Maxfield, Clive: *The Design Warriors Guide to FPGAs*, Elsevier, 2004.
- Mclachlan, Robert: “Symplectic Integration of Hamiltonian Wave Equations”, in: *Numer. Math* 66 (1994): 465–492.
- Meissner, Jochen, Ulrich Muecke, and Klaus Weber: *Schwarzes Amerika. Eine Geschichte der Sklaverei*, Muenchen: Verlag C. H. Beck, 2008.
- Mersenne, Marin: *Harmonie universelle: Contenant la théorie et la pratique de la musique. (Paris 1636)*, Reprint Centre nat. de la recherche scientifique, Paris: Springer, 1965.
- Meyer-Baese, Uwe: *Digital Signal Processing with Field Programmable Gate Arrays*, 2nd ed., Berlin, Heidelberg: Springer, 2007.
- Mingyue, Liang: *Music of the Billion*, ed. by Ivan Vador, New York: Heinrichhofen Edition, 1985.
- Moore, Brian E.: “Conformal multi-symplectic integration methods for forced-damped semi-linear wave equations”, in: *Mathematics and Computers in Simulation* 80.1 (2009): 20–28.
- Moore, Brian E. and Sebastian Reich: “Multi-symplectic integration methods for Hamiltonian PDEs”, in: *Future Generation Computer Systems* 19.3 (2003): 395–402.
- Moore, Brian and Sebastian Reich: “Backward error analysis for multi-symplectic integration methods”, in: *Numerische Mathematik* 95.4 (2003): 625–652.
- “Backward error analysis for multi-symplectic integration methods”, in: *Numerische Mathematik* 95.4 (2003): 625–652.
- Mores, Robert: “Vowel Quality in Violin Sounds”, in: ed. by R. Bader, C. Neuhaus, and U. Morgenstern, Peter Lang, 2010, chap. 6.
- Morse, Philip M. and K. Uno Ingard: *Theoretical Acoustics*, Princeton University Press, 1968.
- Motuk, E., R. Woods, and S Bilbao: “Implementation of Finite-Difference Schemes for the Wave Equation on FPGA”, in: *IEEE International Acoustics Speech and Signal Processing ICASSP 2005 3* (2005).
- Motuk, E. et al.: “Design Methodology for Real-Time FPGA-Based Sound Synthesis”, in: *IEEE Transactions on signal processing* 55.12 (2007).

Bibliography

- Motuk, Halil Erdem: “System-On-Chip implementation of real-time finite difference based sound synthesis”, PhD thesis, Queen’s University Belfast, 2006.
- Münxelhaus, Barbara: *Pythagoras musicus: Zur Rezeption der pythagoreischen Musiktheorie als quadrivieraler Wissenschaft im lateinischen Mittelalter*, Verlag für Systematische Musikwissenschaft Bonn-Bad Godesberg, 1976.
- Myers, John: *The Way of the Pipa*, Kent, Ohio: Kent State University Press, 1992.
- Mylar polyester film: Physical-Thermal Properties*, DuPont Teijin Films, 2003.
- Nealen, Andrew et al.: “Physically Based Deformable Models in Computer Graphics”, in: *Computer Graphics Forum* 25.4 (Dec. 2006): 809–836.
- Nesterenko, Vitali F.: *Dynamics of Heterogeneous Materials*, ed. by Lee Davidson and Yasuyuki Horie, Springer-Verlag, 2001.
- Neumann, John von and R. D. Richtmyer: “A Method for the Numerical Calculation of Hydrodynamic Shocks”, in: *Journal of Applied Physics* 21 (1950).
- Omelyan, Igor, Ihor Mryglod, and Reinhard Folk: “Optimized Forest-Ruth- and Suzuki-like algorithms for integration of motion in many-body systems”, in: *Computer Physics Communications* 146.188 (2001).
- Paladino, Sascha: *Throw Down Your Heart*, Motion picture, 2009.
- Palmer, Bill: *A Scientific Method for Determining the Correct Head Tension For Your Banjo*, [Online; last accessed 20-January-2014], 2006, URL: <http://www.banjowizard.com/hedtens.htm>.
- Pfeifle, F. and R. Bader: “Measurement and physical modelling of sound hole radiations of lutes”, in: *J. Acoust. Soc. Am.* 130.4 (2011): 2507–2507.
- “Musical Acoustics, Neurocognition and Psychology of Music”, in: Frankfurt am Main, Germany: Rolf Bader, 2009: 71–86.
- “Real-time virtual banjo model and measurements using a microphone array.”, in: *J. Acoust. Soc. Am.* 125.4 (2009): 2515–2515.
- Pfeifle, Florian: “Multisymplectic Pseudo-Spectral Finite Difference Methods for Physical Models of Musical Instruments”, English, in: *Sound - Perception - Performance*, ed. by Rolf Bader, vol. 1, Current Research in Systematic Musicology, Springer International Publishing, 2013: 351–365.
- “Systematic Musicology: Empirical and theoretical Studies”, in: ed. by Albrecht Schneider and Arne von Ruschkowsky, Frankfurt am Main, Germany: Peter Lang Verlag, 2011, chap. Air Modes in Stringed Lute-like Instruments from Africa and China. 137–152.
- Pierce, A.D.: *Acoustics*, New: McGraw, 1981.
- Pitteroff, R. and J. Woodhouse: “Mechanics of the contact area between a violin bow and a string. Part I: Reflection and transmission behaviour”, in: *Acta Acustica united with Acustica* (1998): 543–562.
- Raman, C. V.: “Experiments with mechanically played violins”, in: *Proc. Indian Association for the Cultivation of Science* 6 (1920): 19–36.
- “On the mechanical theory of vibrations of bowed strings”, in: *Indian Assoc. Cult. Sci. Bull.* 15 (1918): 243–276.
- Rastogi, Vikas, Amalendu Mukherjee, and Anirban Dasgupta: “A Review on Extension of Lagrangian-Hamiltonian Mechanics”, in: *Journal of the Brazilian Society of Mechanical Science and Engineering* 18.1 (2011): 22–33.
- Rossing, Thomas D.: *Science of Percussion Instruments*, World Scientific, 2008.

Bibliography

- Rowland, David R. and Colin Pask: “The missing wave momentum mystery”, in: *American Journal of Physics* 67.5 (1998): 378–388.
- Sachs, Curt: *Real-Lexikon der Musikinstrumente, zugleich ein Polyglossar für das gesamte instrumentengebiet*, (Reprint d. Ausg. Berlin 1913), Stuttgart: Olms, 1972.
- Saldner, H.O., N.E. Molin, and E.V. Jansson: “Vibration modes of the violin forced via the bridge and action of the soundpost.”, in: *J. Acoust. Soc. Am.* 100 (1996): 1168.
- Sathej, G. and R. Adhikari: “The eigenspectra of Indian musical drums”, in: *arXiv preprint arXiv:0809.1320* (2008).
- Sauter, Stefan A. and Christoph Schwab: “Springer series in computational mathematics”, in: *Boundary Element Methods*, ed. by R. Bank et al., Springer Verlag, 2011.
- Schelleng, J. C.: “The violin as a circuit”, in: *J. Acoust. Soc. Am.* 35 (1963): 326–338.
- Schilling, Robert J. and Sandra L. Harris: *Fundamental of Digital Signal Processing using MATLAB*, 2nd ed., Cengage Learning, 2012.
- Schwarz, Hans Rudolf and Norbert Köckler: *Numerische Mathematik*, 6., Wiesbaden: Treubner Verlag, 2006.
- Sha, Wei et al.: “Survey on Symplectic Finite-Difference Time-Domain Schemes for Maxwell’s Equations”, in: *IEEE Transactions on Antennas and Propagation* 56.2 (Feb. 2008): 493–500.
- Shen, Jing et al.: “High-order symplectic FDTD scheme for solving a time-dependent Schrödinger equation”, in: *Computer Physics Communications* (2012).
- Shen, Sin-Yan: *Chinese Music and Orchestration: A Primer on Principles and Practice*, Chicago: Chinese Music Society of North America, 1991.
- Shuang, Kai et al.: “Converting Analog Controllers to Digital Controllers with FPGA”, in: *(ICSP2008) Proceedings* (2008).
- Skeel, R.D.: “Symplectic integration with floating-point arithmetic and other approximations”, in: *Applied numerical mathematics* 29.1 (1999): 3–18.
- Smith, Julius O.: “Digital Waveguide Architectures for Virtual Musical Instruments”, in: *Handbook of Signal Processing in Acoustics*, ed. by David Havelock, Sonoko Kuwano, and Michael Vorländer, Springer New York, 2009: 399–417.
- Spa, Carlos, Adan Garriga, and Jose Escolano: “Impedance boundary conditions for pseudo-spectral time-domain methods in room acoustics”, in: *Applied Acoustics* 71.5 (2010): 402–410.
- Stephey, Laurie A. and Thomas R. Moore: “Experimental investigation of an American five-string banjo”, in: *The Journal of the Acoustical Society of America* 124.5 (2008): 3276–3283.
- Strikwerda, J.: *Finite difference schemes and partial differential equations*, 2nd ed., Philadelphia: SIAM, 2005.
- Strikwerda, John and Bruce Wade: “A survey of the Kreiss matrix theorem for power bounded families of matrices and its extensions”, in: *Banach Center Publications* 38.1 (1997): 339–360.
- Synthesis and Simulation Design Guide (UG626)*, version 13.2, Xilinx, 2011.
- Taylor, Michael E.: *Partial Differential Equations I*, Berlin and Heidelberg: Springer, 1996.
- Teixeira, Fernando L.: “FDTD/FETD Methods: A Review on Some Recent Advances and Selected Applications”, in: *J. of Microwaves and Optoelectronics* 6.1 (2007): 83–95.

Bibliography

- Thom e, Vidar: "From finite differences to finite elements: A short history of numerical analyses of partial differential equations", in: *journal of computational and applied mathematics* 128.1-2 (2001): 1–54.
- Trefethen, L.N.: *Spectral methods in MATLAB*, vol. 10, Society for Industrial Mathematics, 2000.
- Truesdell, C.: "Outline of the History of Flexible or Elastic Bodies to 1788", in: *The Journal of the Acoustical Society of America* 32.12 (1960): 1647–1656.
- Tuttle, Matthew David: "Plucked Instrument Strings: A Combined Frequency - Time Domain Wave Approach to Investigate Longitudinal forces at the Bridge Support", Master's Thesis, Chalmers University of Technology, 2007.
- tweddle, Ian: *James Stirling's Methodus Differentialis: An Annotated Translation of Stirling's Text*, Springer Verlag, 2003.
- Ullmann, Dieter: *Chladno und die Entwicklung der Akustik von 1750-1860*, Birkh user Verlag, 1996.
- V lim ki, Vesa et al.: "Model-Based Sound Synthesis", in: *EURASIP Journal on Applied Signal Processing*, Hindawi Publishing Corporation, 2004.
- Vargas-Jarillo, C. and G. Gonzalez-Santos: "A Numerical Study of Discrete Nonlinear Elastic Strings in Two Dimensions", in: *Proceedings of the CCE 2010* (2010): 400–405.
- Veggeberg, K. and A. Zheng: "Real-time noise source identification using programmable gate array FPGA technology", in: *Proceedings of Meetings on Acoustics* 5 (2009).
- Ventsel, Eduard and Theodor Krauthammer: *Thin Plates and Shells: Theory, Analysis and Applications*, Marcel Dekker, 2001.
- Verlet, Loup: "Computer "Experiments" on Classical Fluids. I. Thermodynamical Properties of Lennard-Jones Molecules", in: *Phys. Rev.* 159.1 (July 1967): 98–103.
- Virtex-6 FPGA Configurable Logic Block User Guide*, version 1.2, Xilinx, 2012.
- Von Herzen, B.: "Signal Processing at 250 Mhz Using High-Performance FPGAs", in: *IEEE Transactions on very large scale integration (VLSI) Systems* 6.2 (1998).
- Vyasarayani, Chandrika P., Stephen Birkett, and John McPhee: "Modeling the dynamics of a vibrating string with a finite distributed unilateral constraint: Application to the sitar", in: *The Journal of the Acoustical Society of America* 125.6 (2009): 3673–3682.
- Wang, Z. et al.: "FPGA implementation of Downlink DBF Calibration", in: *Antennas and Propagation Society International Symposium* (2005).
- Webb, Robert L.: "Ring the banjo!", in: *Canadian folk music bulletin* 2.4 (1979).
- Wegner, Ulrich: *Afrikanische Saiteninstrumente*, Berlin: Staatlich Museen Preu ischer Kulturbesitz, 1984.
- Wegst, Ulrike G. K.: "Wood for sound", in: *Am. J. Bot.* 93.10 (2006).
- Wheeler, G. F. and W. P. Crummett: "The vibrating string controversy", in: *American Journal of Physics* 55 (Jan. 1987): 33–37.
- Wilen, A.H., J.P. Schade, and R. Thornburg: *Introduction to Pci Express: A Hardware and Software Developer's Guide*, Engineer to Engineer Series, Intel Press, 2003.
- Woitowitz, R. and K. Urbanski: *Digitaltechnik*, 5th ed., Berlin, Heidelberg: Springer, 2007.
- Woodhouse, J.: "On the "Bridge Hill" of the Violin", in: *Acta Acustica united with Acustica* 91 (2005).
- Woodhouse, J. and P.M. Galluzzo: "The bowed String As We Know It Today", in: *Acta Acustica united with Acustica* 90 (2004): 579–589.
- XILINX: *Configurable Logic Block User Guide*, XILINX, 2010.

Bibliography

- Yee, Kane: "Numerical solution of initial boundary value problems involving Maxwell's equations in isotropic media", in: *IEEE Transaction on Antennas and Propagation* 14.3 (1966): 302–307.
- Zölzer, Udo et al.: *DAFX: Digital Audio Effects*, ed. by Udo Zölzer, John Wiley & Sons, May 2002.
- Zulehner, Walter: *Numerische Mathematik*, Mathematik Kompakt, Basel: Birkhäuser Verlag, 2011.

Eidesstattliche Erklärung

Vor- und Zuname:

Florian Pfeifle

Geburtsdatum:

14.07.1978

Geburtsort:

Hamburg

Hiermit erkläre ich an Eides statt,

dass ich die vorgelegte Dissertation selbständig und ohne unzulässige fremde Hilfe angefertigt und verfasst habe, dass alle Hilfsmittel und sonstigen Hilfen angegeben und dass alle Stellen, die ich wörtlich oder dem Sinne nach aus anderen Veröffentlichungen entnommen habe, kenntlich gemacht worden sind;

dass die Dissertation in der vorgelegten oder einer ähnlichen Fassung noch nicht zu einem früheren Zeitpunkt an der Universität Hamburg oder einer anderen in- oder ausländischen Hochschule als Dissertation eingereicht worden ist.